

Thesis submitted for the degree of
Doctor of Philosophy

Vibrations of precast and partially prestressed floor systems under moving loads

Development of a dynamic fork-lift truck model for vibration
serviceability analysis and its application



Andreas Ehland
Magdalen College

Department of Engineering Science

University of Oxford

Hilary Term 2009

27th March 2009

Thesis submitted for the degree of Doctor of Philosophy

“Vibrations of precast and partially prestressed floor systems under moving loads”

Andreas Ehland – Magdalen College, Oxford

Hilary term 2009, 27th March 2009

Abstract

This project studies the dynamic response of a composite floor system to excitations from moving fork-lift trucks. The floor system analysed is a system of precast and partially prestressed double-tee elements with a cast in-situ topping. Currently, there are concerns whether the vibrations caused by fork-lift trucks might exceed acceptable limits due to an ongoing trend towards structures of higher slenderness. This study investigates the mechanical background of the excitation and the current design of the floor system. The study is divided into three major chapters:

Dynamic fork-lift truck model A dynamic load model of a fork-lift truck is developed which can be used in the analytical verification of the vibration serviceability of structures. The model is based on tests performed on four fork-lift trucks in various configurations. The tests are analysed for the spectrum of accelerations. The analysis results in a simple two-degree-of-freedom model. Its only variables are velocity and time. All other values are constant throughout a simulation and depend on the geometry of the specific fork-lift truck and its payload. The frequencies and phase delays are constants and they are verified as eigen-frequencies of a three-degree-of-freedom model.

FE-simulation of vibrations of a composite floor system The fork-lift truck model is applied to a three-dimensional model of a composite floor system. The finite-element model is developed to simulate the construction process of the composite floor system and its influence on the in-service properties of the structure. As part of this work a preliminary investigation of the damping potential of the joint between precast and cast in-situ concrete is undertaken.

A linear time-step analysis of the structure is performed and the nodal accelerations are analysed for their magnitude, dependence on the excitation and frequency content.

Field test In order to verify the FE-model of the floor system and the results of the dynamic analysis a field test was undertaken: a floor system was monitored under service conditions. The field data comprise the accelerations of the floor and the fork-lift truck and the position of the truck relative to the points of measurement. A comparison of the field data and the simulation results proves the validity of both the dynamic fork-lift truck model and the FE-model of the floor system.

Acknowledgments

Many people were involved in this project. It seems almost impossible to express my gratitude to everyone who helped during its completion. To all who should be mentioned for their generous assistance, my warmest thanks.

In particular, I would like to express my gratitude to my supervisors Prof. Dr. Martin S. Williams and Prof. Dr. Tony Blakeborough, both for accepting me as a research student and for three years of inspiring discussions. I am very privileged to have been a member of the Structural Dynamics research group in the Department of Engineering Science in Oxford.

I am equally grateful to my referees Mrs Dipl.-Arch. Heide von Wehrden-Liebich of HOCHTIEF, Univ.-Prof. i.R. Dr.-Ing. Ulrich Quast of the Hamburg University of Technology (TUHH) and Mr Dipl.-Hdl. Gerd Loch of Deutsche Bundesbank who volunteered their support for my application to Oxford. It was their references which actually opened the door to Oxford for me in the first place.

This project would also not have been possible without the support of several sponsors. In particular, I would like to take this opportunity to acknowledge the support of:

- HOCHTIEF Construction AG (Germany) who provided me with financial support and guaranteed me a job upon my return from study. I would especially like to thank Dr. Karl Reinitzhuber, whose encouragement of my research aspirations made me confident that I had made the right decision to pursue my research project in Oxford.
- EURO-TYRE (Netherlands) who not only gave me the opportunity to test fork-lift trucks on their site, but also provided financial support for my studies. In this regard, I would like to acknowledge the contribution of the managing director Mr Siegfried Schlacks.
- EVAUGE (Germany) and its branch manager Mr Ingo Holzadt who kindly allowed me to test fork-lift trucks on their site.
- LAFARGE (UK) who provided me with high quality cement for my experiments.
- SOFiSTiK AG (Germany) who allowed me to use their finite element software program and who also provided continuous support.
- MWH Metallwerke Helmstadt (Germany) who allowed me to carry out the essential field test in their building.

I would also like to thank my friends in College and “Room 11” in the Jenkin Building.

It goes without saying that I would not be where I am today if it were not for the love and support of my parents. They have always encouraged my siblings and myself

to pursue our educational ambitions, which has resulted in more than 35 years with at least one of their children in an educational institution. When, after almost six years working in industry, I decided to return to university to undertake this project, they not only accepted my decision but also actively encouraged and helped me to achieve my goal. I am also grateful for the support of my whole family, for it is their encouragement which gives me the confidence to explore “new worlds”: I must mention my sister Anne-Ruth who provided me with generous financial support which not only allowed me to eat three meals per day, but also enabled me to participate in the social opportunities available in Magdalen College (and also provided me with a London base should I need to escape the hectic pace of student life in Oxford); my sister Friederike and her husband Oliver (with their daughters Hannah and Leah) who looked after some of my belongings whilst I was in Oxford and my brother Christoph who not only looked after some of my belongings and provided me with financial support but who also paid me regular visits. Thank you so much - I am indebted to you all for your assistance beyond measure.

This thesis has gone through a phase of significant change since its first submission in November 2007. It was not easy to finish this project while working fulltime. I am grateful for the support and help I received during this time from my supervisors, employer, friends and above all my parents.

In particular, I would like to thank Mr. Roy M. Pinkerton, who volunteered to check my grammar and spelling.

Last but not least, I would like to express my gratitude to my examiners, Prof. James M.W. Brownjohn and Dr. Peter D. McFadden, for volunteering to examine me.

Oxford, 27th March 2009

A. E.

Contents

Nomenclature	10
Preface: practical context	13
1 Introduction	14
1.1 Executive summary	14
1.2 Preliminary observations	15
1.3 Precast concrete structures	16
1.3.1 General introduction to precast concrete	16
1.3.2 Flooring systems	19
1.3.3 Production of double-tee elements	20
1.3.4 Design of double-tee elements	22
1.4 Material Science: concrete	23
1.4.1 Time dependency of properties	23
1.4.2 Cracks	26
1.4.3 Tension stiffening	27
1.5 Vibration behaviour of concrete structures	28
1.5.1 Vibration transmission path: the structure	31
1.5.2 Vibration source: dynamic excitations	36
1.5.3 Two case studies on floor vibrations caused by vehicular traffic .	41
1.5.4 Field monitoring of vibrations	43
1.5.5 Acceptability criteria of accelerations	44
1.6 Fork-lift trucks	49

1.6.1	Remarks on the general configuration of fork-lift trucks	49
1.6.2	Fork-lift trucks as loading on structures	50
1.7	Research needs and scope of thesis	51
2	Development of a dynamic load model for a fork-lift truck	53
2.1	Executive summary	53
2.2	Design of structures: the dynamic load factor	55
2.3	Existing dynamic models of fork-lift trucks	57
2.4	Proposed dynamic load model of a fork-lift truck	60
2.4.1	Simplifying assumptions	60
2.4.2	Two-dimensional load model	62
2.5	Experiment set-up and data recording	75
2.6	Experiment execution	79
2.6.1	Fork-lift truck specifications	80
2.7	Results	82
2.7.1	Frequencies of vertical accelerations	83
2.7.2	Cross-correlation of accelerations at front and rear axle	91
2.7.3	Amplitudes of accelerations	95
2.7.4	Ratio of amplitudes	106
2.7.5	Correlation between surface roughness and accelerations	108
2.8	Load model of the fork-lift truck	109
2.8.1	Summary of the results found in the experiments	109
2.8.2	Dynamic load model of a fork-lift truck	110
2.8.3	Generalised load models of general fork-lift trucks	111
2.8.4	Final remarks on the dynamic load model	113
3	Numerical simulations of vibrations of a (sample) floor system	114
3.1	Executive summary	115
3.2	Preliminary observations	116
3.3	Finite element program	118

3.3.1	SAP2000 and ABAQUS	118
3.3.2	SOFiSTiK	120
3.4	Benchmark testing	121
3.4.1	Sample structure (two-dimensional)	121
3.4.2	Verification of static states	127
3.4.3	Verification of eigen-frequencies	128
3.4.4	Conclusions of benchmark testing	131
3.5	Three-dimensional sample floor system	132
3.5.1	Special features of the floor model	133
3.5.2	Dynamic loading	138
3.5.3	Results of the simulations of a 3-D floor system	142
3.5.4	Summary of results of the simulations	150
4	Field test: dynamic response of the Helmstadt floor system to fork-lift truck loading	151
4.1	Executive summary	151
4.2	The Helmstadt floor system	153
4.2.1	Description of the structure	153
4.2.2	Experiment set-up	155
4.2.3	Natural frequencies of the Helmstadt floor	157
4.3	The fork-lift truck	159
4.3.1	Model Mariotti Mycros 13C	159
4.3.2	Experiment set-up	160
4.4	Test execution and results	160
4.5	Finite-element model of the Helmstadt floor	164
4.5.1	Structure	164
4.5.2	Time-dependent properties	165
4.5.3	Damping properties of the structure	165
4.5.4	The dynamic fork-lift truck load model implemented	166
4.5.5	Results of finite-element simulation	168

4.6	Acceptability of accelerations in Helmstadt	174
5	Conclusions	175
5.1	Concrete joint between precast and cast in-situ concrete	175
5.2	Fork-lift truck load model	176
5.3	Simulation of floor vibrations under moving load	178
5.4	Final observations	179
5.5	Future work	180
5.5.1	Fork-lift truck model	180
5.5.2	Analysis of floor system	181
5.5.3	Investigation of concrete joint	181
A	Investigation of the damping behaviour of the joint between precast and cast in-situ concrete	183
A.1	Preliminary observations	183
A.2	Preparation of specimen	186
A.3	Cyclic loading	187
A.4	Results of cyclic testing	189
A.4.1	Influence of cyclic loading on ultimate strength	189
A.4.2	Influence of cyclic loading on stiffness	190
A.4.3	Influence of cyclic loading on hysteresis loop	191
A.4.4	Estimate of damping from hysteresis loop	192
A.5	Conclusions from the investigation of the joint	193
B	Evaluation of fork-lift truck tests	195
B.1	Specification of test equipment	195
B.2	Summary of configuration of tests performed	196
B.3	Frequency analysis	196
B.3.1	Total record	196
B.3.2	Correlation of velocity and frequencies	201
B.3.3	Correlation of driving direction and frequencies	207

B.3.4	Modal analysis	213
B.3.5	Summary of frequencies	214
B.4	Cross-correlation and coherence	220
B.5	Amplitude analysis	222
B.5.1	Theoretical model of amplitudes	222
B.5.2	Correlation of velocity and accelerations	223
B.6	Ratio of amplitudes	230
C	Procedure and source code in SOFiSTiK	232
C.1	Calculation procedure	232
C.2	The input file for the fork-lift truck model	233
D	Results of the field test in Helmstadt	236
E	Results of the finite-element simulations of the floor in Helmstadt	240
	References	244

Nomenclature

The Nomenclature for structural design is chosen according to EC2 (2004), Chapter 1.6. The symbols for structural design and dynamic analyses used in this report are given below:

Roman Symbols

Statics

C	Concrete
E	Young's modulus
L	Length
PS	Prestressing steel
S	Steel
f	Strength, Stress
g	Selfweight
h	Height of cross-section
I	Second moment of area
q	Service load

Dynamics

a	Acceleration
c	Coefficient of viscous damping
f	Frequency
g	Gravity
J	Mass moment of inertia
k	Spring-stiffness
m	Mass
U	Amplitude
u	Deformation
v	Velocity

Greek symbols

Statics

ε	Strain
σ	Normal stress
ϕ	Dynamic load factor
κ	Ageing factor (creep model)
τ	Shear stress
ψ	Reduction factor of service loads

Dynamics

δ	Logarithmic decrement of damping
ζ	Viscous damping ratio
φ	Phase delay/angle (in Matlab figures: ϕ)
μ	Ratio of amplitudes
Ψ	Shape function (Rayleigh)
ω	Circular frequency
$\bar{\omega}$	Excitation frequency

Subscripts

Statics

c	Concrete
k	Characteristic
m	Mean value
p	Prestressing
s	Reinforcement
t	Tensile

Dynamics

cr	Critical
d	Damped (natural frequency)
flt	Fork-lift truck
f	Front (axle)
n	Natural (frequency)
r	Rear (axle)
tot	Total (mass)

Acronyms

Static

A_p	Cross-section area of a prestressing strand
B_{bottom}	Width of web at bottom
C50/60	Concrete, cylinder/cube compressive strength
DLF	Dynamic load factor
$E(t)$	Time-dependent Young's modulus (creep model)
F_{axle}	Axle load of a fork-lift truck
f_{cm}	Mean value of compressive strength (concrete)
$f_{p0,1}$	0.1% proof stress of prestressing steel
f_{pk}	Tensile strength of prestressing steel
f_y	Yield strength of reinforcement
H_{ci}	Height of cast in-situ topping
H_{pc}	Height of precast slab
H_{web}	Height of web
n_{op}	Number of strands per web
PS1570/1770	Prestressing steel, $f_{p0,1}$, f_{pk}
R^2	Determination of linear regression
S500	Steel, f_y
SLS	Serviceability limit state
ULS	Ultimate limit state
W_{flange}	Width of flange
$\varphi(t, t_p)$	Creep coefficient

Dynamic

AFC	Absolute frequency change
[C]	Damping matrix
COG	Centre of gravity
Δf	Increment of frequency in discrete psd

DOF	Degree(s) of freedom
fft	Fast fourier transform
$E_{c,dyn}$	Dynamic Young's modulus of concrete
$[K]$	Stiffness matrix
L_f	Length from COG to front axle
L_r	Length from COG to rear axle
LI	Load carried, indoors
LO	Load carried, outdoors
$[M]$	Mass matrix
MDOF	Multi-degree-of-freedom system
NLI	No load carried, indoors
NLO	No load carried, outdoors
P_{xx}	Power spectral density of front axle
P_{yy}	Power spectral density of rear axle
PSD	Power spectral density
SDOF	Single-degree-of-freedom system
T_{max}	Maximum kinetic energy
V_{max}	Maximum potential energy
VDV	Vibration dose value
$w(n)$	Window function (frequency analysis)
WB	Wheelbase of a fork-lift truck
x', x''	First, second derivative with respect to location
\dot{x}, \ddot{x}	First, second derivative with respect to time
XC(f)	Cross-correlation function
Z_0	Reference amplitude (Rayleigh)
z_{ssr}	Steady state response

This study has been carried out using the following hard- and software:

Computer	Fujitsu-Siemens, Pentium 4, 3.0 GHz, 1024 MB Ram
Operating system	Microsoft Windows XP Professional, SP 2
Finite Element analysis	SOFiSTiK Version 23, ABAQUS 6.4-1
Static analysis of beams	ABaSW32 Version 05/09/2000 by TUHH, Germany
Moment-curvature analysis	INCA 2.62 (11.04.2004) by TUHH, Germany
Technical computing	MATLAB R2006a
Spreadsheet calculations	Excel

Preface: practical context

This project originates from my professional experience as an engineer working with precast concrete structures in an industrial environment. First as a design engineer in the technical office of a precast plant¹ and later as head of tenderworks in that plant the question arose occasionally whether the ongoing trend towards structures of higher slenderness might lead to vibration serviceability problems if loading from fork-lift trucks has to be considered as a factor in the design.

When storage facilities or warehouses built with precast floor systems were inspected under service conditions, floor vibrations caused by fork-lift trucks were often noticeable. In one case where a too heavy fork-lift truck² was used, unacceptable deflections (and vibrations) were found.

Improvement of the vibration serviceability after a structure has been built is a costly project which is likely to disrupt or at least impede normal use of that building for a while. Furthermore (and from a business point of view more importantly), repairing a newly built structure is not the best way to win the client's trust and to inspire confidence in one's company for future projects.

To avoid poor vibration performance in the future, this project investigates the dynamic response of a precast and partially prestressed composite floor system to loading from fork-lift trucks. How a fork-lift truck excites vibrations in a structure and whether current structures still fulfil the acceptability criteria of vertical accelerations will be investigated.

The aim is to provide means for a serviceability check of a composite floor system under fork-lift truck traffic which can be easily included in the design procedures and can thus reduce the likelihood of poor vibration performance of these floor systems.

¹HOCHTIEF Construction AG, Stockstadt am Rhein, Germany

²About 25% (1000 kg) heavier than the floor was designed for.

Chapter 1

Introduction

1.1 Executive summary

This chapter summarises the basic background to the elements of this study and the state of the scientific debate on them to date.

This study investigates the dynamic response of a precast structure to fork-lift truck traffic. Like every practical vibration problem it is divided into the investigation of three elements: vibration source, path and receiver. The receiver is not of particular interest here, but it could be either a human being or machinery. Of particular interest are the vibration source and path.

As the path is a precast structure, basic information will be given about these structures to show their properties and to explain why they are used more frequently in modern buildings, especially precast concrete flooring systems made of double-tee elements. As concrete is the important material in these systems its key properties will be discussed including shrinkage, creep, cracks and tension stiffening. The state of research and the relevant standards will be described.

The source of vibration here is fork-lift truck traffic. Therefore basic information on fork-lift trucks will be given and two case studies on floor vibrations caused by vehicular traffic will be discussed to show the state of research and the relevant standards.

The literature review shows that at present neither the relevant standards nor

the scientific research deal satisfactorily with vibration problems in precast concrete structures caused by fork-lift truck traffic. The need for further research to achieve the desired aim of a serviceability check on a composite floor system under fork-lift truck traffic is discussed, and from this, the scope of this thesis is defined.

1.2 Preliminary observations

In recent years an ongoing trend towards structures of higher slenderness combined with multi-storey buildings for industrial usage can be noted. In Figures [1.1] and [1.2] are shown typical applications of precast concrete: a distribution centre during construction. Typical buildings in an industrial context are skeleton structures which have up to three storeys.



Figure 1.1: Industrial precast concrete building



Figure 1.2: Industrial precast concrete building (distribution centre)

The trend towards a higher structural slenderness is caused by several factors, the main ones being:

- the ever-increasing prices for land, which make multi-storey buildings more economical than a single-storey building on a bigger site (Pan et al., 2001),
- the economic pressure on the building market combined with the improved production methods and materials which lead, especially for precast elements, to

very slender structures and high stress intensity.

It is this trend that gives rise to concerns over whether the old design methods of floors for fork-lift truck traffic are still suitable. In the past a check on the vibration serviceability has not been part of the design process. It was (and currently still is) assumed that the dynamic effects caused by a fork-lift truck are negligible: the service weight of the fork-lift truck is increased to cover all dynamic effects and it is applied statically in the design process. This project will investigate whether and how a fork-lift truck causes vibrations in a floor system.

1.3 Precast concrete structures

1.3.1 General introduction to precast concrete

Elliott (2002) gives two useful definitions for precast concrete. One focuses on the production: “[...] it is concrete which has been prepared for casting, cast and cured in a location which is not its final destination.”

The other focuses on the structure:

...a precast concrete element is, [...], of a finite size and must therefore be joined to other elements to form a complete structure.[...] A precast structure is an assemblage of precast elements which, when suitably connected together, form a 3D framework capable of resisting gravitation and wind (or even earthquake) loads. The framework is ideally suited to buildings such as offices, retail units, car parks, schools, stadia and other such buildings requiring minimal internal obstruction and multi-functional leasable space.

Areas without any obstructions from columns of about 100 – 200 m² are possible for precast industrial buildings and up to 400 m² for offices and retail units. Therefore, precast concrete elements are widely used for building projects in the industrial world. Elliott (2002) states that nowadays about 50% of multi-storey buildings are built at least partly with precast concrete elements.



Figure 1.3: Assemblage of a 40 m roof girder

Furthermore, several other advantages of precast concrete elements have ensured their continuous usage since their introduction in the 1900s (Glover, 1964). The arguments given by Billig (1955), Glover (1964), Richardson (1991) and Elliott (2002) have not changed significantly over the years and may be divided into three main categories¹:

- Quality
 - Production in factory and so independent of weather conditions and with other relevant conditions able to be controlled.
 - Consistent high quality of concrete.
 - The employment of the most appropriate method of production and curing.
 - Employment of skilled workers and further training of them.
 - Technical control in the production factory is usually better than on site.
 - Amount of concrete cast in-situ is reduced and the work on site is kept cleaner and drier.

¹There is no strict separation between the items and the category they are placed in. Not all of these items may be true for every precast element on every site.

- Economy
 - In the cost of formwork, shuttering and in cost by re-using the same moulds.
 - Mass production due to standardisation resulting in economy in labour and increased productivity.
 - Lighter and often cheaper structures compared to cast in-situ structures.
 - Speed of construction on site is usually greatly increased.
 - Delivery of complete elements on site compared to the delivery of different building materials.
 - No need for scaffolding and shutterings on site.

- Structure
 - Main effects of shrinkage are worn off when elements are assembled on site.
 - Provisions for thermal and moisture movements are possible in joints.
 - Joints can be used for the insulation of noise and vibrations.

Glover (1964) also gave some disadvantages of precast concrete structures. These can be summarised as:

- Larger and more heavily reinforced sections due to static systems of simply supported beams.
- Provision for stresses due to demoulding, handling, transportation and erection.
- Care in handling and erection of units.
- Difficulties in providing convenient and safe support during formation of in-situ jointing.

Care in handling is necessary for all building materials and as modern joints are constructed “ready-to-use” and do not need additional supports during construction,

there is no significant difference in cost or difficulty of erection in comparison to a steel construction.

Provisions for transient stresses during production and transportation are usually negligible, but the simply supported beam construction is still the most common static system which leads to more reinforcement compared to a cast in-situ beam of the same quality. However, on most sites it is rarely possible to use high performance concrete and this therefore reduces the disadvantages of precast concrete.

1.3.2 Flooring systems

The demand for precast flooring systems is steadily growing, as their advantages are obvious: slender constructions are possible which reduce building heights; no formwork is needed on site and therefore cost-intensive foundations for props can be omitted. Assembly is fast, so that large areas can be covered in a short time, thus enabling other trades to start work earlier (Elliott, 2002). Usually a greater span-width can be covered without supports than cast in-situ constructions allow. During construction time the assembled precast concrete elements provide safety for all trades on site: they are useable as a floor from the first moment and thus temporary constructions like scaffolding are not required.

Since the 1950s, separate strands of development can be observed: precast elements without topping and precast concrete elements with a structural topping, which are divided into plank elements and slab girder elements.

Composite plank floors with toppings cast in-situ are mainly used for short spans, since for spans larger than 4.50 m props are needed. The selfweight is identical to that of a cast in-situ floor. Thin precast slabs are laid between supports and used as permanent formwork for a cast in-situ topping (Elliott, 1996).

As a result of the development of lighter structures with larger span-width, prestressed hollow-core elements have been designed. Hollow-core systems are suitable for buildings with an elastic floor covering (Elliott, 2002). The elements are produced with a maximum width of 1.20 m and allow covering spans from 3.00 m to about 16.00 m.

However, no dynamic loading is permitted on these elements.

Glover (1964) stated that the most forceful types of development of light floors are those where the structural elements are reduced to two webs and a thin slab connecting the webs. The slab will then be covered by a structural topping. He gave examples for these systems (so called “channel”-elements, “Y.T. units” and “floor-beams”). It is from these that the modern “double-tee” cross-section has been developed.

Compared to the systems in use before 1964, modern systems have a higher slenderness ratio and need less cast in-situ topping [e.g. Libby (1984)]. These observations can be explained by the use of high performance concrete, prestressing and modern production technologies in the precast plant. The precast concrete element is produced with a higher precision and can withstand higher stresses allowing a higher slenderness during construction. Today the slenderness is usually limited by deformation criteria during production (storage), construction (assembling on site) and under service loads.

Typical span-widths for double-tee elements used in industrial buildings are from 10 m to 25 m, but Elliott (2002) showed an example with a span-width of 39.00 m for a conference centre. Usually the width of the element is not greater than 3.00 m (limited for easy transportation), and most elements have a width of 2.50 m to 3.00 m. Therefore, fewer elements have to be assembled on site compared to hollow-core elements.

The slenderness ratio (span-width over height (including topping): L/h) of a double-tee element depends largely on its width and its service load, but in general it is in the range of 20 - 28 in office buildings (Chen, 1999) while a ratio of 15 - 25 is found in an industrial environment.

1.3.3 Production of double-tee elements

The production of prestressed double-tee elements is carried out in a span-bed. Usually long span-beds (often ≈ 100 m) are used which enable the economic production of several elements in one cast. The mould consists of three major elements: the core element, the two outer elements and the end bearings against which the prestressed strands will be anchored during production. Figure [1.4] shows a cross-section of a

span-bed mould.

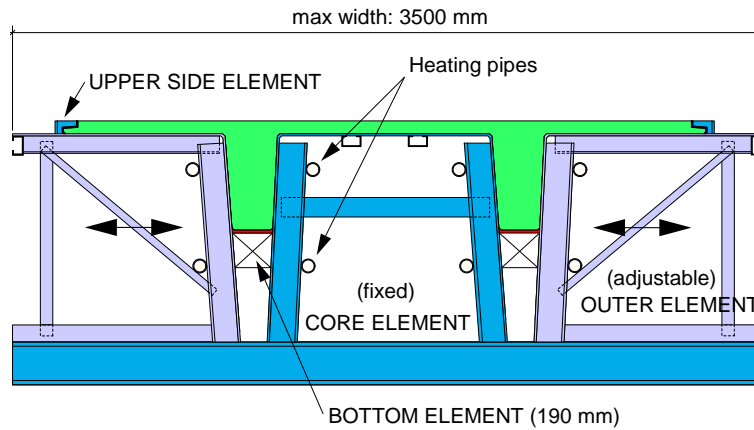


Figure 1.4: Cross-section of mould for double-tee elements

The core element is fixed. After the height of the webs is adjusted by moving the bottom element (usually 190 mm wide), the outer elements are then fixed to the system and the two upper side formworks are positioned to define the width of the slab.

The web has a side gradient of $1/20$. Thus demoulding of the element is possible without moving the outer formwork. Detensioning the strands and striking the upper side element of the formwork are all that is necessary for each cast.

The main steps of the production are: mould preparation, placing of web reinforcement, pulling through the strands, placing of slab reinforcement, prestressing the strands, casting and compacting of concrete, curing, detensioning of strands, striking upper side formwork, demoulding element, cutting ends of strands and covering them with concrete, storage until transportation to construction site.

Usually, the most economical frequency of production is one cast per day (per mould) for double-tee elements: demoulding takes place about 18 hours after casting. This has an important influence on the concrete mixture, which needs to attain a high early strength with an acceptable workability of the concrete during casting (Elliott, 2002).

1.3.4 Design of double-tee elements

For this project, all units are in SI. The Standards used for structural design are:

EC 1 (2002): EN 1991-1-1:2002, Eurocode 1: Action on structures. General actions. Densities, selfweight, imposed loads for buildings.

EC 2 (2004): EN 1992-1-1:2004, Eurocode 2: Design of concrete structures; Part 1: General rules and rules for buildings. Its predecessor, EC 2 (1991), was used for the design of the structure used for the field test described in Chapter 4, which was built in the year 2000.

In the Eurocodes two different levels of prestressing are defined: fully prestressed and partially prestressed. In a “fully prestressed” structure the tension zones of all cross-sections have to be in compression under service loads and tension is only allowed at the top end of the cross section under selfweight, while for “partial prestressing” cracks of a defined width are allowed at the serviceability limit state. Inside a building where normal conditions (humidity and temperature) are guaranteed both types of prestressing are allowed.

The design of double-tee elements, which are used inside buildings, is normally carried out with the aim of creating a partially prestressed structure, thus reducing the required prestressing force and reinforcement.

According to the design standards, the design process is divided into two steps:

1. Proof of stability at the ultimate limit state (ULS).
2. Proof of fitness for use (deformations and cracks) at the serviceability limit state (SLS).

At ULS the necessary reinforcement including the number of prestressing strands is determined for the maximum loading including safety factors and the prestressing is limited to an allowable maximum. At SLS the desired prestressing force is determined to secure serviceability with respect to deformations (under full load as well as during assembling, but without safety factors) and the minimum reinforcement is determined to fulfil the desired crack width.

“Special” load cases have to be checked for precast elements in addition to the “common” load cases. These special cases are “demoulding” (at a young age with lower compressive strength) and “assembling”: the static system of the precast element is a simply supported beam which has to bear the load of casting the topping.

Modern production methods and building materials have enabled the production of highly slender and light double-tee elements. Today many dimensions of a double-tee element are governed by non-structural design criteria: e.g. the width of the web is governed by the minimum width to fulfil the fire resistance criteria, the side gradient of the web is determined to simplify the production processes and the thickness of the transverse slab (precast slab plus cast in-situ topping) has to fulfil the requirements for allowing vehicular traffic.

1.4 Material Science: concrete

Here, it is not intended to give a full introduction to the building materials used for the production of precast concrete structures (a comprehensive overview of concrete can be found in Neville (1995)), but some properties of particular interest will be discussed briefly.

1.4.1 Time dependency of properties

Concrete changes its properties from the moment of casting over its whole lifetime. To define the strength of concrete as the strength achieved after 28 days is a useful, but arbitrary, convention. The strength continues to increase over years. But even though the compressive strength reached after 28 days can increase up to 50% over four years depending on the ambient environment (Persson, 1999), changes in Young’s modulus are negligible after a few days, as this mainly depends on the aggregates which do not change their strength or stiffness at all. However, the change of compressive strength is of little interest to this work which focuses on the serviceability limit state well below

the maximum compression.

Therefore, the time-dependent properties of interest are critical alterations like shrinkage and creep. These effects begin after setting of concrete and loading respectively and carry on over years.

1.4.1.1 Shrinkage

Shrinkage is the result of the drying process of concrete. Concrete contracts in this process. If contraction is not possible due to constraints a tensile stress is imposed on the structure, which might lead to cracks, if the tensile strength is exceeded.

EC 2 (1991), EC 2 (2004) and Kordina (1992) give estimates for shrinkage based on proposals made by CEB-FIP (1990). These estimates are based on the dependency of the magnitude of shrinkage on the compressive strength, cement type and local conditions, where the humidity is the main factor of interest. However, this is a simplification due to the lack of knowledge of concrete mixture during the design process. A formula to estimate maximum shrinkage after 70 years is given. A second set of formulae allows estimates at any desired time. Estimates obtained with these formulae have a deviation of $\pm 35\%$ from observed values.

Gardner (2004) compared several predictions of drying shrinkage (and creep). He compared the methods used in national and international standards: American Concrete Institute (ACI 209-82) and the 1990 Comité euro-international du Béton (MC1990-99) and two proposals from latest research called B3 and GL2000. He determined the accuracy of the predictions on the basis of an international database (RILEM¹) and concluded that the prediction with the method MC1990-99 (which is used in CEB-FIP (1990)) usually underestimates shrinkage, while the model GL2000 gives the most accurate results (although still showing deviations of about 20%).

Bischoff (2001) studied the influence of shrinkage on tension stiffening and cracking of reinforced concrete. His results showed an apparent effect of shrinkage on tension stiffening: shrinkage seemed to reduce tension stiffening. However, he showed that if

¹Réunion Internationale des Laboratoires et Experts des Matériaux, Systèmes de Constructions et Ouvrages

the additional strain from shrinkage is taken into account for the calculation of overall strain the results become identical with those obtained from similar strains without shrinkage. The observed effect was only a shift of strains and if the strain due to shrinkage was added to the strains due to load the tension stiffening was as expected.

1.4.1.2 Creep

Creep is defined as an increase of deformation under constant loading over time.

It can therefore be modelled as either a decrease in stiffness, in particular a decrease in Young's modulus, or as an additional strain leading to further deformations.

Trost and Wolff (1970) suggested an easy formula to model the creep effects, that found its way into several standards:

$$E(t) = \frac{E_c}{1 + \chi\varphi(t, t_p)} \quad (1.1)$$

where $E(t)$ is Young's modulus as function of time t and t_p (which marks beginning of loading), E_c is Young's modulus as chosen for the design process and χ is an ageing coefficient. The factor $\varphi(t, t_p)$ is the creep coefficient. Sapountzakis and Katsikadelis (2003) used this formula for Young's modulus in connection with the formula given in EC 2 (1991) and EC 2 (2004) for the creep coefficient to model creep effects. The results obtained by this formula matched their test results with good approximation.

In EC 2 (1991) a formula is given to estimate maximum creep after 70 years. The values in this formula are chosen in such a way that a creep deformation (under constant loading) over another 70 years would not exceed 5% of the creep deformation after the first 70 years. A second set of formulae allows estimates at any desired time. Estimates obtained with these formulae have a deviation of $\pm 20\%$ ¹ from observed values.

Sapountzakis and Katsikadelis (2003) studied the influence of creep and shrinkage in the dynamic analysis of slab-beam structures. They introduced the effects of creep and shrinkage as normal forces in the slab and the beam. From their results, they concluded

¹Estimates of shrinkage are more uncertain than estimates of creep, because the effects of shrinkage depend much more on the concrete mixture and water/cement-ratio than the effects of creep do (Kordina, 1992).

that effects of creep and shrinkage cannot be neglected in the analysis. Furthermore, the eigen-frequencies decreased with time due to the fact that creep predominates over shrinkage.

1.4.1.3 Creep and shrinkage of high-performance concrete

Li and Yao (2001) studied creep and drying shrinkage of different high-performance concrete mixtures. Three different binders were investigated: Portland cement (mixture A), GGBS¹ (mixture B) and a combination of GGBS and SF² (mixture C).

A comparison of their results for mixture A³ with the results obtained for this mixture by formulae in EC 2 (2004) shows that the levels of creep and shrinkage are consistently predicted to be about 30% higher than they actually are, which is in the expected range of deviations.

1.4.2 Cracks

In a reinforced, or partially prestressed, concrete construction, cracks are inevitable. Cracks themselves, however, are not a problem for the structure. Only if moisture can get into the structure is the reinforcement at risk of corrosion. To avoid serious damage from rusting reinforcement, it is necessary to design the reinforcement so that cracks are small. In EC 2 (2004) a maximum crack width of 0.20 mm is allowed under service loading for elements located inside buildings with a constant relatively dry environment.

These requirements can be met by limiting the maximum stress in reinforcement at the SLS. The allowable maximum stress depends on the diameter of reinforcement, because the crack width tends to be proportional to the diameter of reinforcement, whilst the crack distance tends to be inversely proportional (EC 2, 1991).

¹Ultrafine ground granulated blast-furnace slag

²Silica fume

³Mixture A is similar to the mixture used for precasting the double-tee elements of the structure used in the field test

1.4.3 Tension stiffening

CEB-FIP (1990) gives a good description of tension stiffening:

“In a cracked cross-section all tensile forces are balanced by the steel only. However, between adjacent cracks, tensile forces are transmitted from the steel to the surrounding concrete by bond forces. The contribution of the concrete may be considered to increase the stiffness of the tensile reinforcement.”

This additional stiffness can be taken into account at the serviceability limit state. Doing so will increase the stiffness and thus reduce deformations to more realistic values. Tension stiffening should only be included in the analysis if a smeared-crack approach is used. If the cracks in a beam are modelled discretely and the area between two cracks is taken into account with its full stiffness, tension stiffening is inherent to the model. However, most programmes use a smeared-crack approach as this reduces the computational effort significantly. All programmes used in this study use that approach.

Several models are proposed in the literature to simulate the tension stiffening effect: see Figure [1.5] for some common approaches. Lately, Torres et al. (2004) suggested simulating the first crack by a sudden drop of tension at cracking strain. From that point, the tension should decrease linearly with increasing strains. They showed experimentally that a total loss of tension stiffening can be expected at a strain of 15 times the cracking strain. Consequently, they defined 15 times the cracking strain as the maximum strain for tension stiffening effects in their model. This seems to be a simple approach and it represents the phenomenon well, but for a computer-based simulation this approach leads to instability, as a change of tension for a fixed strain does not give a unique solution.

Other approaches like those provided by Scott (1983) or Busjaeger and Quast (1990) use a bi-linear stress-strain relation, which gives less accurate results for strains slightly larger than cracking strain, but are easier to compute and lead to stable results in FE-

analyses for all strains. For strains smaller than the cracking strain, the stress increases with increasing strains. Beyond the tensile strength, the stress decreases from that maximum to zero with increasing strains.

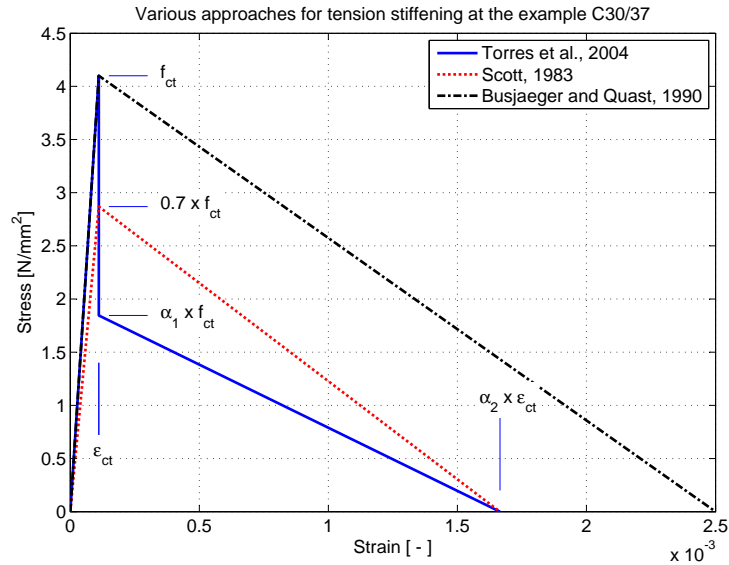


Figure 1.5: Various approaches of tension stiffening

The software package SOFiSTiK which was used for the finite element simulation takes tension stiffening into account using the approach presented in Heft 400¹ of the German Concrete Society (DAfStb) [developed by Schießl, similar to Busjaeger and Quast (1990)]: a bi-linear stress-strain relation.

1.5 Vibration behaviour of concrete structures

The vibration behaviour of concrete floors and structures has been of interest for a long time. Already in 1965 King and Rea had published a paper on the vibration behaviour of slender prestressed concrete beams (King and Rea, 1965) and in 1975 Murray published a paper entitled “Design to prevent floor vibrations” (Murray, 1975).

In 1986, however, the ASCE’s Ad Hoc Committee on Serviceability Research stated that “as standards evolve toward probability-based limit states design methods, serviceability issues are expected to become an increasingly important design consideration.”

¹Edited by Bertram and Bunke (1994).

And

“... current serviceability guidelines are not useful in many cases of new construction. The absence of meaningful criteria may be interpreted by some to mean that serviceability is not important ... [but] with the continuing trend towards high-strength, flexible structures, efficient structural systems and limit state design, this casual attitude will likely lead to costly problems in many buildings. ... Additional research must be undertaken in numerous areas in order to develop or complete the data base needed to prepare rational and practical serviceability guidelines.” (ASCE, 1986)

Since that time, the development of high performance building materials and the optimisation of production methods of precast elements have led to more slender systems, which are more vulnerable to vibration problems.

In 1996 Beards was still concerned about the lack of vibration analyses carried out in the design process:

“It is essential to carry out a vibration analysis of any proposed structure. [...] There have been many cases of systems failing or not meeting performance targets because of resonance, fatigue or excessive vibration of one component or another. Because of the very serious effects that unwanted vibrations have on dynamic systems, it is essential that vibration analysis be carried out as an inherent part of their design; when necessary modifications can most easily be made to eliminate vibration or at least to reduce it as much as possible.

It is usually much easier to analyse and modify at the design stage than it is to modify a structure with undesirable vibration characteristics after it has been built.” (Beards, 1996)

At the same time BS 6399-1 (1996) stated:

“...static load design is not sufficient where dynamic loading occurs in buildings and structures that are susceptible to dynamic excitation. In such

cases, the design should take account of the load-structure interaction and natural frequency, mass, damping and mode shape of the structure.”

However, no detailed guidance was given as to how this analysis should be carried out. Thus several associations developed their own guidelines to check vibration serviceability¹ [e.g. AISC D811 (1997), SCI 076 (1989) for steel-concrete composite structures and Concrete Society TR43 (2005) for post-tensioned concrete structures] and in only one national standard is guidance given: NBC (1995). Caverson et al. (1994) compared several vibration guidelines particularly with regard to their applicability to concrete floors. They found that guidelines written for other building methods of floors can be adopted but the whole matter is not straightforward. Furthermore, they found in several field tests that modern structures are close to the acceptability limits of accelerations and a further increase in slenderness might result in the “vibration [serviceability] becoming the governing design criterion”.

Pavic and Reynolds (2002a, 2002b) reviewed the current knowledge of the vibration serviceability of long-span concrete building floors. They focussed on cast in-situ post-tensioned concrete floors under dynamic loading from walking. They gave a detailed summary of the structural systems possible, the likely excitations and the research carried out to date on the subject. In this review they stated that the behaviour of a precast concrete structure will be significantly different from the behaviour of a cast in-situ concrete structure due to the different ways in which columns are connected to beams and beams to slab elements. In a cast in-situ structure these joints are usually all monolithic but in a precast structure they are more difficult to describe: from pin-jointed to fully restrained. Thus the procedures for modelling a cast in-situ post-tensioned concrete structure cannot be directly adapted to model a precast structure.

This project investigates the dynamic response of a precast and partially prestressed composite floor system to loading from fork-lift trucks. Of particular interest, therefore, are publications dealing with the dynamic behaviour of prestressed concrete structures:

¹Most guidelines concern vibrations caused by walking.

several researchers have worked on the vibration of (prestressed) concrete beams to discover the influence of composite action or cracks on natural frequencies and their damping behaviour. Their findings are summarised in the following sections.

1.5.1 Vibration transmission path: the structure

According to ISO 10137 (2007) a reliable assessment of the vibration behaviour of a system needs the identification of some key factors. One of them is the vibration transmission path, which is characterised by the mass, stiffness and damping of the floor structure, which define its natural frequency. The following sections summarise publications on the structure's dynamic response.

1.5.1.1 Natural frequency

Partial prestressing means that cracks of a certain width are permitted under service loads at the SLS. The cracks influence the stiffness and thus the dynamic properties of the structure. The natural frequencies decrease over the lifetime of the structure due to the formation of cracks which result from the reduction of prestressing force due to relaxation, creep and shrinkage.

Different approaches have been proposed to model the effects of cracks on a beam's dynamic behaviour. One is the "open-crack model" in which the stiffness is locally reduced if the maximum tensile stress of concrete is exceeded. For example, Neild et al. (2001) presented an analytical model for cracked beams. They modelled the beam as a set of discrete masses connected with springs representing the stiffness. The stiffness is varied depending on crack distribution and size.

Hamed and Frostig (2004) tested and modelled vibrations of prestressed and cracked beams. They produced different stages of crack distribution due to static external loads and measured the natural frequencies of the cracked beams. They were able to show a significant drop in the natural frequency of up to 50% for a "fully" cracked beam in comparison with the uncracked beam. They used an open-crack model to calculate the eigen-frequencies, which matched the experimental data well.

The other model used frequently is a “breathing-crack model”. Several approaches for this model were developed [e.g. Abraham and Brandon (1995), Cheng et al. (1999)]. In general these models assume that the cracks close if the load that caused the crack to form in the first place is taken away. This leads to a recovery of the stiffness under loads smaller than those which cause cracks to form. Furthermore the cracks can open and close in one cycle of a vibration, thus changing the stiffness. Law and Zhu (2004) stated that in an analytical investigation with “... reinforced concrete, this mechanism would be very complicated [to implement]” and Neild et al. (2002) noted that these models with a “... bi-linear assumption [of the crack state] proved inaccurate... [and] in reinforced concrete the problem becomes more complex [as]... loose aggregate may prevent the crack from closing”.

1.5.1.2 Damping

The damping governs the amplitude of the response, if an excitation is close to the natural frequency of the system. Damping is the dissipation of energy by the whole system during vibrations. Therefore, it is useful to focus rather on the damping properties of structures built with reinforced or prestressed concrete as one composite system than on the concrete as the building material.

Bachmann and Dieterle (1981) worked on the damping behaviour of cracked and uncracked beams. They suggested a model which included viscous damping for uncracked beams and additionally friction damping for cracked beams. They showed that the overall damping after cracking is dominated by friction damping for low stresses and a long cracked zone. At higher stresses¹ friction damping is almost completely lost and the damping is entirely viscous. Neild et al. (2002) investigated the non-linear behaviour of cracked concrete beams under various levels of loading. For 100% of the failure load they identified a different behaviour than for lower levels of loading which they explained as resulting from a breakdown of frictional effects, thus setting the limit of this effect higher than Bachmann and Dieterle.

¹They set a limit of $\sigma_c < 0.5f_{cm}$

1.5 Vibration behaviour of concrete structures

However, the proposal from Bachmann and Dieterle is qualitatively in good compliance with the results shown in Table 1.1: after increasing from uncracked to cracked conditions, damping decreases for higher stresses.

Bachmann (1995) gave a survey of the range of damping of concrete structures, see Table 1.1: the damping properties of concrete structures depend mostly on the crack development and the level of utilisation (stress intensity) and non-structural members can contribute significantly to the overall damping [e.g. Falati (1999)].

Viscous damping ratio ζ

Construction type	min.	mean	max.	Description
Bare structure:				
Reinforced	0.007	–	0.010	uncracked, low stress intensity
Reinforced	0.010	–	0.040	cracked, medium stress intensity
Reinforced	0.005	–	0.008	cracked, high stress intensity
Prestressed	0.004	–	0.007	uncracked
Partially prestressed	0.008	–	0.012	slightly cracked
for comparison:				
Steel	0.001	–	0.002	
Structure including non-structural elements:				
Reinforced	0.014	0.025	0.035	sport floors
Prestressed	0.010	0.020	0.030	sport floors

Table 1.1: Viscous damping ratio ζ of concrete structures, Bachmann (1995)

Caneiro et al. (2006) investigated the damping behaviour of concrete beams using a pseudo-dynamic method. They found the equivalent viscous damping of the system [as defined by Constantine (1994)] to be between 5.5% for low reinforced beams of low concrete strength and 2.5% for high reinforced beams of high concrete strength. These values are higher than the data presented by Bachmann (1995) if they are compared with a medium stress intensity.

Others developed empirical functions to formulate the damping properties dependent on the crack state [e.g. Chowdhury et al. (2000)]. However, these approaches lack

a mechanical derivation and their quality depends on the number of tests they are based on. Furthermore, there are doubts whether generalisations for other geometries than those used to formulate the functions are feasible.

Another development does not focus on the amount of reinforcement but on the dynamics. Jeary (1986) developed a model of damping that is vibration-amplitude dependent: for lower amplitudes the damping is constant but it increases to a maximum for high amplitudes. This finding was supported by field tests [Li et al. (2000, 2003)]. Additionally, he found a time-dependent reduction of damping for higher stresses due to smoothing of the rubbing surfaces which reduces frictional effects. His amplitude-dependent damping model gives similar values for low amplitudes to those given by Bachmann (1995) for a medium stress intensity: $\zeta \approx 1.0\%$.

However, Jeary (1996) stated that

[...] in the case of concrete even the foregoing mechanistic description [of damping mechanisms] is too simplistic.

When he carried out a microscopic evaluation of concrete samples taken from a high-rise building before and after dynamic loading from a typhoon, he found that the concrete changed its crystallographic structure, which he explained by reference to the dynamic stress levels evoked during the typhoon (Jeary, 1996).

The models of damping offered by Jeary and Bachmann disagree for increasing amplitudes and stresses respectively. While Jeary's model predicts an increase in damping for higher amplitudes, Bachmann and Dieterle's model predicts a reduction in damping for higher levels of loading.

It is not possible to identify either of these models as the correct one, but as the levels of vibration investigated in this study can be classified as low amplitude, the contradiction between the models for higher amplitudes is not of importance.

In this context Chen (1999) presented an interesting study of the vibrations of double-tee elements used in office buildings. The typical excitation he considered is walking

(heel drop). The study is based on linear FE-simulations with a simplified geometry of the structure.

Parameter studies were undertaken for the span width and thus the geometry of the web. The change of the response due to variations in the damping ratio, in the weight of materials used, in cracks at double-tee element joints, in the thickness of the topping and in the Young's modulus was analysed.

As an acceptability criterion the maximum peak acceleration as a function of the natural frequency was used, as defined by Allen. Another criterion used was the required damping as proposed by Murray¹.

He observed that to satisfy the defined acceptability criteria it was necessary to assume a damping ratio of 3%, which is about equal to and partly beyond the upper limit found by Bachmann for damping, and a crack at the joint between two double-tee elements which prevented carriage of moment over the joint reduces the natural frequency slightly and reduces the maximum acceleration at mid-span.

From these observations he concluded that

- virtually all composite precast concrete floors met the acceptability criteria, if the damping ratio was 3.0 - 3.5%,
- damping was the main factor in determining the response and additional damping can be obtained from non-structural members like suspended ceilings or furniture which greatly improve the floor vibration acceptability (this agrees well with Falati (1999)),
- the influence of the density of the material, cracks at joints and variation in Young's modulus is not significant.

The focus of this project is on industrial buildings and storage houses where only a few non-structural members are found. Therefore, the contribution of these elements cannot be taken into account for damping. From Chen (1999) it seems that vibration problems may occur for double-tee elements in an industrial environment: elements

¹Both criteria are based on unpublished correspondence.

designed with high slenderness, little non-structural damping and dynamic loading from fork-lift truck traffic.

1.5.1.3 Dynamic Young's modulus

In vibration tests an increase in stiffness is often observed. This is interpreted as an increase in Young's modulus for short time loading, called Dynamic Young's modulus. Neville (1995) summarised different results of empirical evaluations of the dynamic Young's modulus. The easiest formula, proposed by Lydon and Balendran (1986), gives a direct relation between the static and the dynamic Young's modulus: $E_{c,dyn} = \frac{1}{0.83} E_c$. Others considered the influence of the density of the concrete on the dynamic Young's modulus.

In opposition to these proposals Bachmann (1995) presented a function¹ where the change of the dynamic Young's modulus depend on the velocity of vibration:

$$\frac{E_{c,dyn}}{E_{c,stat}} = \left(\frac{\dot{\epsilon}}{\dot{\epsilon}_0}\right)^{0.025} \quad \text{if } \dot{\epsilon} \geq 3.0 \times 10^{-5}/\text{s}$$

with $\dot{\epsilon}_0 = 3.0 \times 10^{-5}/\text{s}$. Similar functions were proposed for increase in compression strength and ultimate strain.

Without further investigation, it seems reasonable to consider the dependency of Young's modulus on the velocity of the vibrations because for a "slow" vibration the dynamic Young's modulus is reduced to the static one.

However, the dynamic Young's modulus is only used to adjust numerical simulations to experimental data and it has no mechanical background.

1.5.2 Vibration source: dynamic excitations

For a reliable prediction of the vibration response of a structure the dynamic loading as the vibration source has to be identified (ISO 10137, 2007).

Two major areas of research interest can be identified. One form of excitation

¹From CEB (1988)

investigated arises from human activity in buildings and on footbridges. The other form of excitation arises from traffic on bridges and in buildings.

Human occupants In most practical cases people are the receiver of (floor) vibrations. However, it became apparent that often the receiver is the source of vibration as well. Research into walking or jumping on the part of single individuals [e.g. Ellis and Ji (1997)] and crowd loading, e.g. of cantilever grandstands [e.g. Sachse et al. (2004), Reynolds and Pavic (2006)] has shown the effects of people as both sources and receiver of vibrations.

Sachse et al. (2003) gave an overview of how human occupants of a structure can excite it and how they influence the response and Zivanovic et al. (2005) reviewed literature on the vibration serviceability of footbridges under human-induced vibration.

However, human occupants and fork-lift trucks, which are the scope of this study, have little in common and the former are therefore not further reviewed.

Vehicles Dynamic vehicular models are mainly of interest for the analysis of bridges [e.g. Green and Cebon (1994), Kwark et al. (2004)] and the analysis of roadsurfaces [e.g. Hardy and Cebon (1993)]. Only a few publications are concerned with vehicular traffic inside buildings (Pan et al., 2001), and only one publication is known where a fork-lift truck is considered as a dynamic load (Eriksson, 1994).

The excitation from vehicles and the structure's response are described in the following section.

1.5.2.1 Response of concrete structures to dynamic vehicular excitation

This section summarises investigations into the response of concrete structures to dynamic loading: starting from linear-elastic modelling of the structure subjected to defined forces and the more complex model of dynamic interaction, non-linear studies which take the effects of cracks into account are then presented. The effects of surface roughness and velocity for the definition of an impact factor are considered in these studies.

Lin (2006) presented an analytical solution for the “response of a bridge to a moving vehicle load” for a linear elastic bridge of constant stiffness. He investigated the total deflection of the bridge which can be calculated as the sum of the static deflection of a stationary vehicle load and the deflection due to the dynamic part of the load model. He concluded that the response is governed by the surface roughness of the bridge and the natural frequencies of the vehicle. Furthermore the deviation of midspan deflection due to the dynamic load “is proportional to the square root of the pavement roughness coefficient¹ for a specified vehicle speed.”

His findings are similar to those presented by Green and Cebon (1994, 1997) who investigated the response of a bridge to a two-axle vehicle with four degrees of freedom by modal superposition. They showed the importance of the modelling of the excitation as (pre-defined) dynamic forces or even as an interactive dynamic system. The response changes significantly compared to that caused by a constant force. In terms of the peak accelerations, the interactive model gives values of only about half of the accelerations due to the pre-defined dynamic forces.

Other investigations modelling the structure as a linear elastic material are presented by Senthilvasan et al. (2002) and Kwark et al. (2004), who showed the influence of the velocity of a load travelling over a bridge on the response: both below, and well above, a critical speed, the influence of speed on vibrations was minor, but if the critical speed was reached the amplitude increased significantly.

Fryba (1999) presented the analytical solution of vibrations under moving loads for various structural systems. He focussed on linear elastic relations or linear elastic - perfect plastic relations. Therefore, his approaches do not cover the response of cracked concrete structures but could be used as a starting point for future analytical studies.

Law and Zhu (2004) stated that, “...despite the ever increasing number of research publications on the dynamic response of structures with moving loads, there is few

¹A scaling factor that increases by a factor of 4 from “good” (1) via “ordinary” (4) to “damaged” (16)

publication on the dynamic response of beams with inherent cracks under the action of moving loads.” They gave a summary of publications on cracked concrete structures subject to moving loads. They focussed on the influence of cracks (“damage”) on the natural frequencies to obtain a tool for the assessment of bridges.

They used two different models for cracks: the open-crack model and a breathing-crack model. They modelled the load either as a moving mass or as a four-degree-of-freedom system to include suspension and flexibility of tyres. Additionally, they considered the effects of moving speed and road surface roughness.

They carried out simulations and experiments to validate their models.

First, they measured free vibrations of the undamaged beam and then of the beam with small or large damage. They observed a significant drop in natural frequencies and an increase in damping from the undamaged to the damaged case. The change in damping was negligible from small to large damage. These findings agree well with Hamed and Frostig (2004) in terms of the natural frequencies and Bachmann (1995) in terms of the damping effects.

Then they tested different types and ratios of dynamic loading: moving mass and moving oscillator. The maximum ratio for moving mass to weight of the system was 0.2 (which is similar to typical ratios of fork-lift trucks to double-tee elements). They investigated numerically the effects of loading for a four-degree-of-freedom system. They concluded that,

- both models for cracks were suitable for the investigation of effects on vibrations due to cracks,
- the roughness of the surface had little impact for the definition of a dynamic impact factor (compared to local irregularities).

Their conclusion that the roughness has only little impact corresponds with observations from Major (1980), who gave increase factors for dynamic loading due to the state of road surface, because they varied the roughness only slightly. Liu et al. (2002) presented similar results in a study which was concerned with the dynamic impact of

moving loads.

Characteristic of surface	Increase factor
Roads in good conditions	5 - 10%
Sudden braking	10 - 20%
Bad condition + sudden braking	25 - 30%
Extreme effect	40 - 50%
Bump-like	80%

Table 1.2: Dynamic effects observed by Major (1980)

The definition of an impact factor (or dynamic load factor, according to the Eurocodes) has to consider the condition of the surface driven on and the effects of velocity and resonance.

For this study it can be assumed that the surface quality of a floor in an industrial building is “in good condition”, so that the main dynamic effects would be expected from “sudden braking”. However, this is a large dynamic force of a short duration and it is assumed that continuous excitation from driving gives a bigger dynamic response.

Conclusions drawn from vehicle-excited vibrations The best predictions of the response of a structure to excitations from vehicular traffic are made with an interactive load model. The interactive model considers the deformability and damping not only of the suspension system but of the wheels as well. The weight of the underbody and its movement independent of the body are taken into account: see sketch in Figure [1.6].

In the literature one can find various interactive models of diverse levels of complexity. Simple models reduce a vehicle to a one-degree-of-freedom system [e.g. Green and Cebon (1997)], while more complex models not only consider the number of axles but also the influence of the underbody on the overall dynamics [e.g. Pan et al. (2001)]. These models allow a good approximation of the real case, but for a numerical simulation of how it will be carried out at the design stage of floor systems, they are difficult to implement and computationally expensive. For this reason a model of defined forces will be developed in this study, allowing an easy implementation of and a comparatively

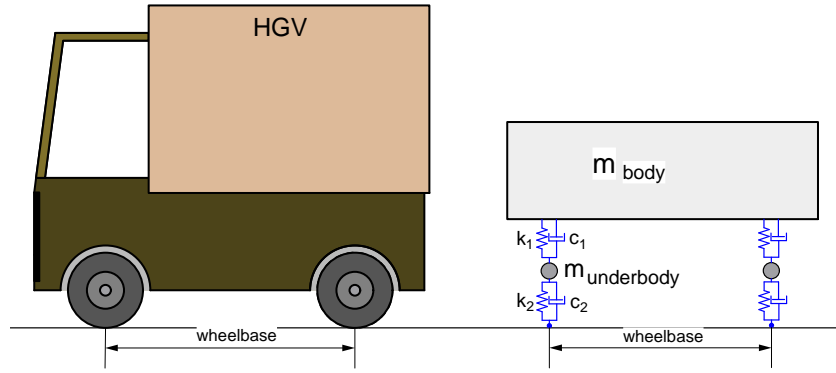


Figure 1.6: 4dof-model of a heavy goods vehicle

fast solution to the finite-element simulation.

1.5.3 Two case studies on floor vibrations caused by vehicular traffic

1.5.3.1 Fork-lift truck traffic on a suspended floor

In his doctoral thesis on dynamic forces and response prediction of the vibration of low-frequency floors, Eriksson (1994) presented a concise chapter on vehicular traffic as a source of vibration. While the thesis is mainly concerned with walking as a source of excitation the fifth chapter summarises the investigation into the response to excitation from three vehicles: an electric truck, a pallet truck and a fork-lift truck.

He stated that “fork-lifts cause significant dynamic forces which have resulted in clearly perceptible floor vibrations.”

The floor system he investigated was a typical composite floor. The main beams were steel girders cased into a rectangular concrete cross-section and the floor elements were t-beams. Main beams and floor beams were cast together with in-situ cast concrete to form a continuous floor. The experimentally obtained natural frequency was $f_n = 7.83$ Hz with a damping of $\zeta_n = 1.3\%$.

The vehicles were driven on two defined paths and the accelerations of the floor were measured in specific positions. From these records the spectral densities of the force input of the vehicles were calculated. Eriksson summarised the results of the

analysis as follows:

In the spectrum representing the AT [the fork-lift truck], it can be seen that the acceleration caused by this vehicle is concentrated to the frequency band 6 - 15 Hz. Outside this band there is virtually no response at all. [...] The frequency of the spectral density peak was also seen to drop slightly when the fork-lift was loaded. The conclusion is therefore that this represents a resonance in the vehicle, presumably a rigid-body vibration mode, and that the vehicle imposes relatively high forces on the floor at this frequency.

From the spectral density of the fork-lift truck with and without a payload he calculated input forces which he validated against a single-degree-of-freedom model of forces vibration. He stated that “...the model describes only a single rigid body mode of vibration of the fork-lift truck but serves nevertheless an illustrative purpose.”

The maximum force input was predicted to be 10 kN at 6.7 Hz. However, he concluded from a comparison with measured values that the worst case scenario of surface roughness and a one-degree-of-freedom model may be too simplistic.

The section on the fork-lift truck ends with a reflection on the effects if the resonance frequency of the floor and the excitation frequency of the truck had coincided. The root-mean-square (RMS) acceleration of the floor would have been $> 0.5 \text{ m/s}^2$ and Eriksson concluded that “...pure luck seems to have made this floor serviceable.”

This statement from Eriksson further strengthens the concern as to whether modern slender precast structures will fulfil vibration acceptability criteria in the future and demonstrates the necessity of a more detailed investigation into the dynamics of fork-lift trucks.

1.5.3.2 Vehicular traffic in a building

Pan et al. (2001) investigated the dynamic response of floors of a multistorey building to excitation from heavy goods vehicles (40 ft container trucks). The building has access for vehicles on all four storeys (ground floor and three elevated floors).

The dynamic loading arose from road roughness and was applied with two different methods in the numerical analysis: the first method was the decoupled dynamic nodal loading (DNL) which ignored the interaction with the structure while the second method took the dynamic interaction between the truck and the floor into account (“fully coupled dynamic finite element method for a vehicle-structure system”). The truck was modelled as a three-degree-of-freedom model.

They showed that the accelerations calculated with the decoupled dynamic loads were about twice the magnitude of the accelerations calculated with the coupled (interactive) system. They pointed out that the easier, computationally less expensive decoupled model should yield results of “good engineering precision” if the stiffness of the vehicle is much smaller than the stiffness of the structure.

All vibrations excited by the vehicular traffic were very localised.

1.5.4 Field monitoring of vibrations

Despite the ever increasing effectiveness of numerical simulations, field tests are still a common (and indispensable) method of determining the dynamic properties of structures.

The results are used either to adjust the numerical model [e.g. Pavic and Reynolds (2003), Brownjohn et al.(1989, 2000), Zong et al. (2005)] or to investigate specific types of excitation which are then modelled numerically [e.g. influence of human occupants on the dynamic response: Brownjohn (2001), Rainer et al. (1988)].

As mentioned earlier in this section, Caverson et al. (1994) investigated the guidelines published for the vibration serviceability check applied to concrete structures. They stated that the simplifications undertaken in most guidelines to calculate the eigen-frequencies do not reflect the (complex) real structure and thus falsify the results. To demonstrate this they investigated five floors: it took considerable adjustments to calculate the same eigen-frequencies with an equivalent beam approach (as used in most guidelines) as those natural frequencies measured on site. The definition of boundary conditions in the model proved especially difficult. Furthermore the

two-span characteristics of a floor system influenced the behaviour considerably, which demonstrates the necessity of field tests to prove a model. Ellis and Littler (1988) had the opportunity to test nine similar buildings during construction and stated that “...a large difference between [dynamic] characteristics of two of the buildings shows that it may never be possible to provide exact calculations [...] at the design stage [...]”

Modal testing A frequently applied testing method during field tests is “modal testing” [e.g. Ewins (2000) and He and Fu (2001)]. Modal testing allows the calculation of the response functions and mode shapes from defined excitations (generated by, e.g., a mechanical shaker or instrumented impact hammer) in specified locations and the record of the accelerations of the floor. This method gives a precise picture of the dynamic properties of a system, but it can be time consuming (and expensive) for a big floor system¹.

Pavic et al. (1995) investigated a (precast) multi-storey car park numerically and with a comprehensive modal test. They concluded that the experimental data are needed to adjust a FE-model, but a numerical analysis prior to the field test is recommended to identify the modes of vibration and thus the best locations of accelerometers and excitation.

Another example illustrating the complexity of this method is the study of a high-strength concrete floor by Pavic and Reynolds (2003): the testing programme on a floor of 225 m² supported by four columns comprised 49 locations of excitation.

1.5.5 Acceptability criteria of accelerations

Since the early 1930s the perception of vibrations and the acceptability of floor accelerations have been investigated by many researchers². They agree that the perception of accelerations depends not only on the amplitude of the accelerations and their frequency but also on the occupation of the person being the receiver and possibly the

¹It would have been an appropriate method for recording the dynamic properties of the floor found in the field test, but limited time and financial constraints prevented a modal test.

²H. Reiher and F.J. Meister are widely credited for their fundamental research in the field, e.g. see Allen and Rainer (1976).

1.5 Vibration behaviour of concrete structures

source of vibration as well. Therefore two different types of guidelines have been developed over the years: general guidelines which give allowable maximum accelerations and more specialised guidelines which consider the influence of the frequencies on the perception.

For example, general guidelines are NBC (1995) (where maximum accelerations depending on the occupation are defined, see Table 1.3) and ISO 10137 (2007) which gives maximum accelerations depending on the usage of the building: 0.5%g for offices and 1.5%g for shopping malls.

Occupation	Maximum accelerations			
Aerobics	10.0	% g	≈	1.0 m/s ²
Dining beside dance floor	2.0	% g	≈	0.2 m/s ²
Lying / sitting still	0.5	% g	≈	0.05 m/s ²

Table 1.3: Allowable accelerations for various occupations according to NBC (1995)

The acceptable accelerations for the occupation “dining beside a dance floor” shown in Table 1.3 are (for the relevant frequency range) similar to the values already suggested by Allen and Rainer in 1976 for “quiet human occupancies - residences, offices and schoolrooms” in their (frequency-dependent) guideline “Vibration criteria for long-span floors” (Allen and Rainer, 1976).

Two frequently used standards will be described in more detail: ISO 2631, i.e. part 1 and part 2, which is virtually identical to BS 6472 (1992), and DIN 4150 which is applicable to the evaluation of the measurements of the field test carried out in Germany.

1.5.5.1 DIN 4150

The standard DIN 4150 Teil 2 (1999) is an example of a guideline which takes the frequency dependency of the perception into account. It was one of the earliest guidelines and it has been revised several times over the last 70 years. An “intensity perception value” (KB) is defined that has to be taken into account to calculate the acceptable floor accelerations.

The easiest version of a vibration serviceability is defined in part 2 from 1975¹: depending on the usage of the building, the duration of the vibration (continuous or transient) and the time of the day (daytime or nighttime) different values of a maximum KB are defined. Important values are summarised in Table 1.4. From the natural frequency of the floor and the peak acceleration a_0 a KB is calculated:

$$KB = \frac{0.8f^2}{\sqrt{1 + 0.032f^2}} \cdot \frac{a_0}{4\pi^2} \quad (1.2)$$

which has to be smaller than the tabled maximum value. The relation of the acceptable combinations of RMS-accelerations and natural frequencies for various levels of perception are plotted in Figure [1.7].

For the structures investigated two different occupations are possible, which seem representative of many industrial buildings: one is manual labour like assembling items for production or packing them for shipping. The other one is clerical work in offices adjacent to the storage area. Hence two interpretations of the standard are possible:

1. It is an industrial environment and the vibrations are transient (only local excitation of vibrations by the fork-lift truck).
2. The occupation is clerical work (in adjacent offices) and the vibrations are transient.

Both occupations lead to the same value: $KB = 12.0$ (see Table 1.4). The allowable root-mean-square acceleration of the relevant frequency range (3-8 Hz) can be found in a chart: the acceptable RMS-acceleration is about 0.5 m/s^2 . A plot of the KB values is shown in Figure [1.7] where the ISO base curve is plotted as well.

1.5.5.2 ISO 2631

Similarly in ISO 2631-1 (1997) there is defined a base curve of acceptable RMS-accelerations. Depending on the occupation and on the time and duration of vibration

¹This part has not been superseded by the latest version from 1999.

1.5 Vibration behaviour of concrete structures

Building type	Time	Continuous vibration	Transient vibration
Rural, residential and holiday resort	day	0.20	4.00
	night	0.15	0.15
Small town and mixed residential	day	0.30	8.00
	night	0.20	0.20
Small business and office premises	day	0.40	12.00
	night	0.30	0.30
Industrial	day	0.60	12.00
	night	0.40	0.40

Table 1.4: Acceptable KB values according to DIN 4150 Teil 2

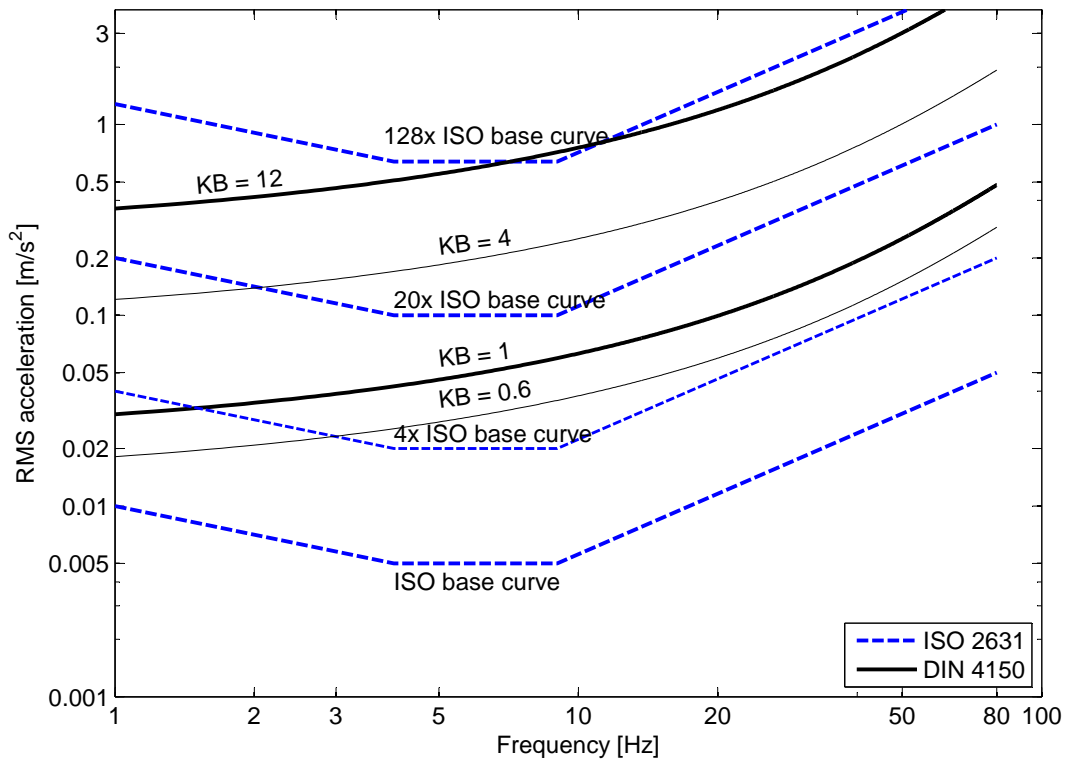


Figure 1.7: Allowable RMS-accelerations according to DIN 4150 and ISO 2631

weighting factors are defined to calculate the allowable accelerations, see Table 1.5. Furthermore, in ISO 2631-2 (2003) methods are defined for the application of weighting factors depending on the frequency of vibration to calculate the allowable magnitude.

1.5 Vibration behaviour of concrete structures

Place	Time	Continuous vibration	Transient vibration
Critical working areas	day or night	1	1
Residential	day	2 - 4	60 - 90
	night	1.4	20
Office	day or night	4	128
Workshop	day or night	8	128

Table 1.5: Weighting factors according to ISO 2631-1 (1997)

Transient vibration in a workshop would lead to a factor of 128, which in turn results in an allowable RMS-acceleration of vertical vibration of $a \approx 0.6 \text{ m/s}^2$ in the frequency range of 3 - 8 Hz. A frequency weighting factor is not applied as it depends on the occupation of the receiver which is, as mentioned before, not of special interest in this study.

1.5.5.3 Eriksson's observation on the calculation of RMS-accelerations

When Eriksson (1994) calculated the RMS-accelerations of the floor caused by fork-lift truck traffic, he stated that due to the vibration lasting for only a few seconds (and so being localised) the calculation of a one minute RMS-acceleration is not a good measure for the severe vibrations caused by a fork-lift truck. He suggested using a shorter time period to calculate the RMS-acceleration.

In this study a shorter time period is chosen to calculate the RMS-acceleration of a floor with respect to the duration of vibration caused by a fork-lift truck passing the point of measurement which is severe for a period of $t \approx 10 \text{ s}$, and this RMS-acceleration will be denoted as $a_{RMS,10}$.

1.5.5.4 Vibration dose value

Another commonly used measure of acceptable accelerations is the vibration dose value (*VDV*) as defined in BS 6841 (1987). It takes the duration (T) of a vibration event

into account:

$$VDV = \left(\int_0^T a^4(t) dt \right)^{0.25} m/s^{1.75} \quad (1.3)$$

According to BS 6841 (1987) the limit of acceptable vibrations is 0.8 - 1.6 in a workshop environment depending on the duration of exposure (24 h to 1 s).

1.6 Fork-lift trucks

1.6.1 Remarks on the general configuration of fork-lift trucks

Counterbalance fork-lift trucks used for indoor goods handling share some construction details across all manufacturers.

The chassis is not suspended with a separate underbody. The axles are directly connected to the chassis and no spring-damper system exists. The suspension and damping of the truck comes from the deformability (and loss of energy when deforming) of the solid rubber tyres. Almost all trucks are fitted with solid rubber tyres; only very few models are fitted with pneumatic tyres.

Virtually all trucks have rear steering and front drive through a differential and automatic gearbox. Battery-powered and most combustion-engine-powered trucks have only two gears: one for driving forward and one for driving backwards.

The distance from the centre of gravity of the truck to the payload is similar to the length of the wheelbase of the truck which leads to a considerable weight at the rear axle (about the same size as the truck's capacity) to keep the truck balanced in all load states.

These characteristics make them very different from conventional vehicles, where the wheelbase is large and any payload is carried close to the centre of gravity of the vehicle. Furthermore, since the fork-lift trucks have no separate suspension system, the damping is low and no underbody has to be modelled. Thus it is difficult to adapt a dynamic model of a heavy goods vehicle for the simulation of a fork-lift truck.

1.6.2 Fork-lift trucks as loading on structures

In the design process of a floor the loading from a fork-lift truck is taken into account with its quasi-static load. This means that the selfweight of the fork-lift truck is multiplied by a factor to achieve the same static deformation when this quasi-static load is applied to the structure as if the dynamic action of the fork-lift truck would had considered.

Hence it is no surprise that very little is known about the dynamic properties of fork-lift trucks for dynamic investigations of structures: for the structural design this factor (so called Dynamic Load Factor: DLF) is the only one of interest.

Most investigations of the dynamic behaviour of fork-lift trucks have focussed on the health assessment of the drivers: extensive research has been carried out to evaluate the “whole body vibrations” of fork-lift truck drivers [e.g. Malchaire et al. (1996), Bovenzi et al. (2002), Lemerle et al. (2002)].

The other area in which research on the dynamic behaviour of fork-lift trucks has been carried out is the design of fork-lift trucks. However, in the case of design loading only extreme situations are considered like driving over joints, swells or through bumps (Beha, 1989). These loads are far too big in comparison to loads excited under normal service conditions, see Table 1.2, where the influence of the surface conditions on dynamic effects on a bridge are compared.

1.7 Research needs and scope of thesis

The need for research in the area of floor vibrations of precast and partially prestressed composite floors under loading from fork-lift trucks can be summarised as follows:

- Precast elements are going to be used even more widely than today, because they deliver economical advantages as well as high quality. The construction times are reduced, thus disturbance to neighbours is reduced and an earlier return of the investment is guaranteed.
- The slenderness of a double-tee element is usually governed by the deformations at the serviceability limit state. Thus it is important to model all loads at this level realistically.
- Prestressing leads to slender systems with low damping, which are vulnerable to vibration serviceability problems.
- The influence of the joint between the precast part and the cast in-situ topping on the overall damping properties of the composite floor has not been investigated to date.
- In the past loading of fork-lift trucks has been considered unable to excite vibrations of floor systems. But today, due to low natural frequencies of the floor system an excitation is possible. Hence the dynamic properties of fork-lift trucks have to be investigated to set up a dynamic load model for a reliable vibration serviceability check.
- Research into the dynamic response of the double-tee element floor system has been over-simplified in the past. Time-dependent effects of concrete (creep and shrinkage) as well as the influence of the crack distribution have to be incorporated in a realistic simulation.

From the research needs listed above the scope and the objectives of this thesis are deduced:

1. To develop a dynamic load model of a driving fork-lift truck. - This will be based on mechanical derivations of the vibration sources. The modal analysis of a three-degree-of-freedom model determines the eigen-frequencies and the amplitudes are determined with a one-degree-of-freedom model. The model is validated against experimental data obtained from testing four fork-lift trucks tested in various configurations. The load model and its derivation are presented in Chapter 2.
2. To develop a finite-element model of a composite (sample) floor system and validate it. - The model will incorporate not only the time-dependent effects and the loading but also the construction process and its influence on the in-service properties of the structure. As part of this work a preliminary investigation of the damping potential was undertaken. The finite-element model will be used to simulate the floor's response to loading from the dynamic fork-lift truck model developed in Chapter 2. The numerical simulations are presented in Chapter 3.
3. To carry out a field test to measure the vibrations excited by fork-lift trucks on a composite floor. The experimental data will be compared with the results of the finite-element simulation to verify the models, both of the fork-lift truck and of the floor system. The field test and the comparison with the finite-element simulation are presented in Chapter 4.

The investigation of these three objectives will enable a realistic reproduction of a precast composite floor system under fork-lift truck traffic in a finite-element program. The simulation of the dynamic response can be used for a vibration serviceability check by adapting the geometry of the double-tee elements (most likely by limiting the slenderness) to fulfil the existing acceptability criteria for floor accelerations.

Chapter 2

Development of a dynamic load model for a fork-lift truck

2.1 Executive summary

This chapter gives an overview of the consideration of loads from fork-lift trucks in the design process and a review of fork-lift truck dynamics in the literature, and explains the development of the dynamic load model of a fork-lift truck. The dynamic load model will be used in finite-element analyses of the vibration response of floor systems to loading from fork-lift trucks and, as such, be a tool for the serviceability check.

The fork-lift truck is analysed as a three-degree-of-freedom system and it is shown that the third mode is unlikely to be relevant for the excitation of low-frequency floors. The model is, therefore, reduced to a two-degree-of-freedom model by ignoring the relative motion between the mast and the body of the truck.

The load model is two-dimensional and based on the two-degree-of-freedom model. The front axle and the rear axle are modelled as springs. The model comprises geometric and dynamic constants and two variables: current (horizontal) velocity and time. The constants are the mass and the mass moment of inertia of the truck, the mast and the payload. The dynamic constants are the natural frequencies of the vibration, the phase angle between the front and the rear axle and the amplitude ratio of the

axles. The dynamic properties are found mathematically as well as experimentally. The mathematical modelling included a three-degree-of-freedom model for a modal analysis to find the eigen-frequencies, a two-degree-of-freedom model to find the reaction forces on the floor and a single-degree-of-freedom model of forced vibration which is used to predict the amplitudes of vibration.

The experimental test programme tested four fork-lift trucks in twelve different configurations. The evaluation of the experiments is shown for one configuration. Each configuration was analysed for its frequency content with respect to the main variables during a test: the current velocity and the driving direction. The analyses were compared with the analysis of the data set without distinction of the main variables. The analysis of the amplitudes was focussed on the influence of the current horizontal velocity. The influence of the driving direction was analysed as well.

It was found that the dynamic behaviour of a fork-lift truck is governed by the natural frequencies of the truck and its current velocity, whereas the driving direction has no significant influence. The relation between driving velocity and the magnitude of vibration is complex but a simple linear envelope function is used to model the effects.

The load model comprises two time-variable forces¹ a fixed distance apart. Each force is the product of a mass matrix and an acceleration vector. The acceleration vector is the product of an amplitude factor and a frequency factor which, in turn, is the sum of two sinusoidal functions with a constant phase angle between front and rear axles:

$$\begin{aligned} \text{Force} &= \text{Mass matrix} \cdot \text{Acceleration function} \\ \begin{bmatrix} F_f(t, v) \\ F_r(t, v) \end{bmatrix} &= \begin{bmatrix} M_{11} & M_{12} \\ M_{21} & M_{22} \end{bmatrix} \cdot \begin{bmatrix} a_f(t, v) \\ a_r(t, v) \end{bmatrix} \\ \\ \text{Acceleration} &= \text{Amplitude} \cdot \text{Periodic function} \\ \begin{bmatrix} a_f(t, v) \\ a_r(t, v) \end{bmatrix} &= (Cv + D) \cdot \begin{bmatrix} \mu \sin(2\pi f_1 t) & + \sin(2\pi f_2 t) \\ \mu \sin(2\pi f_1 t + \pi) & + \sin(2\pi f_2 t) \end{bmatrix} \end{aligned}$$

¹to which the static loads due to gravity have to be added.

The geometric values and natural frequencies depend on the specific type of truck whereas the amplitude function is generally valid for all models in the range of capacity investigated. However, a generalisation of the geometric values enables the serviceability to be checked at the design stage before it is known which specific truck will be used on that site. Data for such generalised models are presented for a range of truck capacity from 1000 kg to 6000 kg.

2.2 Review of the design load of fork-lift trucks on structures: the dynamic load factor

Note: what in the Eurocodes is called either “dynamic load factor” or “dynamic magnification factor” is called “dynamic amplification factor” in some other publications. However, the meaning is the same. In accordance with the standards used for this study the term dynamic load factor (DLF) will be used.

To simplify the design process of floor systems (and of the whole structure), in several national and international design codes the load from fork-lift trucks is considered as a quasi-static load, e.g. the Eurocodes EC 1 (2002) and the German DIN 1055 (1978): the static load (mass multiplied by gravity) of a fork-lift truck is multiplied by a dynamic load factor and the resulting load is applied statically to the structure in the design process.

It is assumed that the loading from a moving (dynamic) load can be modelled by the dead load multiplied by the dynamic load factor, which will cover the effects from dynamic loading, i.e. this method will guarantee that the deformations will be similar in both cases and thus the stress level will be also similar. However, Palamas et al. (1985) stated that the current DLFs

“are generally not based upon well defined mechanical considerations or systematic experiments.”

This statement is still valid today: the current version of the DIN 1055 Teil 3

(2006) still uses the same values as were already defined in the last version from 1978 and Eriksson (1994) stated that

“information on force input from fork-lifts is, however, limited or non-existent, making the floor design process highly uncertain.”

In the DIN and the earlier versions of the Eurocode, the DLF for fork-lift truck traffic has a fixed value of 1.4 (DIN) and 1.6 (EC). The latest version of the Eurocode 1 gives for the first time a differentiated value for the “dynamic magnification factor” according to the wheel material of the fork-lift truck. Furthermore, this version of the Eurocode defines the source of dynamic effects: hoisting of loads. It seems that “driving” was not regarded as a cause of vibration problems. However, there are several indicators that this approach is over-simplifying the real case.

EN 1991-1-1:2002, 6.3.2.3 (4): The dynamic load factor ϕ takes into account the inertial effects caused by acceleration and deceleration of the hoisting load and should be taken as:

$\phi = 1.40$ for pneumatic tyres,

$\phi = 2.00$ for solid tyres.

Palamas et al. (1985) investigated the influence of surface irregularities on the dynamic response of a bridge in order to define a more realistic DLF. The irregularities they investigated are classified into two groups: global and local irregularities. A global irregularity may be either a hog or sag over the whole span which may result from creep and shrinkage due to prestressing forces. Local irregularities comprise pot holes and bumps in the surface of the bridge.

In their analytical and numerical investigation they found the DLF to be just above 1.0 for a perfectly levelled bridge and a moving (constant) load. In the case of a deformed structure they showed that the velocity of the travelling force exercised a strong influence on the magnitude of the response. At a critical velocity the DLF increased by up to 50% compared with that of a perfectly levelled bridge. The DLF

was calculated to be about 1.5 to 1.6 for a globally deformed bridge, while local irregularities led to much higher values: a maximum of 2.0 for a one-span system at a (critical) velocity of 20 km/h.

However, even more interesting for this project is their observation that the dynamic response of a bridge to an oscillating load moving over the bridge is governed by the frequency of the oscillator and the eigen-frequency of the bridge¹, the shape of deformation of the bridge and the velocity of the load.

2.3 Existing dynamic models of fork-lift trucks

The data available in the literature are limited for several reasons: as explained earlier, the loading of fork-lift trucks is considered as a static load on structures, the design of fork-lift trucks is based on the proof against fatigue for the highest loadings and the vibration of the driver's seat is of interest for medical research, but not the load induced by the fork-lift truck on a structure. Furthermore, it is obvious that these studies do not differentiate between the loadings for different velocities as they focus on extreme or long-duration time-averaged situations. One study that investigated briefly the response of a floor system to fork-lift truck traffic is the doctoral thesis by Eriksson (1994) which will be discussed at the end of this section.

Design of fork-lift trucks Beha (1989) investigated the dynamic loading of fork-lift trucks and their motion performance. His aim was to find the main parameters for the dynamic load factor (and their size) for the design of fork-lift trucks and their lifters. Therefore, he investigated which situation under normal service conditions produced the highest accelerations of different parts of the construction. For the fork-lift truck in motion he investigated two different cases: a change of the road surface level (20 mm), which meant one step (up) for both axles, and a single obstacle of 25 mm height, which meant two steps (up and down) for both axles. He concluded that the dynamic response of the fork-lift truck is governed by the spring characteristics of the wheels, but not

¹As to be expected, due to resonance effects.

2.3 Existing dynamic models of fork-lift trucks

by the working load of the fork-lift truck. For fork-lift trucks ranging from 1500 kg to 6000 kg safe working load, he found no significant difference in the behaviour: the same dynamic load factor could be used for the design of fork-lift trucks in this range¹.

Medical research (1) Although Bovenzi et al. (2006) investigated a large group of professional drivers and measured a significant number of fork-lift trucks, they do not show the measurement records, but only present the calculated ‘frequency-weighted root-mean-square acceleration magnitude of vibration’ as it is defined in ISO 2631-1 (1997), which is used to determine what dose of vibrations is acceptable without causing health issues for the drivers. Their investigation focussed on the peak and average accelerations and was not concerned with the influence of velocity.

Medical research (2) Lemerle et al. (2002) presented a method for designing suspended cabs for fork-lift trucks. They took the main vibration frequency of the fork-lift truck to be 6 Hz. When driving over an obstacle of 20 mm height, the peak acceleration at the rear axle was found to have a value of about 8 m/s², whereas the peak acceleration at the front axle was about 5 m/s².

Medical research (3) Lewis and Griffin (1998) compared alternative standards for the prediction of whole-body vibrations of the driver on different vehicles. For a fork-lift truck they gave a power spectral density as shown in Figure [2.1]. These data were obtained by measuring the accelerations of the driver’s seat and confirm the natural frequency of the fork-lift truck to be < 10 Hz (actually about 3-5 Hz).

Medical research (4) Malchaire et al. (1996) investigated the “vibration exposure on fork-lift trucks”. They investigated five different trucks with several configurations of tyres to discover which factors influence the magnitude of vibration and how these factors interact. The capacity of the trucks was in the typical range of indoor usage (1500 to 4000 kg).

¹The results of this study accord with this finding: all models had similar dynamic behaviour. However, the range of tested models was small: 1500 kg to 2500 kg.

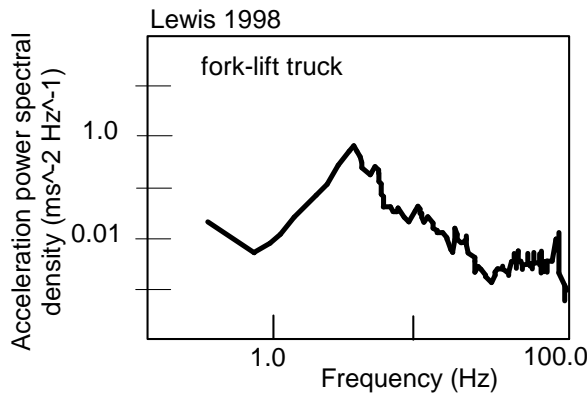


Figure 2.1: Power spectral density of unweighted accelerations on the seat of a fork-lift truck according to Lewis and Griffin (1998)

The maximum weighted acceleration they found for the body of the fork-lift truck was 5.19 m/s^2 . They found that the main factors that affect the magnitude of vibration are the roughness of the track, the driving speed and the quality of the seat (which is not of interest for this study):

	Driving speed [km/h]	Truck body a_{Zw} [m/s ²]
Load		
- empty	12.7	1.98
- loaded	11.0	1.55
Track		
- concrete	12.4	1.26
- paved	11.2	2.27

Table 2.1: Average weighted acceleration in the vertical axis and mean driving speed from Malchaire et al. (1996)

Table 2.1 summarises the effects of the main factors of interest for this study. Whether a payload is carried or not influences the driving speed which results in different accelerations of the fork-lift truck body (reduction in speed results in a reduction in accelerations of 27%). The table also shows that the condition of the track influences the driving speed (12.4 km/h on a smooth concrete track and 11.2 km/h on a rough paved track). However, the roughness has a significant influence: the accelerations on a rough track are 80% higher than on a smooth one.

2.4 Proposed dynamic load model of a fork-lift truck

They found the dominant frequencies to be in the range of 3-6 Hz.

Research on floor vibration Eriksson (1994) investigated methods for predicting dynamic forces (mainly due to human movement) and the response of low-frequency floors. In this context he investigated the dynamic loading of three different vehicles for “indoor goods handling”. The results of this investigation are presented in a concise chapter. One of the vehicles investigated is a fork-lift truck. Eriksson presented an estimated power spectral density plot of the fork-lift truck which has a peak at 6.7 Hz for the unloaded truck and at 6.4 Hz for the loaded truck. He stated that the lower frequency for the loaded truck is explained by its higher mass while the other properties remain constant. In agreement with Malchaire et al., he found that the forces excited from the loaded truck are smaller than from the unloaded truck using the same explanation of a lower driving speed.

To predict the amplitudes of the force input he set up a single-degree-of-freedom model that takes the roughness of the surface into account. While he stated that it seems to be too simplistic it is a useful model to predict the order of magnitude of the vibration.

2.4 Proposed dynamic load model of a fork-lift truck

For the simulation of the dynamic response of the floor system to a fork-lift truck a dynamic (time- and velocity-dependent) load model is necessary to model the loading realistically. The aim is to provide a load model which can be used in numerical (and analytical) verification of the vibration serviceability of a floor system.

2.4.1 Simplifying assumptions

The fork-lift truck is modelled as a rigid body that is resting on springs (which represent the deformability of the wheels) at the front and rear axles. This model is based on the following assumptions:

2.4 Proposed dynamic load model of a fork-lift truck

Symmetry The fork-lift truck and its behaviour are considered symmetrical about the plane containing the vertical and front to rear axles (thus neglecting lateral effects):

- The load distribution is approximately symmetrical, which is correct for the body of the fork-lift truck.
- The payload has to be approximately symmetrical.
- The error due to the mass and the offset of the driver is small. Considering the driver's mass to be ≤ 100 kg and given that the minimum service mass of the fork-lift trucks tested was 2840 kg, the maximum error is $\frac{100}{(2840+100)} \leq 0.034 \approx 3.4\%$. This is small compared to the uncertainties of the mass distribution of the payload and the fork-lift truck, and thus may be neglected. (The driver's mass during the execution of the experiments for this study was ≈ 65 kg giving a maximum error of 2.2%.)

The mass distribution (high load on the rear axle if no payload is carried and a small load if a payload is carried) makes pitching a likely form of movement. The overall length is about twice the length of the wheelbase and about twice the width. Thus rolling will be negligible compared to pitching and the model can be set up two dimensionally as shown in Figure [2.3] and as such comprising the axle forces instead of four individual forces as shown in Figure [2.2].

Stiffness The stiffness of the fork-lift truck is high, so that bending of the body can be neglected. Thus rigid body motion can be assumed. For further discussion of this subject see Beha (1989).

Payload fixed The payload is fixed to the fork. The fork and the mast have a high bending stiffness. Thus fork, mast and payload can be modelled as one rigid system. The assumption of the fixed payload potentially creates a larger error, because in reality the maximum downward acceleration is limited to the acceleration due to gravity otherwise the payload would lift off the fork. However, it is assumed that accelerations of this magnitude do not occur under normal service conditions.

2.4 Proposed dynamic load model of a fork-lift truck

Damping Fork-lift trucks for indoor goods handling do not have an underbody suspension system like heavy goods vehicles or cars. Damping arises from the hysteresis of the tyres when deforming during operation, the mast connections, the payload and the driver. However the damping is low and can be neglected for the load model. The error resulting from this assumption is small¹ as a continuous energy input is considered when the fork-lift truck is in (horizontal) motion and thus a (temporary) steady-state response (vertical) is reached.

Linearity The behaviour of the fork-lift truck is assumed to be linear. This includes modelling the wheels as linear springs. In contrast, Beha (1989) modelled the wheels as non-linear springs, which were characterised by hysteresis loops. However, the effect mainly provided damping², which, as mentioned above, will be neglected.

2.4.2 Two-dimensional load model

2.4.2.1 Overview of load model

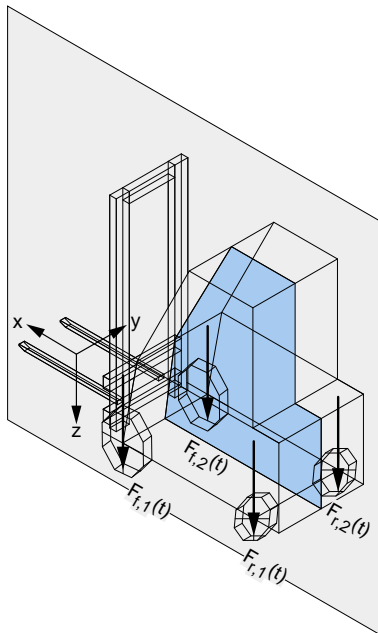


Figure 2.2: Sketch of a fork-lift truck

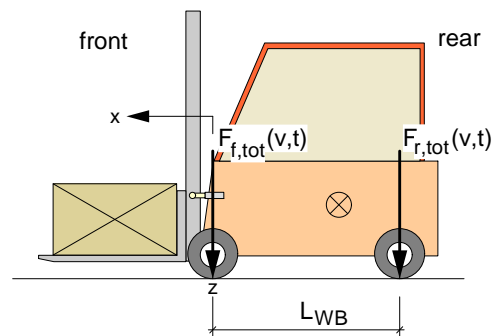


Figure 2.3: 2D model fork-lift truck

¹Except close to the natural frequency.

²With a negligible effect on the frequencies

2.4 Proposed dynamic load model of a fork-lift truck

The proposed two-dimensional model has the following form:

$$\begin{bmatrix} F_{f,tot}(v, t) \\ F_{r,tot}(v, t) \end{bmatrix} = \begin{bmatrix} F_f(v, t) \\ F_r(v, t) \end{bmatrix} + \begin{bmatrix} F_{g,f} \\ F_{g,r} \end{bmatrix} \quad (2.1)$$

The model comprises two vertical time-variable forces ($F_{f,tot}(v, t)$ and $F_{r,tot}(v, t)$) that travel at a fixed distance (WB) over the floor system at a velocity (v). Each force is the sum of a variable part ($F_f(v, t)$ and $F_r(v, t)$) representing the dynamics of the fork-lift truck and a constant part due to gravity ($F_{g,f}$ and $F_{g,r}$), which will not be considered in the further analysis of the dynamic load model. The time-variable forces can be written according to Newton's law as the product of mass and acceleration:

$$\begin{array}{l} \text{Force} \\ \begin{bmatrix} F_f(t, v) \\ F_r(t, v) \end{bmatrix} \end{array} = \begin{array}{l} \text{Mass matrix} \\ \begin{bmatrix} M_{11} & M_{12} \\ M_{21} & M_{22} \end{bmatrix} \end{array} \cdot \begin{array}{l} \text{Acceleration function} \\ \begin{bmatrix} a_f(t, v) \\ a_r(t, v) \end{bmatrix} \end{array} \quad (2.2)$$

The mass matrix contains the mass, its distribution and consequently the mass moment of inertia of the fork-lift truck, its mast and any payload carried. The acceleration vector, in turn, is the product of an amplitude factor and a periodic factor which comprises the frequencies of vertical movement and the phase angles between the front and the rear axle:

$$\begin{array}{l} \text{Acceleration} \\ \begin{bmatrix} a_f(t, v) \\ a_r(t, v) \end{bmatrix} \end{array} = \begin{array}{l} \text{Amplitude} \\ \begin{bmatrix} A_f(v) \\ A_r(v) \end{bmatrix} \end{array} \cdot \begin{array}{l} \text{Periodic function} \\ \begin{bmatrix} \sum_{i=1}^n \mu_{1,i} \sin(2\pi f_i t) \\ \sum_{i=1}^n \mu_{2,i} \sin(2\pi f_i t + \varphi_i) \end{bmatrix} \end{array} \quad (2.3)$$

In Equation 2.3 it is assumed that the amplitude of vibration is a function of the driving velocity ($A(v)$) and that the periodic function is represented as the sum of sine-functions of n frequencies (f_i) with fixed ratios of amplitudes ($\mu_{1,i}$ and $\mu_{2,i}$) on each axle and constant phase angles (φ_i) between front and rear axle.

Initially, the analysis will be based on a three-degree-of-freedom model of the fork-

2.4 Proposed dynamic load model of a fork-lift truck

lift truck. However, as will be shown, the third degree of freedom is unlikely to influence the floor vibrations. It is therefore sufficient to model the truck as a two-degree-of-freedom model and as such to set $n = 2$ in Equation (2.3).

2.4.2.2 Modelling and modal analysis of a fork-lift truck

Eriksson (1994) concluded from his investigation of fork-lift truck excitation of floor vibrations that rigid body modes dominate the dynamic behaviour. This finding agrees well with the study of Beha (1989) who tested several degrees of freedom to determine their contribution to the accelerations of parts of a fork-lift truck.

In this study the model is set up with two rigid bodies in which the total mass of the truck and any payload are concentrated. One body represents the chassis including counterbalance weight, engine and driver while the other rigid body represents the mast including fork and any payload carried. It is assumed that the chassis can move vertically due to deformations of the wheels. The mast can rotate about its fixed point at the chassis by longitudinal deformation of the actuator which controls the inclination of the mast. Hence a three-degree-of-freedom model (in two dimensions) is set up and is investigated: see principal sketch on the left hand side in Figure [2.4].

In their investigation of the dynamic response of highway bridges to heavy vehicle loads, Green and Cebon (1994) used a four-degree-of-freedom model as shown on the right hand side in Figure [2.4] which is an easy model to represent the dynamics of a heavy goods vehicle.

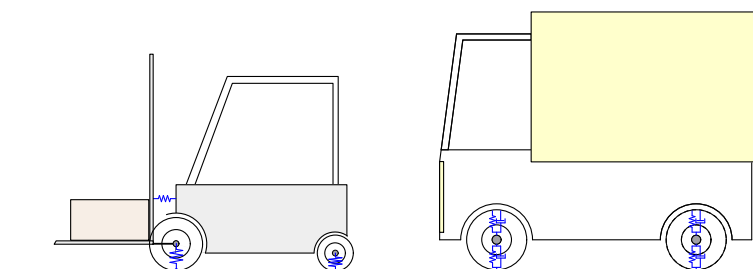


Figure 2.4: Comparison of fork-lift truck as 3dof system with heavy goods vehicle as 4dof system according to Green and Cebon (1994)

The main differences between the heavy goods vehicle model and the fork-lift truck

2.4 Proposed dynamic load model of a fork-lift truck

model shall be discussed briefly: the model by Green and Cebon is set up using coupled spring-damper-systems on each axle. This is done to account for the weight of the vehicle's suspension system (underbody). In the case of a heavy goods vehicle representing a 40 t-lorry, the underbody weighs about 4000 kg (10% of the total mass). In the case of a fork-lift truck for indoor goods handling there is no separate underbody and the total weight is about 6000 kg of which the axles with their wheels weigh about 250 kg (4.2% of the total mass). This means in the case of a fork-lift truck there is no separate system with a significant weight (the underbody) and an additional deformability (wheels). The suspension stiffness (and damping) only results from the deformability of the wheels. Hence a simple two-axle, two-degree-of-freedom model is sufficient to model the motion of the body of the truck. A third degree of freedom is introduced to model the rotation of the mast, see Figure [2.5].

The model of a fork-lift truck shown in Figure [2.6] is a simplified version of the model introduced by Beha (1989), for which he unfortunately did not give a closed solution because he was only interested in single parts. His seven-degree-of-freedom model is reduced to three degrees of freedom as only the main modes are of interest: the degrees of freedom used in the model here are the vertical movement and rotation of the fork-lift truck body (labelled as z_g and φ_g), and the rotation of the mast including any payloads relative to the rotation of the body (labelled as φ_m), see Figure [2.7].

The degrees of freedom omitted here are the horizontal deformability of the wheels, the horizontal and vertical movement of the fork relative to the mast, and the vertical movement of the second stage of the mast, which is small if the fork is in a low position, as is usually the case while driving.

The reactions are calculated based on the assumption that the deformability of the wheels can be modelled by linear springs. As explained above and in agreement with Beha, no separate set of springs to model the underbody is included in the model. The axle forces are products of spring constants and displacements.

The rotation of the mast is governed by the stiffness of the actuator which is modelled as a linear spring as well.

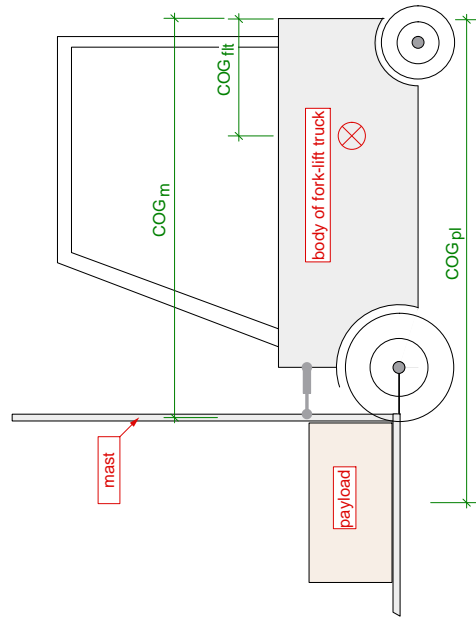


Figure 2.5: Fork-lift truck modelled as three rigid bodies: payload, mast and body of fork-lift truck

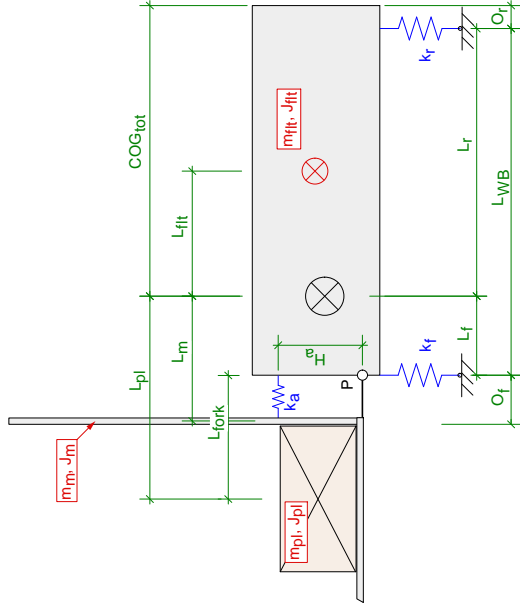


Figure 2.6: Fork-lift truck as three-degree-of-freedom system: modelled properties

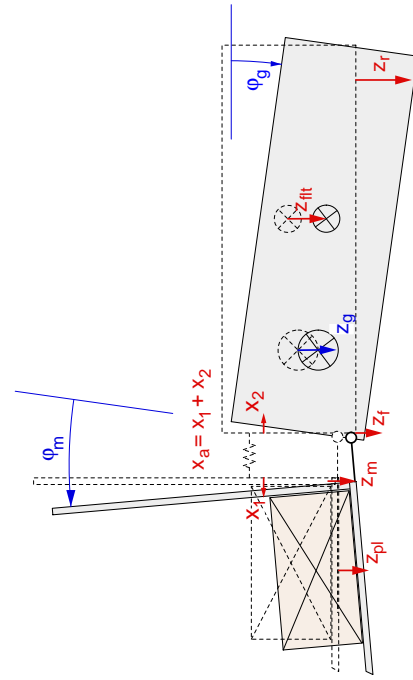


Figure 2.7: Fork-lift truck model: primary variables (in blue) and derived variables (in red)

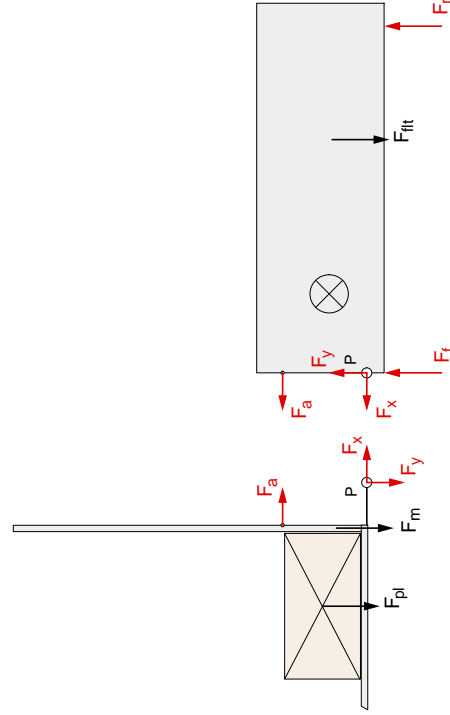


Figure 2.8: Fork-lift truck model: inertia (d'Alembert) forces (in black) and spring / contact forces (in red)

2.4 Proposed dynamic load model of a fork-lift truck

The spring forces are:

$$F_f = k_f z_f \quad (2.4)$$

$$F_r = k_r z_r \quad (2.5)$$

$$F_a = k_a x_a \quad (2.6)$$

The model shown in Figure [2.5] is used to find the eigen-frequencies of the fork-lift truck. The kinematic relations and equations of forces and moments are:

Kinematics :

$$z_f = z_g - L_f \varphi_g \quad (2.7)$$

$$z_r = z_g + L_r \varphi_g \quad (2.8)$$

$$z_{flt} = z_g + L_{flt} \varphi_g \quad (2.9)$$

$$z_m = z_g - L_m \varphi_g + O_f \varphi_m \quad (2.10)$$

$$z_{pl} = z_g - L_{pl} \varphi_g + L_{fork} \varphi_m \quad (2.11)$$

$$x_a = H_a \varphi_m \quad (2.12)$$

Sum of vertical forces for whole system :

$$F_f + F_r = F_{flt} + F_m + F_{pl} \quad (2.13)$$

$$k_f z_f + k_r z_r = -m_{flt} \ddot{z}_g - m_m \ddot{z}_m - m_{pl} \ddot{z}_{pl} \quad (2.14)$$

$$\begin{aligned} & \ddot{z}_g (m_{pl} + m_m + m_{flt}) + \ddot{\varphi}_g (m_{flt} L_{flt} - m_{pl} L_{pl} - m_m L_m) + \dots \\ & + \ddot{\varphi}_m (m_{pl} L_{fork} + m_m O_f) + z_g (k_f + k_r) + \varphi_g (k_r L_r - k_f L_f) = 0 \end{aligned} \quad (2.15)$$

Since the expression $(m_{flt} L_{flt} - m_{pl} L_{pl} - m_m L_m) \equiv 0$ in Equation (2.15), it follows that it may be written as

$$\begin{aligned} & \ddot{z}_g (m_{pl} + m_m + m_{flt}) + \ddot{\varphi}_m (m_{pl} L_{fork} + m_m O_f) + \dots \\ & \dots + z_g (k_f + k_r) + \varphi_g (k_r L_r - k_f L_f) = 0 \end{aligned} \quad (2.16)$$

Sum of moments about the centre of gravity (COG_{tot}):

$$F_f L_f - F_r L_r = M_{tot} \quad (2.17)$$

$$k_f (z_g - L_f \varphi_g) L_f - k_r (z_g + L_r \varphi_g) L_r = J_{tot} \ddot{\varphi}_g - m_{pl} \ddot{\varphi}_m L_{fork} L_{pl} - m_m \ddot{\varphi}_m O_f L_m \quad (2.18)$$

$$J_{tot} \ddot{\varphi}_g + \ddot{\varphi}_m (-m_{pl} L_{fork} L_{pl} - m_m O_f L_m) + z_g (k_r L_r - k_f L_f) + \varphi_g (k_r L_r^2 + k_f L_f^2) = 0 \quad (2.19)$$

2.4 Proposed dynamic load model of a fork-lift truck

with J_{tot} as the mass moment of inertia of all parts about the centre of gravity as a rigid body motion:

$$J_{tot} = J_{ftt}^{COG} + J_m^{COG} + J_{pl}^{COG} \quad (2.20)$$

$$= J_{ftt} + m_{ftt}L_{ftt}^2 + J_m + m_mL_m^2 + J_{pl} + m_{pl}L_{pl}^2 \quad (2.21)$$

which is reduced by the relative rotation of the mast and the payload about the centre of gravity (COG_{tot}): $(-m_{pl}\ddot{\varphi}_m L_{fork}L_{pl} - m_m\ddot{\varphi}_m O_f L_m)$

Sum of moments about point P at the mast system:

$$(J_{pl} + J_m)\ddot{\varphi}_m + m_{pl}\ddot{z}_{pl}L_{fork} + m_m\ddot{z}_m O_f + F_a H_a = 0 \quad (2.22)$$

$$\begin{aligned} \ddot{z}_g(m_{pl}L_{fork} + m_m O_f) + \ddot{\varphi}_g(-m_{pl}L_{fork}L_{pl} - m_m L_m O_f) + \dots \\ \dots + \ddot{\varphi}_m(J_{pl} + m_{pl}L_{fork}^2 + J_m + m_m O_f^2) + \varphi_m(k_a H_a^2) = 0 \end{aligned} \quad (2.23)$$

where $m_{pl}L_{fork}^2$ and $m_m O_f^2$ are the parallel axis theorem contributions of the payload and the mast about point P. Thus the moment of inertia about P can be written as

$$(J_{pl} + m_{pl}L_{fork}^2) + (J_m + m_m O_f^2) = J_{pl}^P + J_m^P \quad (2.24)$$

Equations (2.16), (2.19) and (2.23) with (2.24) can be written in matrix form as:

$$\begin{aligned} \begin{bmatrix} m_{ftt} + m_m + m_{pl} & 0 & m_{pl}L_{fork} + m_m O_f \\ 0 & J_{tot} & -m_{pl}L_{fork}L_{pl} - m_m L_m O_f \\ m_{pl}L_{fork} + m_m O_f & -m_{pl}L_{fork}L_{pl} - m_m L_m O_f & J_{pl}^P + J_m^P \end{bmatrix} \begin{bmatrix} \ddot{z}_g \\ \ddot{\varphi}_g \\ \ddot{\varphi}_m \end{bmatrix} \dots \\ \dots + \begin{bmatrix} k_f + k_r & k_r L_r - k_f L_f & 0 \\ k_r L_r - k_f L_f & k_r L_r^2 + k_f L_f^2 & 0 \\ 0 & 0 & k_a H_a^2 \end{bmatrix} \begin{bmatrix} z_g \\ \varphi_g \\ \varphi_m \end{bmatrix} = \begin{bmatrix} 0 \\ 0 \\ 0 \end{bmatrix} \end{aligned} \quad (2.25)$$

which is the standard formulation of a free vibration problem:

$$\begin{bmatrix} M \end{bmatrix} \begin{bmatrix} \ddot{u} \end{bmatrix} + \begin{bmatrix} K \end{bmatrix} \begin{bmatrix} u \end{bmatrix} = \begin{bmatrix} 0 \end{bmatrix} \quad (2.26)$$

Thus a solution of the form $[u] = [x] \sin(\omega t)$ can be assumed and Equation (2.25) can be solved as an eigenvalue problem of the form:

$$([K] - \omega^2 [M]) [x] = 0 \quad (2.27)$$

$$([M^{-1}K] - \omega^2 [I]) [x] = 0 \quad (2.28)$$

The eigenvalue problem is solved using MATLAB R2006a. The values used for the

2.4 Proposed dynamic load model of a fork-lift truck

numerical solution are derived as follows.

The mass of the fork-lift truck and its dimensions are known from the manufacturer's data sheet (see Table 2.5). The other dimensions (COG_{tot} , COG_{flt} , COG_{pl} , L_f , L_r , L_m , L_{fork} and L_{pl}) can be calculated from the data given (axle loads, wheel base, overhang). The mass moment of inertia of the fork-lift truck can be calculated with some simplifying assumptions and Beha (1989) gives values for the mass of the mast (see Table 2.5) and its mass moment of inertia ($150 - 200 \text{ kg m}^2$).

While the other values are reasonably well defined, the spring constant of the wheels and the actuator can vary over a wider range: according to Beha (1989), the equivalent spring constant of the tyres can vary between $k_{eq} = 0.85 \times 10^6 \text{ N/m}$ and $3.2 \times 10^6 \text{ N/m}$. For the equivalent spring constant of the actuator he gives values in the range of $4.4 \times 10^6 - 4.2 \times 10^7 \text{ N/m}$ for different models of fork-lift trucks.

In his study the range of the model's load capacity is 1500 kg to 6000 kg, thus covering the range investigated in the experiments here (1500 kg to 2500 kg).

In this analysis the values are taken from a generalised model of a fork-lift truck¹ with a capacity of 1600 kg. The equivalent spring constants were chosen to be: $k_f = k_r = 2.1 \times 10^6 \text{ N/m}$ for both load cases and $k_a = 1.0 \times 10^7 \text{ N/m}$ for the unloaded case, while $k_a = 3.0 \times 10^7 \text{ N/m}$ was chosen for the loaded case.

In Table 2.2 the results of the modal analysis for a 1600 kg-model are presented in terms of the vertical displacement (z_g) and rotation of the centre of gravity (φ_g) and the rotation of the mast (φ_m). The modes of the case "no payload carried" are illustrated in Figures [2.9 to 2.11] while the modes of the case "payload carried" are illustrated in Figures [2.12 to 2.14].

¹General models with various capacities will be presented later, see Section 2.8.2.

2.4 Proposed dynamic load model of a fork-lift truck

Modal Analysis		Mode 1	Mode 2	Mode 3
Without a payload carried:				
Eigen-vector	$\begin{bmatrix} z_g \\ \varphi_g \\ \varphi_m \end{bmatrix}$	$\begin{bmatrix} -0.02 \\ 1.00 \\ -0.13 \end{bmatrix}$	$\begin{bmatrix} 1.00 \\ 0.06 \\ 0.15 \end{bmatrix}$	$\begin{bmatrix} -0.07 \\ 0.10 \\ -1.00 \end{bmatrix}$
Eigen-frequency	[Hz]	4.8	5.7	14.6
With a payload of 1600 kg carried:				
Eigen-vector	$\begin{bmatrix} z_g \\ \varphi_g \\ \varphi_m \end{bmatrix}$	$\begin{bmatrix} -0.78 \\ 1.00 \\ -0.17 \end{bmatrix}$	$\begin{bmatrix} -1.00 \\ -0.78 \\ -0.17 \end{bmatrix}$	$\begin{bmatrix} -0.38 \\ 0.30 \\ 1.00 \end{bmatrix}$
Eigen-frequency	[Hz]	2.5	5.4	11.1

Table 2.2: Summary of modal analysis (3dof)

Modal analysis, no payload carried:

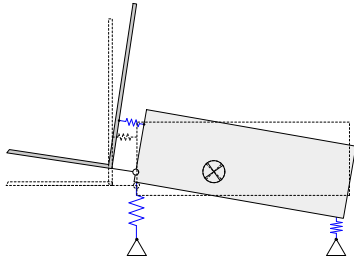


Figure 2.9: Mode 1

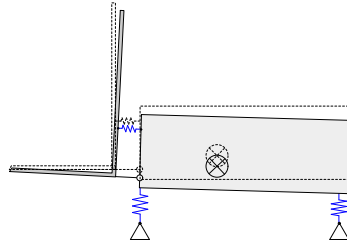


Figure 2.10: Mode 2

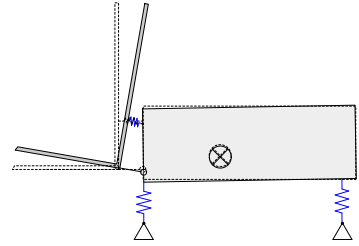


Figure 2.11: Mode 3

Modal analysis, payload carried:

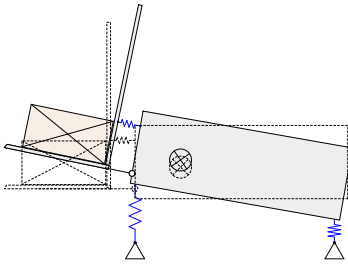


Figure 2.12: Mode 1

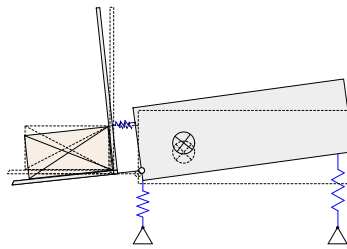


Figure 2.13: Mode 2

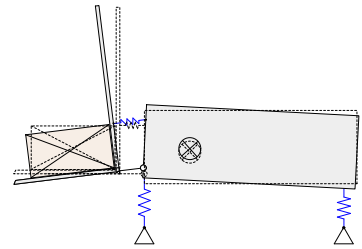


Figure 2.14: Mode 3

In the unloaded case the chosen parameters lead to eigen-vectors which are close to motion in a single degree of freedom for each mode, i.e. mode 1: pitch (φ_g dominates), mode 2: bounce (z_g dominates) and mode 3: mast pitch (φ_m dominates). When a payload is carried it is not possible to separate the modes as clearly as in the unloaded

2.4 Proposed dynamic load model of a fork-lift truck

case: in particular, it becomes harder to distinguish the first and the second mode due to interaction between the first (z_g) and the second (φ_g) degree of freedom. For certain configurations both modes are in-phase instead of anti-phase as in the unloaded case. However, an adjustment of the spring constants for the loaded case was not made.

Reduction of the number of degrees of freedom For the sake of a simple model, the third mode is neglected in the further investigation and the set-up of the load model. This is permissible for two reasons: for the unloaded case, which is known to excite higher forces (see Eriksson (1994), Malchaire et al. (1996)), the contribution of the third degree of freedom (rotation of the mast φ_m) to the vertical reactions is small. In the loaded case the contribution is slightly higher but is still small. Furthermore, the modal frequencies of the third mode are considerably higher (i.e. 14.6 Hz and 11.1 Hz) than are relevant for the floor systems investigated here, i.e. those with low eigenfrequencies (3.0 to 5.0 Hz). Therefore, the third degree of freedom will be neglected for the derivation of the axle forces, i.e. the actuator is assumed to be rigid: the equivalent spring constant k_a is set to ∞ .

The effect of reducing the three-dof system to a two-dof system is negligible for the case “no payload carried” as each mode is close to a single-degree-of-freedom motion. In the case “payload carried” it changes the frequencies slightly, but it does not change the behaviour significantly, see Table 2.3.

Modal Analysis	Mode 1	Mode 2
Without a payload carried:		
Eigen-vector	$\begin{bmatrix} z_g \\ \varphi_g \end{bmatrix}$	$\begin{bmatrix} 1.00 \\ 0.00 \end{bmatrix}$
Eigen-frequency	[Hz] 4.6	5.8
With a payload of 1600 kg carried:		
Eigen-vector	$\begin{bmatrix} z_g \\ \varphi_g \end{bmatrix}$	$\begin{bmatrix} -0.77 \\ 1.00 \end{bmatrix}$
Eigen-frequency	[Hz] 2.6	5.5

Table 2.3: Modal analysis of 3dof model with $k_a = \infty$ and thus $\varphi_m = 0$

2.4.2.3 2DOF load model

Based on the preceding modal analysis, a two-degree-of-freedom model is deemed sufficient to represent the fork-lift truck. To formulate the mass matrix of the load model (see Equation 2.2) the fork-lift truck is reduced to one (total) mass and is assumed to be rigid (see Figure [2.5] with $k_a \rightarrow \infty$), and the reaction forces at the front and rear axle, which are the sought forces, can be found as functions of the front and rear axle accelerations (a_f and a_r respectively) of the rigid body motion.

The kinematics of the two-degree-of-freedom system with z_g as the vertical displacement and φ_g as the rotation of the centre of gravity are:

$$\ddot{z}_g = a_f \frac{L_r}{L_{WB}} + a_r \frac{L_f}{L_{WB}} \quad (2.29)$$

$$\ddot{\varphi}_g = a_f \frac{-1}{L_{WB}} + a_r \frac{1}{L_{WB}} \quad (2.30)$$

Thus in matrix form:

$$\begin{bmatrix} \ddot{z}_g \\ \ddot{\varphi}_g \end{bmatrix} = \frac{1}{L_{WB}} \begin{bmatrix} L_r & L_f \\ -1 & 1 \end{bmatrix} \begin{bmatrix} a_f \\ a_r \end{bmatrix} \quad (2.31)$$

The equation of forces with $F_{tot} = F_{flt} + F_m + F_{pl}$ and the equation of moments with M_{tot} as the moment about the centre of gravity are:

$$\sum V = -F_{tot} + F_f + F_r = 0 \quad (2.32)$$

$$\sum M = M_{tot} + F_f L_f - F_r L_r = 0 \quad (2.33)$$

Thus

$$F_f = F_{tot} \frac{L_r}{L_{WB}} - M_{tot} \frac{1}{L_{WB}} \quad (2.34)$$

$$F_r = F_{tot} \frac{L_f}{L_{WB}} + M_{tot} \frac{1}{L_{WB}} \quad (2.35)$$

With $F_{tot} = m_{tot} \ddot{z}_g$ and $M_{tot} = J_{tot} \ddot{\varphi}_g$, where m_{tot} and J_{tot} are the total mass and mass moment of inertia about the centre of gravity, it follows in matrix form:

$$\begin{bmatrix} F_f \\ F_r \end{bmatrix} = \frac{1}{L_{WB}} \begin{bmatrix} L_r & -1 \\ L_f & 1 \end{bmatrix} \begin{bmatrix} F_{tot} \\ M_{tot} \end{bmatrix} = \frac{1}{L_{WB}} \begin{bmatrix} L_r & -1 \\ L_f & 1 \end{bmatrix} \begin{bmatrix} m_{tot} \ddot{z}_g \\ J_{tot} \ddot{\varphi}_g \end{bmatrix} \quad (2.36)$$

2.4 Proposed dynamic load model of a fork-lift truck

$$\begin{aligned}
 \begin{bmatrix} F_f \\ F_r \end{bmatrix} &= \frac{1}{L_{WB}^2} \begin{bmatrix} L_r & -1 \\ L_f & 1 \end{bmatrix} \begin{bmatrix} m_{tot}L_r & m_{tot}L_f \\ -J_{tot} & J_{tot} \end{bmatrix} \begin{bmatrix} a_f \\ a_r \end{bmatrix} \\
 &= \frac{1}{L_{WB}^2} \begin{bmatrix} m_{tot}L_r^2 + J_{tot} & m_{tot}L_fL_r - J_{tot} \\ m_{tot}L_fL_r - J_{tot} & m_{tot}L_f^2 + J_{tot} \end{bmatrix} \begin{bmatrix} a_f \\ a_r \end{bmatrix}
 \end{aligned} \tag{2.37}$$

It follows from this that the load model can be expressed by means of constants (specifications of the fork-lift truck and the payload) and the (periodic) functions of accelerations a_f and a_r . The acceleration function can be expressed using modal superposition:

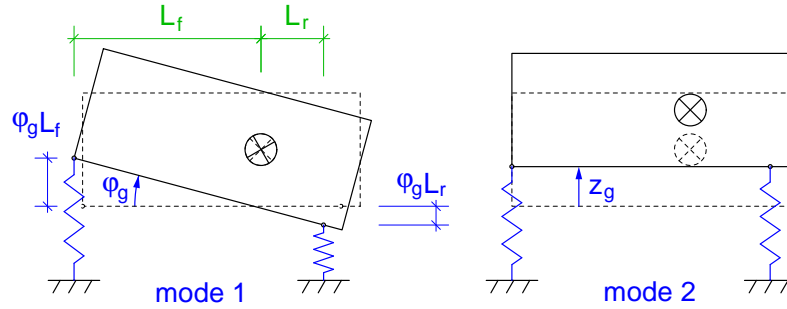


Figure 2.15: Modal modes of 2dof model

According to Figure [2.15] the modes are:

$$\text{mode 1: } \begin{bmatrix} a_f \\ a_r \end{bmatrix} = \begin{bmatrix} -L_f \\ L_r \end{bmatrix} \varphi_g \tag{2.38}$$

$$\text{mode 2: } \begin{bmatrix} a_f \\ a_r \end{bmatrix} = \begin{bmatrix} 1 \\ 1 \end{bmatrix} z_g \tag{2.39}$$

This allows the acceleration function to be formulated, based on the mode shapes in the time-domain, as:

$$\begin{bmatrix} a_f \\ a_r \end{bmatrix} = A_1 \begin{bmatrix} -L_f \\ L_r \end{bmatrix} \sin(2\pi f_1 t) + A_2 \begin{bmatrix} 1 \\ 1 \end{bmatrix} \sin(2\pi f_2 t) \tag{2.40}$$

where A_1 and A_2 are the modal acceleration amplitudes, which are functions of the

driving conditions - principally the forward velocity v .

Since the model parameter will be investigated experimentally and the aim is to develop a model easy to implement in the time-domain, it is convenient to re-formulate and simplify Equation (2.40).

Amplitudes The amplitudes and their dependence on current (horizontal) velocity are measured in the experiments. The peak acceleration will be used to define the model amplitudes. These modal amplitudes A_1 and A_2 therefore have to be transformed into a single, velocity-dependent (time-domain) amplitude. The measured peak acceleration is $A(v)$ and a modal amplitude ratio is considered as μ .

Pitch mode It will be shown later that the bounce mode is the important mode for the excitation of the floor driven on. To simplify the model and to allow a general non-truck-specific model to be developed, the dependence of the amplitudes of the pitch mode on the distances of the axles from the centre of gravity (L_f and L_r) is neglected in the model and set to unity: $\begin{bmatrix} -1 & 1 \end{bmatrix}^T$. The resulting error is small if no payload is carried ($L_f \approx L_r$), but it is significant if a payload of the maximum capacity is carried. However, it will be shown later that the pitch mode is not of the same importance for the excitation of a floor system as the bounce mode. And thus, keeping in mind the need for an easily applicable model, this variable will be neglected.

With these modifications the acceleration function can be formulated in the time-domain as:

$$\begin{bmatrix} a_f \\ a_r \end{bmatrix} = A_1 \begin{bmatrix} -1 \\ 1 \end{bmatrix} \sin(2\pi f_1 t) + A_2 \begin{bmatrix} 1 \\ 1 \end{bmatrix} \sin(2\pi f_2 t) \quad (2.41)$$

$$\begin{aligned} \text{Acceleration} &= \text{Amplitude} \cdot \text{Periodic function} \\ \begin{bmatrix} a_f(t, v) \\ a_r(t, v) \end{bmatrix} &= A(v) \cdot \begin{bmatrix} \mu_1 \sin(2\pi f_1 t) + \sin(2\pi f_2 t) \\ \mu_2 \sin(2\pi f_1 t + \varphi_1) + \sin(2\pi f_2 t) \end{bmatrix} \end{aligned} \quad (2.42)$$

From the set-up of the load model it is clear which data are required for the load

model:

- to define the amplitude function:
 - The amplitudes of vertical accelerations.
 - The influence of velocity on the amplitudes.
 - The ratio of amplitudes at the considered frequencies.
- to define the periodic function:
 - The frequencies of vertical accelerations, which will be validated against the modal frequencies based on the three-degree-of-freedom model.
 - The influence of the driving velocity and direction (forwards and backwards), which should have no influence if the natural frequencies of the truck are excited.
 - The phase angle between the front axle and the rear axle, which will be validated against the mode shapes.

These values required for the development of the load model are found experimentally.

2.5 Experiment set-up and data recording

To fulfil the requirements previously outlined, it is necessary to record the accelerations at the front and the rear axle during the experiment as well as the velocity, without restricting the execution of the experiment to a pre-defined space. Thus all equipment used to record the accelerations and displacements must be mounted on the fork-lift truck itself and has to be independent of any stationary parts such as a power supply or computer.

The equipment for the experiments comprised two PCB accelerometers (338B35) with signal conditioners (480E09) and two infra-red tracking systems that were connected to a data acquisition card (DT9804)¹. The card was accessed with the Software

¹For the specifications of the equipment see Appendix B.1.

programme DT Measure FoundryTM (Version 4.0.7) and the data stored on the hard drive of a laptop (operating system Microsoft Windows XP Professional). The infra-red tracking system needed a constant power supply of 5 V, which was supplied from a 12 V lead-acid battery. The voltage was reduced with an electronic converter to the desired voltage.

The accelerometers were fixed to the chassis of the truck with G-clamps. The locations were chosen within the limits of accessibility as close as possible to the axles.

Acceleration record It should be noted here that no physical low-pass filter was available for the experiment execution. Therefore special attention had to be paid to the problem of aliasing of high frequency components, e.g. due to engine noise.

During the test execution the sampling frequency of the records was increased from 50 Hz up to 1250 Hz (per channel of acceleration record). The records did not show a significant change over the range of sampling frequencies and in the records with a higher sampling frequency no significant peaks were noted in the range from 50 to 100 Hz which could have been aliased into the relevant frequency band of 0 to 15 Hz.

A further confirmation of the recorded natural frequencies is the modal analysis of the three-degree-of-freedom model and the agreement between the results of the experiments carried out here and the natural frequencies of fork-lift trucks presented in other publications: see Section 2.3.

Infra-red tracking system The purpose-built infra-red tracking system was used to record the horizontal travel of the front axle. A combined infra-red emitter-sensor (OPT760T) with a range of 15 mm was used. After testing various materials for the reflectors, it was found that PTFE was the best suited material. It had to be made certain that only the reflectors triggered the switch of the sensor and that dirt and other spots on the wheels should not trigger the switch. PTFE allows setting the sensor to its maximum distance to pick up the reflected signal, so that any reflection of other (less reflective) materials were not detected. Reflectors with a diameter of 10 mm were fixed with double-sided tape to the side of the tyres. Eight reflectors were

attached to each wheel and when the reflector passed the sensor, it switched on, giving a peak of 5 V in the time-record for the time the reflector passed the sensor. From this, the driven path and speed could be derived. The accuracy of this measurement was dependent on the tyre diameter. For the fork-lift trucks used in the experiments the maximum error of horizontal displacement was $\Delta s = \frac{\pi D}{8} = 0.24$ m. The error for the fork-lift trucks of special interest (the battery powered ones) was $\Delta s = 0.19$ m. This was a negligible error in terms of the total driven path. In terms of the correlation of an event to the velocity this meant a possible delay between the event and the actual velocity of about 0.2 s at a velocity of 1 m/s reducing to 0.05 s at a velocity of 4 m/s. This was acceptable, because the influence of velocity will be analysed not for a specific velocity but for velocity bands.

The data were stored as a .txt file. Each line of a file comprised a time stamp, the outputs from the front and rear accelerometers and the information whether the IR-sensor was switched on or off. Additionally notes were recorded of some test parameters. These parameters noted whether the test was performed driving forwards or backwards, with or without payload, on which surface it was performed and whether bumps were crossed during the test.

The calculation of the velocity of the fork-lift truck is explained, because the method had an influence on the later analysis.

Velocity The infra-red tracking system recorded the passing of a reflector as a 5 V peak in the record of the channel. The length of each peak was determined by the time the reflector needed to pass the sensor barrier. The time lag from the beginning of one peak to the next was used to calculate the velocity of a wheel from the known displacement related to two signals (1/8 of a wheel's perimeter). To account for errors during the passing of a reflector (voltage may drop if the reflection is not clear over its whole surface) a minimum time lag for the distance of two peaks was introduced into the evaluation and the velocity was smoothed by averaging over three calculated points. The outcome at the end of this procedure was a smooth, averaged, record of

the velocities of each of the front wheels.

From the record of the displacements (and the derived velocity) of both front wheels the resultant velocity of the fork-lift truck was calculated. It was the mean of the two front wheel velocities.

Driven path From the record of the displacements of each front wheel, the driven path was calculated: see for example Figure [2.16]. However, no influence from a change of direction on the dynamics of the truck could be noted (except the change of velocity) and thus it was disregarded in the further analysis: if the spectral analysis was carried out for time windows while driving in a curve, the results did not differ from those obtained while driving in a straight line.

Figure [2.16] shows the result of a typical record.

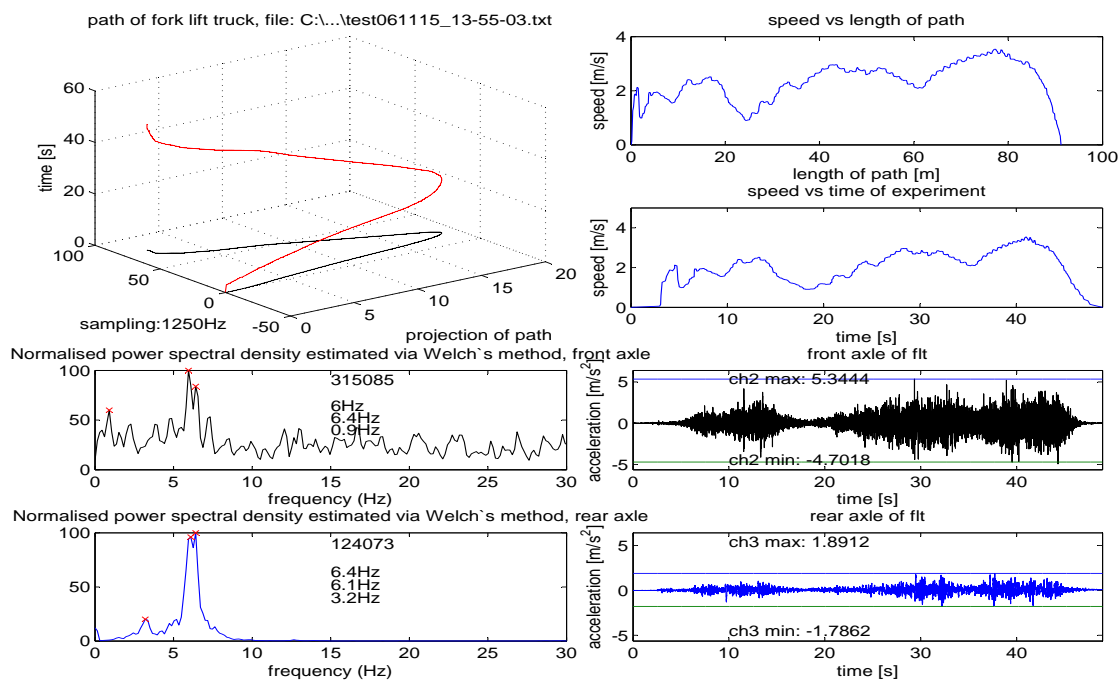


Figure 2.16: Record and analysis of a test with NISSAN16 (payload, indoors)

The plot in the top left corner shows the driven path in the xy-plane and the time in the z-direction.

The plots on the top right show the velocity plotted versus the length of the driven path and versus time, respectively.

In the bottom half is shown the record of accelerations on the right hand side and on the left hand side the evaluation of their frequency range.

2.6 Experiment execution

The test programme was performed in Germany and the Netherlands after a series of initial tests were carried out on the site of the Engineering Science Department in Oxford to check the workability of the set-up with a gas powered fork-lift truck. In Germany and the Netherlands a total of four different fork-lift trucks were tested:

2 battery-powered models: Nissan GNX 1L16HQ, Nissan FP01 R15

1 gas-powered model: Jungheinrich TFG16 AK

1 diesel-powered model: OM Pimespo XD25

Unfortunately, the access to the fork-lift trucks was limited in time as normal service on site had to continue around the tests. Each fork-lift truck could only be tested for about two hours (including set-up time). Due to this limitation, the lack of additional help during the experiments (staff on site had to do their own business) and the financial constraints, only basic data could be collected (in particular an instrumented hammer test could not be carried out as it was not feasible to transport such equipment).

The focus of this project is on battery-powered fork-lift trucks, because these are usually used inside buildings (and on upper floors) as they do not produce any exhaust. The gas-powered and diesel-powered models were tested to find out whether there is a trend to be found independent of the type of engine of the fork-lift truck.

The tests were carried out in twelve different configurations:

Fork-lift truck	Payload	Surface	Indicator
Nissan 16	600 kg	indoor (smooth concrete)	N16-LI
	600 kg	outdoor (sett paving)	N16-LO
	no load	indoor (smooth concrete)	N16-NLI
	no load	outdoor (sett paving)	N16-NLO
Nissan 15	420 kg	indoor (smooth concrete)	N15-LI
	420 kg	outdoor (sett paving)	N15-LO
	no load	indoor (smooth concrete)	N15-NLI
	no load	outdoor (sett paving)	N15-NLO
Jungheinrich 16	350 kg	outdoor (tarmac)	J16-LO
	no load	outdoor (tarmac)	J16-NLO
Pimespo 25	350 kg	outdoor (tarmac)	P25-LO
	no load	outdoor (tarmac)	P25-NLO

Table 2.4: Fork-lift truck test configurations

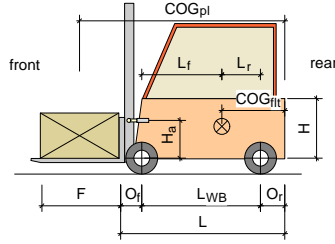
2.6.1 Fork-lift truck specifications

The following sections will explain the tests executed and give more details of the fork-lift trucks. The main dimensions and weights of the fork-lift trucks¹ tested are given in Table 2.5. At the top is shown the nomenclature used throughout the analysis.

The fork-lift trucks set up for testing are shown in Figures [2.17] to [2.20]. In total 166 (successful) tests were carried out. The length of the tests varied between a few seconds and about four minutes, with an average of about 70 seconds: see Appendix B, Section B.2 for a comprehensive summary of the test configurations. Next to the fork-lift trucks set up for testing, the figures show a sketch of the positions of the accelerometers (■).

From the figures it can be seen that the accelerometers could not be placed directly on the axles. An offset from the axle influences the pitch mode of the trucks. Since the truck body is effectively rigid, a correction could be applied. However, this has not been done in the evaluation of the tests, since, as will be shown, the bounce mode is the important mode for the excitation of floor systems.

¹Table 2.5 also gives the values for a fifth model. This model, a Mariotti Mycos 13C, which was used during the field test. However, testing it on solid ground instead of the (suspended) floor system was not possible and thus the results were not considered for the derivation of the load model.



Specification \ Model		Nissan N16	Nissan N15	Jungheinrich J16	Pimespo P25	Mariotti M13
Load capacity	m_{pl}	kg 1600	1500	1600	2500	1300
Service mass	m_{flt}^*	kg 3020	3120	2840	3980	2185
incl. mass of mast ***	m_m	kg 500	500	500	580	500
Axle load with payload	front	kg 4145	3815	3930	5775	3030
	rear	kg 475	805	520	705	450
Axle load without payload	front	kg 1550	1285	1330	1760	800
	rear	kg 1470	1835	1510	2220	1385
Length without fork	L	mm 1980	1980	2236	2592	1490
Height of body	H	mm 935	1105	1049	1095	800
Wheelbase	L_{WB}	mm 1395	1270	1495	1620	1088
Front overhang	O_f	mm 365	370	398	482	235
Rear overhang	O_r	mm 220	340	343	490	167
Length of fork	F	mm 900	1070	1150	1000	1000
Centre of gravity:						
... of fork-lift truck *	COG_{flt}	mm 936	863	1043	1206	565
... to front axle *	L_f	mm 679	747	795	904	690
... to rear axle *	L_r	mm 716	523	700	716	398
... of payload *	COG_{pl}	mm 2485	2482	2773	3092	1990
Position of hydr. actuator **	H_a	mm 400	400	400	400	400
Tyre size (front axle)		mm 460	490	520	620	330
Breadth	B_{flt}	mm 1090	1120	1080	1180	895
(*) calculated value, (**) estimated value, (***) estimated from Beha (1989)						

Table 2.5: Specifications of tested fork-lift trucks (1)



Figure 2.17: Nissan GNX 1L16HQ and sketch of positions of accelerometers



Figure 2.18: Nissan FP01 R15 and sketch of positions of accelerometers



Figure 2.19: Jungheinrich TFG16 AK and sketch of positions of accelerometers



Figure 2.20: OM Pimespo XD25 and sketch of positions of accelerometers

2.7 Results

The evaluation of the data recorded during the experiments is carried out with the software package MATLAB R2006a. All procedures for the evaluation used in this section are provided by either the software package “MATLAB R2006a” by The MathWorks (2006) or the book “NUMERICAL RECIPES” by Press et al. (1988).

The analysis is governed by the properties sought for the load model: the frequencies of vertical accelerations, their amplitudes, the ratio of these amplitudes and the phase angle between front and rear axle.

The analysis of the data will be explained for the example of the configuration Nissan16-LI. The results from other configurations will be summarised in tables and Appendix B.

2.7.1 Frequencies of vertical accelerations

In this section the experimental data will be analysed for their frequency contents to validate the assumption of Section 2.4 that the excitation frequencies in the load model are the natural frequencies of the trucks.

The analysis comprises the evaluation of the total record of data for each configuration and a more detailed analysis, where the influence of the driving direction (see Section 2.7.1.3) and velocity (see Section 2.7.1.2) is investigated. The results of all investigations concerning the frequencies are summarised in tables for an easy comparison. The results for Nissan16-LI are summarised in Table 2.10.

The raw data are passed through an electronic low-pass filter to get rid of high frequencies, which are not of interest for this project. Depending on the sampling frequency, which was changed during the experiments to find an optimal compromise between accuracy and size of files, a 10th order Butterworth filter with a cut-off frequency of 100 Hz is designed as a low-pass filter and applied to the dataset. Obviously, the low-pass filter is only applied if the sampling frequency is above 100 Hz.

2.7.1.1 Total record of experiments

The frequency content of the acceleration record is evaluated using P. Welch's method, which is readily available in MATLAB R2006a.

This method analyses the frequency content of intervals of the total data set. The intervals are windowed with a Hamming window to reduce the ends of the intervals, overlapped and time-averaged to smooth the spectrum. From each interval the frequency content is calculated with the discrete fast Fourier transform (FFT). The length of the intervals was set to 5 seconds and the overlap to 50%. The length (n) of the

FFT is determined according to the sampling frequency during the experiment. It is $n = f_{ds}l_{int}$ where f_{ds} denotes the frequency of data sampling (1250 Hz in most tests) and l_{int} is the length of an interval (here 5 s)¹.

For each configuration the average power spectral density of all tests performed is calculated. The averaging takes into account the fact that the sampling frequency could vary throughout one test configuration and that therefore the frequency increment of the discrete power spectral density does not remain constant. The averaged power spectral density is normalised to 1. Figure [2.21] shows the result of this averaging: the results of the front axle on the left and rear axle on the right.

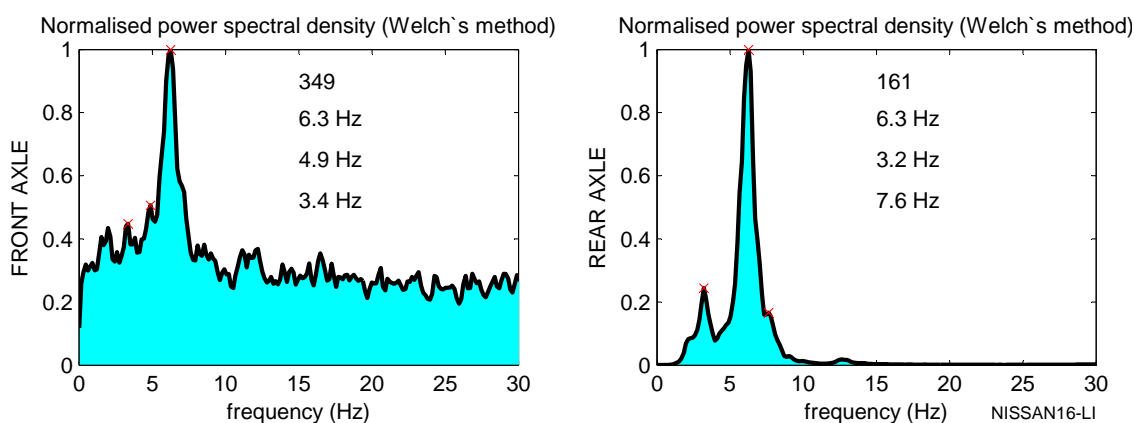


Figure 2.21: Nissan16, loaded, indoors

The plots are characterised by one to three distinct peaks and a variable noise level. For Nissan16 the noise level is higher on the front axle, while at the rear axle hardly any noise is recorded. This trend is found in most tests. It may be explained by the drivetrain which transmits the power to the front axle. Another possible explanation of the front axle noise is the influence of the vibrations of the mast, which is attached to the body of the fork-lift truck at the front axle. This assumption is supported by the observation that the noise level increases when a payload is carried which leads to more degrees of freedom at the mast system, because the payload is not (as assumed for the load model) rigidly fixed to the fork.

¹A detailed summary of the configuration of the tests is given in Appendix B, Section B.2.

The peaks denote the natural frequencies of the fork-lift trucks in a specific load situation. In the plots the peaks fulfil the requirement of a local maximum.

For the Nissan16 fork-lift truck the significant peaks are similar at the front and the rear axle and may be assumed to be natural frequencies¹. The first peak is about 6 - 7 Hz (smaller in the case “payload carried”) and the second peak is about 3 - 4 Hz (again smaller if loaded). The change of frequencies from the unloaded to the loaded case is to be expected from the modal analysis and the literature (Eriksson, 1994).

A brief discussion of the results of the frequency analyses of the other models can be found in Appendix B.3. However, the results follow the trend found for the Nissan16: significant peaks in the range of interest from 0 - 10 Hz.

2.7.1.2 Correlation of velocity and frequencies

Reminder: the velocity is measured in the (horizontal) xy-plane, while the accelerations of interest are vertical, thus in the z-direction! Hence here $\frac{dv(t)}{dt} \neq a(t)$.

To analyse the influence of the velocity on the vertical accelerations the data records are split into four “velocity bands”. The velocity bands are

$$v_1 \leq 1 \text{ m/s} < v_2 \leq 2 \text{ m/s} < v_3 \leq 3 \text{ m/s} < v_4$$

The velocity bands are chosen with respect to the maximum velocity of the fork-lift trucks. They have a maximum of about 14 to 16 km/h ($\hat{=}$ 3.8 to 4.5 m/s), thus leading to four equally sized bands. A finer division is not desirable, because, as will be explained later, it would lead to more errors in the frequency analysis.

Each line of the record is associated with a velocity, which is assumed to be constant between two signals from the infra-red tracking system. The data record is segmented according to the velocity bands. The segments related to a velocity band are then concatenated to form four continuous sub-data sets. Consider the extract of a record as an example:

¹For an easy comparison the results of the frequency analyses are summarised in Table 2.10.

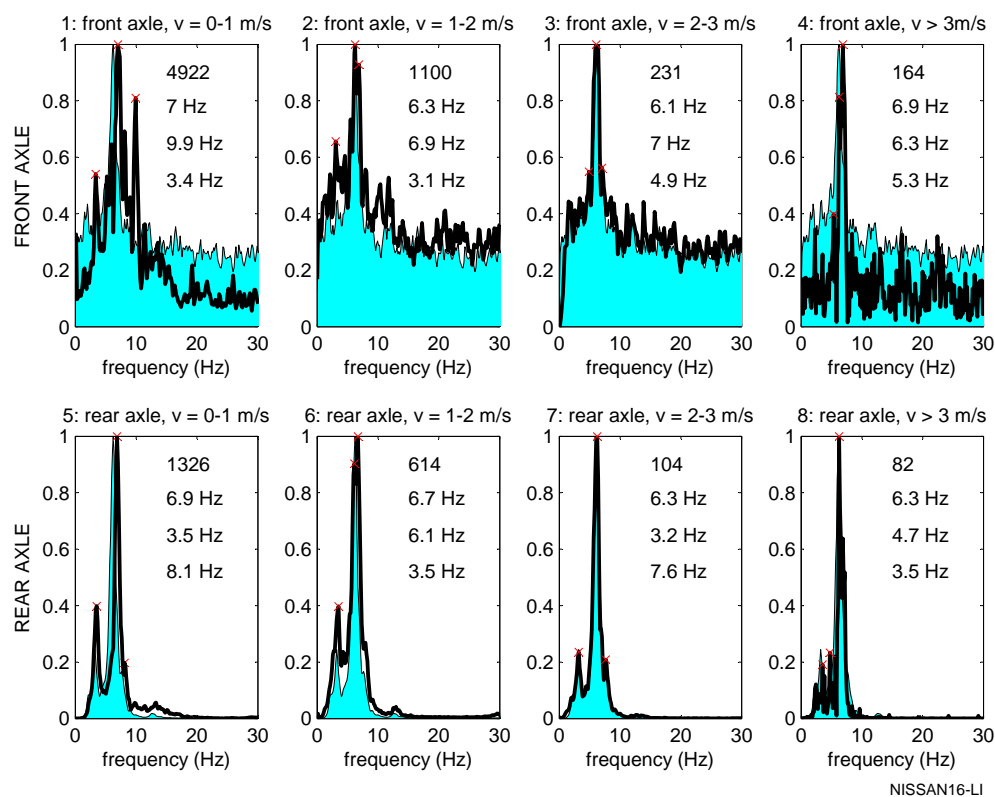


Figure 2.22: Nissan16-LI, Influence of velocity on frequencies

However, as will be seen later in a comparison of all frequency related analyses (see Table 2.10), the analysis of the influence of the velocity on the frequencies shows the biggest errors. This can be explained by reference to the procedure of creating the sub-data sets: first the total record is broken into segments of equal velocity bands and then the segments are concatenated to form one sub-data set. However, at the joints of two segments the continuity is not guaranteed, which consequently produces errors in the Fourier transform¹. The more joints are in the sub-data sets, the more errors are introduced. The more bands considered, the more joints exist. Thus, more velocity bands would lead to more errors and less meaningful results.

¹See the example, sub-data set v_2 : line 873 and 1216 are adjacent lines in the sub-data set, but the voltage of the accelerometers at the front and the rear axle is not continuous.

2.7.1.3 Correlation of driving direction and frequencies

The driving direction was noted for each test during the execution. Thus, it is easy to divide the complete data set into two sub-sets: driving forwards and driving backwards. The normalised power spectral density from each member of both sets is known from the analysis of the total data set (Section 2.7.1.1).

So, the same averaging process is carried out as earlier¹, only with a distinction between the sub-sets. The results are plotted in Figure [2.23]. The figure shows the power spectral density of configurations when driving forwards ([2.23.1] and [2.23.3]) and when driving backwards ([2.23.2] and [2.23.4]). The power spectral density of the total data set is plotted shaded in the background for an easy comparison. In all plots the same normalisation factor is used. The natural frequencies found are summarised in Table 2.7.

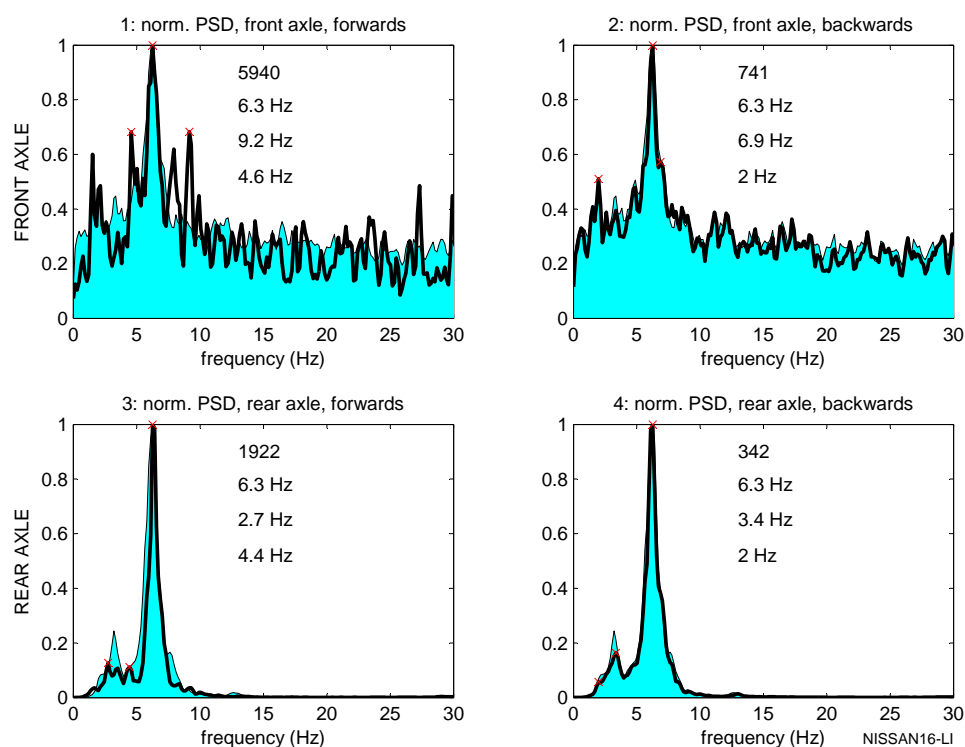


Figure 2.23: Nissan16-LI, power spectral density for different driving directions

The variation in the shape of the power spectral density determined for the different

¹See Section 2.7.1.1

Analysis	Axle	Frequency [Hz]					
Total data set	front	-	3.4	4.9	6.3	-	-
	rear	-	3.2	-	6.3	-	7.6
Driving direction							
forwards	front	-	-	4.6	6.3	-	9.2
	rear	-	2.7	4.4	6.3	-	-
backwards	front	2.0	-	-	6.3	6.9	-
	rear	2.0	3.4	-	6.3	-	-

Table 2.7: Nissan16-LI, Influence of driving direction on frequencies

driving directions is small. The biggest peak at 6.3 Hz matches exactly for both driving directions. The deviation of the second peak (3.4 Hz) is 0.7 Hz for the rear axle when driving forwards. The other combinations match the frequency well.

It is concluded that the direction of driving has no significant influence on the power distribution in the power spectral density. This is to be expected, if the frequencies excited are natural frequencies.

2.7.1.4 Modal analysis of the fork-lift truck

The three-degree-of-freedom model introduced in Section 2.4.2, Figure [2.5] is used to verify the measured frequencies as natural frequencies of the fork-lift truck. The equivalent spring constants are adjusted for the unloaded case to: $k_f = 2.3 \times 10^6$ N/m, $k_r = 2.8 \times 10^6$ N/m and $k_a = 4.0 \times 10^6$ N/m.

The same values are chosen for the loaded case and show a good match of the eigenfrequencies and the measured natural frequencies. The modal analysis of the Nissan16 is summarised for both load cases in Table 2.8.

The results of the modal analyses of all models tested are summarised in Table 2.9.

Modal Analysis		Mode 1	Mode 2	Mode 3
Without a payload carried:				
Eigen-vector	$\begin{bmatrix} z_g \\ \varphi_g \\ \varphi_m \end{bmatrix}$	$\begin{bmatrix} -0.30 \\ 1.00 \\ -0.28 \end{bmatrix}$	$\begin{bmatrix} -1.00 \\ -0.79 \\ -0.22 \end{bmatrix}$	$\begin{bmatrix} -0.10 \\ 0.14 \\ 1.00 \end{bmatrix}$
Eigen-frequency	[Hz]	5.2	6.7	9.7
With a payload of 600 kg carried:				
Eigen-vector	$\begin{bmatrix} z_g \\ \varphi_g \\ \varphi_m \end{bmatrix}$	$\begin{bmatrix} -0.49 \\ 1.00 \\ -0.47 \end{bmatrix}$	$\begin{bmatrix} -1.00 \\ -0.83 \\ -0.25 \end{bmatrix}$	$\begin{bmatrix} -0.30 \\ 0.15 \\ 1.00 \end{bmatrix}$
Eigen-frequency	[Hz]	3.3	6.3	8.9

Table 2.8: Summary of modal analysis for Nissan16

Configuration Model		Frequency [Hz]			Eq. spring constant [N/m]		
		Mode 1	Mode 2	Mode 3	k_f	k_r	k_a
Nissan 16	L	3.3	6.3	8.9	2.3×10^6	2.8×10^6	4.0×10^6
	NL	5.2	6.7	9.7			
Nissan 15	L	3.3	5.4	9.8	2.1×10^6	2.1×10^6	4.0×10^6
	NL	4.3	5.7	9.6			
Jungheinrich 16	L	3.6	5.8	9.2	2.1×10^6	2.1×10^6	1.0×10^7
	NL	4.9	6.1	14.6			
Pimespo 25	L	3.4	4.9	17.7	2.1×10^6	2.0×10^6	4.2×10^6
	NL	4.0	5.1	24.5			

Table 2.9: Summary of modal frequencies for all configurations

2.7.1.5 Summary of frequency analyses

The frequencies found in the analyses and calculated with the 3dof model are summarised for Nissan16-LI in Table 2.10 and for the other configurations in Tables B.6 to B.16.

A good agreement between the calculated eigen-frequencies and the measured natural frequencies is found throughout all configurations. The frequencies prove to be independent of the velocity and the driving direction. Hence they can be assumed to be the natural frequencies of the trucks and can be used in the load model.

They form one part of the periodic factor of the acceleration function as defined in

Nissan16 - LI							
Analysis	Axle	Frequency [Hz]					
			1^{st}_{mode}		2^{nd}_{mode}		3^{rd}_{mode}
Modal:	-	-	3.3	-	6.3	-	8.9
Experimental:							
Total data set	front	-	3.4	4.9	6.3	-	-
	rear	-	3.2	-	6.3	7.6	-
Velocity							
v_1	front	-	3.4	-	-	7.0	9.9
	rear	-	3.5	-	-	6.9	8.1
v_2	front	-	3.1	-	6.3	6.9	-
	rear	-	3.5	-	6.1	6.7	-
v_3	front	-	-	4.9	6.1	7.0	-
	rear	-	3.2	-	6.3	7.6	-
v_4	front	-	-	5.3	6.3	6.9	-
	rear	-	3.5	4.7	6.3	-	-
Driving direction							
forwards	front	-	-	4.6	6.3	-	9.2
	rear	2.7	-	4.4	6.3	-	-
backwards	front	2.0	-	-	6.3	6.9	-
	rear	2.0	3.4	-	6.3	-	-

Table 2.10: Nissan16-LI, summary of frequencies

Section 2.4, Equation 2.42. The second part of that factor (the phase angles) will be considered in a separate analysis: see Section 2.7.2.

2.7.2 Cross-correlation of accelerations at front and rear axle

The cross-correlation and coherence are calculated to analyse the dependency of the accelerations at the front and the rear axle. Ultimately, this allows for the calculation of the phase angle between the vertical accelerations of the front and rear axle which are needed for the load model as proposed in Section 2.4.

The cross-correlation and the coherence are calculated using the discrete fast Fourier transform of windowed intervals, which overlap¹. Each test is split into intervals of 5 seconds length, which overlap by 50%. The interval is then multiplied with a Hamming window to reduce the effects of the (non-zero) ends. From each windowed interval the

¹The procedure is similar to P. Welch's method, but it is not readily available in Matlab for the calculation of the cross-correlation.

Fourier transform is calculated for both axles. The number of points (n) of the Fourier transform is determined according to the sampling frequency during the experiment. It is: $n = 2^m$ where $2^m < f_{ds}l_{int} < 2^{m+1}$.

From the Fourier transforms the power spectral densities are calculated. They are $P_{xx,i}(f)$ at the front axle and $P_{yy,i}(f)$ at the rear axle:

$$P_{xx,i} = [FFT_{front,i}] \cdot [FFT_{front,i}]^* \quad (2.43)$$

$$P_{yy,i} = [FFT_{rear,i}] \cdot [FFT_{rear,i}]^* \quad (2.44)$$

where $(\cdot)^*$ denotes the complex conjugate. The cross-correlation of each interval is the product of the two Fourier transforms:

$$XC_i = [FFT_{front,i}] \cdot [FFT_{rear,i}]^* \quad (2.45)$$

The cross-correlation of each interval is normalised and the average taken of all intervals (see continuous line in Fig. [2.24]). As $XC_i \in \mathbb{C}$ the phase angle φ is found as

$$\varphi = \arctan\left(\frac{Re(XC_i)}{Im(XC_i)}\right) \quad (2.46)$$

For the natural frequencies found in Section 2.7.1 the distribution of the phase angle of all intervals is plotted in Figure [2.24]. The frequency of occurrence (cardinality) of each angle is plotted against the phase angle. The average phase angle and the phase angle with the maximum cardinality are denoted.

The coherence is calculated as

$$C_{xy,i}(f) = \frac{|XC_i|^2}{P_{xx,i} * P_{yy,i}} \quad (2.47)$$

$C_{xy,i}(f)$ denotes the coherence of an interval and is a function of the frequency. All intervals of all tests are added up and the average calculated by dividing the sum by the number of intervals analysed. The coherence is plotted in Figure [2.24] as a dashed line: the higher the coherence for a particular frequency, the more likely it is that the signals are linked to the same source of vibration.

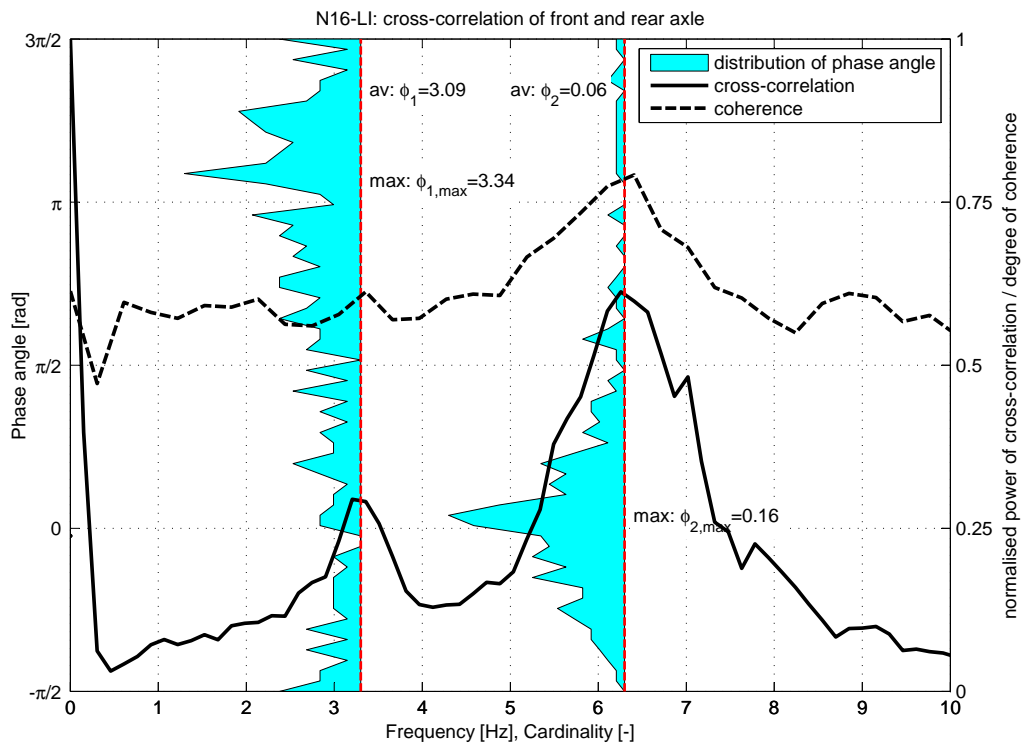


Figure 2.24: Nissan16-LI, Cross-correlation of front and rear axle

Correlation and coherence The results for Nissan16-LI are plotted in Figure [2.24]. The cross-correlation has its peaks at the natural frequencies (3.3 Hz and 6.3 Hz) and the coherence is about 0.6 and 0.8 for these frequencies.

For all configurations the cross-correlation shows its major peaks at the natural frequencies found in the previous section (see Section 2.7.1) and the coherence is 0.6-0.8 for the relevant frequencies (with few exceptions: N15-NLO: $f=4.3$ Hz $C_{xy}=0.4$, J16-LO: $C_{xy}=0.4$, P25-LO: $f=3.4$ Hz $C_{xy}=0.4$).

While the level of coherence is not very high, the results are clear enough for the desired determination of the phase angles as calculated in the modal analysis.

Phase angles of Nissan 16 The averaged phase angle for the first mode is $\phi_{1,av,N16} = 3.09 \approx \pi$, which is in good agreement with the modal analysis: mode 1 is anti-phase. The averaged phase angle for the second mode theoretically is 0 (in-phase) and is found to be $\phi_{2,av,N16} = 0.06$.

Phase angles in load model The average phase angles calculated from all configurations are shown in Table 2.11. The distribution of the phase angle for the second mode is a bell-shaped curve, with an average calculated from all configurations of $\phi_{2,av} = 0.003$. Thus, the phase angle in the load model is, in agreement with the modal analysis, set to zero.

The average phase angle of the first mode calculated from all configurations, however, does not show such a clear picture, but still a distinct peak can be found close to π . The average phase angle for the first mode is $\phi_{1,av} = 2.94$, which is, consistently with the modal analysis, rounded to π for the load model.

Configuration	Average phase angle		
	mode 1	mode 2	
N16	LI	3.09	0.06
	NLI	3.08	0.24
	LO	3.07	-0.15
	NLO	2.78	-0.02
N15	LI	2.96	-0.48
	NLI	2.92	0.05
	LO	3.23	0.23
	NLO	2.12	0.14
J16	LO	3.00	0.04
	NLO	3.11	0.04
P25	LO	2.97	-0.13
	NLO	2.90	0.02
Average	2.94	0.003	
	$\approx \pi$	≈ 0	

Table 2.11: Summary of average phase angles of mode 1 and 2 for all fork-lift trucks

The analysis of the cross-correlation provides the phase angles for the load model proposed in Section 2.4, Equation 2.42. With this information the periodic part of the acceleration function can be set up. To complete the acceleration function the amplitude function is still needed. This will be determined in the next Section.

2.7.3 Amplitudes of accelerations

This Section analyses the amplitudes and the relation of the driving velocity to the amplitudes of vibration. The amplitudes govern the magnitude of the forces applied through the load model to the structure. An amplitude function will be defined to be used in the load model according to Equation 2.42.

2.7.3.1 Definition of peak accelerations

The amplitudes have to be extracted from the continuous record of accelerations during the experiments. The extraction is performed with a simple routine that finds a certain number of maxima and minima per second. It is assumed that 20 extrema are sufficient to represent the amplitudes of the record, which means that the peaks of frequencies up to 20 Hz are considered. This is well above the natural frequencies extracted in the previous section of this study. First, the search routine finds all local extrema per second (e.g. maxima: $acc_f(n-1) < acc_f(n) > acc_f(n+1)$) and then saves only the 20 biggest and 20 smallest extrema. In a second step the absolute value of the extrema is taken, thus giving 40 peak accelerations per second. For illustration, see Figure [2.25]: all extrema are found and the 20 biggest (smallest) are extracted (here boxed).

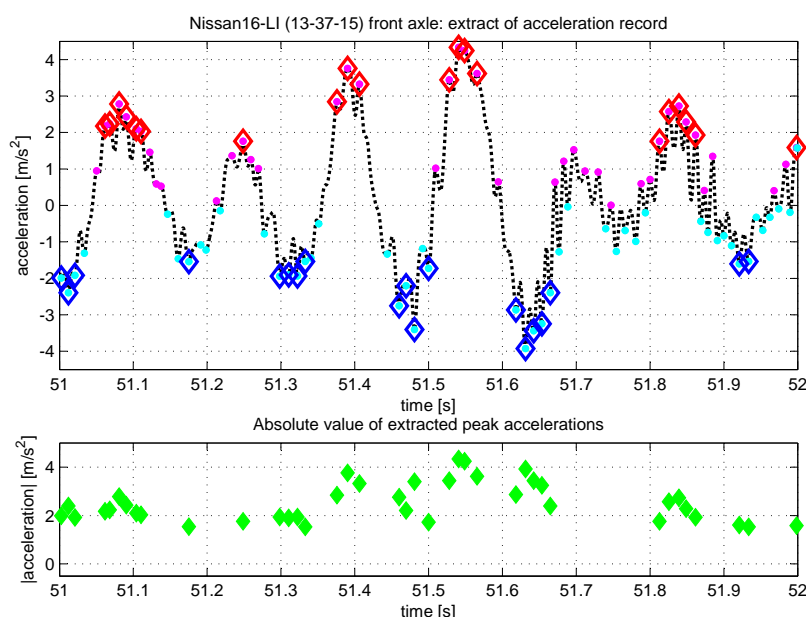


Figure 2.25: Extraction of peak accelerations

2.7.3.2 Model of vibration excitation by velocity

The source of excitation is the roughness of even a smooth concrete floor. Surface roughness can take several forms: a single bump, periodic or randomly distributed surface bumps and surface undulations. On a good quality surface inside a building bumps can (almost certainly) be excluded as a source of periodic excitation of the truck. Most likely the residual irregularities from a well levelled floor excite the truck periodically.

In the next section a simple model will be set up to predict the influence of the horizontal velocity on the vertical accelerations of the fork-lift truck. It is based on the one-degree-of-freedom model presented by Eriksson (1994) to predict the force input of a fork-lift truck on a suspended floor. However, Eriksson did not take into account the influence of velocity. The change of velocity changes the excitation frequency. This effect will be incorporated in the one-degree-of-freedom model of forced vibration here.

Figure [2.26] shows how an imperfection of the floor could lead to a vertical displacement and thus to an (vertical) acceleration of the wheel. The variables in the figure are: R radius of the wheel, ΔR height of the imperfection, α and β angles during the rotation over the imperfection.

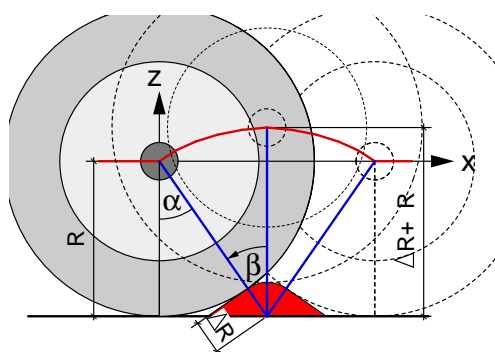


Figure 2.26: Theoretical model of excitation: single bump

While the truck travels at a velocity v and thus the wheel rotates with an angular velocity $\omega_r = \frac{v}{R}$ it makes contact with the block with a height of ΔR , as it has an angle of $\alpha = \beta_{max} = \arccos\left(\frac{R}{R+\Delta R}\right)$ to the centre of rotation. If that block is assumed to be

rigid (as it would be as it is concrete), the centre of rotation (the axle) has to move upwards while moving over the block. The angle β can be expressed as a function of time:

$$\beta(t) = \left[\alpha - \frac{vt}{R} \right] \quad (2.48)$$

the vertical movement, velocity and acceleration are described as

$$\begin{aligned} z(t) &= (R + \Delta R) \cos(\beta(t)) \\ z(t) &= (R + \Delta R) \cos\left(\alpha - \frac{vt}{R}\right) \end{aligned} \quad (2.49)$$

$$\dot{z}(t) = \frac{dz(t)}{dt} = (R + \Delta R) \frac{v}{R} \sin\left(\alpha - \frac{vt}{R}\right) \quad (2.50)$$

$$\ddot{z}(t) = \frac{d^2z(t)}{dt^2} = (R + \Delta R) \left(\frac{v}{R}\right)^2 \cos\left(\alpha - \frac{vt}{R}\right) \quad (2.51)$$

Thus the acceleration $\ddot{z}(t) \propto \left(\frac{v}{R}\right)^2$.

However, on a high quality floor inside a building it is more likely that the undulations are within the limits of defined tolerances. In Figure [2.27] the undulation is modelled as a continuous sine function.

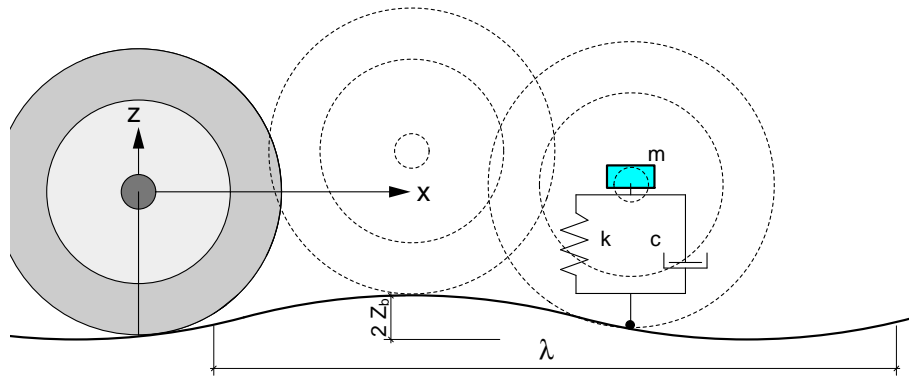


Figure 2.27: Theoretical model of excitation: undulation

For example, in Germany the evenness of floors in industrial buildings is specified according to DIN 18202 (2005), Table 3: the acceptable tolerances are defined as deviations from a level floor. The tolerances of a ready-to-use floor (appropriate for most industrial floors) are defined in line 3 or line 4, if the requirement of higher

precision is defined, see Table 2.12.

Line	Description	Maximum tolerance in mm			
3	Top of ready-to-use floor	2	4	10	12
4	Top of ready-to-use floor (higher requirements)	1	3	9	12
Distance of points of measurement in m:		0.10	1.00	4.00	10.00

Table 2.12: Allowable tolerances according to DIN 18202 (2005)

Measurements of the concrete floors used for the experimental work gave irregularities considerably smaller than the allowed values: except for a few locations the undulation was in the range of 1 mm if the measurement points were 1.00 m apart.

The tolerances defined in DIN 18202 (2005) are twice the amplitude of the undulation: it is measured the maximum sag between two points of measurement, which are peaks on the floor.

In the model, the floor undulation acts as a support motion, which can be written as differential equation¹:

$$m\ddot{z} = -k(z - z_b) - c(\dot{z} - \dot{z}_b) \quad (2.52)$$

The floor undulation is assumed to be $z_b = Z_b \sin(2\pi f_b t) = Z_b \sin(\frac{2\pi v t}{\lambda})$, where Z_b is the amplitude of the floor undulation and f_b its frequency. The frequency is velocity dependent with $f_b = \frac{v}{\lambda}$ where v is the driving speed of the fork-lift truck and λ the wavelength of the undulation. The solution of the differential equation is

$$z(t) = \left[\frac{k + i\frac{2\pi v}{\lambda}c}{k - m\left(\frac{2\pi v}{\lambda}\right)^2 + i\frac{2\pi v}{\lambda}c} \right] Z_b e^{i\frac{2\pi v}{\lambda}t} \quad (2.53)$$

and the acceleration is found as the second derivate of $z(t)$:

$$\ddot{z}(t) = \left[\frac{k + i\frac{2\pi v}{\lambda}c}{k - m\left(\frac{2\pi v}{\lambda}\right)^2 + i\frac{2\pi v}{\lambda}c} \right] \left[i\frac{2\pi v}{\lambda} \right]^2 Z_b e^{i\frac{2\pi v}{\lambda}t} \quad (2.54)$$

¹See for example Thomson (1988).

The values can vary in a range as given in Table 2.13.

Variable	Range of values		
Natural frequencies of the fork-lift truck	f_n	2.0 - 7.0	Hz
Mass supported by the axle	m	800 - 4800	kg
Equivalent spring constant of the wheel	k	2.0 - 3.2	MN/m
Damping constant	c	0.05	1/s
Wavelength of undulation	λ	0.02 - 1.00	m
Amplitude of undulation	Z_b	1 - 2	mm

Table 2.13: Parameter study of response to undulations

In Figure [2.28] the relation between forward velocity and vertical acceleration is plotted for various axle loads with a natural frequency of $f_n = 6.0$ Hz and a maximum undulation amplitude $Z_b = 1$ mm and wavelength of $\lambda = 0.75$ m.

And Figure [2.29] shows three responses of typical configurations. The following observations can be made from these plots:

1. In general the acceleration increases with increasing velocities. A quadratic regression fits the data best in the range $k > m(\frac{2\pi v}{\lambda})^2$, which are, for example, plotted in Figure [2.28].
2. The relation of velocity and acceleration is not monotonic: for $k = m(\frac{2\pi v}{\lambda})^2$ it is not defined on the real axis (resonance). The peak close to the resonance is, for example, shown in Figure [2.29] for the configuration with an eigen-frequency of 3.0 Hz (green line).
3. For $k < m(\frac{2\pi v}{\lambda})^2$ the effect of velocity on the acceleration is small. The velocity can change in a wide range without changing the response.

The relation between the steady state accelerations and the velocity is represented well by a quadratic function. However, for each configuration an individual function would be needed, but a simple bi-linear function is a suitable envelope over the velocity band of interest. The errors are bigger for a velocity band that is of minor interest for the real application: low velocities. Under normal service conditions a fork-lift truck drives at the highest possible velocity.

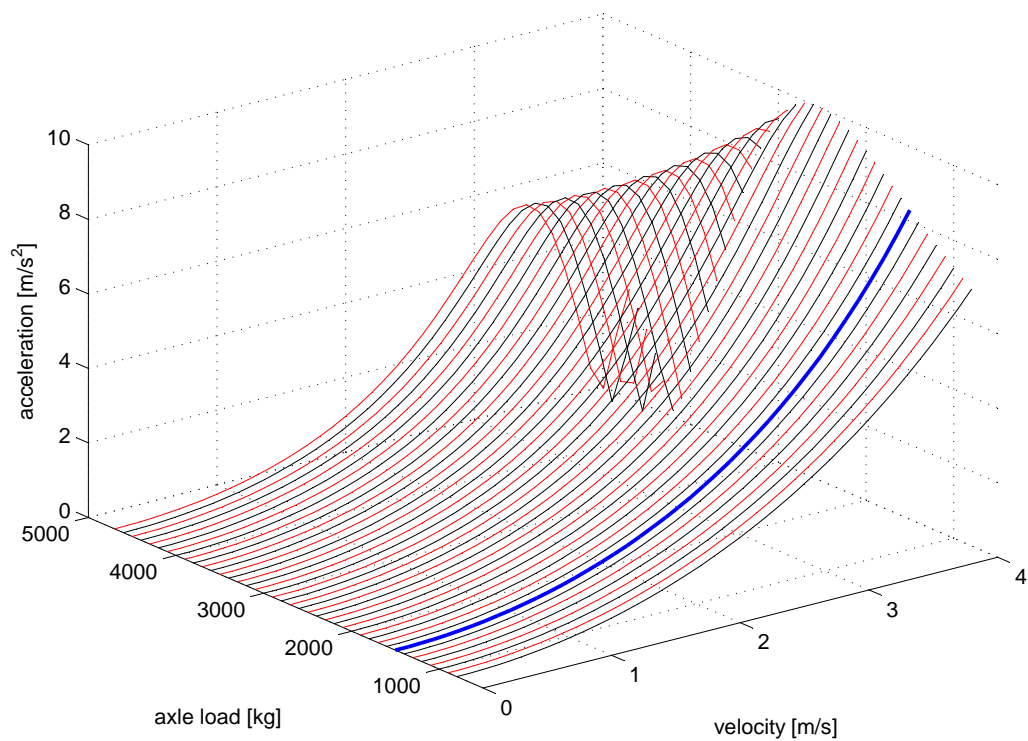


Figure 2.28: Acceleration due to floor undulation for various axle loads with $f_n = 6$ Hz, $\lambda = 0.75$ m and $Z_b = 1$ mm, $m = 1500$ kg plotted in blue

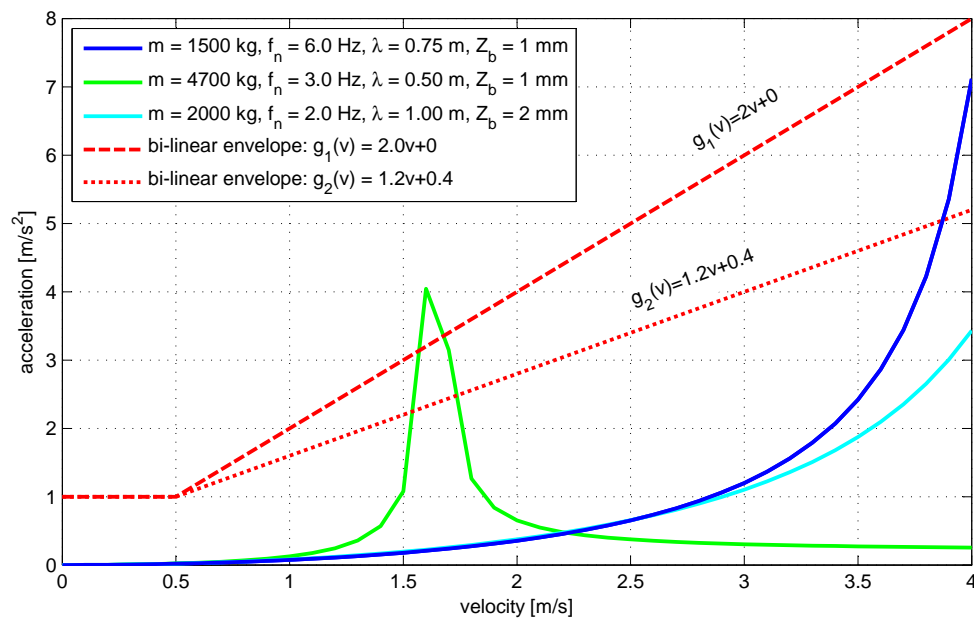


Figure 2.29: Acceleration due to floor undulation for various configurations

The threshold value and the slope of the envelope function are taken as constants. This simplification neglects the fact that the accelerations are functions of the constants defined above where the eigen-frequency has clearly the biggest influence¹ due to resonance effects.

2.7.3.3 Correlation of velocity and amplitudes of accelerations

From the “excitation model” it is assumed that the amplitudes of accelerations are correlated with the velocity of the fork-lift truck. To investigate this effect, the previously explained peak accelerations are associated with the velocity at the time of their occurrence, which is easily done, as for both pieces of information (peak acceleration and velocity) the time stamp is known.

All data pairs of velocity and associated acceleration are sorted into “bins” of a specific velocity and specific acceleration. The size of each “bin” is 0.1 m/s and 0.01 m/s². For example the occurrence of a data pair [$v_j = 2.5$ m/s; $a_{f,j} = 3.0$ m/s²] would be counted in bin(26,301)² which counts all data pairs within the range of $2.5 \leq v < 2.6$ m/s and $3.00 \leq a < 3.01$ m/s². The number of data pairs in each bin is counted and normalised for a specific velocity over all accelerations. The normalisation guarantees that records of all driven velocities are taken into account equally weighted thus allowing meaningful plots of the cardinality.

Figure [2.30] shows the results of the correlation. The figure is divided into two contour plots which show the cardinality for the front axle accelerations and the rear axle accelerations of the configuration “LI”. Additionally the graph shows lines below which lie 95% of all accelerations (henceforth called “the 95% fractile”), the mean of the peak accelerations and the predicted correlation of velocity and accelerations.

The 95% fractile and the mean are of importance for the serviceability analysis: for example EC 2 (2004) uses either the 95% fractile (e.g. Young’s modulus: E_c , which is,

¹In Appendix B, Section B.5.1 is shown a more detailed envelope function that incorporates the eigen-frequency of the fork-lift truck.

²A “bin” is a place in a matrix. This bin would be the entry in line 26 and column 301.

in fact, the 5% fractile¹) or the mean values (E_{cm}) for the serviceability check depending on the type of structure and the type of analysis.

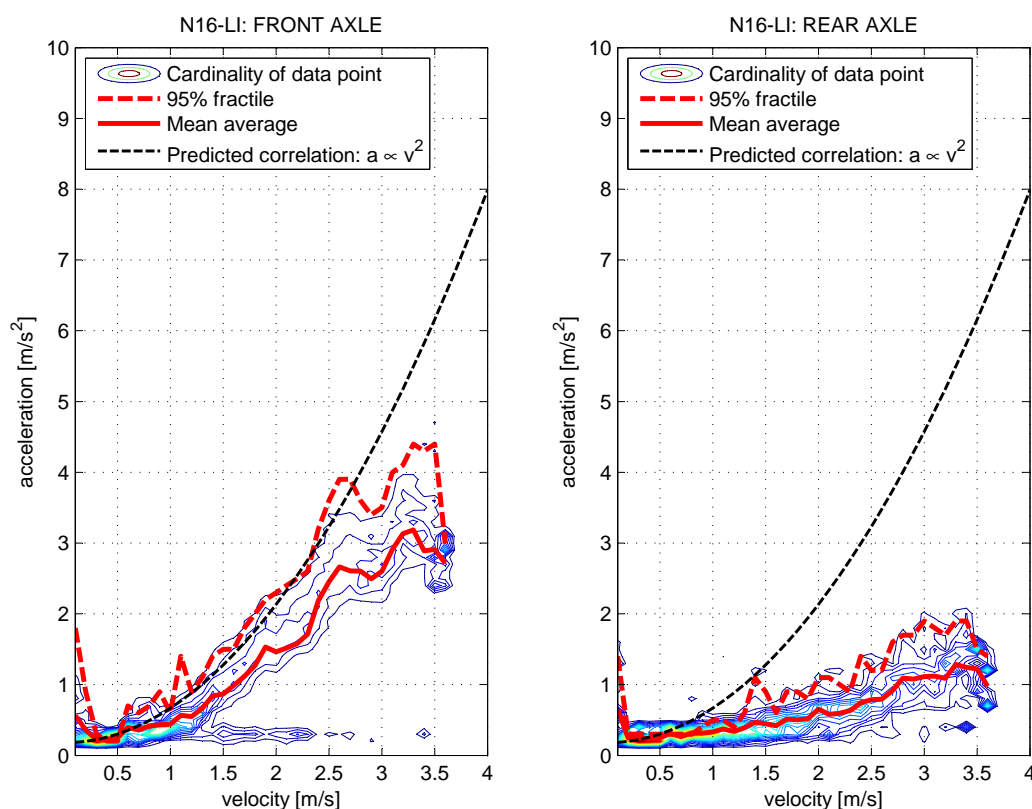


Figure 2.30: Nissan16 loaded indoors, amplitude over velocity for front and rear axle

The quadratic fit matches the 95% fractile data of the Nissan16-indoors very well for the front axle, while the match is still reasonable at the rear axle (better if no payload is carried, see Figure [B.46]). Outdoors, the data are more scattered but still follow the trend. While many maxima (in terms of cardinality) in the contour lie close to the predicted curve, the 95% fractile envelope lies at a higher level than predicted, see Figures [B.47] and [B.48].

In the Appendix the results of the correlation are plotted for the other models as well: see Figures [B.49] to [B.56]. Some of the configurations show severe spikes for one axle (mostly the rear axle) at certain velocities. These spikes can be explained as the result of resonance effects of the rotating parts of the engine and the part of the chassis to which the accelerometer was fixed: local deformations instead of

¹EC 2 uses 95% fractiles for the load-related values and 5% fractiles for material-related values.

the rigid body motions that were aimed for are recorded here. This explanation is supported by the observation that the spikes exceed $10 \text{ m/s}^2 \approx 1g$. If a spike with $a > 10 \text{ m/s}^2$ represented the acceleration of the fork-lift truck, it would have had to leave the ground but such behaviour was not observed. Furthermore, the spikes are bigger for the combustion-powered trucks, which have a higher level of noise caused by the engine, which was running constantly. The spikes or occasionally the total record which has been corrupted by resonance effects have been disregarded in the further analyses.

Even though the results show a “curved” correlation of velocity and accelerations for all models the scatter of the data and particularly the spikes make it difficult to fit a parabola through the data. If a parabola is fitted through the data, it changes its vertex to a maximum instead of a minimum for several configurations and to positive values which means it results in lower accelerations for higher velocities. Hence, the attempt to fit an individual parabola (which would represent the predicted correlation best) was abandoned and a different approach chosen, more suitable for a general (not model-specific) load model: bi-linear envelope functions to cover the mean or 95% of the peak accelerations (the 95% fractile) for any velocity. This means that two load models were set up which are suitable for the various types of serviceability checks. One model predicts the mean acceleration while the other model represents the 95% fractile: the load model predicts accelerations that are only exceeded by 5% of incidences of a given velocity.

In the following figures the mean of various configurations and their envelope are summarised. (The summary of the 95% fractile envelopes is presented in Appendix B, Section B.5.2). In the figures a threshold with a minimum velocity of $v = 0.5 \text{ m/s}$ is introduced under which the measurements are disregarded for the analyses. The introduction of the threshold is undertaken, because for low velocities the measurement of accelerations is not reliable (and not of special interest for the load model): decaying vibrations caused by higher velocities (if slowing down) were recorded and (due to the extraction routine) correlated with a lower velocity. Moreover, even normal operational

service might influence the accelerations as well: for example, from Beha (1989) it is known that any movement of the fork excites vibration at the front axle. However, these vibrations are of a short duration because they are caused by a single force input (the acceleration of the fork and a payload). However, they are likely to occur at low velocities and therefore they were not included in the load model.

Table 2.14 lists the configurations summarised in Figures [2.31] to [2.34].

Figure	Configuration displayed	Models analysed
[2.31]	Indoors, front axle	N16, N15
[2.32]	Indoors, rear axle	N16, N15
[2.33]	Outdoors, front axle	N16, N15, J16, P25
[2.34]	Outdoors, rear axle	N16, N15, J16, P25

Table 2.14: Allocation legend: Summary of mean and envelope

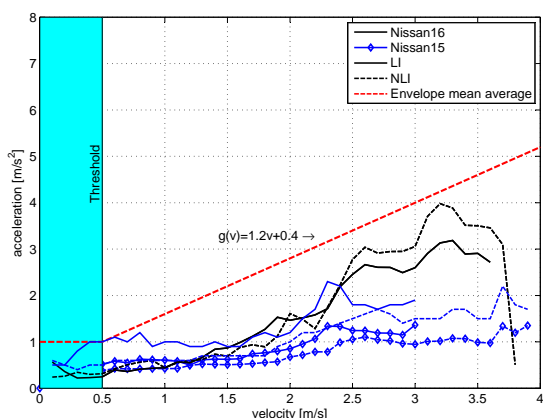


Figure 2.31: Summary: mean accelerations indoors, front axle

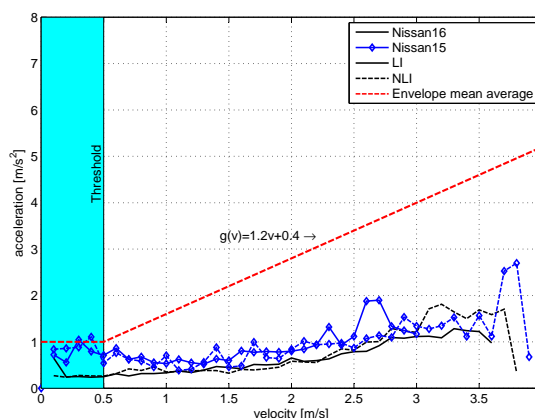


Figure 2.32: Summary: mean accelerations indoors, rear axle

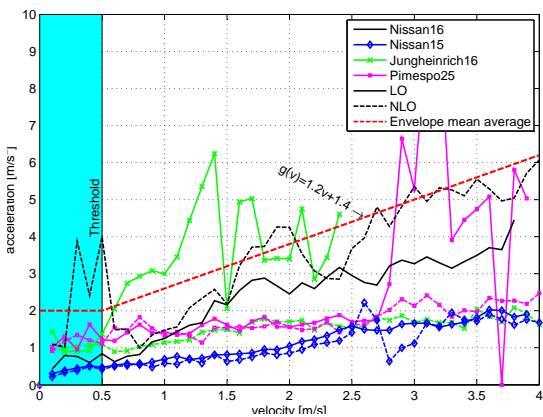


Figure 2.33: Summary: mean accelerations outdoors, front axle

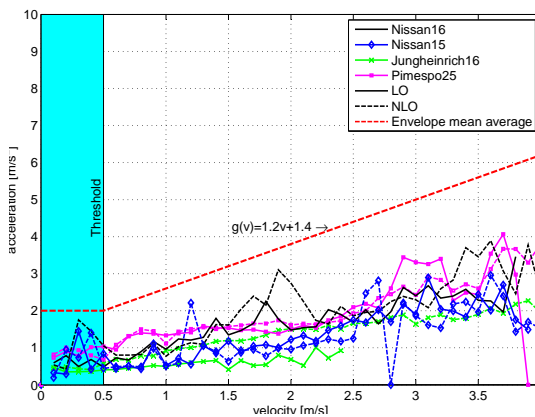


Figure 2.34: Summary: mean accelerations outdoors, rear axle

For the proposed load model a simple function is sought to express the correlation between velocity and the acceleration amplitudes. The bi-linear envelope function is suitable for this purpose and fits the data reasonably well¹.

The bi-linear envelope functions are only exceeded by two average functions: J16-LO and P25-LO. However, these two records show many spikes which can only be explained by resonance effects or errors in the records and thus they can be disregarded. Thus the envelope functions can be expressed as:

$$\begin{aligned}
 A_{av}(v) &= \begin{cases} T_{av} & \text{if } v \leq 0.5 \text{ m/s} \\ C_{av}v + D_{av} & \text{if } v > 0.5 \text{ m/s} \end{cases} & (2.55) \\
 \text{with } C_{av} &= 1.2 \text{ indoors and outdoors} \\
 \text{and } D_{av} &= \begin{cases} 0.4 & \text{indoors} \\ 1.4 & \text{outdoors} \end{cases} \\
 \text{and } T_{av} &= \begin{cases} 1.0 & \text{indoors} \\ 2.0 & \text{outdoors} \end{cases}
 \end{aligned}$$

2.7.3.4 Correlation of driving direction and amplitudes of accelerations

The driving direction does not have an influence on the frequencies excited in the fork-lift truck, and the “excitation model” suggests the independency of the driving direction as well. However, it has to be shown that this is true for the recorded amplitudes in order to verify the theoretical model and to set up a load model which is independent of the driving direction.

If separate records are noted for each driving direction and the analysis of the correlation between acceleration and velocity is plotted for both driving directions similar plots result as shown in Figure [2.30]. The functions of the average accelerations and the 95% fractile are covered by the same envelope functions as defined in the previous section.

Hence, it is shown that the driving direction does not have an influence on the

¹A more detailed envelope function is shown in Appendix B, Section B.5.1

amplitudes of vibration.

2.7.3.5 Summary of amplitude analyses

From the (theoretical) excitation model it is predicted that a quadratic function describes the correlation between velocity and the accelerations. However, the scatter of the data leads to various unsatisfying fits which are not suitable for further use. Thus, an envelope function that gives either the mean or the 95% fractile of all models is chosen for use in the load model. It has been shown that the accelerations are independent of the driving direction. The amplitude function as required for the load model proposed in Section 2.4, Equation 2.42 is set up as a bi-linear function.

The amplitude function represents the total magnitude of the vibration. It does not differentiate between the amplitudes of each of the natural frequencies considered in the load model. The allocation of the amplitudes to a natural frequency is carried out in the next Section 2.7.4.

2.7.4 Ratio of amplitudes

The record of accelerations during the experiments represents the amplitude of the sum of all frequencies. The contribution and the amplitude ratio of the eigen-frequencies of mode 1 (anti-phase motion) and mode 2 (in-phase motion) must be determined for the load model.

For this the power of vibration is considered: it is assumed that the total power of vibration is concentrated in the two frequencies which are sought. This assumption represents the activity well at the rear axle, where very little energy is transmitted at frequencies other than the natural frequencies. For the vibrations at the front axle this assumption means that more energy will be associated with the natural frequencies than with those found in the experiments. However, considering the designated application of the load model, it is desired to have a realistic but simple worst-case model. In this context ‘simple’ means that it is easy to implement into a FE-calculation and ‘worst-case’ means that most of the energy is concentrated in those frequencies which are

likely to excite the structure. As explained in the modal analysis (see Section 2.7.1.4), the eigen-frequencies can be tuned by adjusting the equivalent spring constant of the wheels and the hydraulic actuator.

The power from the accelerations measured during the experiments is the peak acceleration for a certain velocity squared ($P = [A_{peak}(v)]^2$), which is equal to the power of the load model ($P = [A_1 \sin(2\pi f_1 t) + A_2 \sin(2\pi f_2 t)]^2$). The amplitudes of the two frequencies are A_1 and A_2 and it is assumed $A_1 = \mu A_2$. Thus

$$\begin{aligned} P = [A_{peak}]^2 &= [A_1 \sin(2\pi f_1 t) + A_2 \sin(2\pi f_2 t)]^2 = [A_1 + A_2]^2 \\ &= [\mu A_2 + A_2]^2 = [(1 + \mu) A_2]^2 \end{aligned} \quad (2.56)$$

$$A_2 = \frac{A_{peak}}{1 + \mu} \quad (2.57)$$

In the load model the peak accelerations are derived from the measured accelerations in each period (local maxima), of which the mean (and the 95% fractile) are correlated to a driven velocity (see Section 2.7.3).

The peaks of interest are found in the power spectral density plots (see Section 2.7.1, Fig. [2.21] and Appendix B, Fig. [B.1] to [B.3]). Their frequencies and amplitudes are summarised in Table 2.15.

Nissan 16		Frequency and size of peaks:					
		Mode 1		Mode 2		μ_1	μ_2
		[Hz]	[-]	[Hz]	[-]	[-]	[-]
LI	front	4.9	0.5	6.3	1.0	0.5	
	rear	3.2	0.25	6.3	1.0		0.25
NLI	front	5.0	0.6	6.9	1.0	0.6	
	rear	5.0	0.33	6.7	1.0		0.33
LO	front	4.9	0.3	6.1	1.0	0.3	
	rear	3.1	0.1	6.1	1.0		0.1
NLO	front	4.6	0.1	6.1	1.0	0.1	
	rear	4.7	0.15	6.4	1.0		0.15
average						0.38	0.21

Table 2.15: Nissan 16, peak sizes in normalised power spectral density

For the other fork-lift trucks the results are summarised in Appendix B, Tables

B.18 to B.20. The average values for all fork-lift trucks are summarised in Table 2.16.

Fork-lift truck	Front axle $\mu_{1,av}$	Rear axle $\mu_{2,av}$
Nissan 16	0.38	0.21
Nissan 15	0.31	0.78
Jungheinrich 16	0.69	0.86
Pimespo 25	0.47	0.33
average	0.46	0.55

Table 2.16: Ratio μ of peak sizes in normalised power spectral density

The power transmitted from the first mode and the second mode varies over a wide range. At the front axle the ratio varies from $\mu_{1,av} = 0.31$ to $\mu_{1,av} = 0.69$ and at the rear axle from $\mu_{2,av} = 0.21$ to $\mu_{2,av} = 0.88$. However, the average value is about 0.5, which will be used as the ratio between the front axle and rear axle amplitudes in the proposed load model according to Equation 2.42:

$$\mu_1 = \mu_2 = \mu_{av} = 0.50 \quad (2.58)$$

2.7.5 Correlation between surface roughness and accelerations

The experiments were performed on three different surfaces: smooth concrete indoors, herringbone sett paving and tarmac outdoors. It should be determined whether the surface had an influence on the accelerations. If the excitation model (see Section 2.7.3.2) is a good approximation of the real case, a rougher surface (bigger bumps) should lead to higher accelerations.

To analyse the influence of the surface on the vertical accelerations the envelope functions of the amplitudes were compared: a constant difference of $D_{av} = 1.0 \text{ m/s}^2$ ($D_{95\%} = 2.0 \text{ m/s}^2$) was found (see Section 2.7.3.3).

A detailed analysis of the effects of different surfaces was not pursued, because

the surfaces of the relevant floors are either concrete, coated concrete or screed, all of which have a similar roughness and will have been cast with a high accuracy, so that imperfections are generally small. For example DIN 18202 (2005) defines for a cast floor surface, ready to use, a maximum sag of 4 mm (3 mm if higher standards are set) if the reference points are 1.00 m apart and 2 mm (1 mm) if 0.1 m apart.

2.8 Load model of the fork-lift truck

2.8.1 Summary of the results found in the experiments

The load model can be set up independent of the driving direction. Driving forwards or backwards does not change the accelerations in terms of their frequencies or their amplitudes. The modal analysis showed that the frequencies found experimentally are the natural frequencies of the fork-lift trucks.

The amplitudes change linearly with the velocity (due to the linear envelope function, the mechanic relation is quadratic). The surface driven on has an influence on the amplitudes of the accelerations, but it can be assumed that the surface inside the buildings investigated (and to be analysed in the future) fulfil the condition “smooth”. Thus the average of the linear regressions is taken only from configurations “indoors”.

The cross-correlation of the accelerations of the front and the rear axle gives the phase angle between the axles: the frequency related to the in-phase mode showed, as would be expected, a zero phase angle, while the frequency related to the anti-phase mode showed the expected phase angle of π .

Hence the load model can be set up as proposed in Section 2.4.

2.8.2 Dynamic load model of a fork-lift truck

The load model is the product of a mass matrix and an acceleration vector:

$$\begin{aligned}
 \text{Force} &= \text{Mass matrix} \cdot \text{Acceleration function} \\
 \begin{bmatrix} F_f(t, v) \\ F_r(t, v) \end{bmatrix} &= \frac{1}{L_{WB}^2} \begin{bmatrix} (m_{tot}L_r^2 + J_{tot}) & (m_{tot}L_fL_r - J_{tot}) \\ (m_{tot}L_fL_r - J_{tot}) & (m_{tot}L_f^2 + J_{tot}) \end{bmatrix} \cdot \begin{bmatrix} a_f(t, v) \\ a_r(t, v) \end{bmatrix}
 \end{aligned} \tag{2.59}$$

The mass matrix was derived in Section 2.4, Equation 2.37.

The acceleration function was found experimentally and validated against mathematical models of one and three degrees of freedom. The acceleration function is a product of an amplitude function and a periodic function as proposed in Section 2.4, Equation 2.42:

$$\begin{aligned}
 \text{Acceleration} &= \text{Amplitude} \cdot \text{Periodic function} \\
 \begin{bmatrix} a_f(t, v) \\ a_r(t, v) \end{bmatrix} &= A_{av}(v) \frac{1}{1 + \mu} \cdot \begin{bmatrix} \mu \sin(2\pi f_1 t) & + \sin(2\pi f_2 t) \\ \mu \sin(2\pi f_1 t + \pi) & + \sin(2\pi f_2 t) \end{bmatrix}
 \end{aligned} \tag{2.60}$$

$$\text{with} \quad A_{av}(v) = 1.2v + 0.4 \tag{2.61}$$

The amplitude function is set up as an envelope function (of average accelerations) and the averaged ratio of amplitudes of the natural frequencies is taken for the load model. The periodic function uses two natural frequencies which can be found alternatively as the eigen-frequencies of a three-degree-of-freedom model. They can be tuned to the eigen-frequencies of the structure by changing the payload and the equivalent spring constant within the given limits (load capacity and range of spring constant).

For example, in the experiments the Nissan 16 carried a payload of 600 kg, which leads to the eigen-frequencies found in the modal analysis of $f_1 = 3.3$ Hz and $f_2 = 6.3$ Hz.

With the constant phase angles $\varphi_1 = \pi$, $\varphi_2 = 0$ and the amplitude ratio $\mu = 0.5$ the excitation function (of mean accelerations) can be written as:

$$\begin{aligned} a_f(t, v) &= \frac{A_{av}(v)}{1 + \mu} [\mu \sin(2\pi f_1 t) + \sin(2\pi f_2 t)] \\ &= \frac{1.2v + 0.4}{1 + 0.5} [0.5 \sin(2\pi \cdot 3.3 t) + \sin(2\pi \cdot 6.3 t)] \end{aligned} \quad (2.62)$$

$$\begin{aligned} a_r(t, v) &= \frac{A_{av}(v)}{1 + \mu} [\mu \sin(2\pi f_1 t + \pi) + \sin(2\pi f_2 t)] \\ &= \frac{1.2v + 0.4}{1 + 0.5} [0.5 \sin(2\pi \cdot 3.3 t + \pi) + \sin(2\pi \cdot 6.3 t)] \end{aligned} \quad (2.63)$$

which is tied to the specifications of the Nissan 16 with a payload of $m_{pl} = 600$ kg, indoors, giving the load model as:

$$\begin{aligned} \begin{bmatrix} F_f(t, v) \\ F_r(t, v) \end{bmatrix} &= \frac{1}{L_{WB}^2} \begin{bmatrix} (m_{tot} L_r^2 + J) & (m_{tot} L_f L_r - J) \\ (m_{tot} L_f L_r - J) & (m_{tot} L_f^2 + J) \end{bmatrix} \cdot \begin{bmatrix} a_f(t, v) \\ a_r(t, v) \end{bmatrix} \\ &= \frac{1}{1.395^2} \begin{bmatrix} (3620 \times 0.716^2 + 3200) & (3620 \times 0.679 \times 0.716 - 3200) \\ (3620 \times 0.679 \times 0.716 - 3200) & (3620 \times 0.679^2 + 3200) \end{bmatrix} \\ &\quad \cdot \frac{1.2v + 0.4}{1.5} \begin{bmatrix} 0.5 \sin(2\pi \cdot 3.3 t) & + \sin(2\pi \cdot 6.3 t) \\ 0.5 \sin(2\pi \cdot 3.3 t + \pi) & + \sin(2\pi \cdot 6.3 t) \end{bmatrix} \end{aligned} \quad (2.64)$$

However, while the vibration serviceability of a floor has to be verified during the design process of a building, the specific fork-lift truck that will be used in the building is usually not known. Consequently, a more general model, independent of manufacturer, is desirable.

2.8.3 Generalised load models of general fork-lift trucks

From a comparison of the models of several manufacturers, it can be seen that most values of the specifications of fork-lift trucks do not vary significantly for a specific category of load capacity, see Table 2.5 and Beha (1989). They can be averaged for a general model: see Table 2.17.

2.8 Load model of the fork-lift truck

Capacity		1000	1600	2500	6000	kg
Wheelbase	L_{WB}	1.000	1.400	1.500	2.000	m
Centre of gravity* to						
... front axle	$L_{f,npl}$	0.560	0.744	0.825	1.470	m
... rear axle	$L_{r,npl}$	0.440	0.656	0.675	0.530	m
... centre of payload**	$COG_{pl} - COG_{flt}$	1.200	1.500	1.800	2.200	m
Centre of gravity*** to						
... front axle	$L_{f,pl}$	0.170	0.205	0.185	0.340	m
... rear axle	$L_{r,pl}$	0.830	1.195	1.315	1.660	m
Mass moment of inertia	J	2500	3200	5000	10000	kg m ²

* of fork-lift truck without a payload

** for payload smaller than the capacity

*** of fork-lift truck with a payload = capacity

Table 2.17: Specifications for general load model

These values lead to the modal-frequencies for two load cases: “no payload carried” and “payload = capacity carried”, which are summarised in Table 2.18 and thus to the general load model as proposed in Section 2.4.2. Table 2.17 gives the distance from the centre of gravity of the fork-lift truck (without a payload) to the centre of gravity of the given payload. This distance may be used to calculate the modal frequencies for payloads other than the full capacity.

Capacity		Total mass	Mode 1	Mode 2	Static load	
[kg]		m	f_1	f_2	front	rear
		[kg]	[Hz]	[Hz]	[kN]	[kN]
1000	without payload:	2500	3.8	6.4	11.0	14.0
	with payload	3500	2.0	5.3	29.0	6.0
1600	without payload:	3200	4.8	5.8	15.0	17.0
	with payload	4800	2.6	5.5	41.0	7.0
2500	without payload:	4000	4.2	5.1	18.0	22.0
	with payload	6500	1.8	5.0	57.0	8.0
6000	without payload:	7500	3.1	3.4	20.0	55.0
	with payload	13500	1.4	3.2	112.0	23.0

Table 2.18: Modal frequencies and static loads for general load model

The total load of a fork-lift truck applied to the floor is summarised as:

$$F_{f,total} = F_{f,static} + F_f(t, v) \quad (2.65)$$

$$F_{r,total} = F_{r,static} + F_r(t, v) \quad (2.66)$$

In an analysis of the vibration serviceability of a floor system the response to the fork-lift truck should always be tested for both cases: carrying a payload and carrying no payload, since the eigen-frequencies of the fork-lift truck change with the payload.

Furthermore, as mentioned earlier, the equivalent spring constant of the wheels can vary from model to model and thus change the eigen-frequencies. Therefore, if the eigen-frequencies of the floor are found to be close to the frequencies given in Table 2.18, the option should be considered of changing the frequencies in the load model to the eigen-frequencies of the floor to carry out a worst-case analysis.

2.8.4 Final remarks on the dynamic load model

Realistic model of a vehicle's suspension In the literature one can find general agreement that, in order to model a vehicle's suspension realistically, a white noise vibration component has to be included [e.g. Lin (2006)]. However, this component will not be included in the proposed load model for two reasons.

The first reason is that it should be easy to implement the model in a finite element programme so that it can become a part of the standard design procedure without there being too demanding characteristics and difficulties to model.

The second reason is that the proposed model is a worst-case model. This model concentrates the total acceleration in only two frequency components for the excitation. The total acceleration was found experimentally and as such is known as the upper boundary of accelerations. If a white-noise component were to be introduced the total acceleration would have to be split up among three components and as such the accelerations related to the two excitation frequencies would be reduced.

Chapter 3

Numerical simulations of vibrations of a precast and partially prestressed (sample) floor system

Note: The floor system investigated here is a sample structure. It is not the structure investigated in the field test. However, this sample structure allows the methods of the analysis to be explained and makes it easy for the results to be checked.

In Chapter 4 will be explained a field test and its simulation in Sofistik, which will verify both models of the fork-lift truck and of the floor system. However, the development of the FE-model of the floor system is chosen for the following reasons:

- A single double-tee element is introduced that acts as a simple supported beam, which is used for benchmarking of the results calculated with the FE-program chosen for the simulations.
- It shows how the three dimensional floor system can be derived from the single element.
- It allows to focus on a “standard” system without the particularities of the system of the field test.

- A slender system, well within in the limits of the design standards, can be presented that is close to the limits of acceptable vibrations.

3.1 Executive summary

This chapter describes the development of a finite-element model of the composite floor system, explains the loadcases of interest and demonstrates the validity of the results.

This chapter is divided into two major parts: the first part analyses one single TT-element with its cast in-situ concrete topping in two dimensions. The second part investigates a floor system consisting of 3 by 3 elements and the topping in all three dimensions. The dynamic loading from a fork-lift truck moving over the floor is considered.

The program package SOFiSTiK was used for the FE-analysis. The analysis is divided into two tasks: a static and a dynamic analysis of the structure.

Static analysis The static analysis of the floor system determines the stiffness at each construction stage and the resulting deformations of the floor. All construction stages consider the effects of the previous construction stages and their duration:

1. Production of the precast double-tee element including prestressing
2. Storage and transport prior to assembly
3. Assembly of the structure on site using precast main beams
4. Casting of in-situ concrete topping
5. Service

All construction stages are simulated in SOFiSTiK and the results of the analysis are compared with analytical and numerical calculations. A good agreement is found.

Dynamic analysis The dynamic analysis is divided into two tasks: a modal analysis to determine the eigen-frequencies and the mode shapes, and a (linear) time-stepping analysis, which calculated the floor's response to moving loads.

The loading is modelled in two different ways: a moving load of constant magnitude and a time-varying moving load following the load model developed in Chapter 2.

As expected, the response of the floor is considerably larger if the dynamic load model is applied: deformations increase by 10% compared to those caused by the constant load moving over the structure (but these are still smaller than the deformation under the static load of a fork-lift truck increased by the DLF). The accelerations reach values which give rise to concern as to whether the vibration serviceability is still satisfied. The peak accelerations are $a_{peak} = 0.92 \text{ m/s}^2$ ($\hat{=} 10\% \text{ g}$), and the RMS acceleration over a time period of 10 seconds is $a_{RMS,10} = 0.48 \text{ m/s}^2 \approx a_{RMS,DIN4150} = 0.5 \text{ m/s}^2$. In comparison the accelerations caused by the moving constant force are insignificant (smaller than the resolution in SOFiSTiK).

3.2 Preliminary observations

The main properties that influence the response of a floor system to dynamic loading are the system's mass and stiffness (and consequently its natural frequencies) and its damping behaviour.

The structure's stiffness can be modelled easily in an FE-program which supplies the materials with their properties for a linear analysis. More sophisticated is the realistic modelling of the influence of cracks on the stiffness as well as the time-dependent effects which are known to be of significant size in prestressed structures (EC 2, 2004). Both these effects lead to non-linear static behaviour, which has to be considered in the design of prestressed structures. It follows from this that the standard design procedure is a good starting point for the investigation of the dynamic response to fork-lift truck traffic, because it will give a good estimate of the in-service properties of the system.

Chen (1999) showed the importance of damping in the linear FE-analysis of double-

tee elements. As part of the study presented here, an investigation of the joint between the precast and the cast in-situ concrete for additional damping was conducted. A preliminary test was carried out to determine whether a more detailed investigation, which would have resulted in significant costs, was justified. Two types of specimen were cast in two sections to create a joint in the specimen. Each specimen was loaded cyclically for a defined number of times. During the cyclic loading their deformability and hysteresis was measured and after cyclic loading they were tested for their ultimate strength. It was assumed that cyclic loading causes micro cracks to form and the differential movement at the cracks would increase damping. This should be detectable by a change in stiffness, an increase in energy dissipated during a loading cycle and a decrease in ultimate strength. However, the results did not indicate significant damping in the joint and therefore published values for concrete and prestressed concrete structures will be used. The investigation of the joint is summarised in Appendix A.

Palamas et al. (1985) observed in their investigation of DLF-values that the shape of deformation of a bridge had an important influence on the response to a moving 1-dof-system. If the deformation of the structure is similar to its mode shape of vibration, a significant amplification of the dynamic load from a vehicle crossing is to be expected. This observation proves the necessity of realistic modelling over the lifetime of a structure, including the various construction stages, because all of them will influence the deformations under service load.

Hamed and Frostig (2004) showed the influence of cracks on the natural frequencies of prestressed beams when they investigated a load travelling along a beam. In contrast, this project investigates floor systems on which the fork-lift truck could be driving in any direction. From this it follows that the FE-model has to be set up in three dimensions to cover the fork-lift truck travelling both parallel and transverse to the span direction of the double-tee elements.

3.3 Finite element program

This section explains the choice of the FE-program for the analysis of the system. The required capabilities of the FE-program were:

- Non-linear, time-dependent static analysis of the structure to determine the stiffness:
 - Material model of concrete that incorporates cracking in tension, creep and shrinkage
 - Material model of prestressing steel that incorporates relaxation
- Modelling of staged construction:
 - Change of static system
 - Change of stiffness (cast of topping on site)
 - Different ages of construction parts (precast elements and cast in-situ concrete)
- Dynamic analysis:
 - Calculation of eigen-frequencies and mode shapes
 - Loading variable in time and location (moving dynamic loads)
 - Time-step analysis of floor response to moving loads

3.3.1 SAP2000 and ABAQUS

3.3.1.1 SAP2000

SAP2000 is a finite-element program for the design of civil engineering structures and the analysis of their dynamic behaviour, which seemed to satisfy the requirements. However, it was quickly discovered that SAP2000 cannot simulate the cracked conditions of a prestressed concrete structure without engaging in an enormous amount of

detailed element entries. Thus it was decided to seek a general finite-element program able to simulate cracked concrete in a dynamic analysis more easily.

3.3.1.2 ABAQUS 6-5.1

ABAQUS is widely used for finite-element simulations within the Department of Engineering Science at the University of Oxford. It has a library material option ‘concrete’ and can model dynamic processes. The concrete option is capable of non-linear behaviour in compression and the total loss of stiffness in tension after crack formation. When ABAQUS was adopted for the simulation two major problems emerged.

Time to process a job The concrete option in ABAQUS can only be used in conjunction with three-dimensional continuum elements, in which reinforcement is embedded as separate layer elements. To model a crack the concrete option deletes a node of an (concrete) element if its strain exceeds a defined limit. If the element is too big, this leads to stability problems in the calculation process, due to the large change in the stiffness of the structure. To overcome these problems and to get accurate results, the element size and the load increment from step to step in the iteration process have to be “small”. A T-beam (half of a double-tee element) required about 10,000 elements to get accurate results, which took about nine hours on a 3.0 GHz Pentium 4 - PC with 1024 MB RAM, just to calculate the eigen-frequencies in the uncracked and the fully cracked state.

Time-dependent material properties Furthermore the concrete option has not incorporated the effects of creep and shrinkage. However, these effects are known to be significant in prestressed systems. They can match the magnitude of deformations due to external load (EC 2, 2004). Precast structures are particularly prone to creep and shrinkage due to the very young age of the concrete when the prestressing force is applied.

An attempt was made to program a “user-material” in ABAQUS, which would simulate all the desired properties of concrete, but this was given up after a few months.

In this time, a stable model was programmed to model the effects of creep and shrinkage of a single element in compression, but it was unstable in a larger system of several elements or in tension.

A more specialised program for the analysis of civil engineering structures was sought.

3.3.2 SOFiSTiK

The program package SOFiSTiK was chosen because of its capability in modelling concrete behaviour and its capacities for carrying out dynamic analyses of complex structures. It incorporates a concrete model that is capable not only of cracking in tension but also of simulating the time-dependent effects of creep and shrinkage. Furthermore, it can simulate the double-tee elements as “beam” elements, whose behaviour is determined by a calculated moment-curvature relation instead of a stress-strain relation. If desired, the moment-curvature-relation takes into account the effects of tension-stiffening.

This method of analysing the structure is far more efficient, and calculated the results of the previously mentioned sample system in about thirty seconds. The method is so efficient because the moment from the external loading at each point is known and the necessary internal curvature is known from the calculated moment-curvature-relation. Thus the deflected shape and an equivalent stiffness can be calculated by integrating the curvature along the beam. Iterations may be necessary if effects of second-order theory and creep (which is stress-dependent) are to be accounted for.

While SOFiSTiK is a design tool, it is possible to pre-define (and fix) the amount of reinforcement in the cross-sections so that the design module, which has to be run to determine the moment-curvature-relation, does not change the reinforcement: exactly the same cross-section properties can be modelled for different external loadings.

The advantages of SOFiSTiK over the other programs are clear:

1. Realistic concrete model including time-dependent effects

2. Exact cross-section definition including reinforcement and prestressing
3. Several options to model dynamic loading available
4. Efficient solver including time-step analysis for dynamic processes is at the core of the program¹.

3.4 Benchmark testing

3.4.1 Sample structure (two-dimensional)

To verify the program SOFiSTiK, a double-tee element was analysed. To simplify the calculation, a simply supported beam was analysed. While the time-dependent effects were incorporated into the FE-model, they were neglected for the verification, because the methods to verify the FE-calculation were not capable to account for these effects. However, the variables of time-dependent effects and their calculation are explained here as well as part of the general description of the FE-model set up.

The geometry of the system is shown in Figure [3.1] and the main properties are summarised in Table 3.1.

The transmission of the prestressing force to the precast concrete was modelled as a quadratic function over the length of the transmission zone following EC 2 (1991). A loss of prestressing force over time due to relaxation does not need to be considered if prestressing steel with very low relaxation is used (EC 2, 1991), which was assumed here because it is normally used for precast elements to keep the losses of prestress as low as possible. This has clear economic benefits since less prestressing is needed.

The minimum reinforcement according to EC 2 (1991) was sufficient for the precast element. A higher level of shear reinforcement was required only in the transmission zones. The reinforcement of the shear joint between the precast element and the cast in-situ topping was governed by the load of a fork-lift truck. The same would have

¹Even a non-linear dynamic analysis is possible

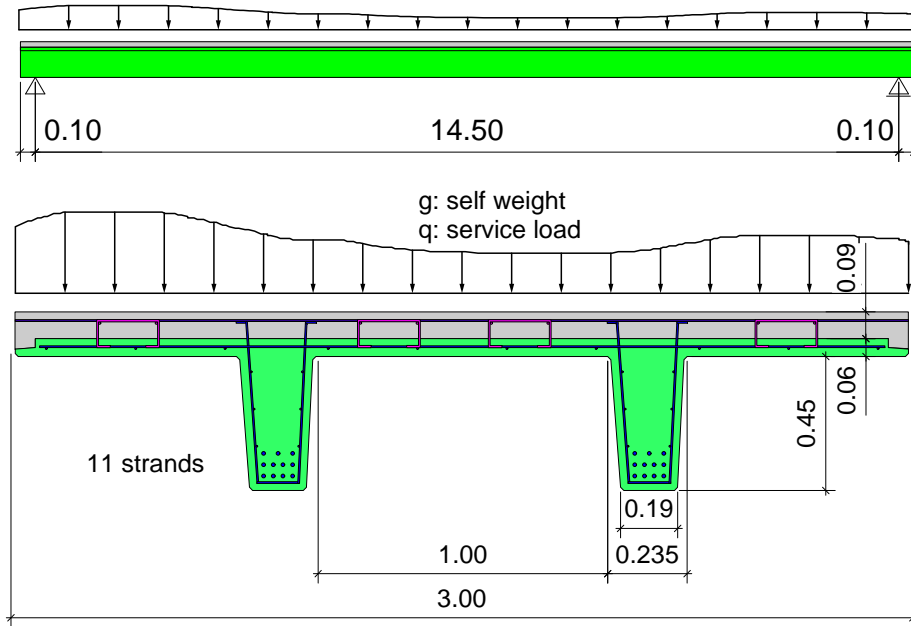


Figure 3.1: System and cross-section of double-tee element

Description	Symbol	Value
Geometry:		
Spanwidth	L	14.50 m
Width of element	W_{flange}	3.00 m
Height of web	H_{web}	0.45 m
Width of web (bottom)	B_{bottom}	0.19 m
Gradient of web's side		1:20
Height of precast slab	H_{pc}	0.06 m
Height of cast in-situ topping	H_{ci}	0.09 m
Cross-section area of a strand	A_p	93 mm ²
Number of strands per web	no_p	11
Loading:		
Selfweight precast concrete	$g_{1,pc}$	4.65 kN/m _{web}
Selfweight topping	$g_{1,ci}$	2.25 kN/m ²
Selfweight screed	g_2	0.25 kN/m ²
Service load	q	5.0 kN/m ²
Reduction factor service load	ψ	0.8
Fork-lift truck $m_{ft} = 3.5$ t	F_{axle}	30.0 kN
Dynamic amplification factor	ϕ	1.4
Material (according to EC 2 (1991)):		
Precast concrete	C50/60	
Cast in-situ concrete	C30/37	
Reinforcement steel	S500	
Prestressing steel	PS1570/1770	

Table 3.1: Geometry, loading and material of sample structure

been true for the transverse reinforcement of the topping. However, transverse action was not considered in this benchmark test.

In Figure [3.2] the moment-curvature relation for the cross-section of the sample structure is shown. The curvature was zero for a moment of about 420 kNm which was about equal to the midspan moment under selfweight ($M_g=440$ kNm), which meant that the element had still a small hog under the dead load. (This was because most of the length had a moment smaller than 420 kNm and thus a negative curvature. Only if time-dependent effects were considered would a sag appear under dead load.)

Figure [3.3] shows the stress distribution in the composite cross-section. The discontinuity in the slab (compression zone) due to the staged construction is noticeable, as is the high tensile stress of the prestressed strands.

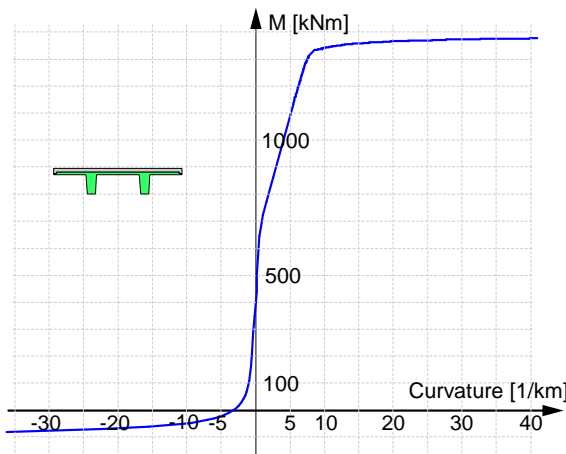


Figure 3.2: Moment-curvature relation for sample structure

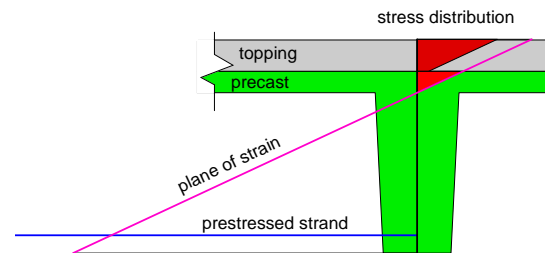


Figure 3.3: Stress distribution in cross-section

To model the behaviour over the lifetime of the double-tee element realistically, the various loadings and time-dependent effects had to be considered.

Creep is dependent on the stress conditions in the cross-section. The stress conditions can change in an infinite number of ways throughout the lifetime of the element, thus making it impossible to model them “correctly”. However, the effects are assessable if some simplifications are made: in its lifetime the precast element has two major phases. The first phase is the precast element from striking the formwork to casting the topping and the second phase is the composite cross-section in service conditions.

In compliance with EC 2 (2004) (and its earlier version EC 2 (1991)) the second phase is modelled with a reduced service load (but constant throughout the lifetime). The two phases were be implemented as:

1. The precast element (pc) from the time of production until assembled on site. The duration from casting to assembly was assumed to be $t_1 = 30$ days.
2. The composite cross-section (pc+ci) from the time of casting the topping (t_1) until the end of its lifetime. After construction a period of 150 days was assumed in which no service loading was present (t_2). The reduction of the service load was $\psi_1 = 0.8$ of the maximum distributed service load, as defined in EC 2 (2004) for storage facilities. Hence 80% of the service load was assumed to be present over the lifetime, which was set to $t_\infty = 70$ years in compliance with EC 2. The age difference between the precast concrete and the cast in-situ concrete was taken into account.

The effects of shrinkage due to the drying concrete in these phases were also taken into account. In SOFiSTiK, the time-dependent effects of creep and shrinkage are calculated automatically by means of a set of functions, which use environmental conditions, material and geometric properties as variables, as set out in EC 2. The environmental conditions considered for the calculation are summarised in Table 3.2.

Time	Environmental conditions
$t_0 - t_1$: 30 days,	20° C, 60 % rel. humidity
$t_1 - t_2$: 180 days,	20° C, 50 % rel. humidity
$t_2 - t_\infty$: 70 years,	20° C, 60 % rel. humidity

Table 3.2: Environmental conditions in SOFiSTiK calculation

The floor loading was divided into seven loadcases, acting in various combinations at different stages of the lifetime. In detail the loadcases were:

LC 1: Selfweight of the precast concrete element

The selfweight acted on the structure throughout the lifetime, from striking the formwork through storage in the precast plant to service in the structure.

LC 2: Selfweight of the cast in-situ topping

The topping started to act on the precast element when it was cast. After curing the composite cross-section with its higher stiffness was ready for service.

LC 3: Selfweight of non-structural screed

After the topping was cured a non-structural screed was applied to the composite structure.

LC 4: Service load, including the “quasi-static” fork-lift truck

The service load acted on the composite structure. The weight of a fork-lift truck was applied with its DLF.

LC 5: Prestressing force

The prestressing force was applied to the precast element when the formwork was struck. Due to the stressing bed method the prestressing steel was in immediate bond with the precast element.

LC 6: Creep and shrinkage of the prestressed precast element

After striking the formwork the selfweight and the prestressing force acted on the cross-section and thus lead to creep, and independently the effects of shrinkage developed.

LC 7: Creep and shrinkage of the complete assemblage

Acted on the composite cross-section during the service-lifetime.

The load cases acted in various time-dependent combinations on the different static systems that resulted from the construction method. The load cases, their combinations, durations and which cross-section bears the load are summarised in Table 3.3.

LC	Description	Acting on	Time	Comment
1	Selfweight precast concrete element			
2	Selfweight cast in-situ topping			
3	Selfweight non-structural screed			
4	Service load (including “static” fork-lift truck)			
5	Prestressing force			
6	Creep and shrinkage of precast element (t_0 to t_1)			
7	Creep and shrinkage of assemblage (t_2 to t_∞)			
Combinations:				
11	= 1+5	pc	t_0	
12	= 11+6	pc	t_0-t_1	
13	= 12+2	pc	t_1	
20	= 13	pc+ci	t_1	maximum stiffness
21	= 13+3+4	pc+ci	t_2-t_∞	
22	= 21+7	pc+ci	t_2-t_∞	minimum stiffness
Only for verification:				
110	= 11	pc	t_0	
130	= 110+2	pc	t_0	
140	= 130+3	pc+ci	t_0	
150	= 140+4	pc+ci	t_0	

Table 3.3: Load cases in SOFiSTiK calculation

3.4.1.1 Simplifications

The results obtained with SOFiSTiK were compared not only with the results of other software packages, but also with simplified manual calculations carried out in a spreadsheet. For a manual estimate two major simplifications were necessary:

Young’s modulus The composite cross-section consisted of two different concretes with different Young’s moduli.

The methods employed to calculate the eigen-frequencies are valid for systems with a constant Young’s modulus. To account for the different Young’s moduli in the composite cross-section, a reduction of the effective stiffness according to EC 4 (2004) was undertaken: the overall second moment of area of each part was multiplied by a factor that gave the ratio of a Young’s modulus to the reference Young’s modulus:

$$n_C = \frac{E_{C30/37}}{E_{C50/60}} = \frac{32000}{37000} = 0.865. \text{ The same was done for the reinforcing and prestressing}$$

steel: $n_S = \frac{E_S}{E_{C50/60}} = \frac{200000}{37000} = 5.405$, which was in fact an increase in stiffness.

This procedure reduced the cross-section to one “representive” Young’s modulus and still took the different material properties into account.

Aged concrete As mentioned before, the methods used to verify the deformations and eigen-frequencies were not capable of simulating the effects caused by creep and shrinkage. Thus, only the deformations and frequencies at a young age were considered for the verification of the results from SOFiSTiK. This meant, for the verification, effects from creep and shrinkage were disregarded: load cases 110 to 150 (see Table 3.3) were therefore calculated.

The final model considered the time-dependent effects and it was assumed that those are realistic because SOFiSTiK has shown that its algorithm calculates the effects according to the standard EC 2 (1991). It was assumed that if the static effects were considered realistically the effects on the dynamic behaviour will also be realistic because the change in stiffness was the major effect.

3.4.2 Verification of static states

The results from the analysis with SOFiSTiK were compared with results obtained with the programs “ABaS” and “INCA2”¹. INCA calculates the moment-curvature for arbitrary cross-sections and is capable of dealing with prestressing forces, tension stiffening and the effects of a staged construction. ABaS is a static programme that calculates the response of beam-structures with non-linear moment-curvatures (as calculated with INCA) to arbitrary loadings.

The authors of ABaS and INCA have shown the accuracy of results obtained with their programmes, see Busjaeger and Quast (1990), Los and Quast (2000) and Pfeiffer (2004). Therefore, these results were taken as a benchmark for the results computed with SOFiSTiK. For comparison, the results obtained earlier by ABAQUS and a manual calculation carried out in a spreadsheet are shown as well.

¹Both programs were developed at TUHH, Germany, and detailed information on the programs may be obtained online there: www.tu-harburg.de/mb

Load case	Mid-span deflection [mm]			
	SOFiSTiK	ABaS	ABAQUS	Excel
110: pc-element installed	-12	-15	-9	-12
130: + weight of wet topping	-4	-5	-1	-2
150: full load on composite structure	13	16	19	15

Table 3.4: Comparison of deflections (sample structure)

The deformations calculated with SOFiSTiK were consistently 20% smaller than those calculated with ABaS. This meant the structure was stiffer in SOFiSTiK than predicted with INCA and ABaS. However, the difference was small enough to assume that the results from SOFiSTiK are trustworthy. If the eigen-frequencies are higher than predicted, the presumption of a stiffer system is confirmed. The results from ABAQUS seemed to be shifted downwards compared with ABaS.

3.4.3 Verification of eigen-frequencies

The eigen-frequencies calculated with SOFiSTiK were compared with the results of the ABAQUS simulation and manual calculations in a spreadsheet.

SOFiSTiK provides two methods for calculating the eigen-frequencies: the direct method according to Lanczos and the simultaneous inverse vector iteration. Here, the Lanczos method was chosen as it is faster than the inverse vector iteration. A huge number of eigen-frequencies is calculated and then filtered for the ones of interest. Of interest were frequencies below 15 Hz as the excitation frequencies of the fork-lift trucks are usually below 7 Hz. Further filtering eliminated those frequencies whose mode-shapes are physically impossible and originate only from the set-up of the FE-model: a beam element was used to model the cross-section, which allowed for the torsional modes that were not expected in a floor system due to a continuous topping in transverse span direction.

For the comparison the eigen-frequencies were calculated manually for the simple supported beam as follows.

Uncracked conditions In the elastic case (uncracked, young concrete) a model using free vibrations of an Euler-Bernoulli beam with distributed mass was chosen:

$$(EIu'')'' + m\ddot{u} = 0 \tag{3.1}$$

$$\Rightarrow \omega_n = \pi^2 \sqrt{\frac{EI}{mL^4}} \tag{3.2}$$

where EI is the stiffness of the beam, m is mass per unit length and L the length of the beam. For three-dimensional floor systems this approach assumes that the structural behaviour and thus the vibration behaviour is only longitudinal. In particular all adjacent beam-slab systems behave similarly and do not influence the vibration of the observed element. For the precast structure this assumption introduced only a minor error and especially for the first mode this was negligible.

Cracked conditions In the loaded case (still without time-dependent effects) the eigen-frequency was calculated with the ‘‘Improved Rayleigh method’’¹.

Firstly the ‘‘normal’’ ‘‘Rayleigh’s method’’ of estimating the eigen-frequency is explained: Rayleigh’s method is based on assumed modes. Rayleigh observed that for undamped free vibrations the motion is a simple harmonic motion, which can be written in the form of Equation 3.3 (Craig, 1981). Furthermore, at any moment of a vibration the sum of potential energy and kinetic energy is constant (conservation of energy, damping is neglected). Thus the maximum kinetic energy is equal to the maximum potential energy. From this, the eigen-frequency is calculated. It can be shown that this estimate is always an upper boundary of the natural frequency.

If the general shape function is expressed as:

$$v(x, t) = \Psi(x)Z_0 \sin \omega t \tag{3.3}$$

¹The advantage of the Rayleigh method for this application is that the static deflection is a good estimate of the first mode. The estimate can be calculated directly from the static deflection without determining the variable stiffness along the beam. The static deflection can be derived from the moment-curvature-relation by integrating the curvature (known from the internal moment’s distribution) over the length of the beam.

where $\Psi(x)$ is a displaced shape and Z_0 an arbitrary reference amplitude¹, this leads to maximum potential energy (V_{max}) and maximum kinetic energy (T_{max}) in the form of:

$$V_{max} = \frac{1}{2} Z_0^2 \int_0^L EI(x) [\Psi''(x)]^2 dx \quad (3.4)$$

$$T_{max} = \frac{1}{2} Z_0^2 \omega^2 \int_0^L m(x) [\Psi(x)]^2 dx \quad (3.5)$$

The eigen-frequency can be extracted as:

$$\omega^2 = \frac{\int_0^L EI(x) [\Psi''(x)]^2 dx}{\int_0^L m(x) [\Psi(x)]^2 dx} \quad (3.6)$$

The accuracy of the estimates depends on the closeness of the assumed shape function of the deformation to the mode shape of the beam. However, errors in the shape function are of second order to the results, thus already giving good results for rough estimates of the deflection. Furthermore, the static deflection is already a reasonable estimate for the shape function.

The accuracy of the estimated eigen-frequency can be improved by applying an iteration called the Improved Rayleigh method, see Clough and Penzien (1975). Basically, the better the assumed shape function fits the real deformation the better the results are.

The idea of this method is to use the calculated eigen-frequency from the Rayleigh's method to compute a better shape function². With this shape function, better results of inertial forces due to the deflection are obtained and this enables the maximum potential energy to be computed more accurately. From this, an improved eigen-frequency can be calculated.

In the next step this result is used to compute an improved maximum kinetic energy, thus leading to a further improved natural frequency.

¹ Z_0 can be used to scale the shape function to desired values.

²Which can be written as $v^{(1)}(x, t) = \omega^2 \Psi^{(1)} \bar{Z}_0^{(1)}$, see Clough and Penzien (1975)

These steps may be repeated till a desired accuracy is reached, but usually the results converge very fast so that three steps are sufficient to obtain accurate results.

The bending stiffness and deflections of the cracked beam, as previously considered, were calculated with INCA and ABaS and were imported into a spreadsheet, where the iteration was carried out.

Comparison of frequencies These methods for finding the eigen-frequencies manually were only capable of finding the first mode for each condition. The second mode was calculated by considering the relation between the first and second mode as: $f_{n=2} = n^2 f_1$.

The eigen-frequencies calculated with the methods previously explained are compared with the SOFiSTiK-computed eigen-frequencies in Table 3.5.

LC	Condition	Description	Eigen-frequencies [Hz]			
			SOFiSTiK	ABAQUS	Excel, method	
140	elastic	1 st mode 	5.0	4.7	4.7	“Euler-Bernoulli”
		2 nd mode 	20.2	17.5	18.8	(= 2 ² × 4.7)
150	cracked	1 st mode 	3.9	3.5	3.2	“Rayleigh”
		2 nd mode 	15.9	15.3	12.8	(= 2 ² × 3.2)

Table 3.5: Comparison of eigen-frequencies (sample structure)

The eigen-frequencies calculated with SOFiSTiK are consistently 5-10% higher than those found in ABAQUS or estimated with “Euler-Bernoulli” or “Rayleigh”. This indicates a higher stiffness which may result from a different modelling of tension stiffening. However, a good agreement among all methods of determining the eigen-frequencies is found.

3.4.4 Conclusions of benchmark testing

The results obtained with SOFiSTiK are in good agreement with the results calculated manually or with ABAQUS. All results obtained with SOFiSTiK are based on a higher

stiffness (smaller deformations and higher eigen-frequencies) than is taken into account from INCA and there is consistency between the results obtained from the static calculation and those from the dynamic verification: if the stiffness is increased by 20% a change in the eigen-frequencies of about 5-10% is to be expected. The slightly higher stiffness can result from the (minimum) reinforcement, which is taken into account in SOFiSTiK, but not in INCA. The cross-section modelled in ABAQUS includes the minimum reinforcement, but the influence of the element size on the results may change them.

Notwithstanding these differences in stiffness the results calculated with SOFiSTiK will be considered correct in the further study, keeping in mind that the stiffness might be slightly overestimated.

3.5 Three-dimensional sample floor system

In the previous section the double-tee element was modelled as a beam in a 2-D analysis (x - z -plane). The third dimension (expansion in y -direction) was not taken into account. In order to simulate a complete floor system realistically, the third dimension has to be included to account for torsional and transverse effects. It should be mentioned that the torsional displacements are negligible compared to the flexural displacements.

The structure is extended starting from the simply supported beam. In order to take into account the response of adjacent double-tee elements to local excitation a sample floor is set up, see Figure [3.4]. The following section explains the major changes that are necessary to model the full system instead of a simple beam.

The sample floor is three double-tee elements wide and three elements long. The double-tee elements rest on the main beam corbels. They span in the x -axis direction, gravity is in the direction of the positive z -axis, and the main beams span in the y -axis direction. In total nine double-tee elements and four main beams are modelled. The columns are not modelled. Figure [3.4] also shows the path of the fork-lift truck as modelled in SOFiSTiK. The starting point is the midspan node of the middle element.

3.5 Three-dimensional sample floor system

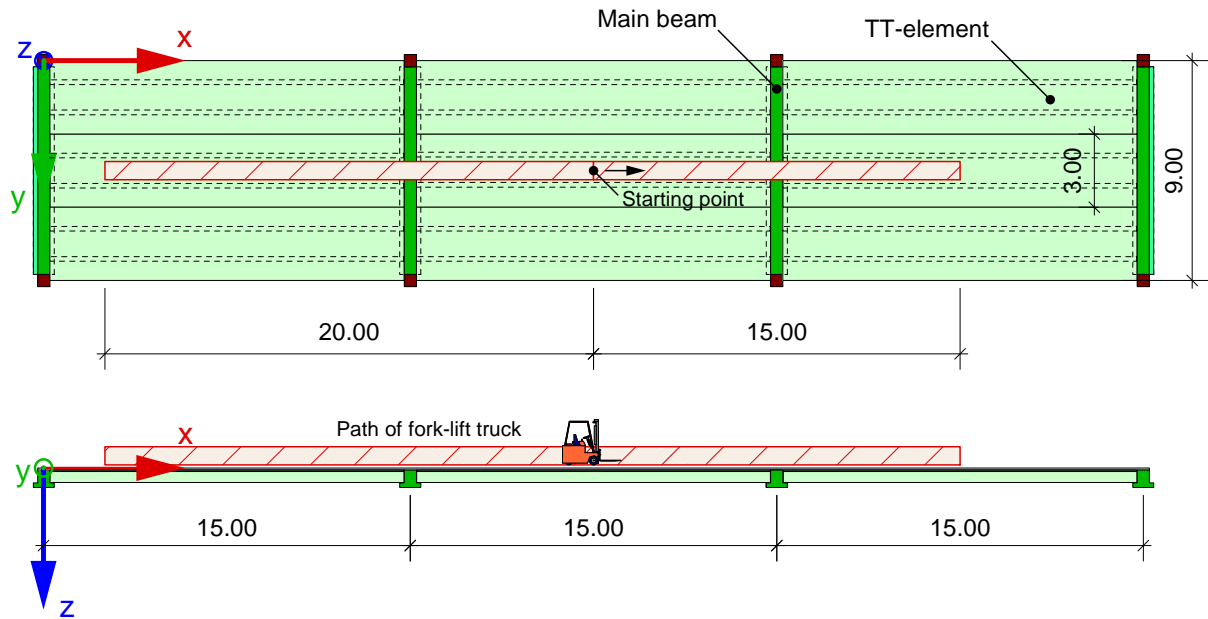


Figure 3.4: Sketch of the sample floor that is set up in SOFiSTiK

From here the truck travels 15 m in the positive x -axis direction. From there it travels 35 m in the negative x -axis direction and then reverses retracing the 35 m in the positive x -axis direction¹.

3.5.1 Special features of the floor model

Distance of TT-elements' webs: load-carrying system in x -direction Due to the production method, the core distance of the webs in one double-tee element is fixed at 1.00 m. Thus, here the axial distance of the webs is $e_1 = 1.00 + 0.235 = 1.235$ m, see Figure [3.1]. The axial distance of two adjacent elements is (for the 3.00 m wide elements) $e_2 = 3.00 - 1.235 = 1.765$ m. For an easy modelling, the double-tee element is split into four symmetrical parts: two T-beams with a slab 1.235 m wide and two slab beam elements, which have rectangular cross sections, each 0.265 m wide, see upper sketch in Figure [3.5].

¹The size of the sample floor only allows a path of the fork-lift truck parallel to the span direction of the double-tee elements. However, the methods developed and procedures used can be explained by this FE-model. The system modelled for the comparison with the field test is significantly bigger, see Chapter 4, Figure [4.11] and solving takes longer.

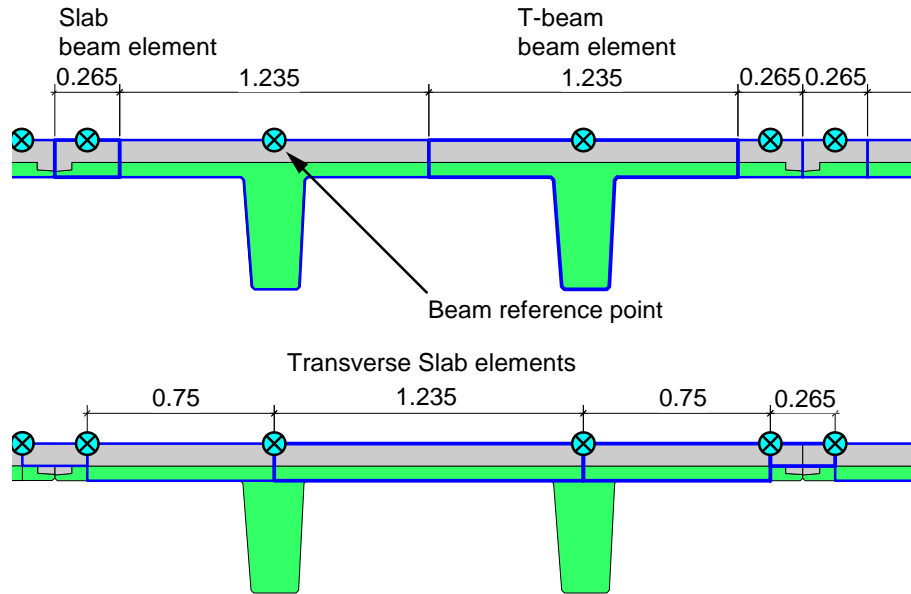


Figure 3.5: Discretisation of double-tee elements which are overlaid in SOFiSTiK

Transverse slab: load-carrying system in y -direction The floor system is modelled as a number of discrete double-tee elements (beam elements). In order to model the longitudinal stiffness realistically (including the effects of creep and shrinkage), they have to incorporate the topping. However, the topping acts as a transverse slab, but this structural behaviour cannot be modelled with the beam elements. To overcome this problem, plate elements with the thickness of the slab are introduced that have only a bending stiffness in transverse direction (EI_{xx}), i.e. the normal stiffness (EA) and the longitudinal bending stiffness (EI_{yy}) are set to zero. In the lower sketch of Figure [3.5] the transverse slab elements are shown. The two structures in Figure [3.5] are overlaid in SOFiSTiK to model the full behaviour.

At the joint between two TT-elements, the lower reinforcement (which is placed in the precast slab) cannot be continuous and an additional lower reinforcement is placed on the precast surface in the topping. Hence the internal lever arm is reduced. The slab element that spans over the joint has therefore a smaller height to account for the lower stiffness at this point, see Figure [3.6].

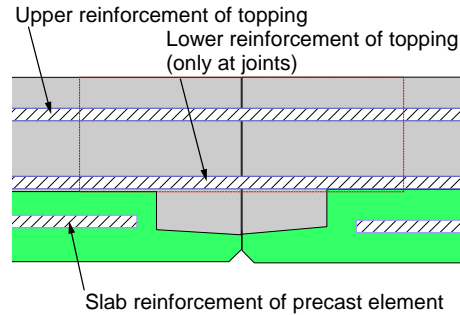


Figure 3.6: Joint between double-tee elements with reduced stiffness

Main beams The main beams are modelled according to Figure [3.7]. In the design process of the main beams the topping is not taken into account to increase the static height, because the additional shear reinforcement that is needed to transfer the forces into the topping exceeds the amount of longitudinal reinforcement that would be saved.

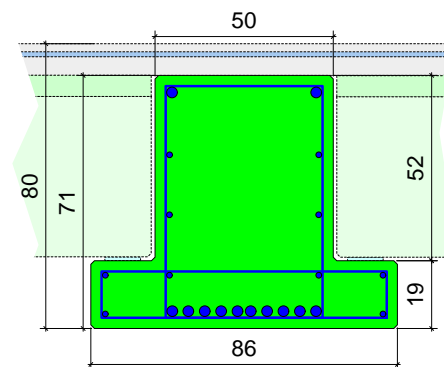


Figure 3.7: Cross-section of main beam

The finite element model is set up including the main beams for all load cases, but the first load cases are concerned only with factors that affect the precast double-tee element, see Table 3.3, load cases 11 to 13. For these load cases all nodes of the main beams are fixed to eliminate the influence of the main beam. For the load cases 21 and 22 the main beams are only supported at their ends and their bending stiffness is taken into account for the complete system.

Rubber bearings To avoid high edge pressures at the joints of precast elements (which might lead to spalling), rubber bearings are placed on the corbel of the main beam under each web of the double-tee elements and on the corbel of the column under

the main beams. Two types of rubber bearings (both from Calenberg Ingenieure) are widely used:

1. “bi-trapez” for pressures up to 10 N/mm² used for the double-tee elements and
2. “Sandwich-Q” for pressures up to 15 N/mm² used for the main beams.

To ensure economical use of the bearings, their size is chosen so that the maximum allowable stress is attained under full load of the precast element. Hence their equivalent spring constant is roughly constant in all practical cases as the deformation depends on the stress:

$$\text{bi-trapez: } C_{p,bi-trapez} = \frac{\Delta F_{service}}{\Delta z} = \frac{52.5}{0.001} \approx 50,000 \text{ kN/m} \quad (3.7)$$

$$\text{Sandwich-Q: } C_{p,Sw-Q} = \frac{\Delta F_{service}}{\Delta z} = \frac{315}{0.0025} \approx 125,000 \text{ kN/m} \quad (3.8)$$

Support conditions The double-tee element is modelled as a statically determinate beam for the construction stages until the topping is cast. The rubber bearings are modelled as a pin joint with linear spring in the vertical direction. The rotation around the x -axis (torsion) is fixed. When the topping is cast (construction completed) the rotation of the double-tee element around the y -axis is partly restrained by the continuous reinforcement in the topping across the main beams. Even more importantly the topping reduces the longitudinal movement of the elements and thus shrinkage introduces stress into the structure.

The main beams are modelled as statically determinate beams. The rubber bearings act as linear springs in the vertical direction. As for the double-tee element the torsional degree of freedom (rotation around y -axis) is fixed.

Damping properties of the structure Damping has to be included in the time-step analysis to achieve realistic accelerations and displacements. The damping properties of each part of the structure are different: the damping for the analysis is chosen to be 1% for precast elements, 3% for the cast in-situ topping and 5% for the rubber bearings.

SOFiSTiK incorporates damping in a time step analysis¹ as mass and stiffness proportional damping. Clough and Penzien (1975) stated that in the case of a non-linear analysis, the damping has to be expressed as a damping matrix. They showed that mass ($[M]$) and stiffness ($[K]$) proportional damping is a suitable approach, which can be expressed as the “Rayleigh damping matrix”. The Rayleigh damping matrix $[C]$ is defined as

$$[C] = a_0 [M] + a_1 [K] \quad (3.9)$$

Craig (1981) explained that the two constants can be defined from the relation of modal damping and modal eigen-frequencies to the proportional factors:

$$\zeta_r = \frac{1}{2} \left(\frac{a_0}{\omega_r} + a_1 \omega_r \right) \quad (3.10)$$

“by choosing ζ_r for two modes (ω_r) and solving for a_0 and a_1 ”.

SOFiSTiK provides an easy means of calculating the proportional factors²: for the calculation of the eigen-frequencies the damping of each participating part can be defined separately. Then the results of a modal analysis state not only the eigen-frequency and the modal mass, but also the modal damping $\zeta_{r,i}$, where i denotes the number of the mode.

In Sofistik the elements d_{ij} of the modal damping matrix are calculated as the product of the mode shape i times the damping matrix C times the mode shape j . This leads to modal damping matrix of which the diagonal elements are then stated as the modal damping $\zeta_{r,i}$, from which the proportional factors of the Rayleigh damping matrix are calculated.

For the program user this is convenient as it reduces the work involved in calculating the required input values manually.

¹Linear or non-linear

²Here another advantage of SOFiSTiK becomes apparent: the modular structure allows a model to be run up to the point where the eigen-frequencies are calculated, then the Rayleigh Damping factors are calculated externally of SOFiSTiK and put in the “ASE” module, that performs the time step analysis without a restart or re-calculation of other modules. Once the results are calculated, they are stored in the database of that project and only over-written if that module is run again.

3.5.2 Dynamic loading

SOFiSTiK calculates the structure’s response to dynamic loading as a time history by using the Newmark-Wilson algorithm. The parameters of the integration are variables which can be user-defined, and the default values (which are used here) correspond to the Newmark method of constant average acceleration (i.e. “Newmark’s $\beta = 1/4$ ”): this is an implicit, unconditionally stable method.

The length of the time steps can be defined to achieve a desired resolution of the motion of the fork-lift truck and the response of the floor system. See Appendix C for the source code of the time history. It is performed in the ASE¹ module “MOVING TRUCK”.

SOFiSTiK treats each time step as a load case. The step width from one “load case” to the next defines the resolution of the response. Here a resolution of 100 Hz is chosen for the analysis (which is roughly ten times the highest excitation frequency). A check was carried out to determine whether a non-linear time-step analysis² changes the results but the stresses and strains imposed by the moving truck are small and thus the change in stiffness is negligible. Hence a linear time-step analysis is performed.

3.5.2.1 Methods available of load modelling

SOFiSTiK provides various means of simulating variable (in time and location) forces on the structure. The most common are:

Constant force The first method is simple: a constant force travels at a constant velocity along a pre-defined path. No interaction with the response of the floor is considered.

Pre-defined forces This method is suitable for the proposed load model of the fork-lift truck as developed in Chapter 2. It takes into account the fact that the force is not

¹ASE = Advanced Solution Engine, the finite-element calculation core of the SOFiSTiK-package.

²In a non-linear time-history analysis SOFiSTiK updates the stiffness of the structure after each load case before the next dynamic load case is calculated.

constant but is in fact a pair of forces of variable magnitude (front axle and rear axle of the fork-lift truck) which travel over the floor.

Programming this is easy: one can program loops in SOFiSTiK which allow several load cases (one per run through the loop) to be defined. In each load case (this is a time step) the (new) position of the fork-lift truck and its forces at the front and rear axle are calculated. Then this load pair is applied while the accelerations and deformations of the previous time step are considered as the initial conditions for this time step.

3.5.2.2 Application of the fork-lift truck load

The dynamic behaviour of the fork-lift truck is applied with the values according to the presented load model. A general model with a load capacity of 1000 kg (giving a total weight of ~ 3500 kg) is chosen:

$$\begin{bmatrix} F_f(t, v) \\ F_r(t, v) \end{bmatrix} = \frac{1}{L_{WB}^2} \begin{bmatrix} (m_{tot}L_r^2 + J) & (m_{tot}L_fL_r - J) \\ (m_{tot}L_fL_r - J) & (m_{tot}L_f^2 + J) \end{bmatrix} \cdot \frac{1.2v + 0.4}{1.5} \begin{bmatrix} 0.5 \sin(2\pi f_1 t) & + \sin(2\pi f_2 t) \\ 0.5 \sin(2\pi f_1 t + \pi) & + \sin(2\pi f_2 t) \end{bmatrix} \quad (3.11)$$

With the values of the constants as defined in Table 3.6 (see Chapter 2, Section 2.8.2 for their derivation) the total load of the fork-lift truck on the floor can be calculated as:

$$F_{f,total} = F_{f,static} + F_f(t, v) \quad (3.12)$$

$$F_{r,total} = F_{r,static} + F_r(t, v) \quad (3.13)$$

The load history of this configuration is shown in Figure [3.8].

The maximum dynamic axle force applied to the structure when the fork-lift truck carries a payload of 1000 kg is $F_{f,total} = 45.9$ kN ($F_{r,total} = 24.6$ kN if no payload is

3.5 Three-dimensional sample floor system

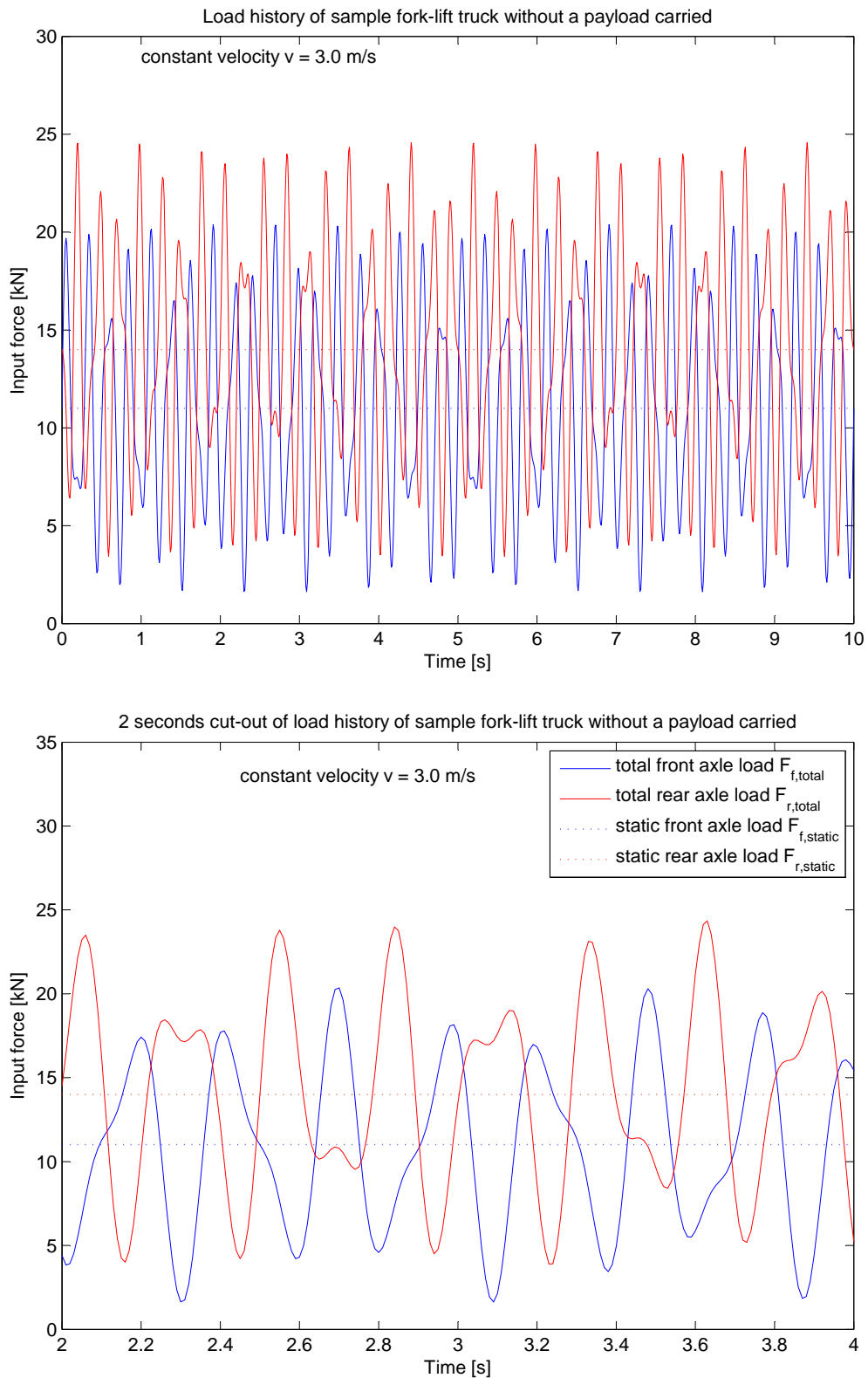


Figure 3.8: Load history of fork-lift truck without a payload carried for a constant velocity as set up for the sample floor system: 10 s window and 2 s section

3.5 Three-dimensional sample floor system

Constant	Symbol	Value	
Wheelbase	L_{WB}	1.000	m
Mass moment of inertia	J	2500	kg m ²
without payload:			
Mass	$m_{tot,npl}$	2500	kg
first mode	f_1	3.8	Hz
second mode	f_2	6.4	Hz
COG to front axle	$L_{f,npl}$	0.560	m
COG to rear axle	$L_{r,npl}$	0.440	m
static load front axle	$F_{f,static}$	11.0	kN
static load rear axle	$F_{r,static}$	14.0	kN
with payload:			
Mass	$m_{tot,pl}$	3500	kg
first mode	f_1	2.0	Hz
second mode	f_2	5.3	Hz
COG to front axle	$L_{f,pl}$	0.170	m
COG to rear axle	$L_{r,pl}$	0.830	m
static load front axle	$F_{f,static}$	29.0	kN
static load rear axle	$F_{r,static}$	6.0	kN

Table 3.6: Values for load model with 1000 kg load capacity fork-lift truck

carried). The design of the structure is carried out according to EC 1 with a quasi-static load. This design load of that truck was $F_{design} = 2.0 \times 30.0 = 60.0$ kN which is 30% above the dynamic load without taking account of any dynamic action.

The dynamic action of the fork-lift truck is divided into several modules in SOFiSTiK. This allows the position of the fork-lift truck to be easily calculated: in one module the velocity (v_{flt}) is either constant or linearly changing (uniform acceleration: positive or negative). The position [$pos(t)$] is then calculated in each module with the start position (x_0) being the end position of the previous module from:

$$pos(t) = \begin{cases} x_0 + \frac{1}{2}a_{flt}t^2 & \text{if } a_{flt} \neq 0 \text{ and thus } v_{flt} = a_{flt}t \\ x_0 + v_{flt}t & \text{if } a_{flt} = 0 \text{ and thus } v_{flt} = \text{constant} \end{cases} \quad (3.14)$$

For the analysis of the sample structure the fork-lift truck at the start of the analysis is at rest at the midspan node of the middle double-tee element, see Figure [3.4]. From that position it accelerates with $a_{flt} = 1.0$ m/s² until it reaches its maximum velocity of

$v_{ft,max} = 3.0$ m/s. Then it travels with a constant velocity ($v_{ft,max}$) until it decelerates to a halt and then reverses. The distances travelled are defined as $L_1 = 15.00$ m (split into $L_{1,1} = 4.50$ m of acceleration, $L_{1,2} = 6.00$ m of constant velocity and $L_{1,3} = 4.50$ m of deceleration), $L_2 = 35.00$ m (reverse, split into $L_{2,1} = 4.50$ m, $L_{2,2} = 26.00$ m, $L_{2,3} = 4.50$ m) and $L_3 = 35.00$ m (forwards again, split into $L_{3,1} = 4.50$ m, $L_{3,2} = 26.00$ m, $L_{3,3} = 4.50$ m), see the dotted line in Figures [3.9] to [3.17] that describes the position of the truck.

The calculation is split over nine modules of either constant (horizontal) acceleration or constant velocity of the truck.

3.5.3 Results of the simulations of a 3-D floor system

3.5.3.1 Static deformations

The deformations for the floor system are in good agreement with the deformations calculated for the simply supported beam. The deformations of the composite structure are smaller than the deformations of the simply supported beam: the midspan deflection is 12 mm under full load without time-dependent effects (compared to 13 mm in the case of the simple supported beam). However, this is to be expected, as the restraining effects of the continuous reinforcement over the main beams in the topping is included, providing a partial rotational constraint.

3.5.3.2 Eigen-frequencies

The eigen-frequencies are calculated for two different stages: firstly, when the composite cross-section is completed and has attained its maximum stiffness (LC 21) and secondly, when the maximum load has been applied and the effects of creep and shrinkage have reduced the stiffness of the structure to a minimum (LC 22*)¹.

¹For the simulation of the fork-lift truck driving over the floor the distributed service load is taken off the floor (thus LC 22 changes to LC 22*). Thus a higher eigen-frequency is calculated than when the distributed service load is included.

3.5 Three-dimensional sample floor system

The frequencies and mode shapes of the relevant bending modes are summarised in Table 3.7. Considered relevant are bending modes whose frequency is below 15 Hz.

The eigen-frequencies of the floor system change over the lifetime of the structure. This demonstrates the importance of modelling the construction stages and age to find the right in-service stiffness of the floor at the relevant time. As the eigen-frequencies of the floor might coincide with truck frequencies during its lifetime it is important to know the band of frequencies.

SOFiSTiK:		LC 20	LC 22*
No.	Mode shape	Eigen-frequency [Hz]	
1		5.0	4.5
2		5.8	4.8
3		6.5	5.4
4		7.3	6.2
5		7.6	6.3

Table 3.7: Comparison of eigen-frequencies (3D-structure)

The eigen-frequencies of the structure over its whole lifetime are similar to the eigen-frequencies found in Chapter 2 for the fork-lift trucks. Therefore an increase in amplitude is to be expected when fork-lift truck traffic is considered on the floor.

3.5.3.3 Response to dynamic loading

The response to the dynamic loading from the fork-lift truck is measured as the time history of the nodal accelerations. The midspan node of the central element is considered for the analysis, which neglects the contribution of the second mode.

3.5 Three-dimensional sample floor system

Moving constant force The displacements and accelerations of the midspan node caused by the constant force are shown in Figures [3.9] and [3.10].

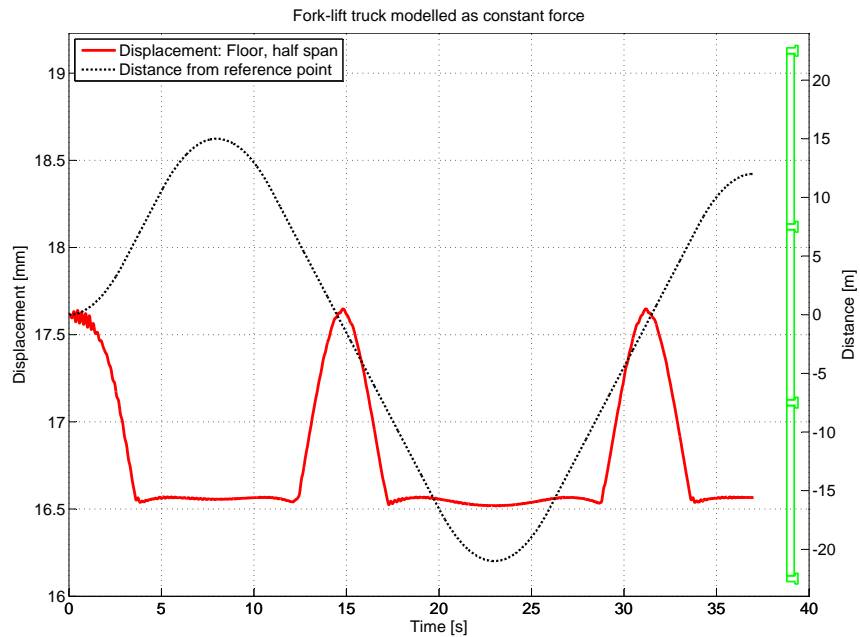


Figure 3.9: Displacement of node with constant force passing

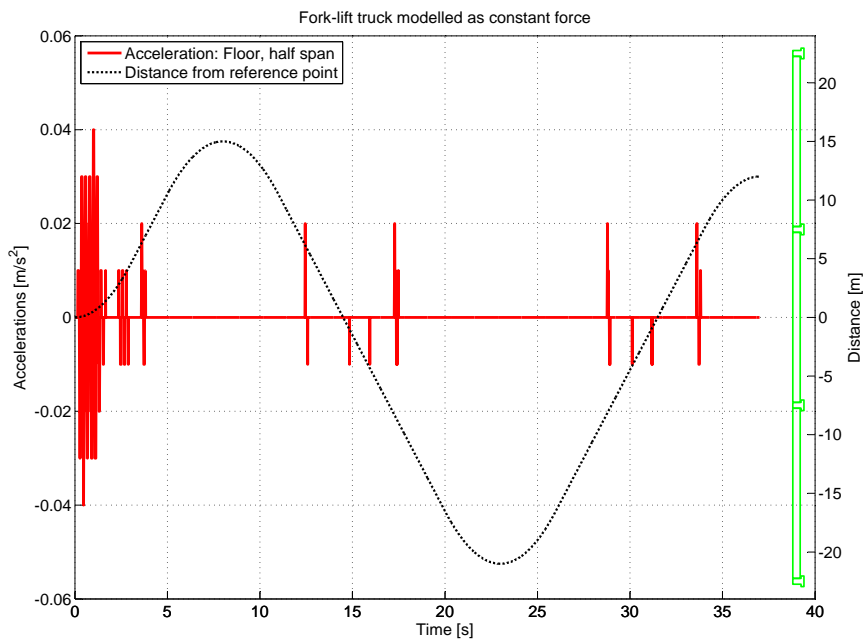


Figure 3.10: Nodal accelerations due to constant force passing

The accelerations excited from the fork-lift truck modelled as a constant force are small and their amplitude is governed by the velocity of the fork-lift truck: the in-

creasing deformation is due to the increasing bending moment of the beam caused by the approaching fork-lift truck which leads to accelerations. The dynamic response of the beam to the removal of the load once the fork-lift truck is over the support and on the next element decays quickly. The displacements caused by a constant force have a maximum of 1.1 mm; the accelerations are less than 0.04 m/s^2 . This is of the same order as the resolution of accelerations in SOFiSTiK which leads to dissatisfying discrete plots, see Figure [3.10].

It has to be concluded that the model of a fork-lift truck as a constant force is not suitable for modelling the dynamic actions.

Dynamic load model of fork-lift truck The dynamic action of the fork-lift truck is simulated for two configurations: with and without a payload carried. The payload used is the maximum capacity of the fork-lift truck: 1000 kg. The evaluation of the reference node's accelerations is undertaken in terms of the time history and the frequency content. The results are shown in Figures [3.11] and [3.12] for the configuration "without payload" and in Figures [3.13] and [3.14] for the configuration "with payload".

Independent of configuration, both simulations show a distinct influence of the dynamic load model (and its position on the floor) on the accelerations, which increase as the fork-lift truck approaches the point of measurement and then decay after it passes. Similarly, the influence of the velocity is visible: increasing velocity (and thus increasing excitation amplitudes) increase the floor accelerations.

The frequency response is governed by the eigen-frequencies of the fork-lift truck model. The first mode determines the response. Significantly smaller peaks are found at the second mode of excitation and the eigen-frequencies of the floor.

The explanation of the amplitudes is more difficult: the peak accelerations are larger for the configuration "no payload" than they are for the configuration "payload". This is in agreement with the findings of Eriksson (1994) and Malchaire et al. (1996). However, their explanation of a lower driving speed when carrying a payload does not

3.5 Three-dimensional sample floor system

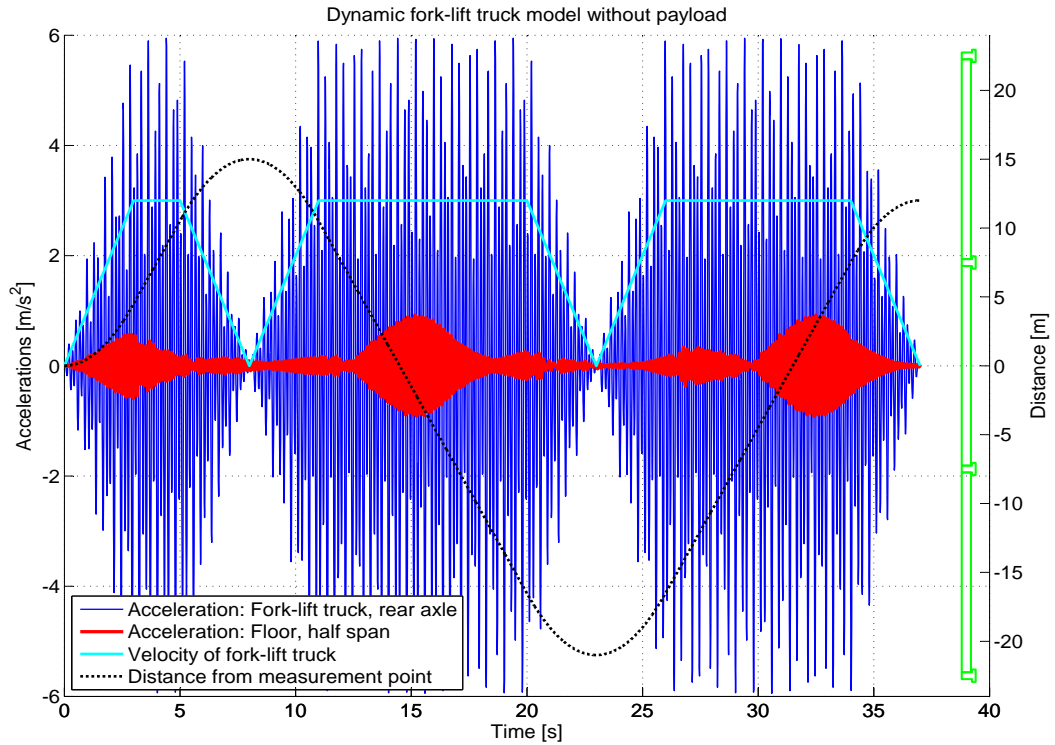


Figure 3.11: Acceleration response of floor system to dynamic fork-lift truck model, without payload

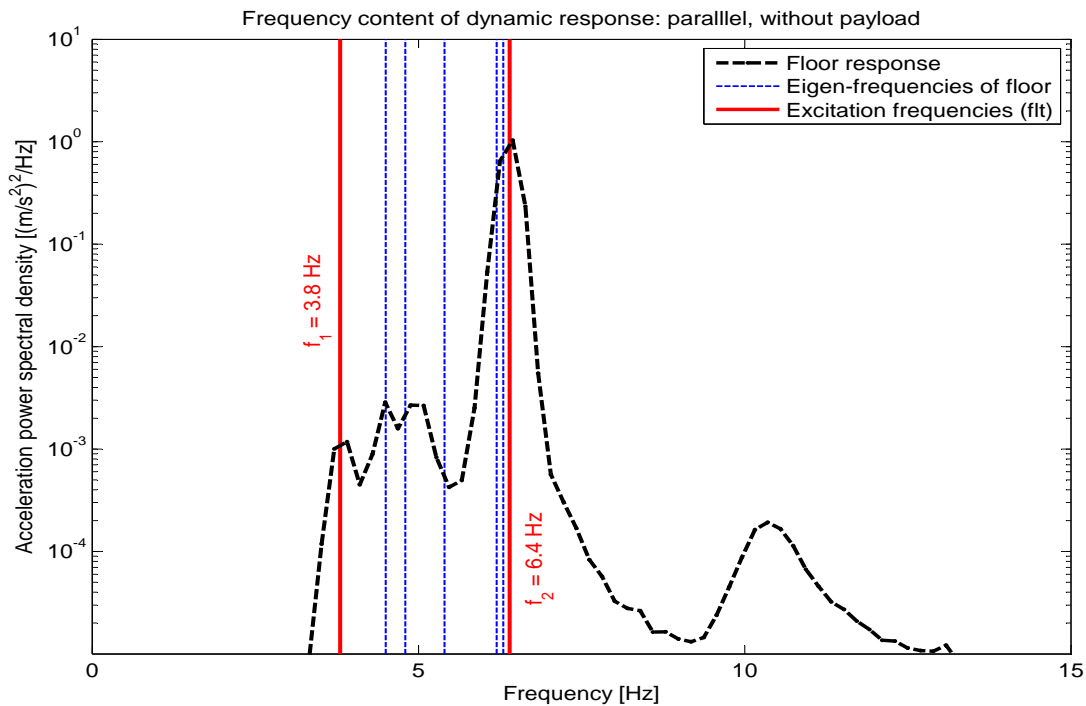


Figure 3.12: Frequency response of floor system to dynamic fork-lift truck model, without payload

3.5 Three-dimensional sample floor system

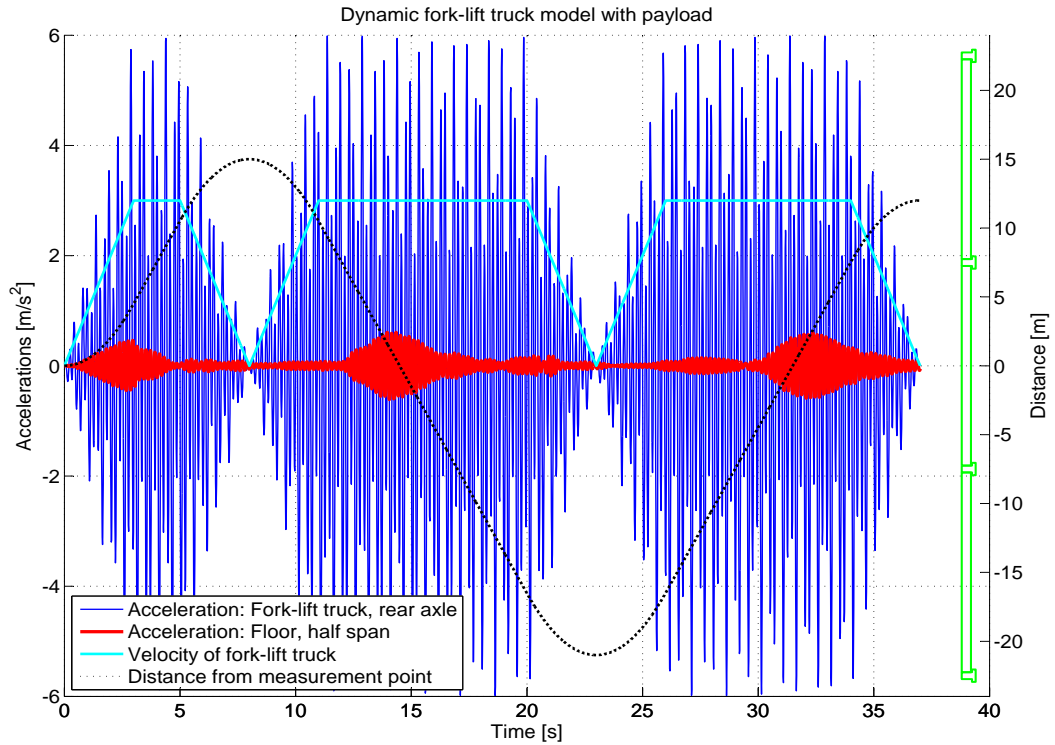


Figure 3.13: Acceleration response of floor system to dynamic fork-lift truck model, with payload: 1000 kg

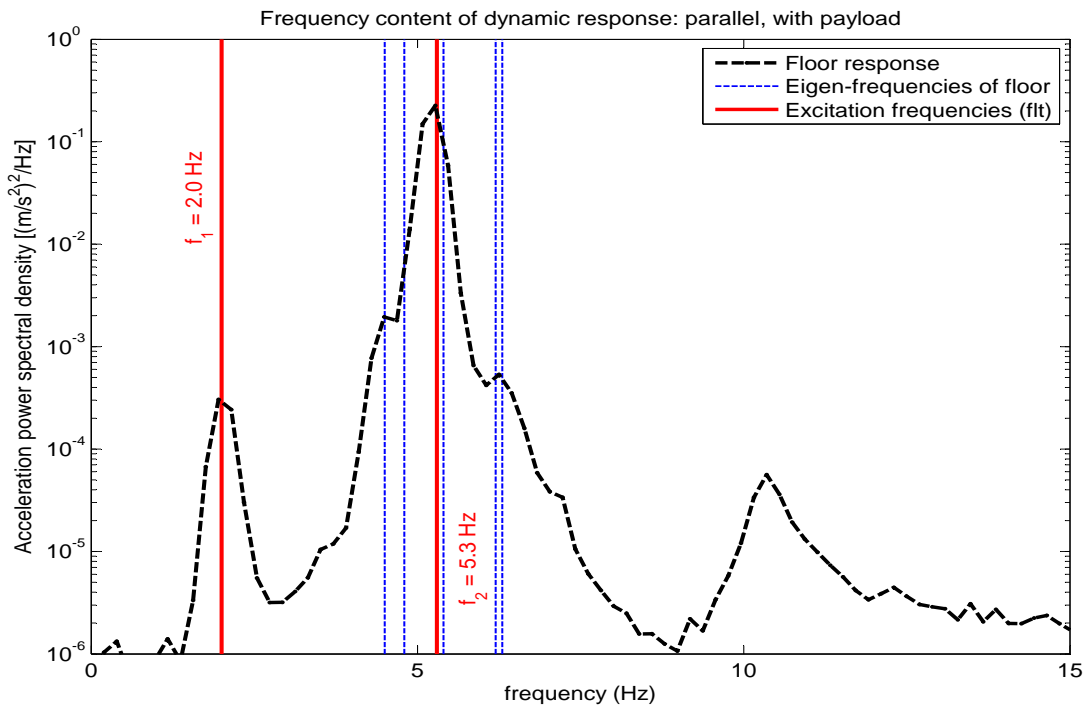


Figure 3.14: Frequency response of floor system to dynamic fork-lift truck model, with payload: 1000 kg

3.5 Three-dimensional sample floor system

work here. The main difference between the two configurations (with the exception of the frequencies) is that the forces of the second configuration are higher and mainly concentrated on one axle (front axle) while they are almost evenly distributed on both axles in the first configuration. However, the dominant second mode of the fork-lift truck excitation is closer to the first eigen-frequency of the floor if no payload is carried, while the second mode of the fork-lift truck's excitation is closer to the third mode of the floor if a payload is carried. From this it is concluded that the second mode of the fork-lift truck vibration (the one in-phase for front and rear axle) governs the response of the floor.

In Section 1.5.5 it was shown that in an industrial environment (either manual labour or clerical work) the limit of acceptable transient (root-mean-square) accelerations is about 0.5 m/s^2 according to DIN 4150 Teil 2 (1999). An analysis of the floor's accelerations shows that the vibration acceptability criteria are just fulfilled: see Figures [3.15] and [3.16] and Table 3.8:

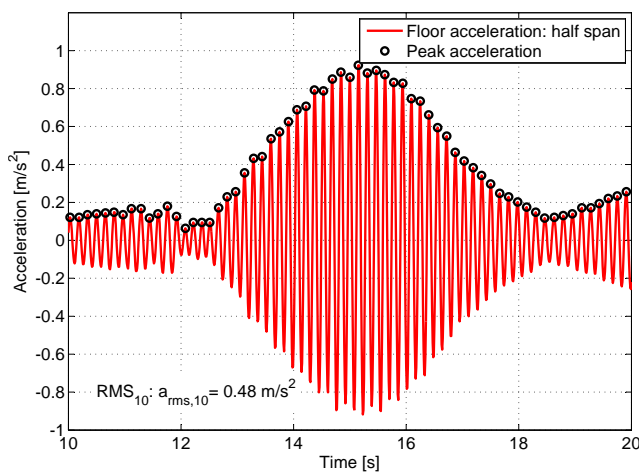


Figure 3.15: Calculation of RMS-accelerations: floor response to truck without payload

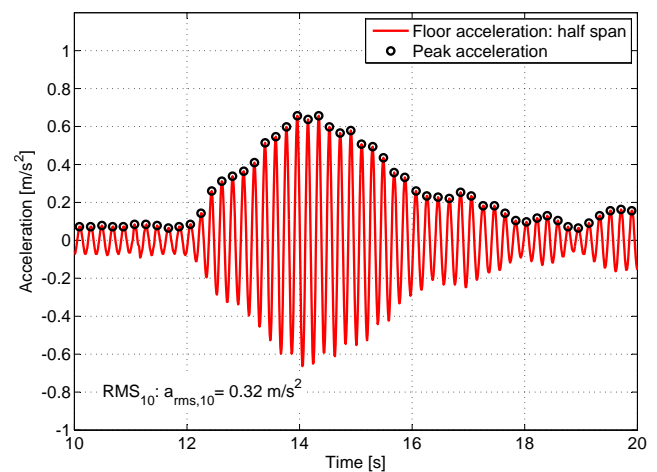


Figure 3.16: Calculation of RMS-accelerations: floor response to truck with payload

The calculation of the root-mean-square acceleration is carried out over a period of 10 seconds, denoted as RMS_{10} . While the configuration “with payload” fulfils the vibration criteria the configuration “without payload” is close to the acceptable limit. A small change in the eigen-frequencies (either of the floor system or of the truck) could lead to a better match of the frequencies and a significant increase in the amplitudes

due to stronger resonance effects.

Configuration	RMS ₁₀ -acceleration [m/s ²]	Peak acceleration [m/s ²]
without payload	0.48	0.92
with payload	0.32	0.66

Table 3.8: Evaluation of accelerations of the floor system

Comparison of displacements In order to identify the influence of the dynamic load model on the displacements they are compared with those calculated for the constant force travelling over the floor, see Figure [3.17]. In this figure the displacement from the current design standards with a dynamic amplification factor of 2.0 for solid tyres is also plotted.

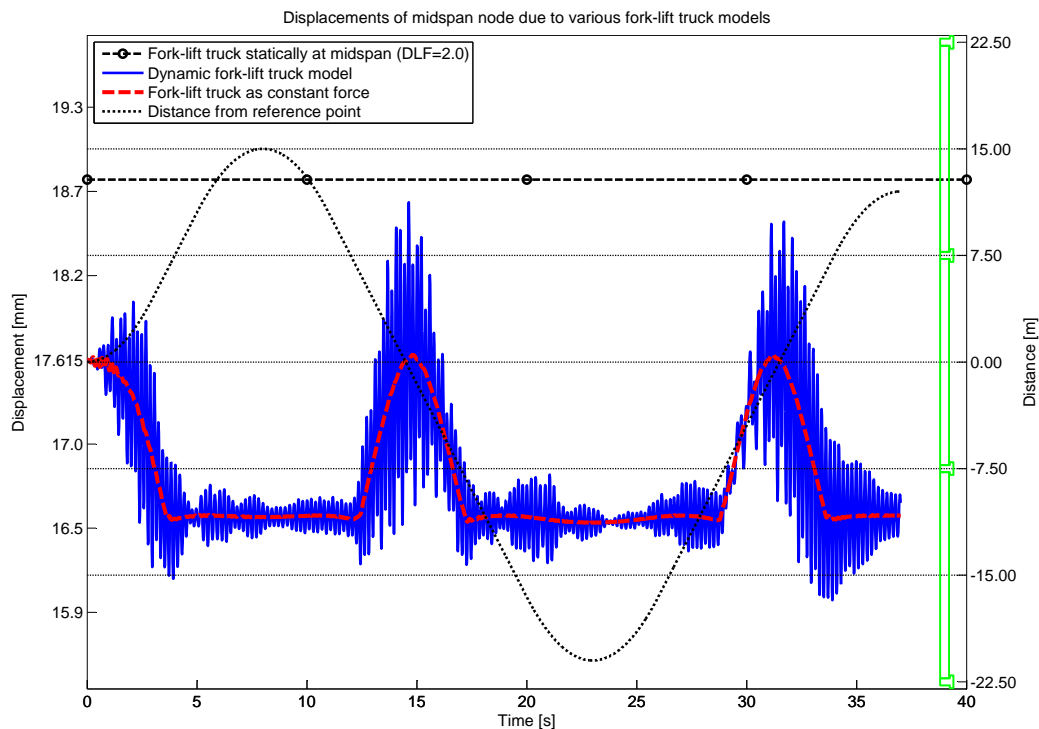


Figure 3.17: Displacements of floor system due to various fork-lift truck models, with payload: 1000 kg

The influence of the dynamic loading is clearly visible. The maximum change in de-

formation caused by the fork-lift truck model travelling along the floor is $\Delta z_{const-force} = 1.1$ mm for the constant force while it is $\Delta z_{flt-model} = 2.7$ mm for the dynamic load model. However, the peak displacements of both methods of applying the load are smaller than the displacement calculated according to the design standard. This is to be expected because the DLF in the design code is set to its value to achieve this effect: the deflection under the dynamic fork-lift truck loading is smaller than that from the quasi-static load from a fork-lift truck increased with the DLF.

3.5.4 Summary of results of the simulations

SOFiSTiK enabled an easy creation of the structural model and its inherent characteristics. The dynamic load model of the fork-lift truck is implemented easily with a few lines of code.

The calculation of the eigen-frequencies at different stages throughout the lifetime of the structures shows the influence of cracks and time-dependent effects: the eigen-frequency of the first mode drops by about 10% and the second mode's eigen-frequency decreases by almost 20%. The absolute values are in good agreement with values calculated with other programs, see Section 3.4.

The floor accelerations show a significant influence of the dynamic load model on the response: compared with a constant force moving over the floor the peak accelerations increase by a factor of 23, while the maximum deflection increases only by 1 mm (both smaller than the deflection calculated with the DLF increased load). However, the deformations vary over a wider range for the dynamic load model compared with the constant force.

It was found that a linear time-step analysis is sufficient to model the effects of the moving truck as imposed changes of strains and stresses are small.

To investigate these results more closely a field test was carried out. If the main effects are found in the field test as well, the load model and the finite element model are suitable for serviceability analysis.

Chapter 4

Field test: dynamic response of the Helmstadt floor system to fork-lift truck loading

4.1 Executive summary

In the previous chapters a load model of the fork-lift truck and a finite element model of a partially prestressed floor system have been developed independently from each other. This chapter summarises a field test that has been carried out to verify that the models developed previously can be tied together as a tool for serviceability checks.

Available for testing was a production and storage facility of MWH in Helmstadt, Germany.

The floor system was excited with a single force input to find the natural frequencies. They were calculated from the acceleration record to be 3.9 Hz and 10.3 Hz. It was not possible to conduct a full modal test of the floor because of a lack of time, equipment and support.

The fork-lift truck available on site was a Mariotti Mycros 13C. Its eigen-frequencies

were calculated with the three-degree-of-freedom model set up during the development of the load model. They were 4.9 Hz and 6.9 Hz in the unloaded case; 3.7 Hz and 6.4 Hz with a payload of 350 kg. All these were close to the measured natural frequencies.

Four different test configurations were executed: with and without a payload carried, driving parallel or transverse to the span direction of the double-tee elements.

The floor accelerations were recorded at a quarter span and at half span of a double-tee element. The record showed a clear correlation between the position of the fork-lift truck and the magnitude of the floor vibration.

The finite-element model of the floor system was calculated at three stages: directly after assemblage with a maximum stiffness, with a reduced stiffness due to cracks from the maximum service load and at the time of testing, considering the effects of creep and shrinkage. During this service time the eigen-frequency of the first mode changed from 6.6 Hz to 4.3 Hz and of the third mode, which matched the measured second mode, from 16.0 Hz to 10.3 Hz.

The fork-lift truck load is implemented as proposed in Chapter 2 with the eigen-frequencies calculated.

The response of the floor was extracted as nodal acceleration of a half span node. The same correlation between the position of the fork-lift truck and the magnitude of vibration was found. From the acceleration record the frequency content was calculated. It was found that the bounce mode of the truck excited the floor to a significantly higher degree than the pitch mode.

A comparison of the measured and calculated floor accelerations showed that the FE-model overestimated the magnitude by less than 0.1 m/s^2 (about 40%). This was to be expected because the load model overestimated the acceleration by about 20%. For a serviceability check this is a conservative and as such acceptable error.

The acceptability of the vibration was checked according to DIN 4150 Teil 2 (1999). The rms-acceleration calculated over a period of 10 seconds was 0.10 m/s^2 when the truck was driven parallel to the span direction and 0.15 m/s^2 when it was driven transverse. Both values were smaller than the allowable rms-acceleration of 0.50 m/s^2 .

4.2 The Helmstadt floor system

A field test was carried out to verify both the fork-lift truck load model and the SOFiSTiK FE-simulation of a floor system. The field test was performed in a production and storage building of the Metallwerke Helmstadt GmbH, Germany (a metal works company which produces garden furniture).

Like the experiments for the development of the fork-lift truck load model the field test had to be conducted without any technical support and under tight time constraints. Testing was only possible for a few hours (including set-up time) because normal service had to continue on site.

4.2.1 Description of the structure

Figure [4.1] shows a sketch of the basic layout with the testing area shaded.

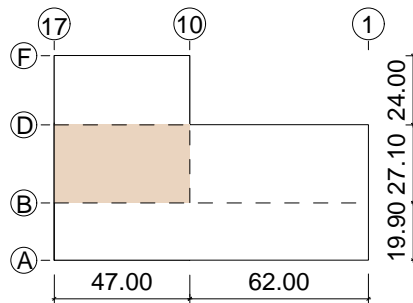


Figure 4.1: Basic layout of the building

The dimensions are approximately 109×71 m. The larger part of the building has two storeys, but the area axis A-B/1-17 has no upper floor because the main production unit extends to a height of two storeys. The building is used for production and loading on the ground floor, and storage of goods and assemblage of components on the upper floor. Fire walls separate the building into several fire compartments. The fire walls are located in axis B/1-17, B-D/10 and D/10-17 on the ground floor. The staircase and the lift shaft are located in axis D-E/10-11. The floor is made from precast and partially prestressed double-tee elements with a cast in-situ topping. It was designed for the loadings given in Table 4.1.

4.2 The Helmstadt floor system

Description	Symbol	Value	Unit
Selfweight precast element	$g_{1,pc}$	5.66	kN/m _{web}
Selfweight topping ($d = 9$ cm)	$g_{1,ci}$	2.25	kN/m ²
Service load	q	15.00	kN/m ²
Reduction factor service load	ψ	0.8	-
Fork-lift truck $m_{total} = 3.5$ t	F_{axle}	30.0	kN
Dynamic load factor	ϕ	1.4	-

Table 4.1: Design loading of the floor system

The cross-sections of the standard precast elements are shown in Figures [4.2] and [4.3]. The precast cross-sections had a strength of C40/50 and the strength of the cast in-situ concrete was C20/25.

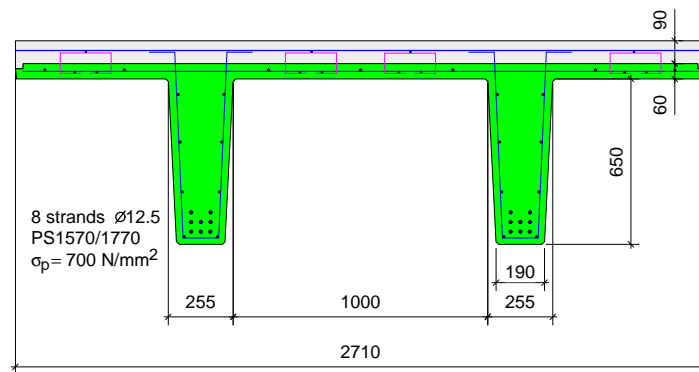


Figure 4.2: Cross-section of a standard double-tee element

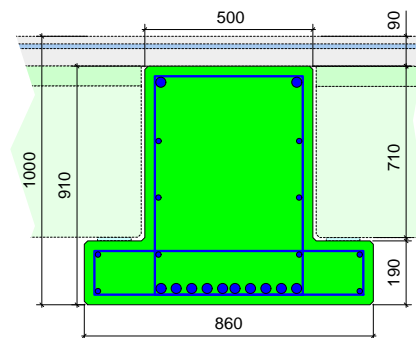


Figure 4.3: Cross-section of a standard main beam

4.2.2 Experiment set-up

In Figure [4.4] a cut-out from the ground plan is shown with a section through the building. The figure shows the ground plan without the cast in-situ topping and thus the general arrangement of the precast elements is visible: each main beam supports two and a half double-tee element. This means that not every bay is identical but only every other.

The locations of the accelerometers on the floor are marked and the paths sketched for the two driving directions: parallel and transverse. Due to goods being stored along axis D, the path “parallel” could not be extended over the axis.

At the time of testing several bays were filled with goods. These are: B-C/10-13, B-C/13'-15, B-C/16-17. Their weight was estimated to be 600 kg/m².

Two accelerometers PCB 393A03 were placed on the joint between two precast elements to measure the floor vibrations. They were placed at a quarter span and at half span. The data were passed through a signal conditioner (PCB 482A22), which was connected to a data acquisition card (DT 9816) and then stored on the hard drive of a laptop (operating system XP Professional): see Figure [4.8].

The sampling rate was set to 1000 Hz. This was well above the frequency range of interest, thus preventing problems of frequency aliasing.

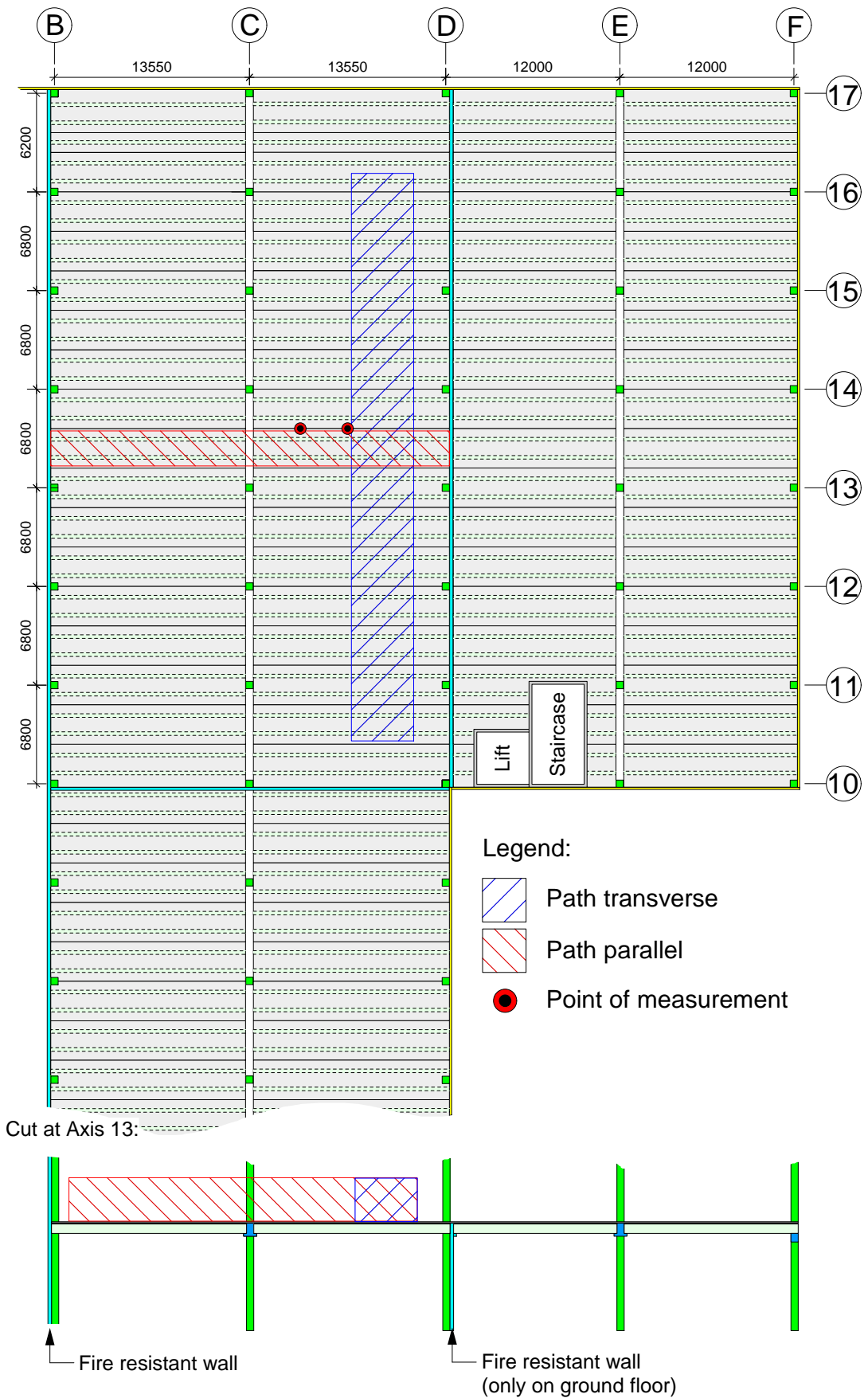


Figure 4.4: Cut out of ground plan and cut through the building

4.2.3 Natural frequencies of the Helmstadt floor

To find the natural frequencies of the floor, it was excited with a short impulse and the response was measured. It was found that dropping the fork gave the best impulse, as it produced a bigger impulse than jumping or “tapping” with a weight. The response lasted longer and thus allowed a finer resolution of the Fourier transform. However, to measure the influence of the fork-lift truck when it was close to the measurement points on the natural frequencies, other methods of excitation were used as well but as expected no significant difference was found¹. The frequency content of all tests was evaluated and averaged. Figure [4.6] shows the results: the natural frequencies were $f_1 = 3.9$ Hz and $f_2 = 10.3$ Hz.

A further peak was found at $f = 7.3$ Hz, but it would have been bold to identify this small peak as a natural frequency. The doubts about this peak were strengthened by the response of the floor to the dynamic excitation: no resonance effects could be found even if the excitation frequency was close to the suspected frequency of 7.3 Hz.

As mentioned earlier, a full modal test of the floor was not possible. However, as will be shown later the natural frequencies match the calculated eigen-frequencies reasonably well.

¹If only the beam action is considered a change of $\sim 4\%$ would be expected. The transverse slab action reduces this change even further.

4.2 The Helmstadt floor system

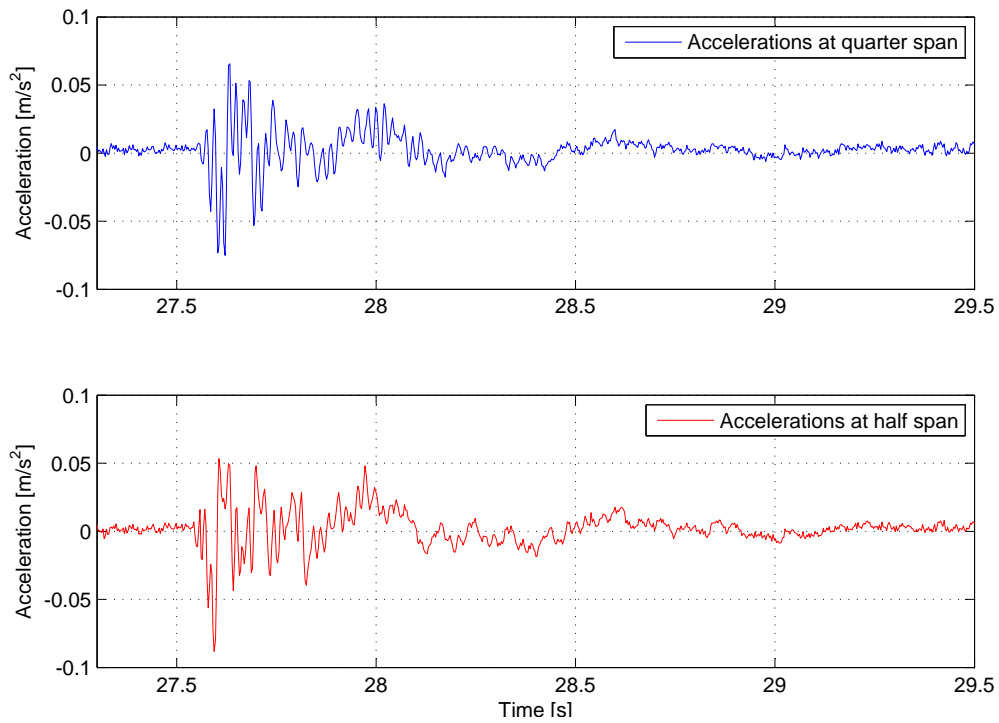


Figure 4.5: A time series of response from which natural frequencies of the floor system are extracted: one jump at half span

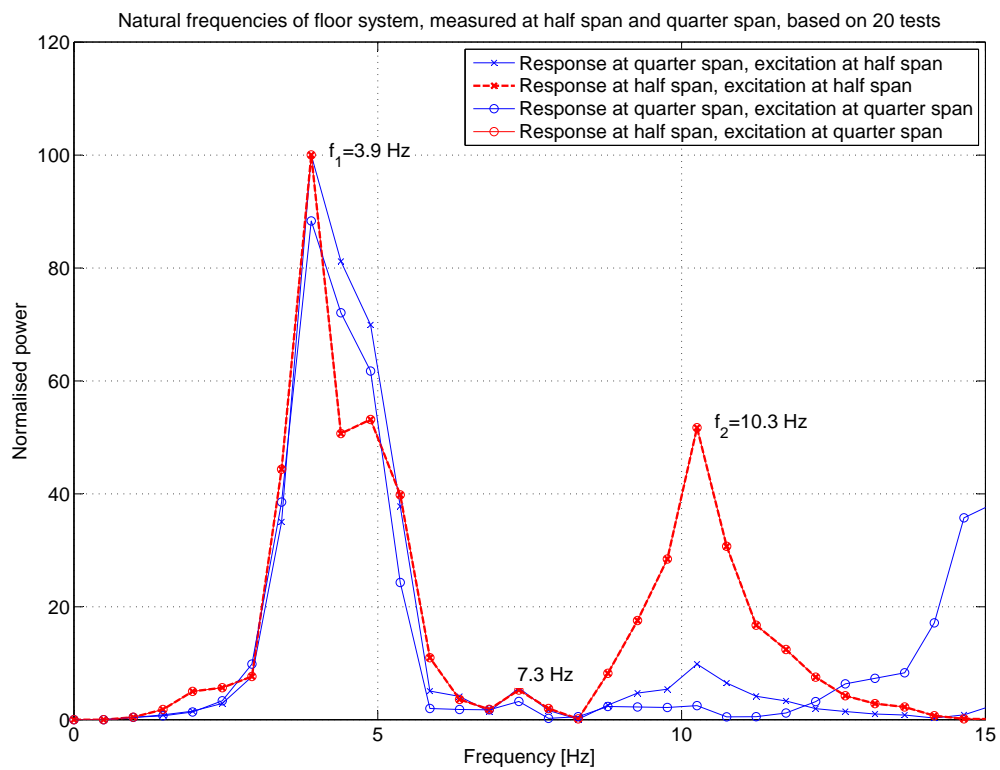


Figure 4.6: Natural frequencies of the floor system averaged from 20 tests

4.3 The fork-lift truck

4.3.1 Model Mariotti Mycros 13C

The fork-lift truck available for testing is a Mariotti Mycros 13C, see Figure [4.7].

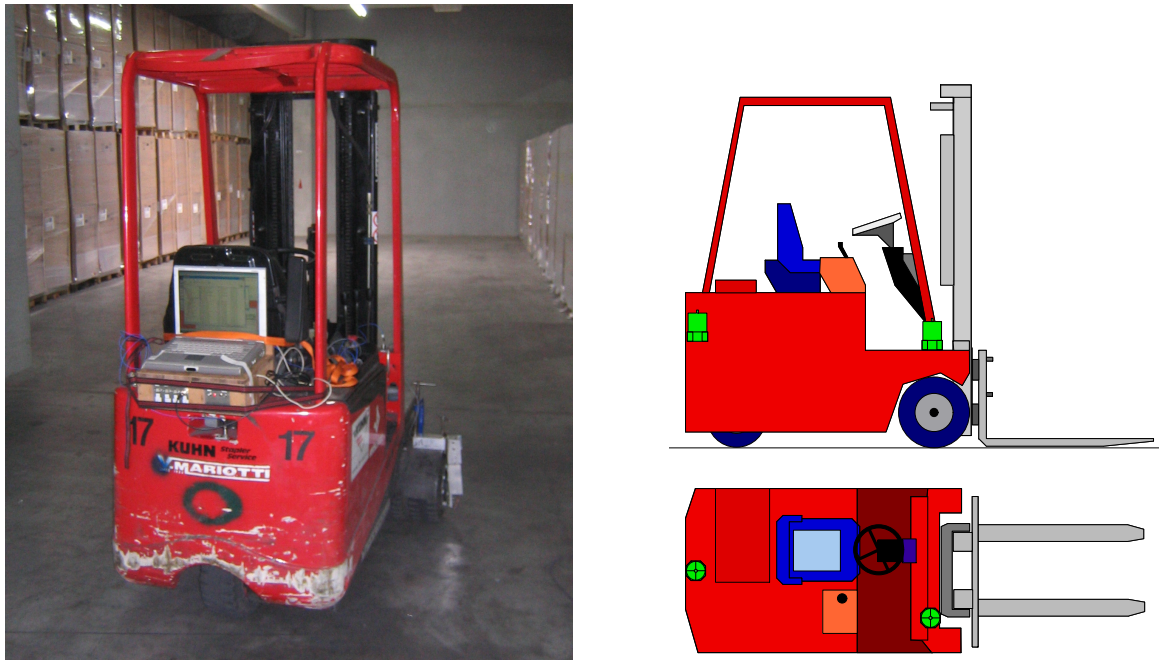


Figure 4.7: Fork-lift truck set up for testing and sketch of positions of accelerometers

The specifications of this model are summarised in Table 2.5. According to the manufacturer's data sheet its maximum velocity is 9 km/h (2.5 m/s) without a payload and 7.1 km/h (2.0 m/s) with the maximum payload. This model is significantly slower than the other models tested (maximum velocity ≈ 4 m/s). However, it can be shown that the same load model can be used to set-up the numerical model as for the other models: the natural frequencies, amplitudes of vibration and the relation between velocity and amplitudes are similar to the behaviour observed in the experimental derivation of the load model: see Chapter 2.

4.3.2 Experiment set-up

For testing the same set-up was used as for the experiments to develop the load model¹: two accelerometers PCB 338B35 (with signal conditioners PCB 480E09) and the infra-red tracking system with the DT9804 data acquisition card and a laptop to record the front axle and rear axle accelerations as well as the path travelled. The data were recorded with a frequency of 500 Hz.

The modal analysis of this model was carried out with the equivalent spring constants set to: $k_f = 2.0 \times 10^6$ N/m, $k_r = 2.0 \times 10^6$ N/m, $k_a = 9.5 \times 10^6$ N/m. The results are summarised in Table 4.2. For both load cases (with and without payload) they are in good agreement with the measured natural frequencies of the truck. The calculated values were used in the load model for the numerical simulation of the response of the floor system to the moving fork-lift truck.

Modal Analysis		Mode 1	Mode 2	Mode 3
Without a payload carried:				
Eigen-vector	$\begin{bmatrix} z_g \\ \varphi_g \\ \varphi_m \end{bmatrix}$	$\begin{bmatrix} 0.32 \\ 1.00 \\ -0.05 \end{bmatrix}$	$\begin{bmatrix} 1.00 \\ -0.52 \\ 0.26 \end{bmatrix}$	$\begin{bmatrix} -0.07 \\ 0.11 \\ 1.00 \end{bmatrix}$
Eigen-frequency	[Hz]	4.9	6.9	15.9
With a payload of 350 kg carried:				
Eigen-vector	$\begin{bmatrix} z_g \\ \varphi_g \\ \varphi_m \end{bmatrix}$	$\begin{bmatrix} -0.10 \\ 1.00 \\ -0.18 \end{bmatrix}$	$\begin{bmatrix} 1.00 \\ 0.30 \\ 0.35 \end{bmatrix}$	$\begin{bmatrix} -0.20 \\ 0.25 \\ 1.00 \end{bmatrix}$
Eigen-frequency	[Hz]	3.7	6.4	10.4

Table 4.2: Summary of modal analysis

4.4 Test execution and results

From Figure [4.8] it can be seen that the recording systems of the fork-lift truck and the floor were independent. They had to be started individually and synchronised later

¹See Chapter 2

in the analysis. To simplify the synchronisation the fork was dropped at the beginning of each record. This distinct peak in the acceleration's record could be easily found in the floor accelerations as well as in the accelerations of the fork-lift truck.



Figure 4.8: Fork-lift truck and floor set up for testing

The tests were carried out in four different configurations: see Table 4.3. Each configuration was tested between 10 and 15 times. The results of all configurations are congruent. Thus only one example for each configuration is presented.

For each configuration the synchronised record of the accelerations combined with the velocity of the truck and its position relative to the point of measurement is shown.

Configuration	parallel	transverse
without payload see Figures	[4.9] & [4.10]	[D.3] & [D.4]
with payload see Figures	[D.1] & [D.2]	[D.5] & [D.6]

Table 4.3: Test configurations

In all tests the influence of the fork-lift truck position relative to the measurement-point is clearly visible. The amplitudes increase as the fork-lift truck approaches and they decay once the fork-lift truck passes that point: the vibrations excited by the

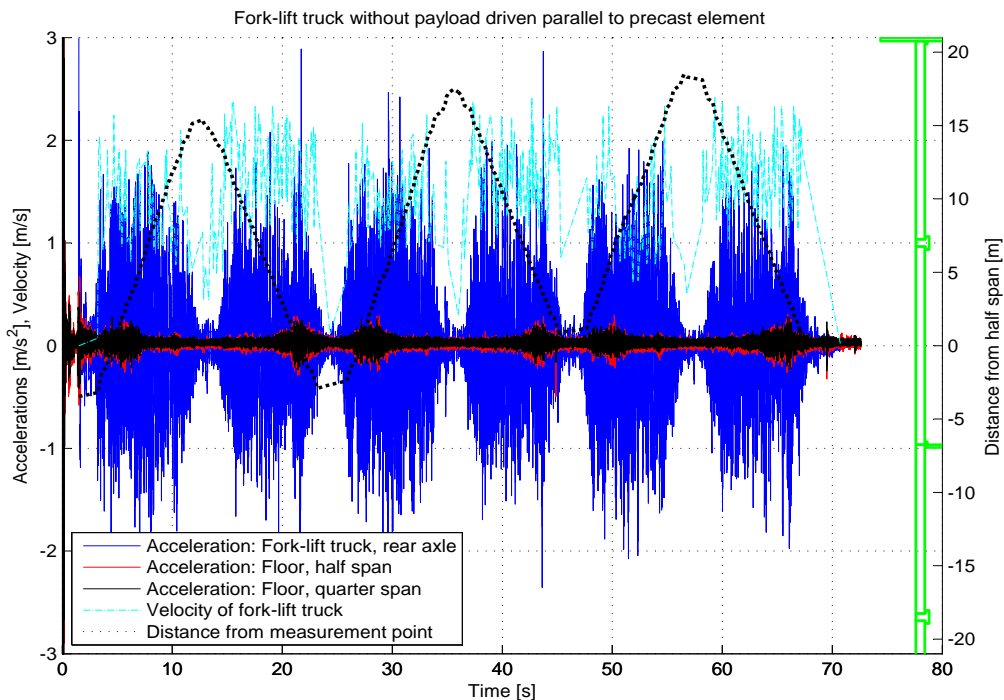


Figure 4.9: Fork-lift truck without payload parallel to precast elements

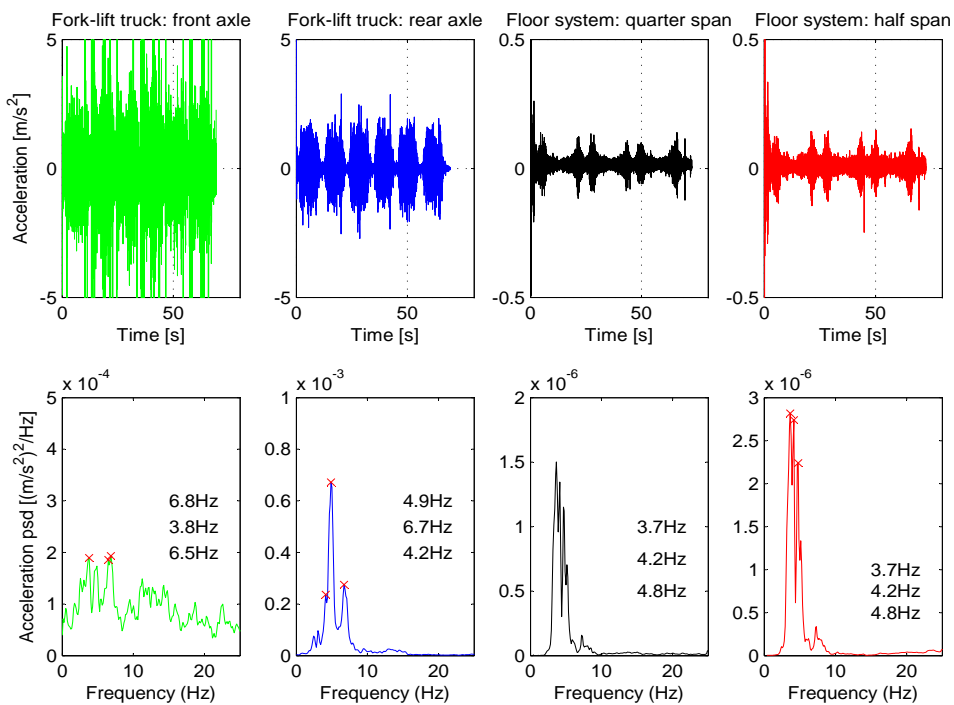


Figure 4.10: Frequency content of the above record (Figure [4.9])

moving fork-lift truck last only for a few seconds.

From Table 4.4 one can see that the driving direction “transverse” excites higher accelerations. They are about 50% higher than those excited by driving parallel to the span direction of the double-tee elements. The difference in the levels of acceleration when driving with or without a payload is less significant.

Configuration	Acceleration [m/s ²]
Driving parallel with payload	0.17
Driving parallel without payload	0.15
Driving transverse with payload	0.24
Driving transverse without payload	0.25

Table 4.4: Magnitude of peak accelerations of measurement point at mid-span

This is explained by reference to the loading of the elements from the moving fork-lift truck: driving parallel means that the element is loaded continuously from one support with an increasing midspan bending moment till the fork-lift truck reaches the mid span position and then the bending moment decreases again (with the truck approaching the next support). The dynamic action arises from the continuous excitation of the fork-lift truck. In the transverse direction, however, there is a more sudden loading of the double-tee element because the transverse load distribution is small: the composite element acts primarily as a beam while only at the joints does the cast in-situ topping act as a transverse slab.

Furthermore the vibrations do not decay as quickly as those excited by driving parallel¹ because the excitation is continuously at mid-span. In contrast to this the excitation from driving parallel constantly changes its position relative to the mid-span position and is positioned over the main beams at some point; thus hardly any excitation of the double-tee elements takes place.

The frequency content of the response is partly governed by the natural frequencies of the floor and partly by the excitation frequencies of the fork-lift truck: all records

¹See Figure [4.4] for a sketch of the driving paths.

show a peak in the range of 3.8 to 4.0 Hz being close to the floor's first natural frequency of 3.9 Hz. The other peaks are close to the excitation frequencies of the fork-lift truck.

4.5 Finite-element model of the Helmstadt floor

4.5.1 Structure

The model used to verify the general suitability of SOFiSTiK could be easily adapted to model the floor found in Helmstadt. Figure [4.11] shows the FE-model. It is a normal assumption that the fire-resistant walls that support the double-tee element in axis B and axis D act as a rigid support. However, as explained in Section 3.5.1 the rubber bearings were taken into account with their equivalent spring constant according to Equation 3.7. The main beams in axis C were modelled with their cross-section and thus their flexibility was taken into account. The supports of the main beams in axis C were considered to be rigid, except for the flexibility of the rubber bearing, see Equation 3.8. The columns were introduced as orientation: they did not contribute to the system.

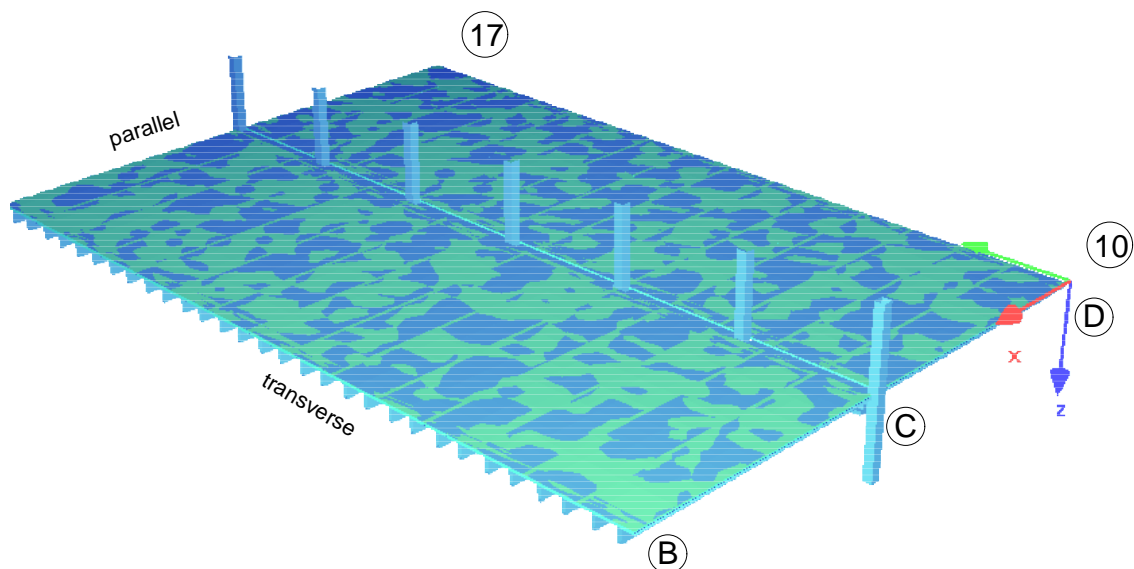


Figure 4.11: Finite-element model of the floor system, colouring shows the overlaid elements

4.5.2 Time-dependent properties

As explained earlier, SOFiSTiK calculates the time-dependent effects according to EC 2 (2004) based on the environmental conditions with the relationships of material properties (strength, cement) and geometric properties. Material and geometric properties are given in Section 4.2.1. The assumed environmental conditions are summarised in Table 4.5.

Time	Environmental conditions			
$t_0 - t_1$:	30	days,	20° C,	60 % rel. humidity
$t_1 - t_2$:	180	days,	20° C,	50 % rel. humidity
$t_2 - t_3$:	2000	days,	20° C,	50 % rel. humidity

Table 4.5: Environmental conditions assumed in SOFiSTiK calculation

4.5.3 Damping properties of the structure

Damping had to be included in the time-step analysis to achieve realistic accelerations and displacements. The damping of each part chosen for the analysis is given in Table 4.6. The damping values were assumed in accordance with Table 1.1 from Bachmann (1995): the mean value for partially prestressed concrete structures was assumed for the double-tee element. Likewise values close to the mean value of cracked reinforced concrete under “medium stress intensity” were chosen for the slab elements and the main beams, where a higher stress intensity was assumed for the main beams, which led to lower damping. The damping value of the support springs (rubber bearings) was set according to the manufacturer’s datasheet.

Part	Damping [%]	Mode	Frequency [Hz]	Modal damping [%]
TT-sections	1	1	4.28	1.2
Composite slab	3	2	4.74	1.1
Support springs	5	3	10.18	1.6
Main beams	2			

Table 4.6: Damping properties for numerical analysis

Table 4.7: Modal eigen-frequencies and damping of cracked, aged structure

4.5 Finite-element model of the Helmstadt floor

With these damping values the modal eigen-frequencies¹ and the modal damping were calculated for the derivation of the Rayleigh damping factors. The values were taken from the cracked, loaded and aged system, see Table 4.7.

From mode 1 and mode 3 the proportionality factors of Rayleigh damping were derived: $a_0 = 0.527094$; $a_1 = 0.000196$

4.5.4 The dynamic fork-lift truck load model implemented

The dynamic behaviour of the fork-lift truck was applied with the following values according to the presented load model² and the modal analysis of the fork-lift truck³:

Constant	Symbol	Value	
Wheelbase	L_{WB}	1.088	m
COG to front axle	L_f	0.690	m
COG to rear axle	L_r	0.398	m
Mass moment of inertia	J	3200	kgm ²
horiz. acceleration	a_{ftt}	1.0	m/s ²
without payload:			
Mass	m_{npl}	2185	kg
first mode	f_1	4.9	Hz
second mode	f_2	6.9	Hz
static load front axle	$F_{f,static}$	8.00	kN
static load rear axle	$F_{r,static}$	13.85	kN
with payload (350 kg):			
Mass	m_{pl}	2535	kg
first mode	f_1	3.7	Hz
second mode	f_2	6.4	Hz
static load front axle	$F_{f,static}$	13.86	kN
static load rear axle	$F_{r,static}$	11.49	kN

Table 4.8: Values for load model with the fork-lift truck: Mariotti Mycros 13C

¹See Section 4.5.5.1

²See Section 2.8.2

³See Section 4.3.1

4.5 Finite-element model of the Helmstadt floor

For example the configuration without a payload carried leads to:

$$\begin{aligned}
 \begin{bmatrix} F_f(t, v) \\ F_r(t, v) \end{bmatrix} &= \frac{1}{L_{WB}^2} \begin{bmatrix} (m_{tot}L_r^2 + J) & (m_{tot}L_fL_r - J) \\ (m_{tot}L_fL_r - J) & (m_{tot}L_f^2 + J) \end{bmatrix} \cdot \begin{bmatrix} a_f(t, v) \\ a_r(t, v) \end{bmatrix} \\
 &= \frac{1}{1.088^2} \begin{bmatrix} (2185 \times 0.398^2 + 3200) & (2185 \times 0.690 \times 0.398 - 3200) \\ (2185 \times 0.690 \times 0.398 - 3200) & (2185 \times 0.690^2 + 3200) \end{bmatrix} \\
 &\quad \cdot \frac{1.2v + 0.4}{1.5} \begin{bmatrix} 0.5 \sin(2\pi \cdot 4.9 t) & + \sin(2\pi \cdot 6.9 t) \\ 0.5 \sin(2\pi \cdot 4.9 t + \pi) & + \sin(2\pi \cdot 6.9 t) \end{bmatrix} \quad (4.1)
 \end{aligned}$$

which results in the total loads applied:

$$F_{f,total} = F_{f,static} + F_f(t, v) \quad (4.2)$$

$$F_{r,total} = F_{r,static} + F_r(t, v) \quad (4.3)$$

The time series of the load pair is plotted for this configuration in Figure [4.12]:

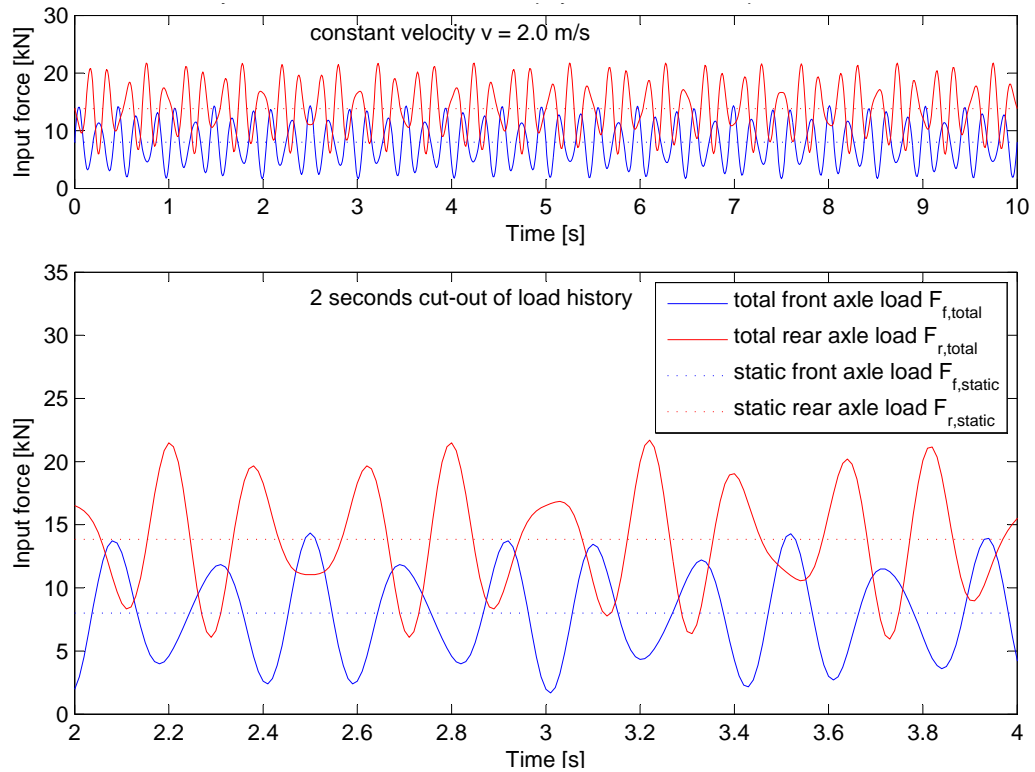


Figure 4.12: Load history of M13 (without payload) as implemented in SOFiSTiK

4.5.5 Results of finite-element simulation

4.5.5.1 Eigen-frequencies of the floor system

The eigen-frequencies were calculated at various stages: see Table 4.9 and Figures [4.13] to [4.15] for the mode shapes.

State	Mode 1	Mode 2	Mode 3	[Hz]
Assembled, unloaded (max stiffness)	6.60	7.37	16.04	
Assembled, loaded (cracked)	4.35	4.78	10.99	
Assembled, cracked, aged (6 years)	4.28	4.74	10.18	

Table 4.9: Eigen-frequencies of the floor system, calculated with SOFiSTiK

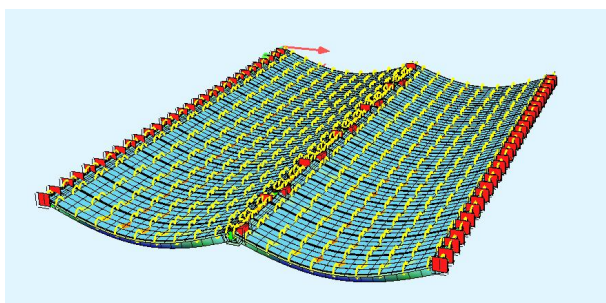


Figure 4.13: Mode 1

Mode 1:
half sine wave in each span with both spans in phase. Hence a bending moment of the topping over the main beam (low stiffness).

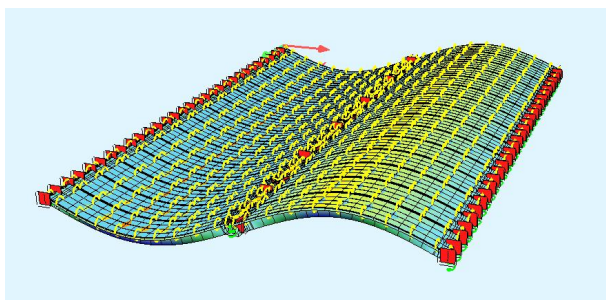


Figure 4.14: Mode 2

Mode 2:
half sine wave in each span with both spans in anti-phase. Hence a torsional moment in the main beams (high stiffness).

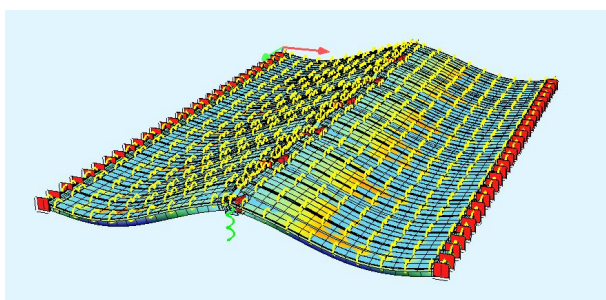


Figure 4.15: Mode 3

Mode 3:
roughly a sine wave over both spans with vertical participation of the main beams and bending of the main beams.

The eigen-frequency calculated for the first mode was about 10% higher than the natural frequency measured for the floor system. This could be accepted as the loading history and environmental conditions were not known. Thus the influence of shrinkage and creep could be different from what was assumed in the simulations. Furthermore a small change in the prestressing force can lead to changes in the stiffness. In agreement with the original design of the floor system according to EC 2 (1991), the simulation did not consider losses of the prestressing force due to relaxation.

The mode shapes of the first and the second mode are similar and it is therefore not surprising that they were not separated clearly in the field test. However, in Figure [4.6] a broad peak around the relevant frequency can be found, which may be interpreted as the merging of the two eigen-frequencies.

4.5.5.2 Peak accelerations of the fork-lift truck and the floor

The peak accelerations were extracted from the simulation results file.

Fork-lift truck accelerations The mean average of accelerations as proposed for the load model show a good agreement in terms of peak accelerations between the field test and the load model:

$$\max a_{flt,field-test} \approx 2.3 \text{ m/s}^2 \text{ and } \max a_{flt,load-model} \approx 2.8 \text{ m/s}^2.$$

The calculated accelerations exceed the measured ones by roughly 20% which is acceptable and would be conservative for a serviceability analysis as part of the design process.

Floor accelerations The measured peak accelerations of the floor (mid-span) are $\max a_{floor,field-test} = 0.25 \text{ m/s}^2$. This is in good agreement with the calculated peak accelerations of the floor which are summarised in Table 4.10. They show a similar pattern to that found in the simulation of the sample structure: the accelerations are bigger for driving transverse than for driving parallel.

As expected, the simulations still overestimated the peak accelerations because the load model concentrates the introduced energy in two frequencies instead of a wider

Configuration	Peak accelerations	
	Simulation	Field test
	$[\text{m/s}^2]$	
Parallel, no payload	0.22	0.15
Parallel, payload	0.23	0.17
Transverse, no payload	0.31	0.25
Transverse, payload	0.34	0.24

Table 4.10: Peak accelerations of the floor system, calculated with SOFiSTiK

range of frequencies which could be clearly found for the front axle of most tests carried out during the development of the fork-lift truck model.

4.5.5.3 Time history of nodal accelerations

The simulation was carried out for all four configurations tested on site. For all configurations the results are in good agreement with the field tests. The configuration “driving parallel without a payload” is presented here and the other results summarised in Appendix E.

Figure [4.16] is set up like the results of the field test (see Figure [4.9]): the nodal accelerations of the midspan node, the accelerations of the fork-lift truck’s front axle, its velocity and its position relative to the midspan node are plotted. From the nodal time history the frequency content of the response was calculated, see Figure [4.17]. The dynamic response is mainly governed by the excitation frequencies of the fork-lift truck model.

4.5 Finite-element model of the Helmstadt floor

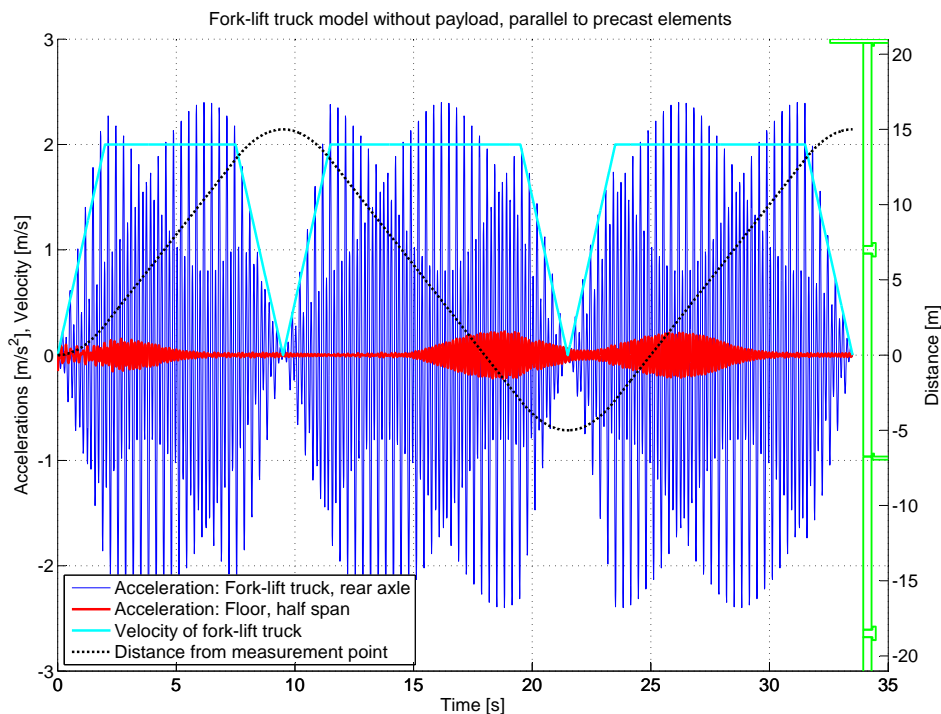


Figure 4.16: Time history of calculated accelerations: “parallel without payload”

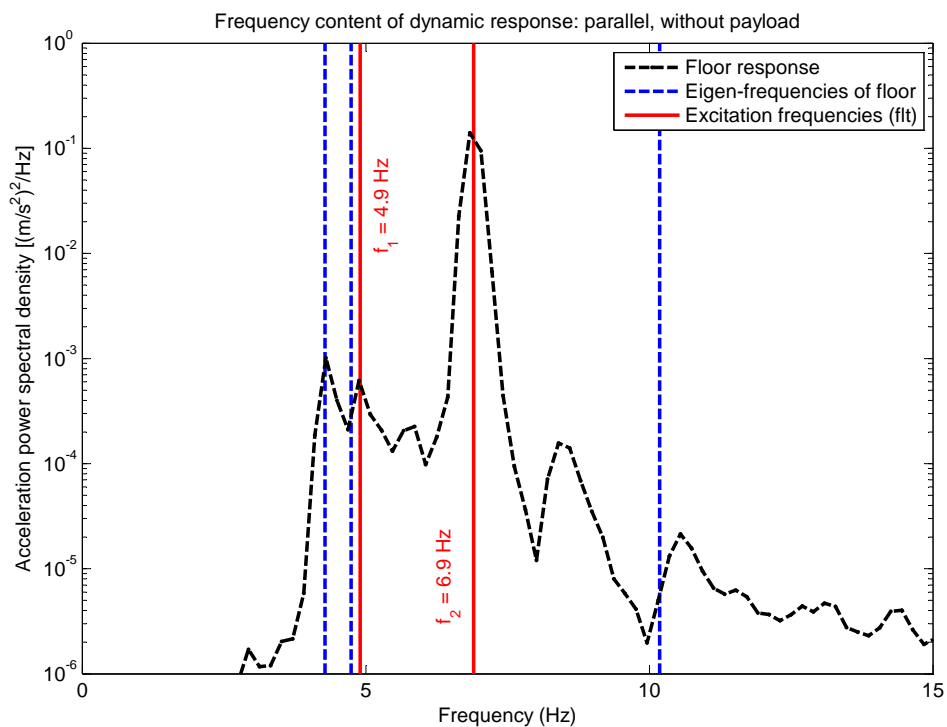


Figure 4.17: Frequency content of calculated floor accelerations: “parallel without payload”

4.5.5.4 Comparison with field test data

In Figure [4.18] the measured accelerations of the midspan node are compared with the calculated accelerations.

A good agreement is found in terms of the peak accelerations and the response relative to the distance between the fork-lift truck and the point of measurement: the peak accelerations calculated are 0.06 to 0.10 m/s^2 bigger than the peak accelerations measured on site. Considering the uncertainties this result is acceptable and with a serviceability analysis in mind, an overestimation of the peak accelerations is a conservative result.

The response to the excitation from the fork-lift truck is similar in both cases. With the fork-lift truck approaching, the amplitudes increase rapidly and then decay quickly after the fork-lift truck passes the point of measurement.

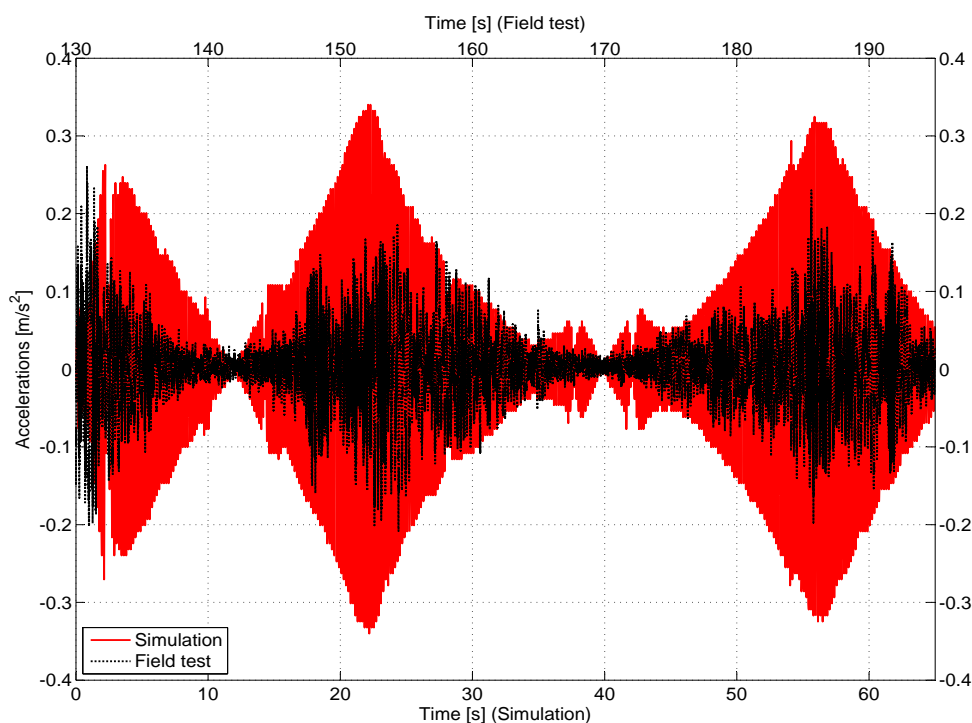


Figure 4.18: Comparison of measured and calculated accelerations

In Figure [4.19] the frequency content of the floor response from the field test is compared with the calculated frequency content of the simulated response: the

4.5 Finite-element model of the Helmstadt floor

frequency contents of the field tests and the simulations shows that while the response during the field tests was spread over a wider range of frequencies the influence of the excitation frequencies from the fork-lift truck on the response is clearly noticeable. However, the floor response was not as closely linked to the excitation as it is in the simulation. This can be explained by the wider range of excitation frequencies in the real case which were not considered in the load model. Hence a higher concentration of energy transmission takes place for the frequencies incorporated in the load model while the real floor shows significant response in its natural frequencies. However, the response in higher modes is bigger in the FE-model.

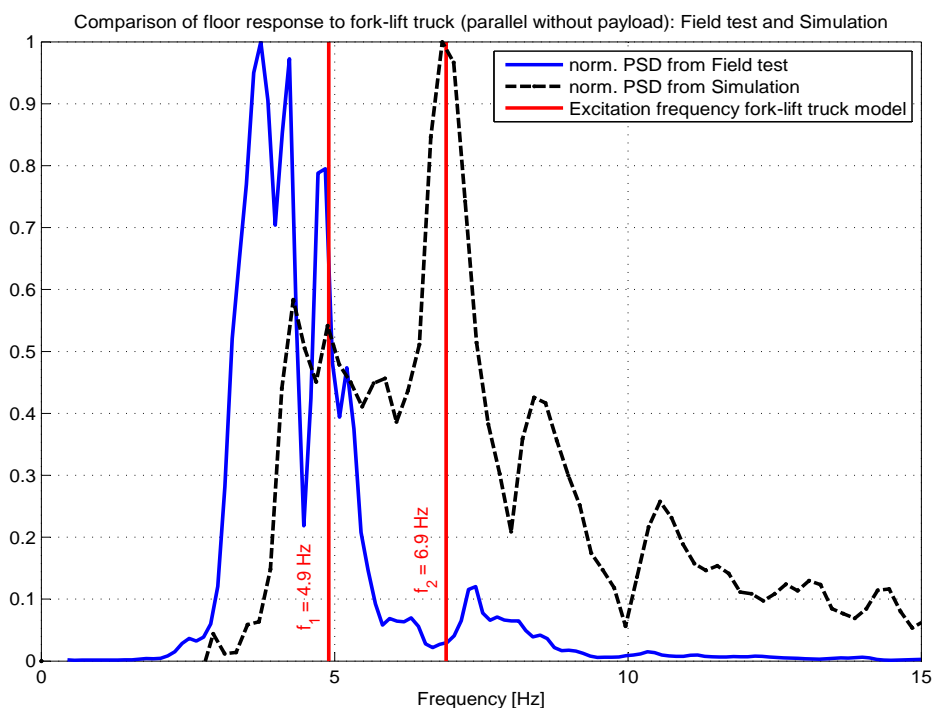


Figure 4.19: Comparison of measured and calculated frequency content of floor response to excitation from fork-lift truck driven parallel without a payload

4.6 Acceptability of accelerations in Helmstadt

In Section 1.5.5 it was shown that in an industrial environment the limit of acceptable RMS-acceleration according to DIN 4150 is about 0.5 m/s^2 , if they are transient.

In Helmstadt the vibrations excited by the passing of a fork-lift truck lasted about 10 seconds, a little shorter if the truck was driven parallel to the double-tee elements and a little longer if it was driven transverse to them. Thus they fulfil the requirement of being transient and the chosen time scale of the RMS-acceleration of 10 seconds is a useful measure.

If the RMS_{10} -accelerations are considered for driving parallel to the span-direction of the double-tee element, it is $a_{\text{RMS},10} = 0.10 \text{ m/s}^2$ and $a_{\text{RMS},10} = 0.15 \text{ m/s}^2$ if driving transverse to it. As expected the acceptability criteria for this floor system are fulfilled: the structure has a low slenderness ratio ($L/h \approx 17.0$) and the fork-lift truck is small (total weight 3.5 t: 35 kN) compared to the distributed design load (15 kN/m^2). These results are in good agreement with comments from the staff in Helmstadt that the floor vibrations are clearly noticeable but not disturbing in any way.

However, even this structure showed significant accelerations and the sample structure analysed in Section 3.5 showed considerably higher accelerations: the RMS-acceleration was about $a_{\text{RMS},10} \approx 0.50 \text{ m/s}^2$. This is equal to the acceptable limits. This sample floor is representative of real, as-built floors¹, showing that the vibration issue has to be taken into account if the trend towards structures of higher slenderness continues. The current design approach will lead to vibration serviceability problems.

¹Unfortunately, those were not available for field testing.

Chapter 5

Conclusions

This project aimed to analyse the dynamic response of a precast and partially prestressed floor system to fork-lift truck traffic. The aim of developing a realistic and useable assessment methodology for floor vibrations caused by fork-lift truck traffic has been achieved.

The project has been divided into three separate studies. These studies are the development of a dynamic fork-lift truck model (see Chapter 2), the development of a FE-model of a composite floor system including all time-dependent effects (see Chapter 3), as part of this a preliminary investigation of the joint between the precast and cast in-situ concrete was carried out (see Appendix A), and a field test to verify the finite element model (see Chapter 4). From each study useful conclusions can be drawn.

5.1 Concrete joint between precast and cast in-situ concrete

A simple preliminary test was performed to find out whether the joint shows damping characteristics worth a closer and more elaborate investigation.

Two different types of specimen were cast to investigate the joint. One type had an inclined joint which resulted in a combined normal and shear stress in the joint, while

the other type transmitted loads through the joint as pure shear stress.

After curing the specimens they were loaded a defined number of cycles to simulate the dynamic loading from fork-lift trucks. During the cyclic loading measurements were taken which allowed for the calculation of the stiffness of the specimen and its hysteresis loop. After cyclic loading they were tested for the ultimate strength.

The investigation of the joint suffered from variability of the materials used. The number of specimens cast in one batch proved to be too small to overcome the variability issues. However, even specimens from the same batch showed significantly different behaviour for the same loading. The results seem almost random. It was concluded that local flaws dominate the results. As even stress levels beyond what is allowable did not evoke a damping mechanism as assumed, it was concluded that no “extra damping” can be activated in the joint and no further investigation was pursued.

5.2 Fork-lift truck load model

Four different fork-lift trucks were investigated experimentally to set up a dynamic load model. During the tests the vertical accelerations of the fork-lift truck at the front and the rear axle were recorded as well as the path travelled of the front axle. The test programme comprised twelve different configurations which allowed a general model to be derived. The model can simulate the dynamics of a fork-lift truck including any payload carried.

For a range of fork-lift trucks and load capacities it was shown that the dynamic behaviour is similar and dominated, in terms of the frequencies, by the natural frequencies of the rigid body motion. The dominating frequencies can be calculated from the modal analysis after making some simplifying assumptions. They are then the eigen-frequencies of a three-degree-of-freedom model. The phase angle between the accelerations of the front and the rear axle was found to be constant: the first mode is in anti-phase and the second mode in phase.

Whereas the relation of horizontal velocity to the amplitudes of vertical accelerations was not as clear as for the frequencies, it is still possible to set up a simple envelope function that represents the relation reasonably well. A linear function after passing a threshold of $v = 0.5$ m/s was adopted. Two envelope functions were developed: one represents the mean of accelerations while the other is only exceeded by 5% of all measured acceleration peaks. The maximum velocity of the truck considered for the model is $v = 4.5$ m/s.

The analysis of the field tests suggests using of the mean of the peak accelerations to model the response realistically. The use of the 95% fractile values is a conservative approach that will leave a larger safety margin for uncertainties in the design.

The ratio of the amplitudes of the two dominant modes was incorporated into the model, and whilst the test results are not conclusive about what the ratio should be, it was set to $\mu = 0.5$.

The model assumes symmetry of the axle's forces and reduces them to a front axle force and a rear axle force. The generalised model for design purposes is set up with constants that are presented for a capacity of from 1500 kg to 6000 kg. The model is dependent on two variables only: time and current velocity.

$$\begin{bmatrix} F_f(t, v) \\ F_r(t, v) \end{bmatrix} = \frac{1}{L_{WB}^2} \begin{bmatrix} (m_{tot}L_r^2 + J) & (m_{tot}L_fL_r - J) \\ (m_{tot}L_fL_r - J) & (m_{tot}L_f^2 + J) \end{bmatrix} \cdot \begin{bmatrix} a_f(t, v) \\ a_r(t, v) \end{bmatrix} \quad (5.1)$$

with the acceleration functions being:

$$a_f(t, v) = \frac{A(v)}{1 + \mu} [\mu \sin(2\pi f_1 t) + \sin(2\pi f_2 t)] \quad (5.2)$$

$$a_r(t, v) = \frac{A(v)}{1 + \mu} [\mu \sin(2\pi f_1 t + \pi) + \sin(2\pi f_2 t)] \quad (5.3)$$

The amplitude function of accelerations for velocities $v > 0.5$ m/s is

$$A_{av}(v) = 1.2v + 0.4 \quad (5.4)$$

$$A_{95\%}(v) = 2.0v \quad (5.5)$$

where A_{av} denotes the mean and $A_{95\%}$ denotes the 95% fractile of peak accelerations.

All constants needed for the generalised load model can be found in Chapter 2, Tables 2.17 and 2.18.

5.3 Simulation of floor vibrations under moving load

The load model was applied to a three-dimensional finite-element model of a precast and partially prestressed floor system. The finite-element model was developed in SOFiSTiK and simulated in good approximation the lifetime of the precast and composite structure. SOFiSTiK proved its suitability for the calculation of the response of the floor to the dynamic (and moving) loading of the fork-lift truck model: a comparison of the measured frequencies and amplitudes during the field test and the results calculated with SOFiSTiK showed a good agreement between both: the field test had validated the method of modelling the fork-lift truck and the floor response calculation.

The structural model is detailed and incorporates the particularities of the precast building method, not only in terms of the geometry, but also in terms of the staged construction: the double-tee elements are modelled realistically (with the non-uniform distribution of the webs), the precast main beams are installed at the right stage and the various stages throughout the lifetime of the element, from storage of the young prestressed element to the composite structure after casting the topping, are calculated step by step. In the calculation of deformations different Young's moduli and ages of the concrete sections are accounted for. The effects of creep and shrinkage on the stiffness (and thus the deformations) are considered throughout the simulation.

The fork-lift truck load model was incorporated in the time-history analysis and

the position on the floor and the forces were calculated and updated for each time step. In SOFiSTiK the set-up of the load model is particularly simple: only the functions to calculate the forces at any time have to be programmed. The evaluation is done automatically in each time step, thus making it unnecessary to evaluate the functions manually and to put in the values for each step as a (potentially long) list.

5.4 Final observations

The aim of this project was the realistic simulation of the dynamic behaviour of a precast and partially prestressed floor system which is designed according to the latest standards (EC 2, 2004) for fork-lift truck traffic: in the design process the fork-lift truck was substituted by a quasi-static load which was placed in the worst possible position to create the highest stresses in the structure. This position usually is at midspan. However, due to this design method no dynamic effects of the fork-lift truck are known for a vibration serviceability check.

In the course of this study a dynamic load model of a fork-lift truck has been developed and was applied to the floor system in a finite-element simulation. The response of the floor system was compared with a field test carried out and a good agreement between observed and calculated behaviour was found.

The load model proved to be a useful tool in the serviceability analysis (and no indication was found that the model cannot be applied to any structure). The generalised model allows it to be tuned within limits if the eigen-frequencies of the structure are found to be close to the eigen-frequencies of the fork-lift truck.

The application of the fork-lift truck model is easy and with suitable software not too time consuming, and thus it should be included in the serviceability check of any structure which has to be designed for fork-lift truck traffic.

The weakness of the serviceability check is the lack of any specialised guideline concerning acceptability criteria for floor vibrations in the industrial environment. The guidance found in DIN 4150 Teil 2 (1999) can only be a starting point as it does not

differentiate between the day-time occupations in an industrial or office environment. Furthermore an investigation could be carried out into how the interaction of vibrations and sensitive machinery (e.g. precision tools) might limit the allowable vibrations.

If the limits of acceptable vibrations as set in DIN 4150 Teil 2 (1999) are taken into consideration it has to be concluded that the current design approach allows structures to be designed that will exceed that limit of accelerations. In the field test a structure was investigated with a low slenderness ratio of $L/h \approx 17.0$ while structures of higher slenderness ratios are possible (and often requested by promoters). An example of a slender floor system with a slenderness ratio of $L/h \approx 24.2$ has been modelled in the course of this thesis which only just fulfils the acceptable criterion according to DIN 4150 Teil 2 (1999): $a_{RMS,10} \approx 0.50 \text{ m/s}^2$. From this it is concluded that the current quasi-static design approach is non-conservative for dynamic loading from fork-lift truck traffic. It must be expected that many floor systems, currently designed and built, are likely to face vibration serviceability problems if the possible slenderness ratios are fully utilised and especially if the trend towards increased slenderness continues in the future.

5.5 Future work

5.5.1 Fork-lift truck model

The fork-lift truck model is robust in terms of the frequencies used to represent its behaviour. The mechanical model for a modal analysis to determine the eigen-frequencies is a suitable tool. It has been proved that the simple mechanical model for the excitation of the vibrations and their amplitudes is valid as well. However, the defined functions of average and 95% fractile accelerations are simple envelope functions which may lead to a falsified representation for certain configurations. It is here where further work should be carried out to make the modelling of the amplitudes in the fork-lift truck model as robust as the frequency model used.

5.5.2 Analysis of floor system

The obvious next step in the continuation of this study would be a full parameter study of various combinations of this precast floor system and different models of fork-lift trucks. This parameter study should identify combinations that lead to a particularly high increase in accelerations. After defining acceptability criteria for accelerations for this type of industrial use, design recommendations could be developed to avoid unsuitable levels of vibrations of these precast structures.

These design recommendations should focus on a new dynamic load factor. The new DLF should be a function of the structure's slenderness and the ratio of fork-lift truck excitation frequencies to the eigen-frequencies of the floor: $DLF_{new} = F(\frac{L}{h}, \frac{f_{floor}}{f_{ft}})$. The DLF should increase with higher slenderness ratios and frequency ratios close to 1. A full parametric study is necessary to investigate the correlations of these values and the accelerations to be expected.

If this new DLF is introduced the design should be possible without many iterations. The slenderness ratio and its mass are known from the initial design and with this the first eigen-frequency can be easily calculated. The eigen-frequencies of general fork-lift trucks are defined in this study.

Another problem to be investigated is the influence of a second fork-lift truck in service on the same floor, as often happens in busy warehouses. Because in most warehouses defined paths have to be followed by all traffic, the fork-lift trucks are likely to come into close proximity to each other regularly. This could lead either to a further increase in the peak accelerations or, if the loadings from the fork-lift trucks are in anti-phase, to a reduction of the amplitudes.

5.5.3 Investigation of concrete joint

The preliminary study reported here has not indicated the potential for significant damping in the joint; however, this may merit detailed study.

The investigation suffered from the influence of local flaws on the overall behaviour.

An ideal test would investigate full-size double-tee element in bending rather than a small specimen in shear. A full-size element would allow to place strain gauges in the joint to monitor any change of local differential deformation. However, not only the size of the specimen would have to be increased, but also the laboratory environment would have to be improved: not only a computer-controlled mixing batch would be necessary to reduce the variation of concrete strength, but also it would need to be climate-controlled to exclude effects from changes of temperature or humidity. Furthermore, lifting equipment in the laboratory would need a capacity of more than 20 tonnes: a double-tee element with a spanwidth of 15.00 m and a width of 2.50 m would have a height of 0.60 m which would result in a weight (including topping) of 23 tonnes.

During the excitation of the element accelerometers would measure the response. From this and the readings from the strain gauges a change of the damping properties would be detectable.

However, apart from a detailed investigation of the standard joint between precast and cast in-situ concrete, an investigation into increasing the damping of the composite structure could focus on the joint surface. One idea might be to add a thin visco-elastic layer between the precast and the cast in-situ concrete to improve the vibration performance. However, the effects on the static performance would have to be considered as well.

Appendix A

Investigation of the damping behaviour of the joint between precast and cast in-situ concrete

A.1 Preliminary observations

Eriksson (1994) investigated numerically the response of a floor system built with double-tee elements to excitation from jumping. He calculated a (root-mean-square) acceleration $a_{RMS} = 0.45 \text{ m/s}^2$, which is close to acceptable limits¹.

Another example is presented by Chen (1999) who analysed the dynamic response of a prestressed TT-floor (“composite floor system”) to heel drops in office buildings with a linear FE-model. He concluded that the additional damping provided by non-structural members in an office building, like light partition walls and furniture, is necessary to achieve the required overall damping (to fulfil the applied acceptability criteria). The damping introduced as structural damping was not sufficient to fulfil the requirements.

¹According to DIN 4150 Teil 2 (1999) an RMS-acceleration of 0.5 m/s^2 is acceptable for transient vibrations in the investigated environment.

In contrast to this, the present project concentrates on industrial buildings, where large areas are unfurnished (as service or traffic areas) and thus damping from non-structural members is small (or even non-existent).

Figure [A.1] shows a cross-section through a floor system built from precast double-tee elements with cast in-situ concrete topping. The joint extends over the whole area of a floor and therefore can potentially have a decisive influence on its overall behaviour.

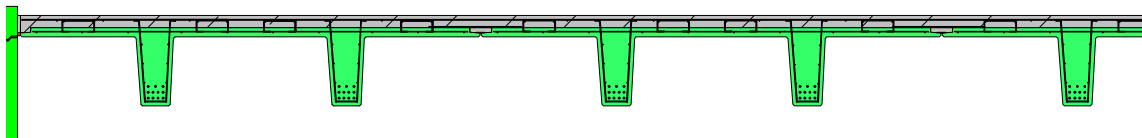


Figure A.1: Cross-section through composite floor system

The damping behaviour is of special importance due to the low natural frequencies of this system and of fork-lift trucks. Eriksson (1994) found more than 10 modes in the range from 4 - 10 Hz. From the literature review of fork-lift trucks it is known that their natural frequency is in the range of 3 - 10 Hz (Lewis and Griffin, 1998). Thus a fork-lift truck should be able to excite the structure close to its resonant frequency, which should lead to a significant increase in its dynamic response, but no cases have been reported where unsuitable dynamic behaviour occurred in conjunction with fork-lift truck traffic¹.

Bachmann (1995) and many other researchers have shown that though concrete structures have higher damping than steel constructions, prestressed concrete ones have only small damping. This may be explained by reference to the mechanism that provides the main part of damping in a concrete structure: differential movement of concrete and reinforcement steel at tension cracks. Prestressing prevents these cracks from forming and thus prevents this kind of damping from occurring. Partial prestressing will show a damping behaviour somewhat in between reinforced and prestressed concrete structures, as cracks can form to some extent under service loading.

This raises the question whether the composite structure of precast (and pre-

¹However, one should bear in mind that building contractors are not interested in making their “failure” public. They will retrofit the structure but not report it.

stressed) concrete elements and an in-situ cast concrete topping provides more damping than a similar concrete structure manufactured in one cast.

The knowledge of the dynamic behaviour of reinforced as well as precast and prestressed concrete structures suggests that further damping can be found only, if at all, in the joint between precast and in-situ cast concrete.

Starting from this hypothesis, it is assumed that the mechanism of damping here would be similar to the damping that occurs at cracks: small cracks form at flaws in the joint like a fatigue process as described in CEB (1996) for reinforced cross-sections. A cracked (and thus delaminated) area could move differentially when vibrating and thus provides damping as a result of energy dissipation due to frictional processes. The mechanism is similar to the damping that occurs for low stresses between cracked concrete and the reinforcement. Bachmann and Dieterle (1981) showed the potential of this damping mechanism and Jeary (1996) explained its relation to fracture mechanics:

[...] current research [into fracture mechanics] suggests that energy is dissipated in materials when microscopic cracks elongate. The work done in elongating represents an energy dissipation mechanism.

The joint carries the normal service load on the surface to the centre of the structure (normal stress in the joint) and it transmits the shear stresses which result from the beam action of the composite structure to the cast in-situ topping (shear stress). The experimental program carried out investigates these two actions of the joint separately: shear and normal stress in the joint, see Figure [A.2], and shear stress in the joint, see Figure [A.3].

It is assumed that the formation of “extra damping” in the joint can be detected by changes in the following properties:

Ultimate strength If the ultimate strength of the (unloaded) specimen is tested in a cube tester it will fail similarly to a standard cube from stresses due to transverse

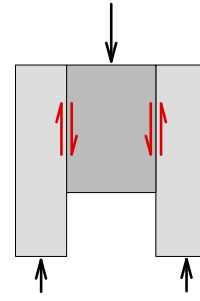
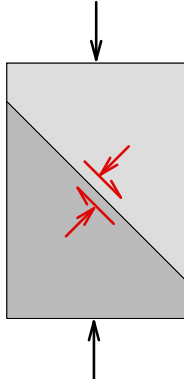


Figure A.2: Sketch of specimen type 1 Figure A.3: Sketch of specimen type 2

expansion (Poisson's ratio). If the predicted effect of delamination weakens the bond in the joint a failure plane along the joint is expected.

Deformability If the predicted effect emerged the delamination of the joint should lead to stress concentrations in smaller (still bonded) areas. The stress concentration should lead to bigger deformations under a constant load.

Hysteresis An increased deformation under constant load levels should lead to increase in the energy dissipation per cycle due to frictional processes at the interface of debonded areas.

All properties of interest could be examined easily with the available equipment (LVDT and Cube tester) without incurring too much cost. Only if these initial tests had shown evidence of the assumed mechanism would a more detailed investigation of the processes in the joint have been conducted.

A.2 Preparation of specimen

Both types of specimen were cast in two sections. To simulate the time gap between casting the precast element and the topping after assemblage on site the second section of a specimen was cast four weeks after the first section was cast. The specimen was cured for another four weeks before the test programme was conducted.

Directly after casting the first section its surface was treated to achieve a rough surface for a good bond of the sections and before casting the second section the surface of the first section was wetted. As Júlio et al. (2004) showed this does not increase the strength, but it ensured a dust-free surface which guaranteed the constant quality of the bond.

From one batch of concrete six to ten specimens could be cast. In total seven sets were cast. Due to the uncontrolled climate conditions in the concrete lab and the different ages of the available cements the actual strength of the concrete mixes varied in a wide range: the first section varied by 20% and the second section by as much as 50%.

The strength of the concrete used to cast the specimen was determined with cube tests. Three standard cubes of $100 \times 100 \times 100$ mm were cast of each batch. In Table A.1 is given the average strength of each set.

Set of specimen	Strength section 1 [MN/m ²]	Strength section 2 [MN/m ²]
13/10	56.2	39.2
14/11	63.7	30.7
23/11	53.4	–
28/03	61.6	47.8
07/07	47.7	41.5
01/12	42.3	41.4
06/12	42.3	37.5

Table A.1: Strength of specimen's concrete

A.3 Cyclic loading

The cyclic loading (as a sinusoidal load) was applied in a DARTEC machine for a defined number of cycles. The extreme values of displacement and load were recorded every 100 (or 1000) cycles.

The stress level was chosen in accordance with the expected stresses in the floor system under service conditions: directly under a wheel a normal stress of ~ 2.1 MN/m² combined with a shear stress of ~ 1.5 MN/m² can be reached:

Normal stress According to DIN 1055 Teil 3 (2006) the footprint of a fork-lift truck's wheel is 200×200 mm and the front axle load of a truck with a capacity of 5 t is $F = 1.4 \cdot 120 = 168.0$ kN where 1.4 is the DLF. From this follows the normal stress under a wheel as: $\sigma_N = \frac{\frac{1}{2} \cdot 168}{200^2} \times 10^3 = 2.1$ MN/m².

Shear stress According to EC 2 (2004) the maximum shear stress in the joint can be estimated as $\tau_{sd} = 1.0 \frac{V_{sd}}{z \cdot b_j}$ where V_{sd} is the shear force, z the leverarm of inner forces and b_j the breadth of the joint. For typical structures the values of these variables can be estimated to $V_{sd} \approx 700$ kN (including safety factors), $z = 0.50$ m, $b_j = 1.25$ m. This gives a shear stress of: $\tau_{sd} = 1.0 \frac{700}{0.50 \cdot 1.25} \times 10^{-3} = 1.1$ MN/m².

However, the configuration of the joint in specimen type 1 led to the same values for shear and normal stress. To account for material safety factors in the design the maximum load was taken as the mean load in the experiments and the amplitude set to 1.0 MN/m².

For the specimen type 2 the stress level was initially $\tau_{mean,1} = 0.5$ MN/m² with $\Delta\tau_1 = 0.25$ MN/m². The stress level was increased over a number of tests to extreme values of $\tau_{mean,2} = 5.0$ MN/m² with $\Delta\tau_2 = 2.0$ MN/m², which were, according to design codes, beyond the allowable shear stress of the concretes cast.

The test programme comprised a range of from 10,000 to 1,000,000 cycles. Each set of specimens was tested over a short period of time to avoid any influence of time-dependent effects within the set.

For the second set of specimens with a vertical joint the testing rig was modified to be able to record the displacements continuously with an LVDT.

A.4 Results of cyclic testing

A.4.1 Influence of cyclic loading on ultimate strength

As described earlier, it was assumed that cyclic loading would evoke a fatigue process that would ultimately result in the failure of the bond. It was of special interest to discover whether the relatively low number of cycles at the given stress levels led to the expected decline or not.

After the cyclic loading the specimens were crushed in a cube tester to determine their ultimate strength. All specimens failed as would be expected for a normal cube test of one material. Only if the cracks reached the joint surface did they then follow it for a short distance, see Figures [A.4] and [A.5].



Figure A.4: Typical failure mechanism of specimen type 1



Figure A.5: Enlarged crack along joint surface

The results are shown in Figures [A.6] and [A.7]. They are normalised to the strength of the un-loaded specimen of each set. The linear regressions (best fit) of each set show an almost random behaviour in the ultimate strength over the number of cycles. Of the seven sets tested, four show an increasing ultimate strength with an increasing number of load cycles.

From the failure mechanism that was observed it can be concluded that no delam-

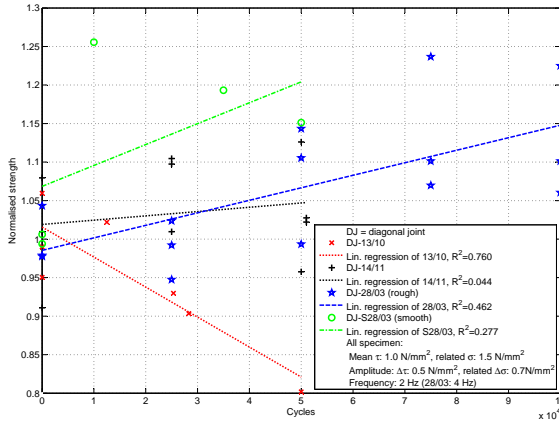


Figure A.6: Normalised strength of specimen type 1

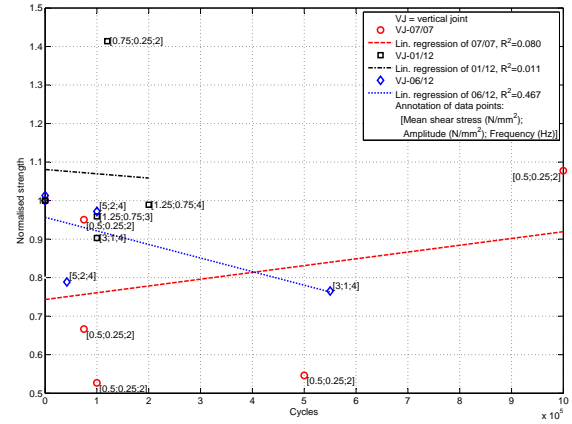


Figure A.7: Normalised strength of specimen type 2

ination of the sections occurred as the result of the applied cyclic loading.

A.4.2 Influence of cyclic loading on stiffness

While the measurement of the ultimate strength did not give conclusive results, the deterioration in the stiffness of the specimens ought to be a better indicator of any delaminating effects: if micro-cracks formed due to the cyclic loading the compliance of the specimen should have increased for a given load because it was transmitted through a smaller effective bond area. Thus higher effective stresses resulted which led to a bigger deformation. This could be interpreted as a deterioration in the stiffness of the specimen. Therefore it was not surprising that the results showed a similar random picture: of the 39 tests executed with a record of the stiffness, only 13 showed a negative slope for the linear regression of the stiffness as a function of the load cycles. Furthermore, the determination R^2 of the linear regressions of the stiffness was low in all tests.

A.4.3 Influence of cyclic loading on hysteresis loop

The measurement of the stiffness and the ultimate strength of the specimens after cyclic loading did not show a conclusive result. As the hysteresis loop is related to the stiffness of the specimen, it is not expected to find a different situation when analysing the hysteresis than was found for the stiffness.

In Figure [A.8] are shown the hysteresis loops of specimen 07/07-VI after 5,000 and 1,000,000 cycles. The energy dissipated was smaller after 1,000,000 cycles than it was after 5,000 cycles. The results for the other specimens show a similarly diverse picture as those of the evaluation of the ultimate strength and the stiffness: of the eleven tests where the hysteresis loop was recorded, only seven showed an increase in energy dissipation with an increasing number of cycles: see Table A.2. The variation in energy dissipation could well be due to errors in the measurement and the analysis¹.

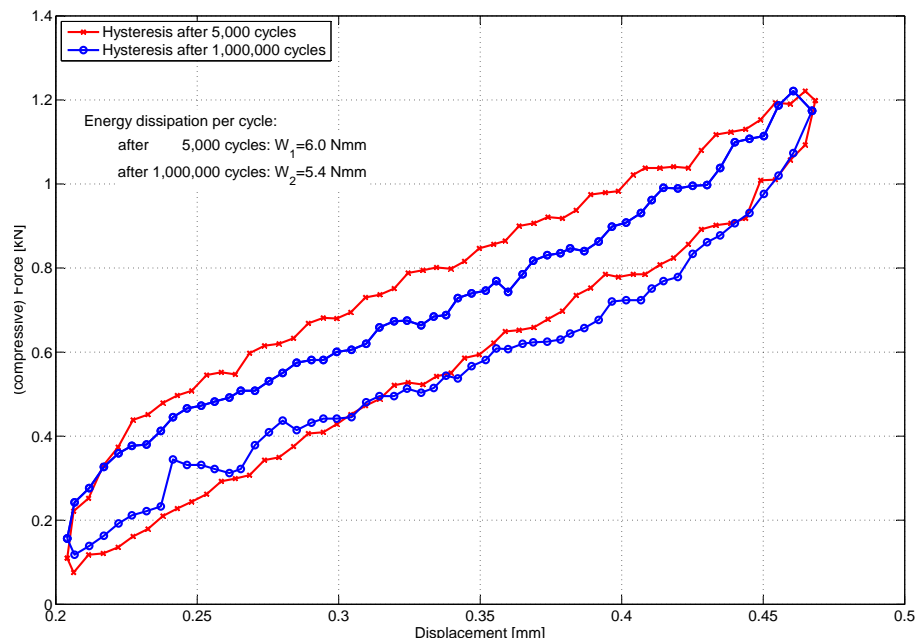


Figure A.8: Hysteresis loop after 5,000 and 1,000,000 cycles of specimen 07/07-VI

¹See Figure [A.8]: the loop is not perfectly smooth, which has an influence on the numerical integration of the area surrounded.

Specimen	Energy [Nmm] dissipated after			
	5000 cycles	max.	number of cycles	
07/07	I	3.0	75,000:	3.2
	II	3.9	75,000:	3.7
	III	2.7	500,000:	2.8
	V	4.2	100,000:	4.4
	VI	6.0	1,000,000:	5.4
	01/12	I	16.3	100,000:
II		18.0	200,000:	18.2
III		30.9	100,000:	30.4
V		7.4	120,000:	6.1
06/12		I	31.2	550,000:
	III	61.6	100,000:	62.4
	IV	58.1	40,000:	57.8

Table A.2: Change of hysteresis loop

A.4.4 Estimate of damping from hysteresis loop

While it is not possible to identify an increase in energy dissipation over the number of cycles tested, it is possible to estimate the damping of the specimen by means of the model of a damped single-degree-of-freedom system:

the energy put into the specimen is the loading branch of the hysteresis: after 5000 cycles it is found to be $W_{5000} = 123.3$ N mm correlated to stress intensity of $\tau_{mean} = 0.5$ MN/m² and an amplitude of $\Delta\tau = 0.25$ MN/m².

If it is assumed that this energy is a load that causes a displacement of a single-degree-of-freedom system which is then released into a free vibration, then this energy would be the potential energy that causes vibration (of the first cycle). The next cycle would have an energy that is equal to the energy of the previous cycle reduced by the dissipated energy during one cycle: $\Delta W_1 = 6.0$ N mm. The energy stored in a one-degree-of-freedom system is known to be:

$$W_i = \frac{1}{2}mU_i^2\omega^2 \Leftrightarrow U_i = \sqrt{\frac{2W_i}{m\omega^2}} \quad (\text{A.1})$$

where U_i is the amplitude of i -th cycle of vibration. Hence the logarithmic damping

decrement may be formulated as:

$$\delta = \ln \left(\frac{U_i}{U_{i+1}} \right) = \ln \left(\sqrt{\frac{2W_i/(m\omega^2)}{2W_{i+1}/(m\omega^2)}} \right) \quad (\text{A.2})$$

$$= \ln \left(\sqrt{\frac{W_i}{W_{i+1}}} \right) = \ln \left(\sqrt{\frac{123.3}{123.3 - 6.0}} \right) = 0.025 \quad (\text{A.3})$$

with the relation between viscous damping and the damping decrement simplified for small amounts of damping ($\zeta < 0.2$):

$$\zeta \approx \frac{\delta}{2\pi} = \frac{0.025}{2\pi} = 0.4\% \quad (\text{A.4})$$

A similar result was obtained after 1,000,000 cycles: $W_{10^6} = 117.2$ N mm, $\Delta W_2 = 5.4$ N mm and thus $\zeta = 0.375\%$.

For a higher stress intensity (test specimen 01/12-V: $W_{5000} = 346.0$ N mm, $\Delta W = 30.9$ N mm, $\tau_{mean} = 1.25$ MN/m², $\Delta\tau = 0.75$ MN/m²) there was calculated a damping value of $\zeta = 0.74\%$.

While these results agree qualitatively with the general findings of Jeary (1986) that an amplitude dependency is to be expected, these calculated damping values are smaller than published values. For example see Chapter 1, Table 1.1: Bachmann gave a value of $\zeta > 0.7\%$ for an uncracked concrete section with a low stress intensity.

A.5 Conclusions from the investigation of the joint

The data collected during the testing of both types of specimen show a very diverse picture. Depending on the type of specimen, the strength of a specimen (or to be more precise the variation in strength of both parts of one specimen) and the stress level during the cyclic loading, the results vary immensely.

Neither the age of a specimen at the time of testing nor the increase in the stress level influenced the results to show a clear trend.

A.5 Conclusions from the investigation of the joint

These findings suggest that local flaws in the specimen have an important influence on the overall behaviour and outcome of a test. Furthermore, the allowable stresses of concrete at service level and at ultimate level during the design incorporate the possible variations of concrete strength and thus they are set to very low (safe) values.

The analysis of the “stiffness” of the specimen also shows huge variations. This suggests that the control of the hydraulic actuator is not precise enough. A change in the testing frequency (which is between 1 Hz and 4 Hz) does not change these variations. Furthermore it is suspected that the change of properties is so small that it is not possible to detect them with the existing equipment.

It is difficult to draw any conclusions from these results, which show such big variations and deviations from the assumed behaviour. However, one should bear in mind that the safety margin for material failure in shear is bigger than for normal stresses and that this might mean that although the applied stress levels are beyond allowable levels, they are still too small to evoke a fatigue process within the limited number of cycles. If that is the case, all changes in the observed behaviour would be due to local flaws. From this it can be concluded that no “extra damping” was activated in the joint.

The estimated damping values of the specimen type 2 are smaller than published values and those (more reliable) values were used for the finite element modelling of the structure in Chapter 3.

The set-up of a more detailed test, which should be able to detect even smallest changes of the damping properties, is described in Chapter 5.

Appendix B

Evaluation of fork-lift truck tests

B.1 Specification of test equipment

Accelerometer:

PCB 338B35

Sensitivity	100 mV/g
Measurement range	± 50 g
Frequency range (± 5 %)	1.0 - 2000 Hz
Frequency range (± 10 %)	0.7 - 3000 Hz
Resolution	0.001 g rms
Resonant frequency	≥ 12 kHz

Signal conditioner:

PCB 480E09

Excitation Voltage to sensor	27 - 29 V (DC)
Maximum DC offset	< 30 mV
Frequency range (± 5 %)	0.15 - 100,000 Hz
Spectral noise at 1 Hz	-113 dB
Spectral noise at 10 Hz	-114 dB
Spectral noise at 100 Hz	-119 dB
Spectral noise at 1000 Hz	-125 dB

Data acquisition card:

DT 9804

Resolution	16 bits
Sampling rate	100 kS/s
Channel acquisition time	5 μ s

Table B.1: Specification of test equipment

B.2 Summary of configuration of tests performed

In Table B.2 are summarised the main test parameters for each of the tested configurations. It states the number of tests performed, the total time of these tests, and the frequency of data sampling which was varied in some tests to find a good compromise between the size of a data file and the quality of the record. Each configuration was tested at least once with the highest data sampling frequency to check the problem of aliasing.

The number of Hamming windows of each configuration that was evaluated in the frequency analysis is stated as well. The analysis is carried out using windows of 5 seconds length and an overlap of 2.5 s, see Section 2.7.1.1.

Configuration	No. of tests performed	Total time of tests	Frequency of data sampling	No. of 5 s windows in frequency analysis	
N16	LI	18	829	1250	330
	NLI	20	1004	1250	400
	LO	14	677	1250	270
	NLO	20	1345	1250	530
N15	LI	16	1114	250; 1250	440
	NLI	13	934	500; 1250	370
	LO	8	880	500; 1250	350
	NLO	8	738	500; 1250	290
J16	LO	9	989	50; 1250	390
	NLO	13	888	500; 1250	350
P25	LO	10	625	500; 1250	250
	NLO	15	1045	500; 1250	410

Table B.2: Summary of configuration of executed tests

B.3 Frequency analysis

B.3.1 Total record

For the plot of Nissan16-LI see Section 2.7.1.1.

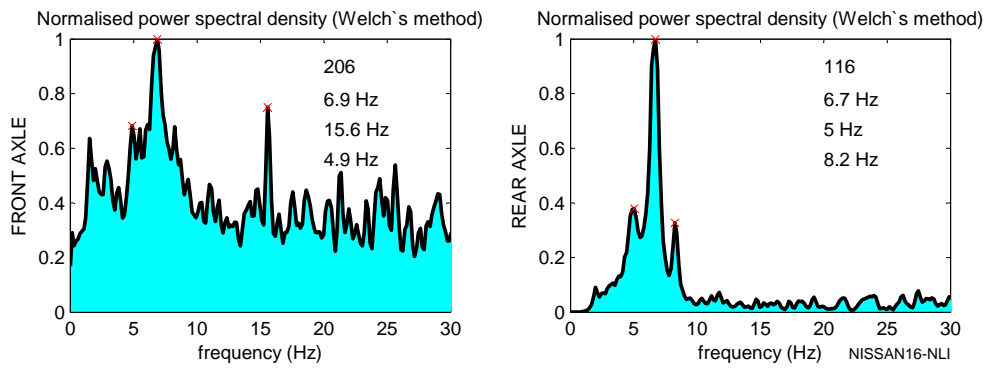


Figure B.1: Nissan16-NLI: indoors without payload

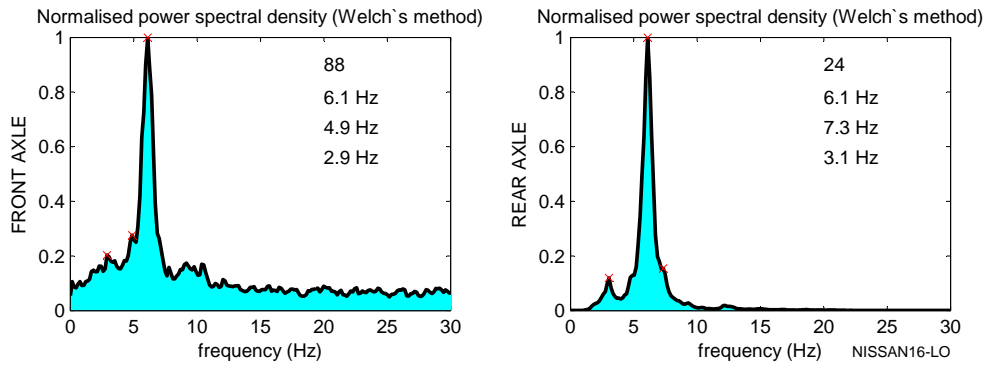


Figure B.2: Nissan16-LO: outdoors with payload

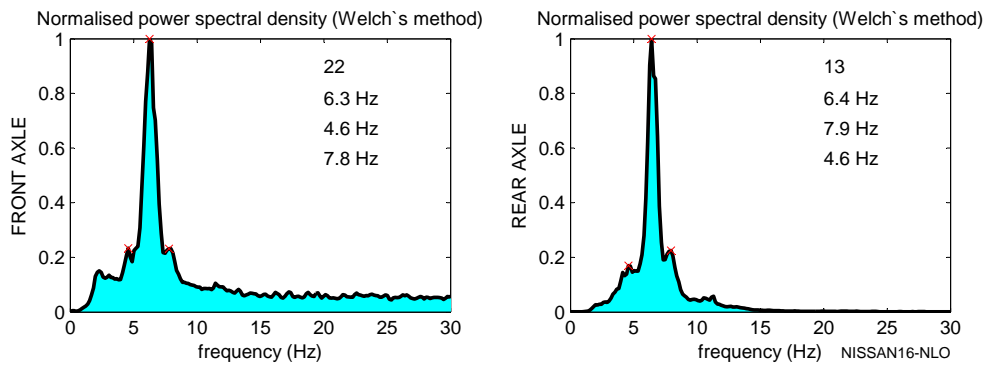


Figure B.3: Nissan16-NLO: outdoors without payload

For the Nissan15 fork-lift truck the significant peaks were found to vary between the front and rear axles as well as in relation to the surface driven on: see Figures [B.4] to [B.7]. While at the front axle for a smooth surface (indoors) the natural frequency of 9.9 Hz is dominant (first peak), it is only the second peak (third, if no payload is carried) outdoors. Here, the natural frequency of about 5.0 - 5.5 Hz is predominant, which is the second peak indoors. The rough surface of the pavement on which the outdoor tests were performed may introduce forced vibration into the system which would explain the changes between the indoor and outdoor tests. However, the main difference between the results from indoors and outdoors is the change in magnitude of vibration and not its frequency.

At the rear axle the picture is clearer: the first peak is about 5.0 - 5.9 Hz and the second peak at 3.0 - 4.4 Hz (smaller in the loaded case for both peaks).

The combustion-engine-powered fork-lift trucks show a less clear picture: for the Jungheinrich16 see Figures [B.8] and [B.9] and for the Pimespo25 see Figures [B.10] and [B.11]. The frequencies induced by the rotating parts of the engine seem to interfere with the natural frequencies of the chassis. The engines run at approximately 1000 - 3000 rpm $\hat{=}$ 16.6 - 50.0 Hz and big peaks are found at 41.0 Hz (J16) and about 26.5 - 30.0 Hz (P25). If these peaks are omitted, the natural frequencies identified are in good agreement with the range of frequencies found for the battery-powered fork-lift trucks.

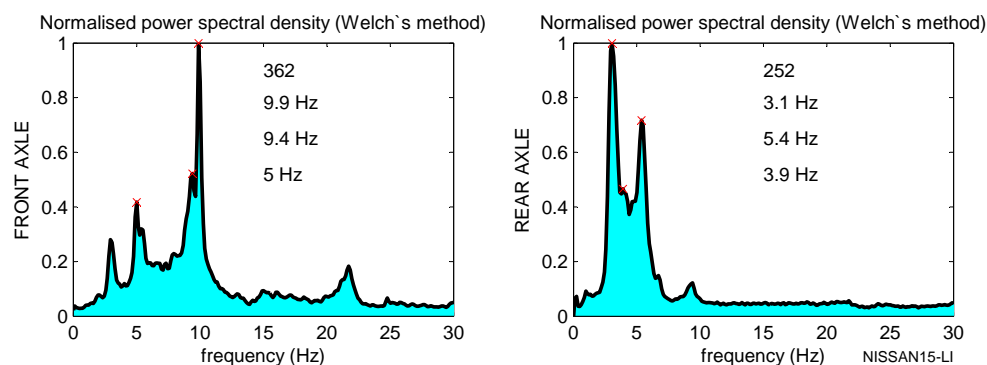


Figure B.4: Nissan15-LI: indoors with payload

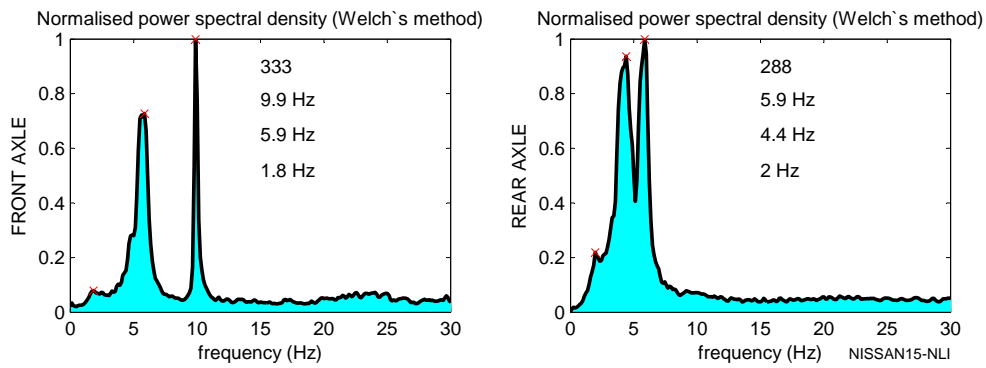


Figure B.5: Nissan15-NLI: indoors without payload

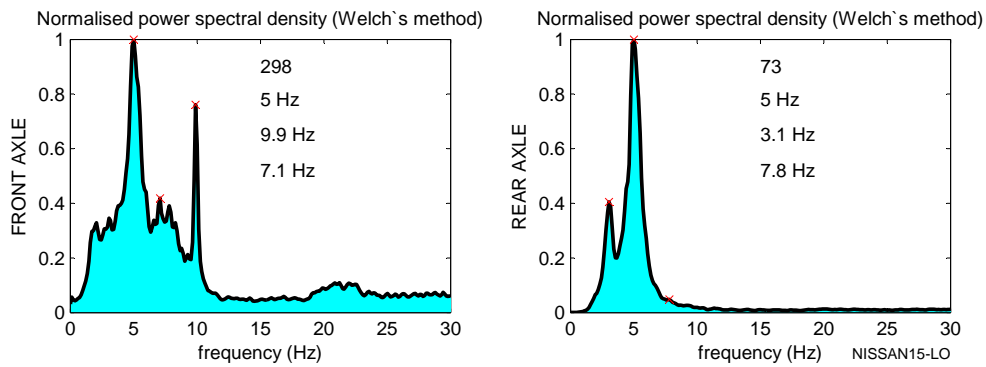


Figure B.6: Nissan15-LO: outdoors with payload

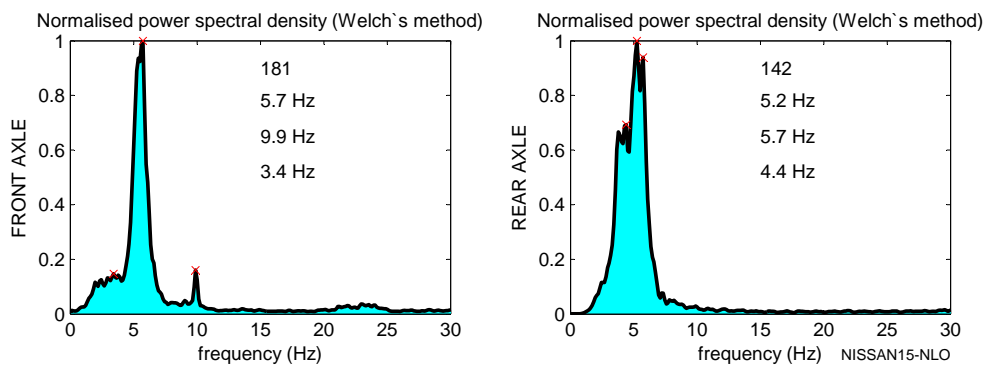


Figure B.7: Nissan15-NLO: outdoors without payload

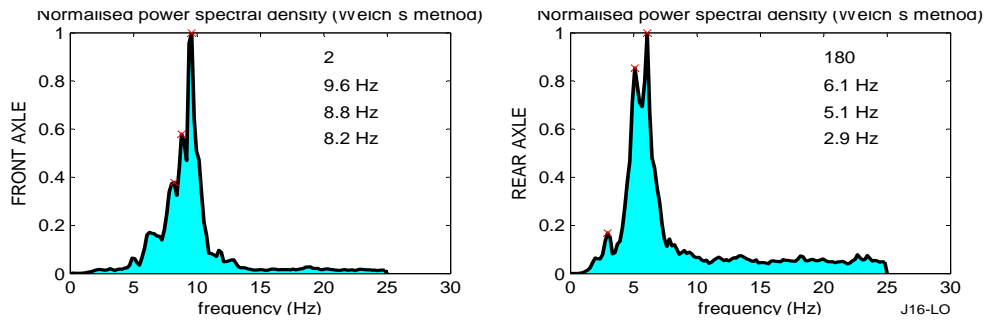


Figure B.8: Jungheinrich16-LO: outdoors with payload

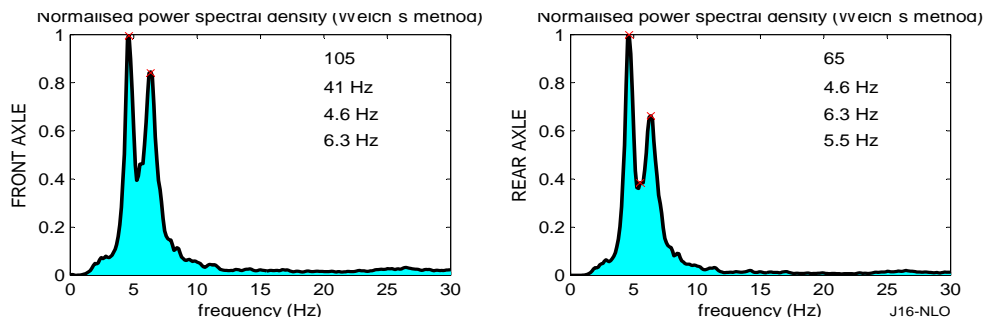


Figure B.9: Jungheinrich16-NLO: indoors without payload

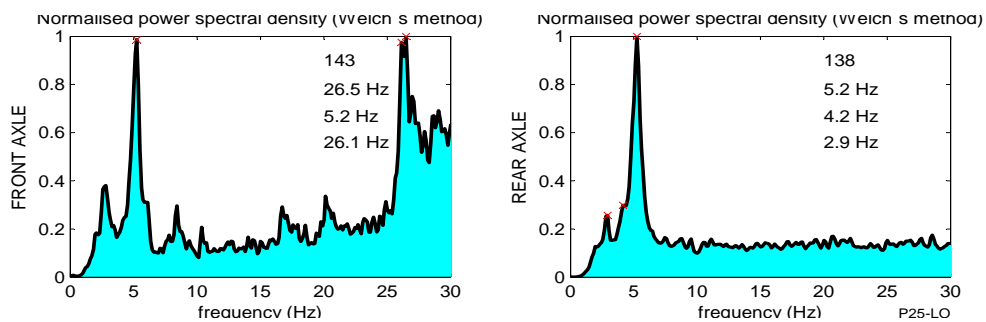


Figure B.10: Pimespo25-LO: outdoors with payload

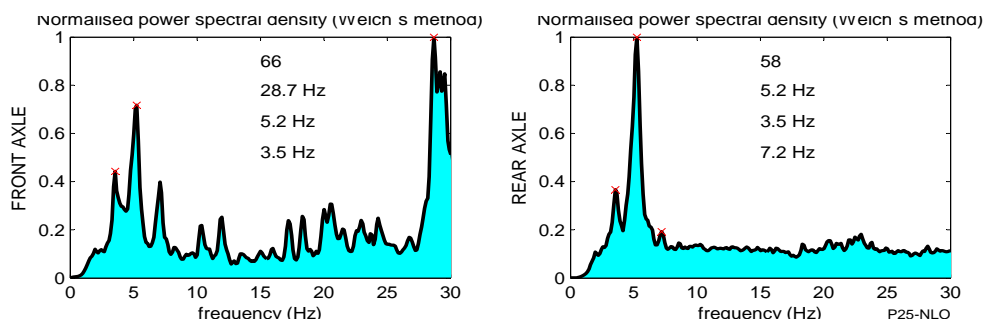


Figure B.11: Pimespo-NLO: indoors without payload

B.3.2 Correlation of velocity and frequencies

For the plot of Nissan16-LI see Section 2.7.1.2.

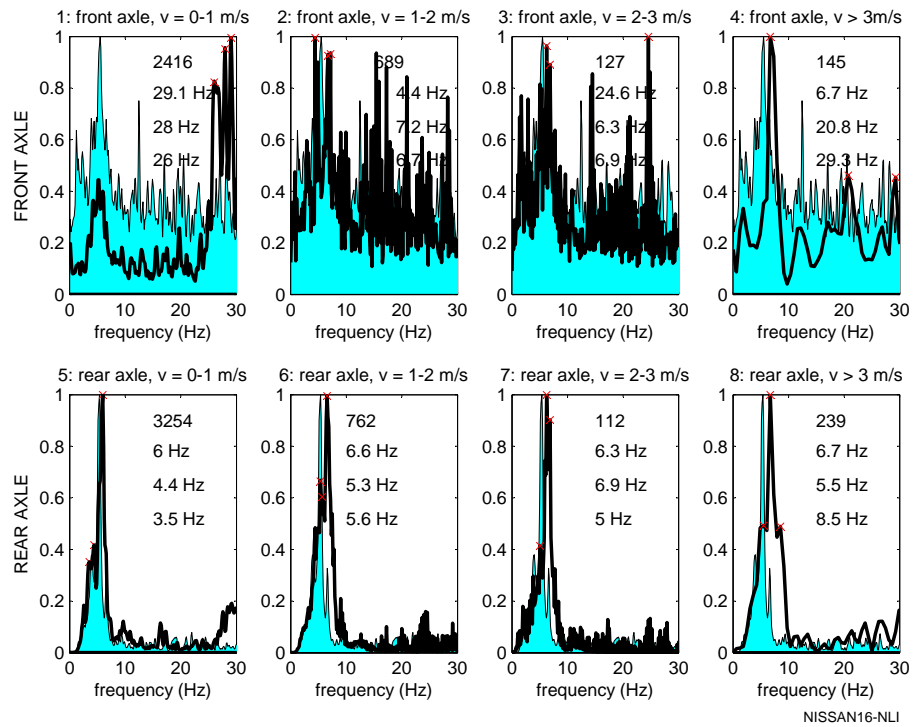


Figure B.12: Nissan16-NLI, influence of velocity on frequency content

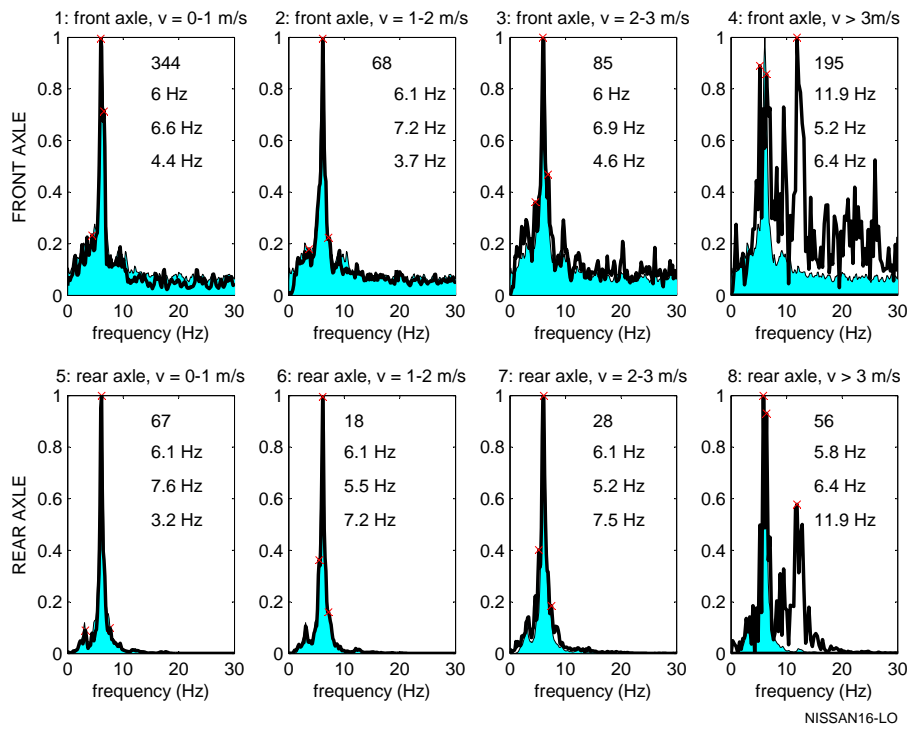


Figure B.13: Nissan16-LO, influence of velocity on frequency content

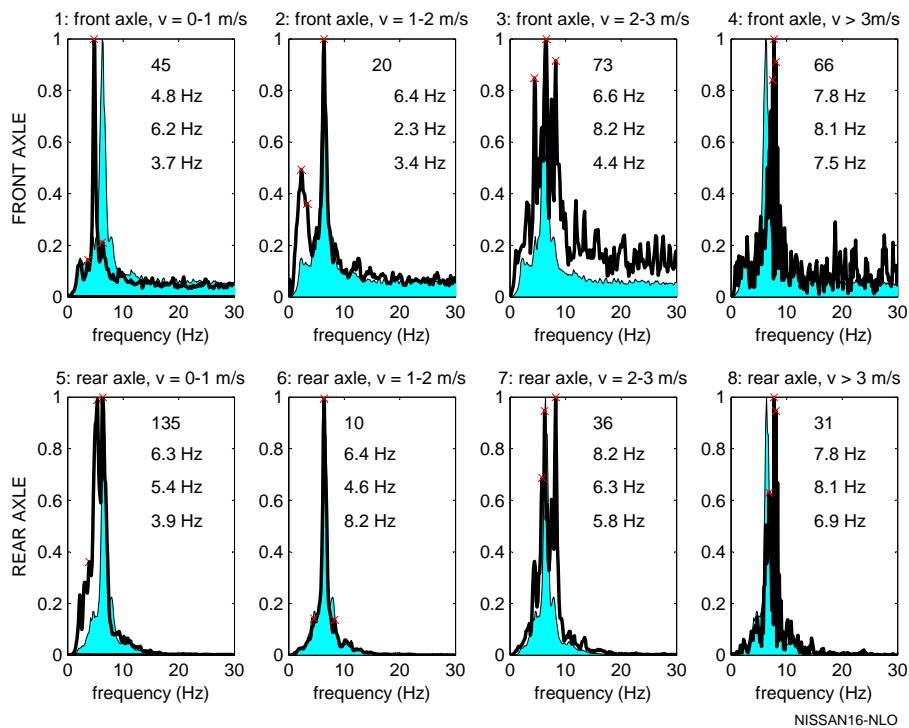


Figure B.14: Nissan16-NLO, influence of velocity on frequency content

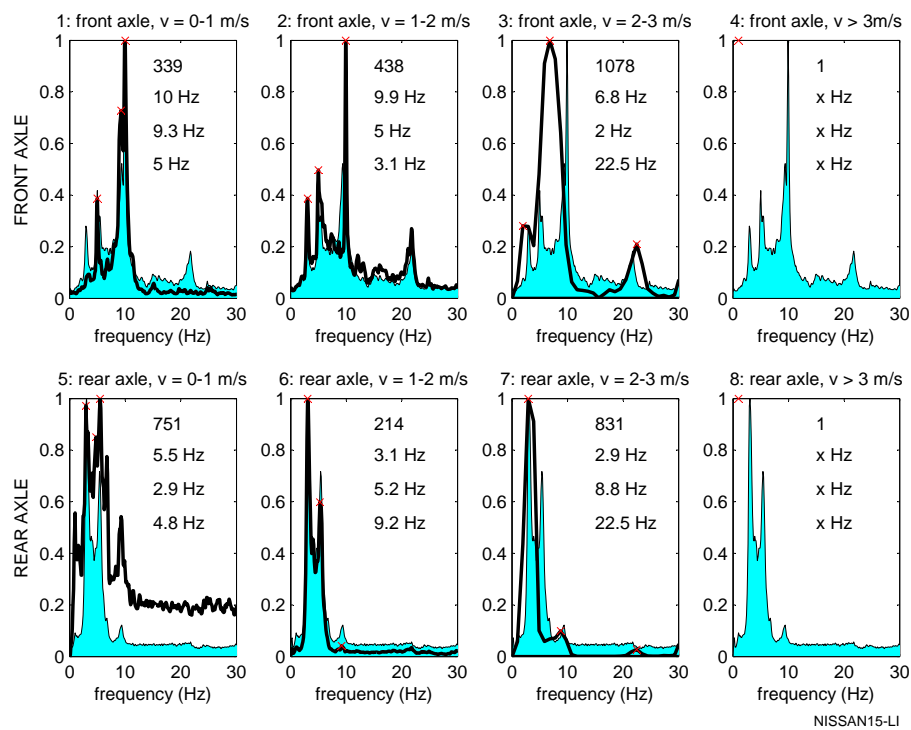


Figure B.15: Nissan15-LI, influence of velocity on frequency content

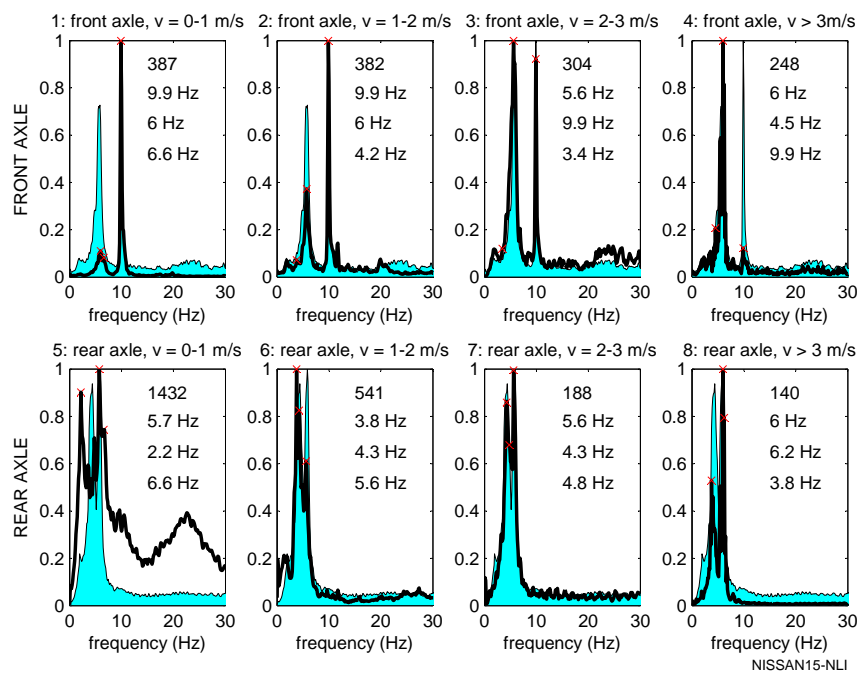


Figure B.16: Nissan15-NLI, influence of velocity on frequency content

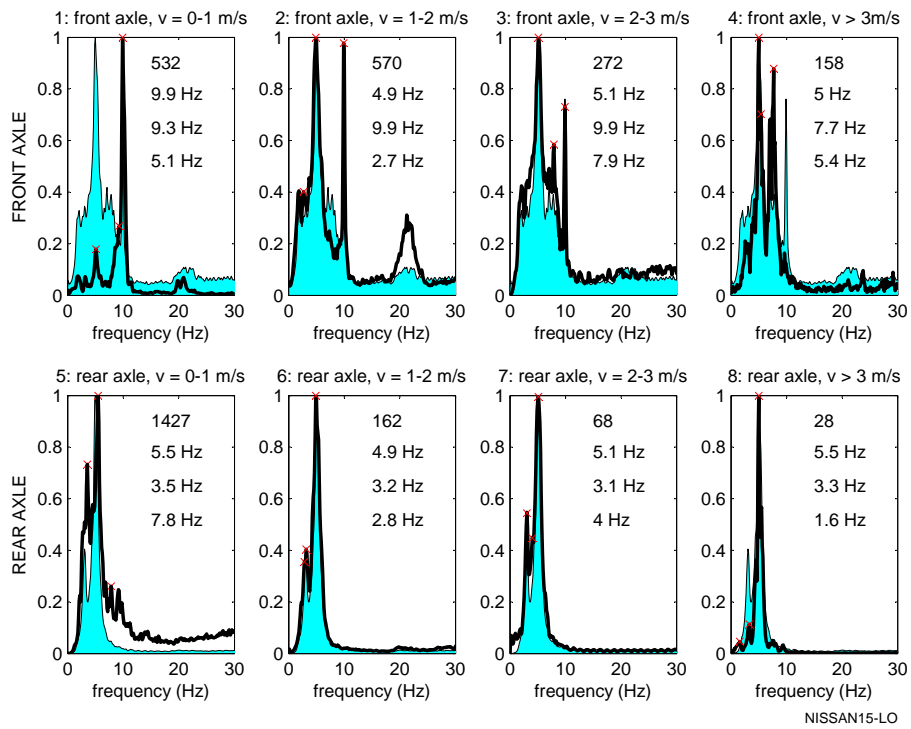


Figure B.17: Nissan15-LO, influence of velocity on frequency content

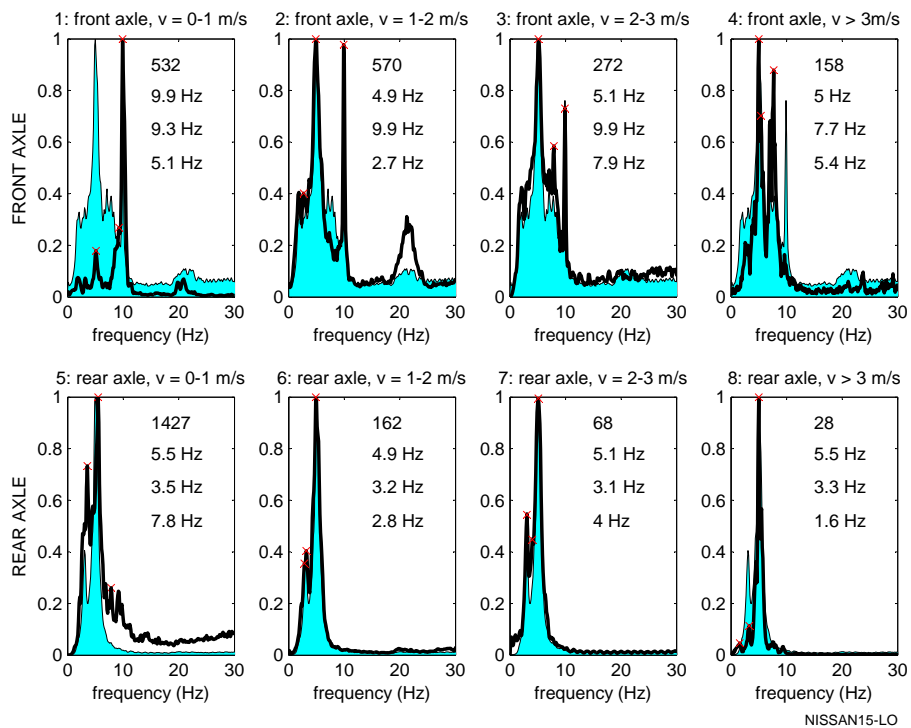


Figure B.18: Nissan15-NLO, influence of velocity on frequency content

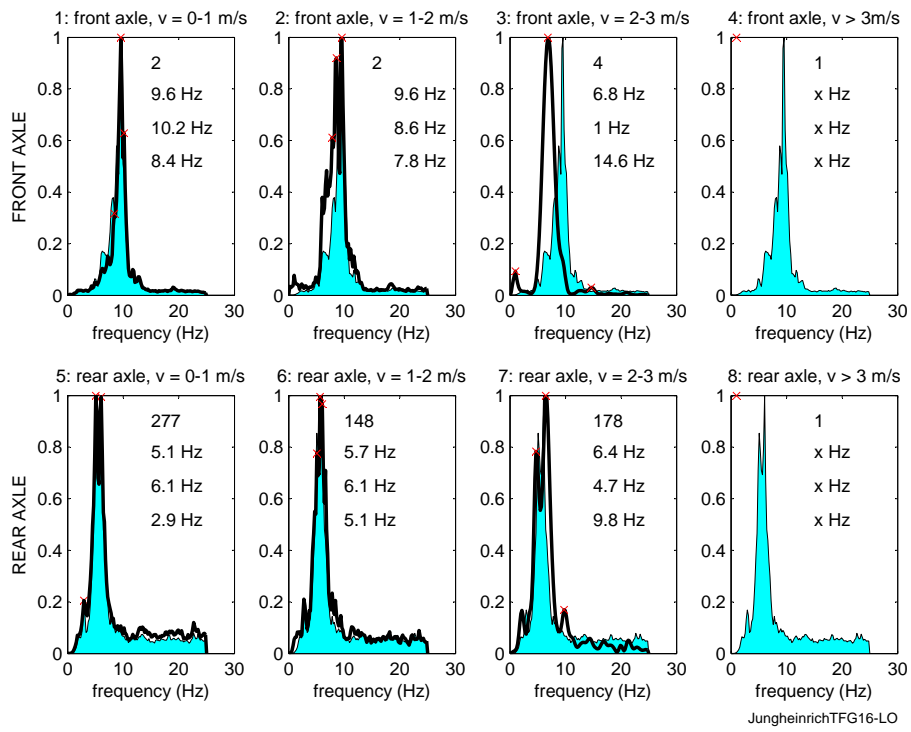


Figure B.19: Jungheinrich16-LO, influence of velocity on frequency content

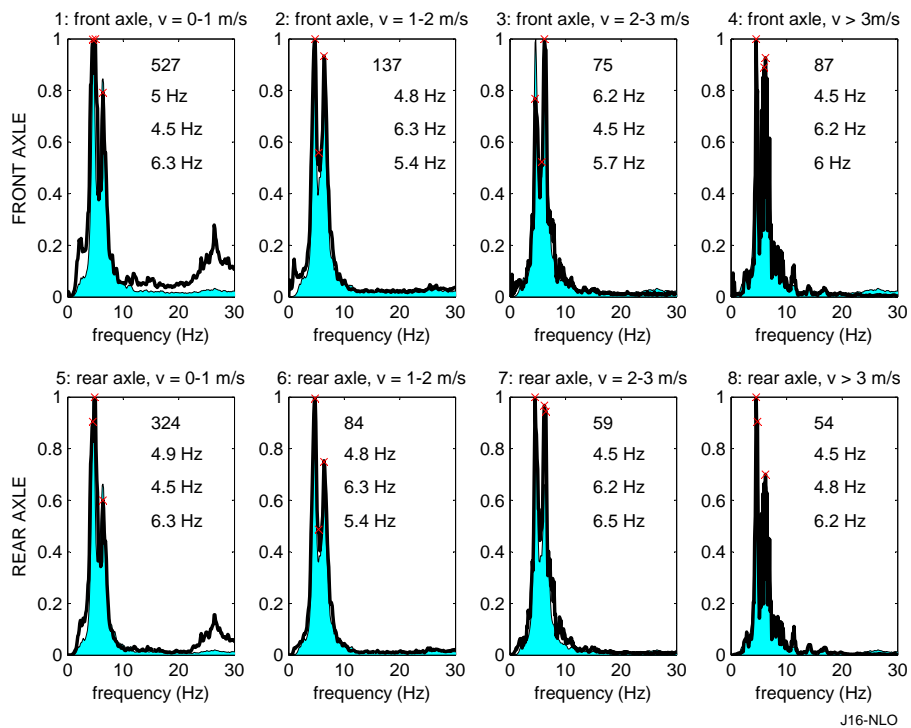


Figure B.20: Jungheinrich16-NLO, influence of velocity on frequency content

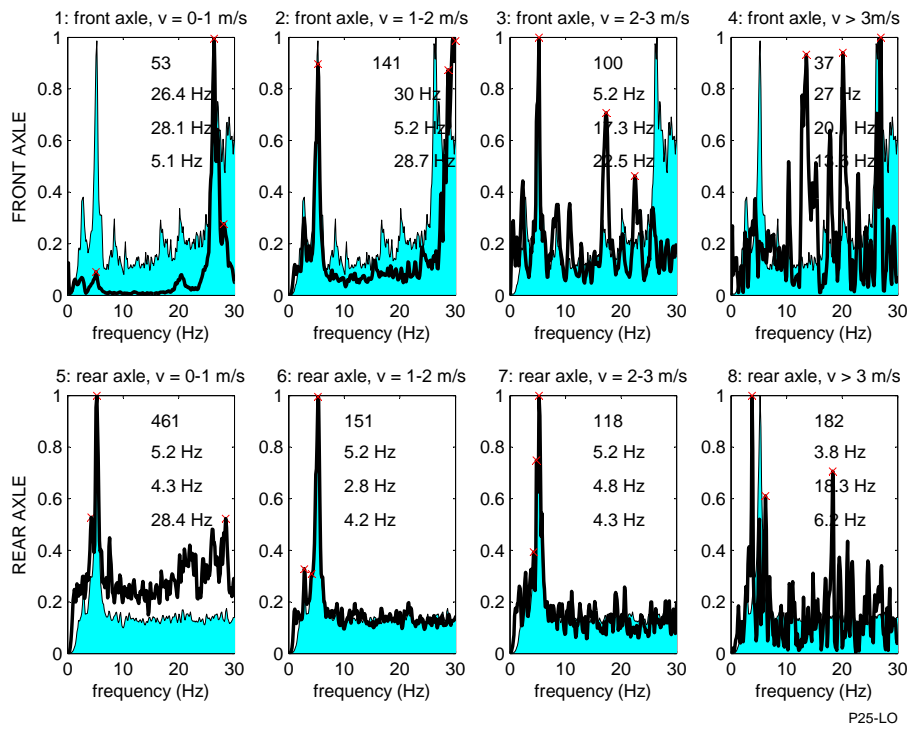


Figure B.21: Pimespo25-LO, influence of velocity on frequency content

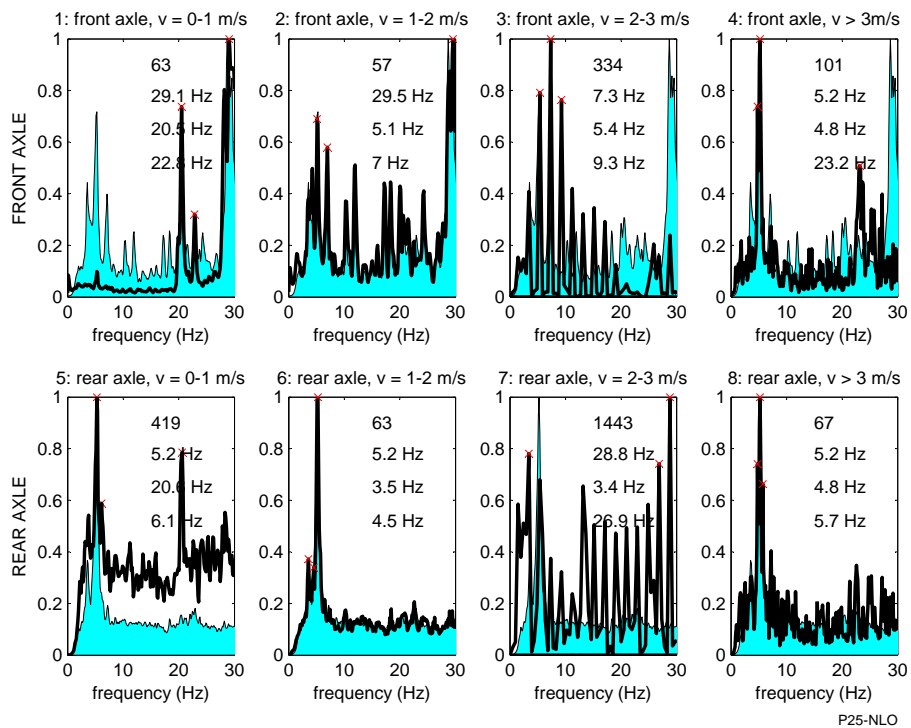


Figure B.22: Pimespo25-NLO, influence of velocity on frequency content

B.3.3 Correlation of driving direction and frequencies

For Nissan16-LI see Section 2.7.1.3.

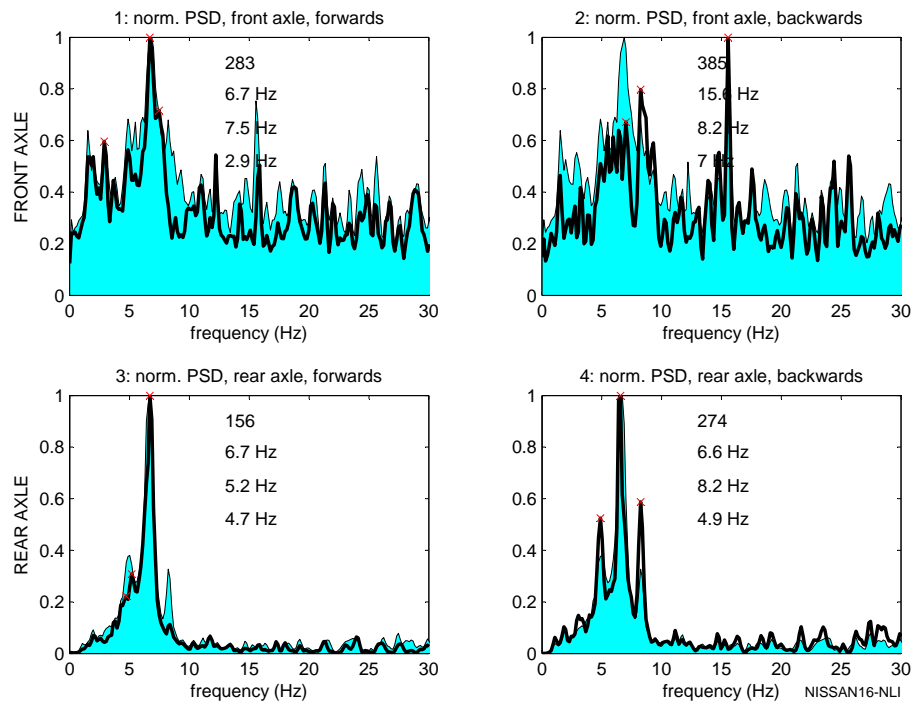


Figure B.23: Nissan16-NLI, power spectral density for different driving direction

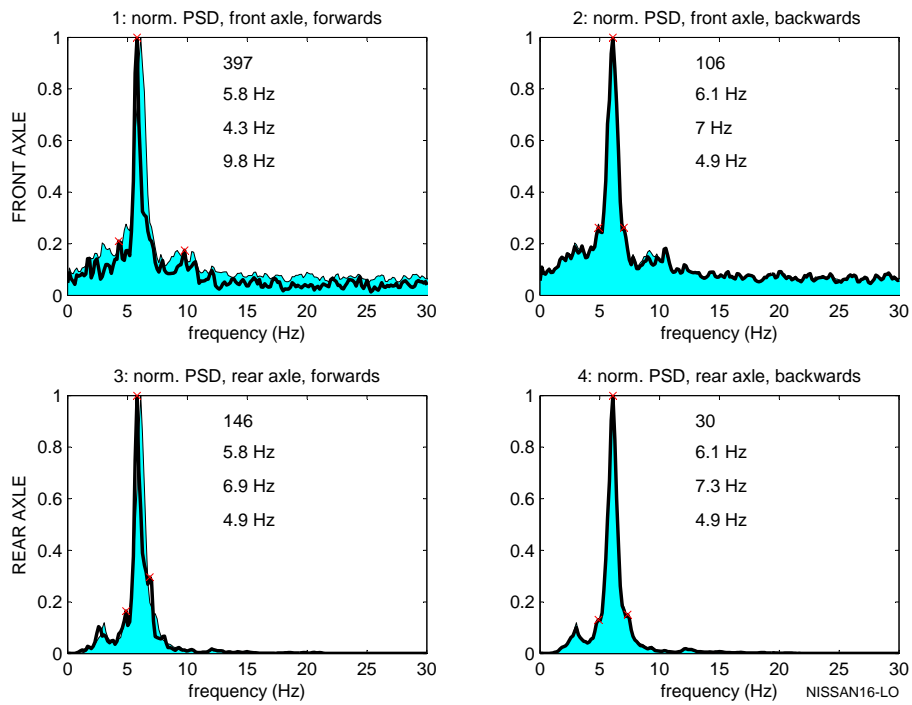


Figure B.24: Nissan16-LO, power spectral density for different driving direction

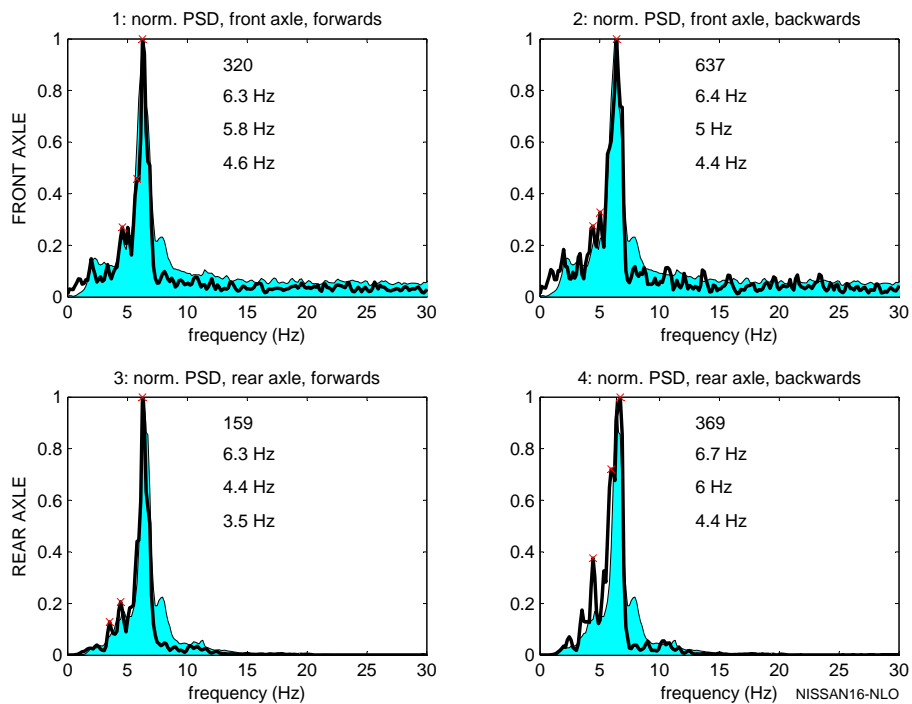


Figure B.25: Nissan16-NLO, power spectral density for different driving direction

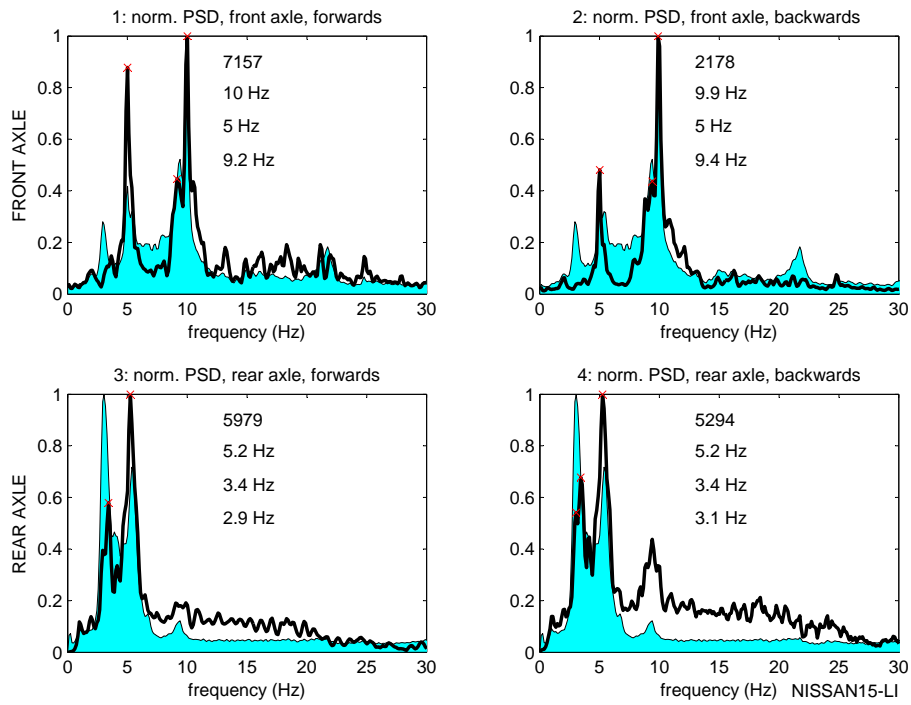


Figure B.26: Nissan15-LI, power spectral density for different driving direction

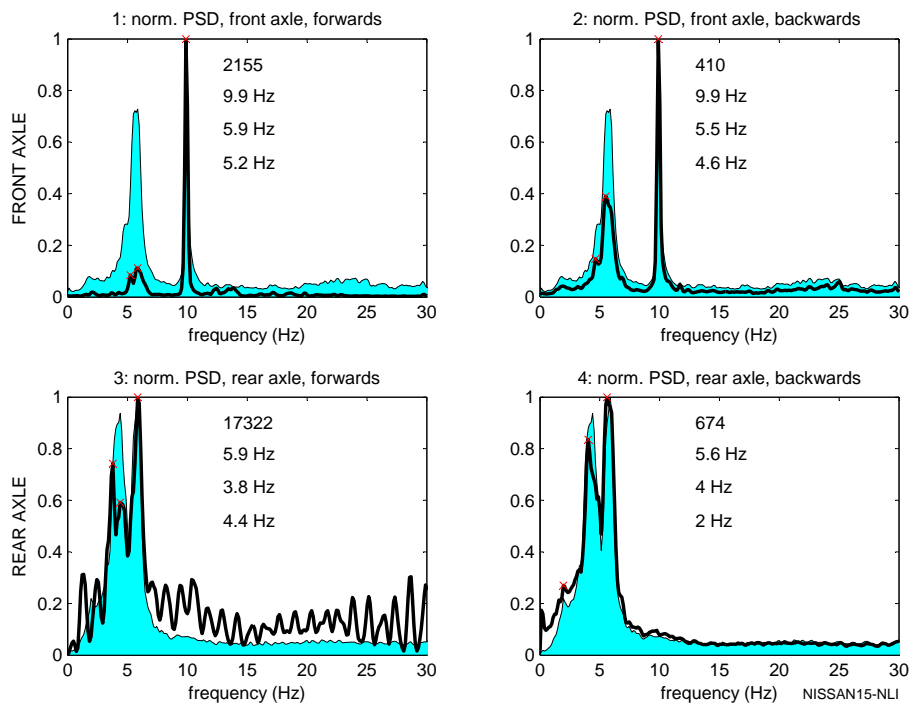


Figure B.27: Nissan15-NLI, power spectral density for different driving direction

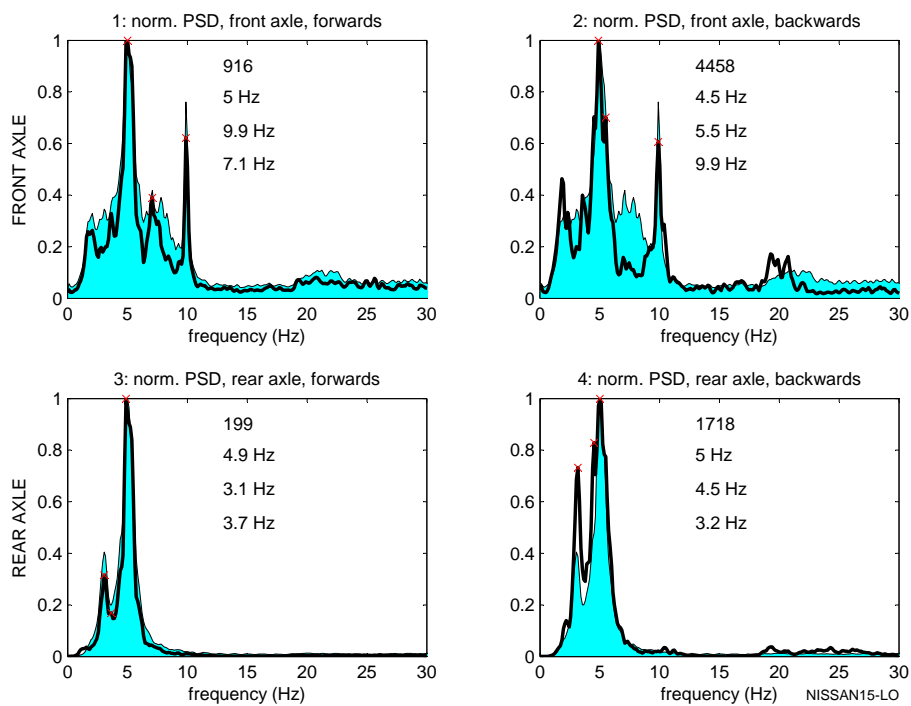


Figure B.28: Nissan15-LO, power spectral density for different driving direction

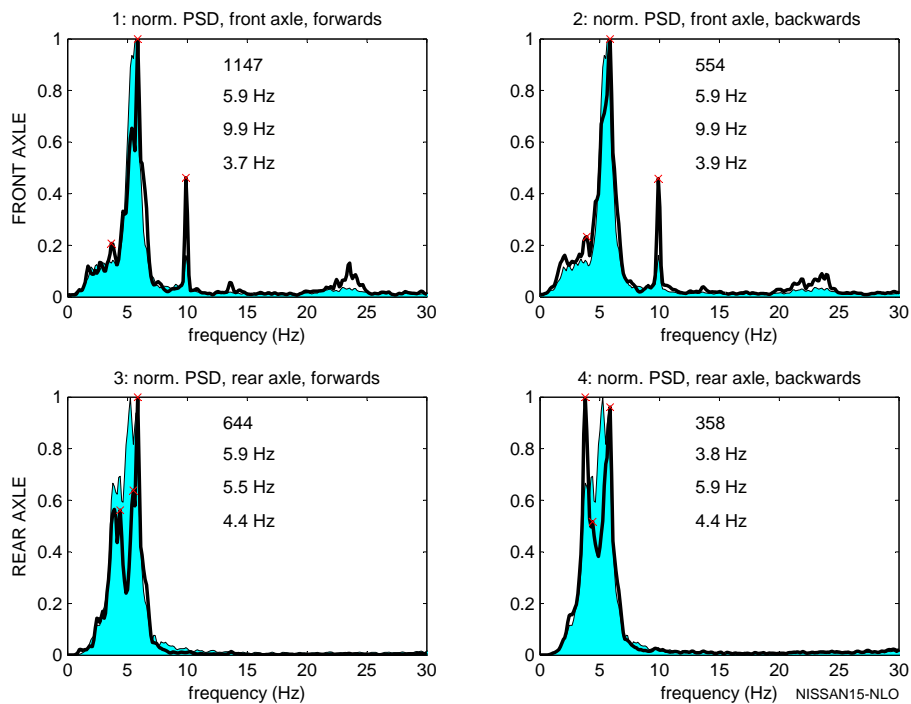


Figure B.29: Nissan15-NLO, power spectral density for different driving direction

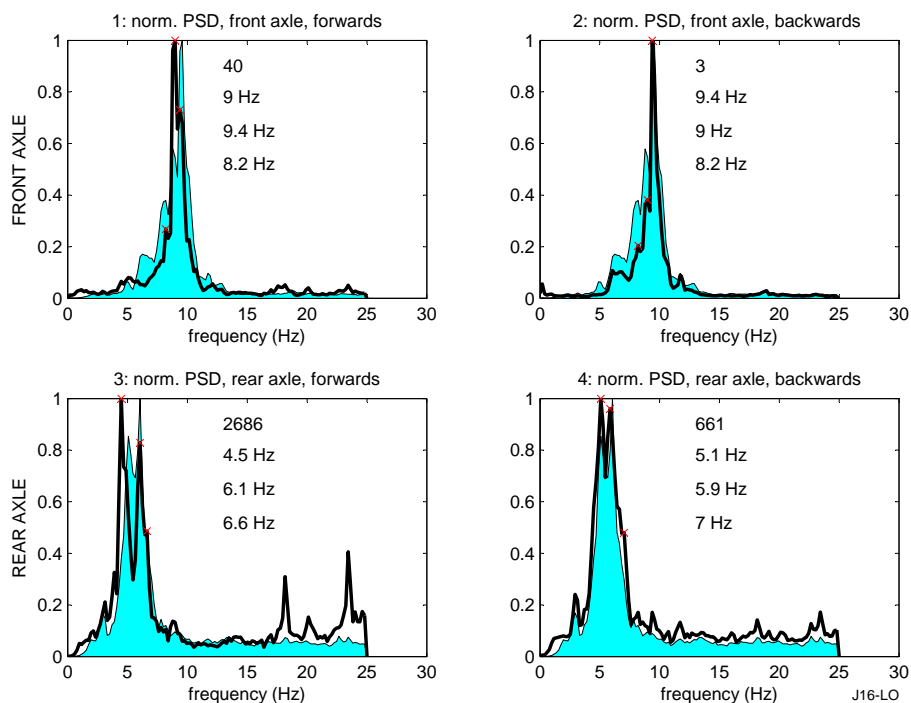


Figure B.30: Jungheinrich16-LO, power spectral density for different driving direction

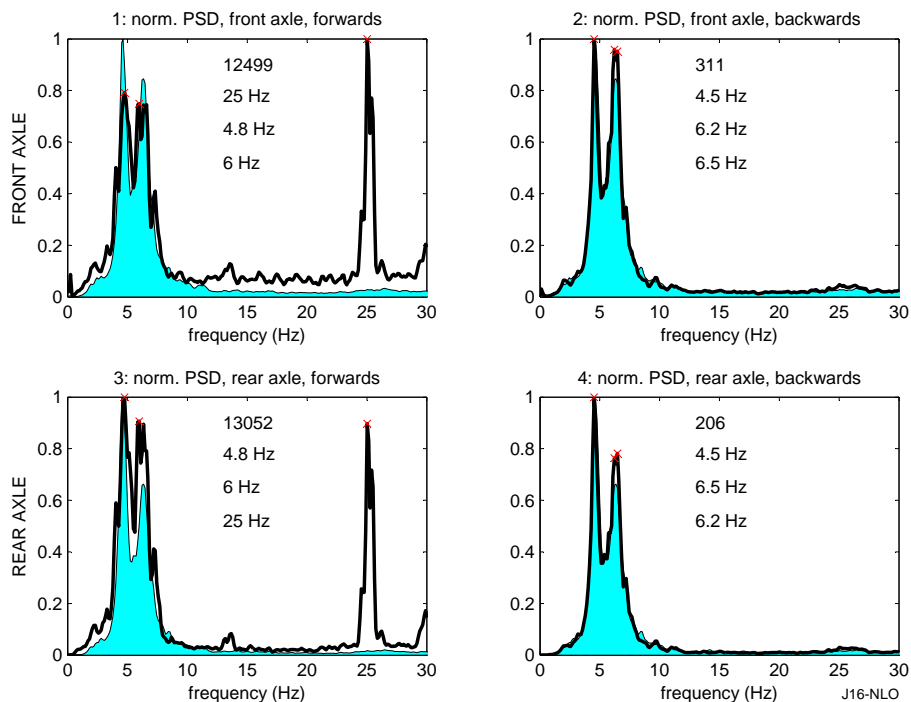


Figure B.31: Jungheinrich16-NLO, power spectral density for different driving direction

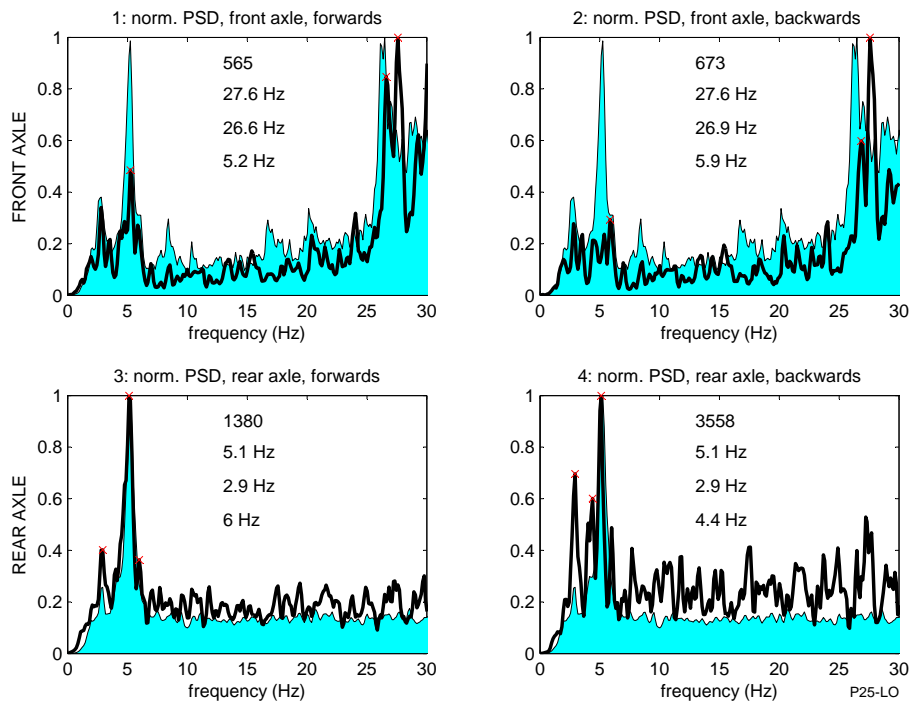


Figure B.32: Pimespo25-LO, power spectral density for different driving direction

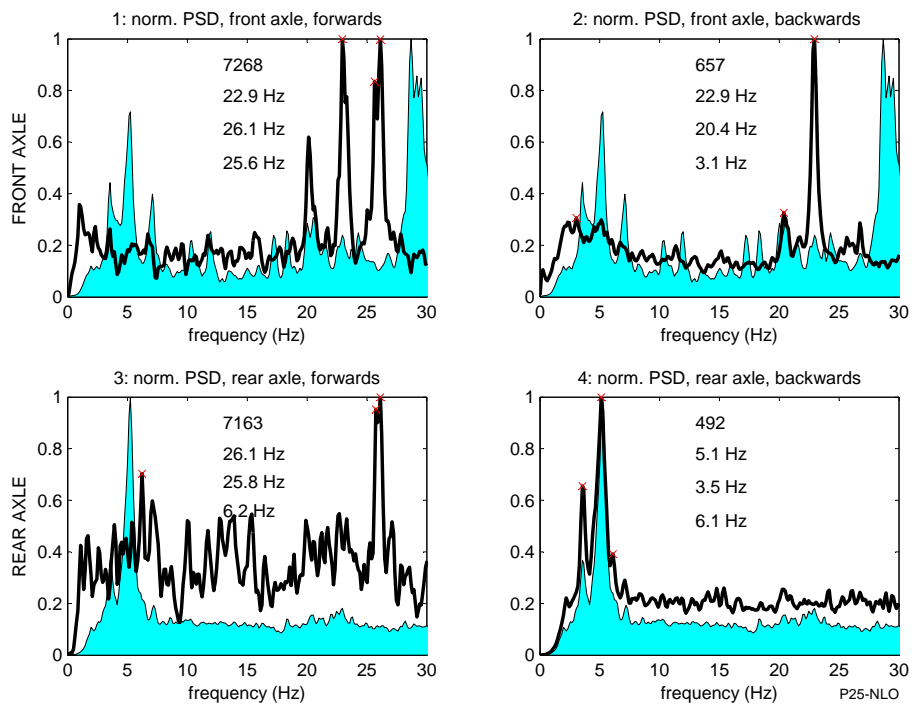


Figure B.33: Pimespo25-NLO, power spectral density for different driving direction

B.3.4 Modal analysis

For the results of the modal analysis of Nissan16 see Section 2.7.1.4.

Modal Analysis: N15		Mode 1	Mode 2	Mode 3
Without a payload carried:				
Eigen-vector	$\begin{bmatrix} z_g \\ \varphi_g \\ \varphi_m \end{bmatrix}$	$\begin{bmatrix} -0.22 \\ -0.95 \\ 0.24 \end{bmatrix}$	$\begin{bmatrix} -0.82 \\ 0.02 \\ -0.57 \end{bmatrix}$	$\begin{bmatrix} 0.10 \\ -0.12 \\ 0.99 \end{bmatrix}$
Eigen-frequency	[Hz]	4.3	5.7	9.6
With a payload of 420 kg carried:				
Eigen-vector	$\begin{bmatrix} z_g \\ \varphi_g \\ \varphi_m \end{bmatrix}$	$\begin{bmatrix} -0.14 \\ 0.96 \\ -0.25 \end{bmatrix}$	$\begin{bmatrix} -0.87 \\ -0.40 \\ -0.30 \end{bmatrix}$	$\begin{bmatrix} -0.21 \\ 0.14 \\ 0.97 \end{bmatrix}$
Eigen-frequency	[Hz]	3.3	5.4	9.8

Table B.3: Summary of modal analysis

Modal Analysis: J16		Mode 1	Mode 2	Mode 3
Without a payload carried:				
Eigen-vector	$\begin{bmatrix} z_g \\ \varphi_g \\ \varphi_m \end{bmatrix}$	$\begin{bmatrix} -0.11 \\ -0.98 \\ 0.14 \end{bmatrix}$	$\begin{bmatrix} -0.97 \\ -0.12 \\ -0.19 \end{bmatrix}$	$\begin{bmatrix} 0.09 \\ -0.10 \\ -0.99 \end{bmatrix}$
Eigen-frequency	[Hz]	4.9	6.1	14.6
With a payload of 350 kg carried:				
Eigen-vector	$\begin{bmatrix} z_g \\ \varphi_g \\ \varphi_m \end{bmatrix}$	$\begin{bmatrix} -0.25 \\ 0.92 \\ -0.32 \end{bmatrix}$	$\begin{bmatrix} -0.85 \\ -0.45 \\ -0.28 \end{bmatrix}$	$\begin{bmatrix} -0.25 \\ 0.16 \\ 0.96 \end{bmatrix}$
Eigen-frequency	[Hz]	3.6	5.8	9.2

Table B.4: Summary of modal analysis

Modal Analysis: P25		Mode 1	Mode 2	Mode 3
Without a payload carried:				
Eigen-vector	$\begin{bmatrix} z_g \\ \varphi_g \\ \varphi_m \end{bmatrix}$	$\begin{bmatrix} -0.28 \\ -0.96 \\ 0.03 \end{bmatrix}$	$\begin{bmatrix} -0.99 \\ 0.10 \\ -0.05 \end{bmatrix}$	$\begin{bmatrix} 0.07 \\ -0.08 \\ -0.99 \end{bmatrix}$
Eigen-frequency	[Hz]	4.0	5.1	24.5
With a payload of 350 kg carried:				
Eigen-vector	$\begin{bmatrix} z_g \\ \varphi_g \\ \varphi_m \end{bmatrix}$	$\begin{bmatrix} -0.08 \\ 0.99 \\ -0.07 \end{bmatrix}$	$\begin{bmatrix} -0.96 \\ -0.26 \\ -0.06 \end{bmatrix}$	$\begin{bmatrix} -0.15 \\ 0.11 \\ 0.98 \end{bmatrix}$
Eigen-frequency	[Hz]	3.4	4.9	17.7

Table B.5: Summary of modal analysis

B.3.5 Summary of frequencies

Analysis	Axle	Frequency [Hz]					
			1^{st}_{mode}		2^{nd}_{mode}		3^{rd}_{mode}
Modal		-	5.2	-	6.7	-	9.7
Experimental							
Total data set	front	-	4.9	-	6.9	-	15.6
	rear	-	5.0	-	6.7	-	8.2
Velocity							
v_1	front	-	5.0	-	-	-	29.1
	rear	3.5	4.4	6.0	-	-	-
v_2	front	4.4	-	-	6.7	7.2	-
	rear	-	5.3	5.6	6.6	-	-
v_3	front	-	-	6.3	6.9	-	24.6
	rear	-	5.0	6.3	6.9	-	-
v_4	front	-	-	-	6.7	-	20.8
	rear	-	5.5	-	6.7	8.5	-
Driving direction							
forwards	front	2.9	-	-	6.7	7.5	-
	rear	4.7	5.2	-	6.7	-	-
backwards	front	-	-	-	7.0	8.2	15.6
	rear	-	4.9	-	6.6	8.2	-

Table B.6: Nissan16-NLI, summary of frequencies

B.3 Frequency analysis

Analysis	Axle	Frequency [Hz]					
			1^{st}_{mode}		2^{nd}_{mode}		3^{rd}_{mode}
Modal		-	3.3	-	6.3	-	8.9
Experimental							
Total data set	front	-	2.9	4.9	6.1	-	-
	rear	-	3.1	-	6.1	7.3	-
Velocity							
v_1	front	-	-	4.4	6.0	6.6	-
	rear	-	3.2	-	6.1	7.6	-
v_2	front	-	3.7	-	6.1	7.2	-
	rear	-	-	5.5	6.1	7.2	-
v_3	front	-	-	4.6	6.0	6.9	-
	rear	-	-	5.2	6.1	7.5	-
v_4	front	-	-	5.2	6.4	-	11.9
	rear	-	-	5.8	6.4	-	11.9
Driving direction							
forwards	front	-	-	4.3	5.8	-	9.8
	rear	-	-	4.9	5.8	6.9	-
backwards	front	-	-	4.9	6.1	7.0	-
	rear	-	-	4.9	6.1	7.3	-

Table B.7: Nissan16-LO, summary of frequencies

Analysis	Axle	Frequency [Hz]					
			1^{st}_{mode}		2^{nd}_{mode}		3^{rd}_{mode}
Modal		-	5.2	-	6.7	-	9.7
Experimental							
Total data set	front	-	4.6	-	6.3	7.8	-
	rear	-	4.6	-	6.4	7.9	-
Velocity							
v_1	front	3.7	4.8	-	6.2	-	-
	rear	3.9	5.4	-	6.3	-	-
v_2	front	3.4	-	-	6.4	-	-
	rear	-	4.6	-	6.4	8.2	-
v_3	front	4.4	-	-	6.6	8.2	-
	rear	-	5.8	-	6.3	8.2	-
v_4	front	-	-	-	-	7.5	8.1
	rear	-	-	-	6.9	7.8	8.1
Driving direction							
forwards	front	-	4.6	5.8	6.3	-	-
	rear	3.5	4.4	-	6.3	-	-
backwards	front	4.4	5.0	-	6.4	-	-
	rear	4.4	6.0	6.7	-	-	-

Table B.8: Nissan16-NLO, summary of frequencies

B.3 Frequency analysis

Analysis	Axle	Frequency [Hz]					
			1^{st}_{mode}		2^{nd}_{mode}		3^{rd}_{mode}
Modal		-	3.3	-	5.4	-	9.8
Experimental							
Total data set	front	-	-	-	5.0	9.4	9.9
	rear	-	3.1	3.9	5.4	-	-
Velocity							
v_1	front	-	-	5.0	-	9.3	10.0
	rear	-	2.9	4.8	5.5	-	-
v_2	front	-	3.1	5.0	-	-	9.9
	rear	-	3.1	-	5.2	-	9.2
v_3	front	2.0	-	-	-	6.8	22.5
	rear	-	2.9	-	-	-	8.8
v_4	front			- no record	-		
	rear			- no record	-		
Driving direction							
forwards	front	-	-	-	5.0	9.2	10.0
	rear	2.9	3.4	-	5.2	-	-
backwards	front	-	-	-	5.0	9.4	9.9
	rear	3.1	3.4	-	5.2	-	-

Table B.9: Nissan15-LI, summary of frequencies

Analysis	Axle	Frequency [Hz]					
			1^{st}_{mode}		2^{nd}_{mode}		3^{rd}_{mode}
Modal		-	4.3	-	5.7	-	9.6
Experimental							
Total data set	front	1.8	-	-	5.9	-	9.9
	rear	2.0	4.4	-	5.9	-	-
Velocity							
v_1	front	-	-	-	6.0	6.6	9.9
	rear	2.2	-	-	5.7	6.6	-
v_2	front	-	4.2	-	6.0	-	9.9
	rear	3.8	4.3	-	5.6	-	-
v_3	front	3.4	-	-	5.6	-	9.9
	rear	-	4.3	4.8	5.6	-	-
v_4	front	-	4.5	-	6.0	-	9.9
	rear	-	3.8	-	6.0	6.2	-
Driving direction							
forwards	front	-	-	5.2	5.9	-	9.9
	rear	3.8	4.4	-	5.9	-	-
backwards	front	-	4.6	-	5.5	-	9.9
	rear	2.0	4.0	-	5.6	-	-

Table B.10: Nissan15-NLI, summary of frequencies

B.3 Frequency analysis

Analysis	Axle	Frequency [Hz]					
			1^{st}_{mode}		2^{nd}_{mode}		3^{rd}_{mode}
Modal		-	3.3	-	5.4	-	9.8
Experimental							
Total data set	front	-	-	-	5.0	7.1	9.9
	rear	-	3.1	-	5.0	7.8	-
Velocity							
v_1	front	-	-	-	5.1	9.3	9.9
	rear	-	3.5	-	5.5	7.8	-
v_2	front	2.7	-	-	4.9	-	9.9
	rear	2.8	3.2	-	4.9	-	-
v_3	front	-	-	-	5.1	7.9	9.9
	rear	-	3.1	4.0	5.1	-	-
v_4	front	-	-	5.0	5.4	7.7	-
	rear	1.6	3.3	-	5.5	-	-
Driving direction							
forwards	front	-	-	-	5.0	7.1	9.9
	rear	3.1	3.7	-	4.9	-	-
backwards	front	-	-	4.5	5.5	-	9.9
	rear	-	3.2	4.5	5.0	-	-

Table B.11: Nissan15-LO, summary of frequencies

Analysis	Axle	Frequency [Hz]					
			1^{st}_{mode}		2^{nd}_{mode}		3^{rd}_{mode}
Modal		-	4.3	-	5.7	-	9.6
Experimental							
Total data set	front	3.4	-	-	5.7	-	9.9
	rear	-	4.4	5.2	5.7	-	-
Velocity							
v_1	front	-	-	5.1	-	9.3	9.9
	rear	3.5	-	5.5	-	7.8	-
v_2	front	2.7	-	4.9	-	-	9.9
	rear	3.2	-	4.9	-	-	-
v_3	front	-	-	5.1	-	7.9	9.9
	rear	3.1	4.0	5.1	-	-	-
v_4	front	-	-	5.0	5.4	7.7	-
	rear	1.6	3.3	-	5.5	-	-
Driving direction							
forwards	front	-	3.7	-	5.9	-	9.9
	rear	-	4.4	5.5	5.9	-	-
backwards	front	-	3.9	-	5.9	-	9.9
	rear	3.8	4.4	-	5.9	-	-

Table B.12: Nissan15-NLO, summary of frequencies

B.3 Frequency analysis

Analysis	Axle	Frequency [Hz]					
			1^{st}_{mode}		2^{nd}_{mode}		3^{rd}_{mode}
Modal		-	3.6	-	5.8	-	9.2
Experimental							
Total data set	front	-	-	-	-	8.8	9.4
	rear	-	2.9	5.1	6.1	-	-
Velocity							
v_1	front	-	-	-	-	8.4	9.6
	rear	-	2.9	5.1	6.1	-	-
v_2	front	-	-	-	-	8.6	9.6
	rear	-	-	5.1	5.7	6.1	-
v_3	front	1.0	-	-	-	6.8	14.6
	rear	-	-	4.7	6.4	-	9.8
v_4	front			- no record	-		
	rear			- no record	-		
Driving direction							
forwards	front	-	-	-	-	9.0	9.4
	rear	-	-	4.5	6.1	6.6	-
backwards	front	-	-	-	-	9.0	9.4
	rear	-	-	5.1	5.9	7.0	-

Table B.13: Jungheinrich16-LO, summary of frequencies

Analysis	Axle	Frequency [Hz]					
			1^{st}_{mode}		2^{nd}_{mode}		3^{rd}_{mode}
Modal		-	4.9	-	6.1	-	14.6
Experimental							
Total data set	front	-	4.6	-	6.3	-	41.0
	rear	-	4.6	5.5	6.3	-	-
Velocity							
v_1	front	-	4.5	5.0	6.3	-	-
	rear	4.5	4.9	-	6.3	-	-
v_2	front	-	4.8	5.4	6.3	-	-
	rear	-	4.8	5.4	6.3	-	-
v_3	front	-	4.5	5.7	6.2	-	-
	rear	-	4.5	-	6.2	6.5	-
v_4	front	-	4.5	6.0	6.2	-	-
	rear	4.5	4.8	-	6.2	-	-
Driving direction							
forwards	front	-	4.8	-	6.0	-	25.0
	rear	-	4.8	-	6.0	-	25.0
backwards	front	-	4.5	-	6.2	6.5	-
	rear	-	4.5	-	6.2	6.5	-

Table B.14: Jungheinrich16-NLO, summary of frequencies

B.3 Frequency analysis

Analysis	Axle	Frequency [Hz]					
			1^{st}_{mode}		2^{nd}_{mode}		3^{rd}_{mode}
Modal		-	3.4	-	4.9	-	17.7
Experimental							
Total data set	front	-	-	-	5.2	-	26.1
	rear	-	2.9	4.2	5.2	-	-
Velocity							
v_1	front	-	-	-	5.1	-	26.4
	rear	-	-	4.3	5.2	-	28.4
v_2	front	-	-	-	5.2	-	28.7
	rear	-	2.8	4.2	5.2	-	-
v_3	front	-	-	-	5.2	-	17.3
	rear	-	-	4.3	4.8	5.2	-
v_4	front	-	-	-	-	13.3	20.1
	rear	-	3.8	-	-	6.2	18.3
Driving direction							
forwards	front	-	-	-	5.2	-	26.6
	rear	-	2.9	-	5.1	6.0	-
backwards	front	-	-	-	-	5.9	26.9
	rear	-	2.9	4.4	5.1	-	-

Table B.15: Pimespo25-LO, summary of frequencies

Analysis	Axle	Frequency [Hz]					
			1^{st}_{mode}		2^{nd}_{mode}		3^{rd}_{mode}
Modal		-	4.0	-	5.1	-	24.5
Experimental							
Total data set	front	-	3.5	-	5.2	-	28.7
	rear	-	3.5	-	5.2	7.2	-
Velocity							
v_1	front	-	-	-	-	20.5	22.8
	rear	-	-	-	5.2	6.1	20.6
v_2	front	-	-	-	5.1	7.0	29.5
	rear	-	3.5	4.5	5.2	-	-
v_3	front	-	-	-	5.4	7.3	9.3
	rear	-	3.4	-	-	-	26.9
v_4	front	-	-	4.8	5.2	-	23.2
	rear	-	-	4.8	5.2	5.7	-
Driving direction							
forwards	front	-	-	-	-	22.9	25.6
	rear	-	-	-	6.2	-	25.8
backwards	front	3.1	-	-	-	20.4	22.9
	rear	-	3.5	-	5.1	6.1	-

Table B.16: Pimespo25-NLO, summary of frequencies

B.4 Cross-correlation and coherence

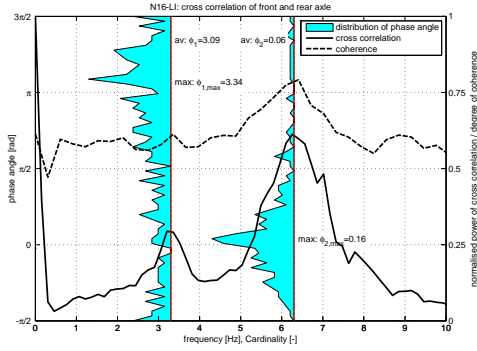


Figure B.34: Nissan16-LI, Cross-correlation of front and rear axle

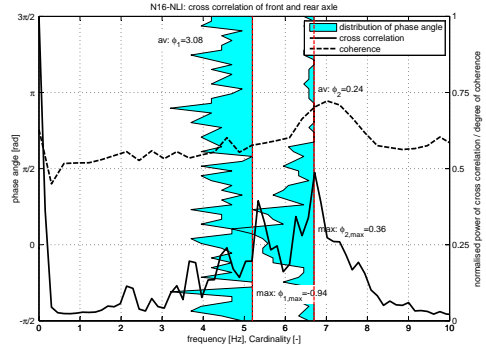


Figure B.35: Nissan16-NLI, Cross-correlation of front and rear axle

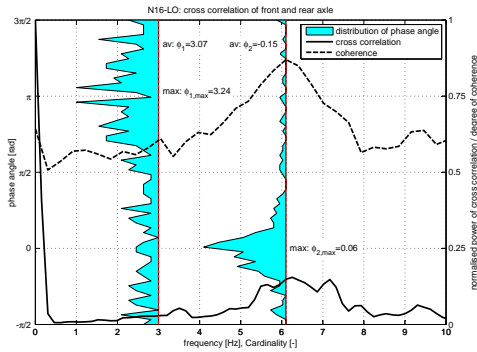


Figure B.36: Nissan16-LO, Cross-correlation of front and rear axle

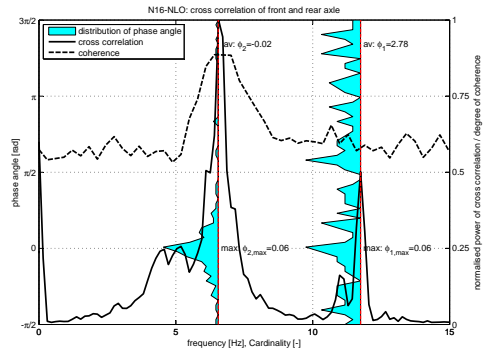


Figure B.37: Nissan16-NLO, Cross-correlation of front and rear axle

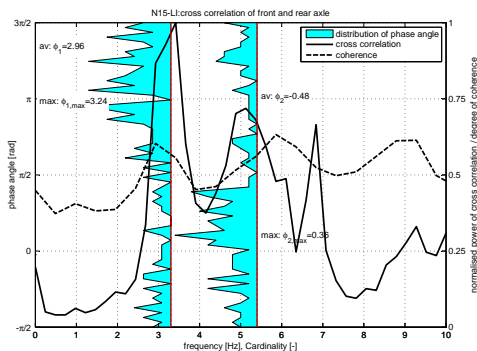


Figure B.38: Nissan15-LI, Cross-correlation of front and rear axle

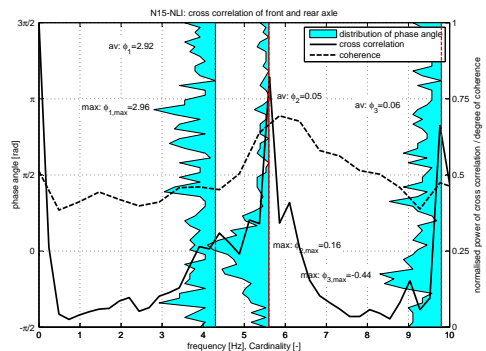


Figure B.39: Nissan15-NLI, Cross-correlation of front and rear axle

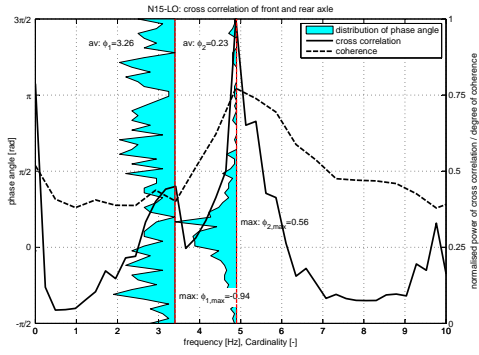


Figure B.40: Nissan15-LO, Cross-correlation of front and rear axle

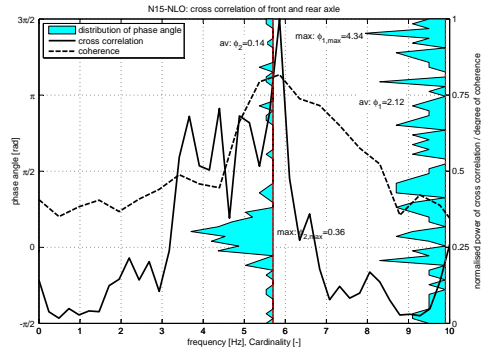


Figure B.41: Nissan15-NLO, Cross-correlation of front and rear axle

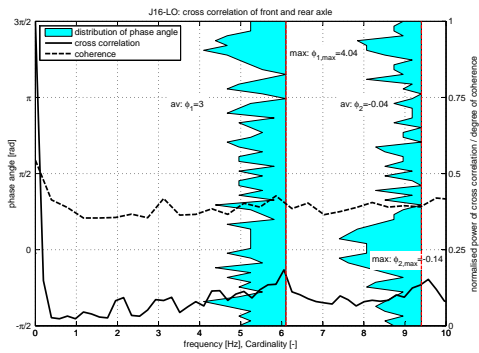


Figure B.42: Jungheinrich16-LO, Cross-correlation of front and rear axle

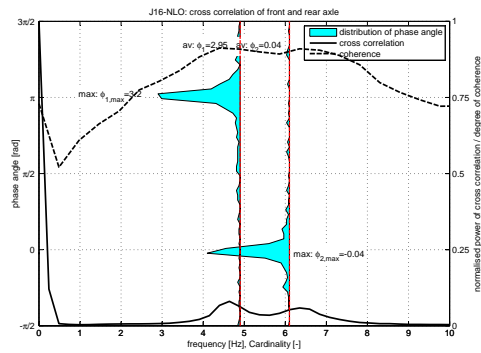


Figure B.43: Jungheinrich16-NLO, Cross-correlation of front and rear axle

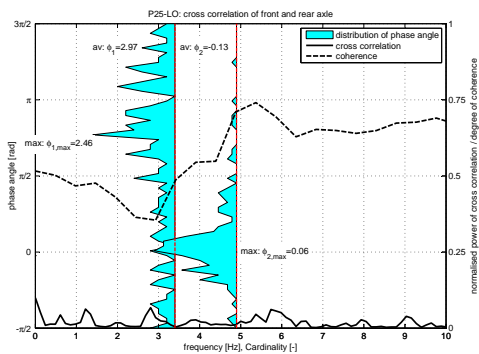


Figure B.44: Pimespo25-LO, Cross-correlation of front and rear axle

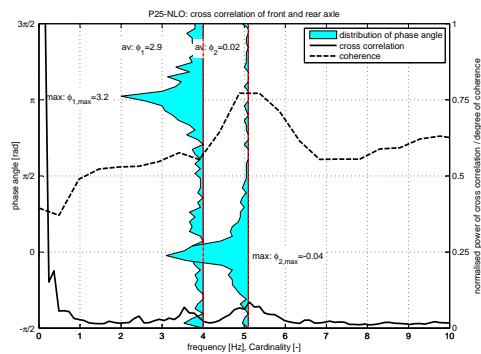


Figure B.45: Pimespo25-NLO, Cross-correlation of front and rear axle

B.5 Amplitude analysis

B.5.1 Theoretical model of amplitudes

The envelope function of the steady state response representing the 95% fractile of accelerations can be expressed as:

For $v \geq 0.5$ m/s:

$$A_{95}(f_n, v) = m_{95}(f_n)v + C_{95}(f_n) \quad (\text{B.1})$$

$$= \frac{1.75 + \frac{5.25}{f_{n,max} - f_{n,0}}(f_n - f_{n,0})}{v_{max} - v_0}(v - v_0) + \dots$$

$$\dots + \left[\frac{0.75}{f_{n,max} - f_{n,0}}(f_n - f_{n,0}) + 0.25 \right] \quad (\text{B.2})$$

With the range of eigen-frequencies $f_{n,0} = 1.0$ Hz, $f_{n,max} = 7.0$ Hz

and the range of velocity $v_0 = 0.5$ m/s, $v_{max} = 4.0$ m/s.

For the “worst” case this simplifies to:

$$A_{95}(f_n, v) = \frac{1.75 + \frac{5.25}{7.0-1.0}(7.0 - 1.0)}{4.0 - 0.5}(v - 0.5) + \dots$$

$$\dots + \left[\frac{0.75}{7.0 - 1.0}(7.0 - 1.0) + 0.25 \right] \quad (\text{B.3})$$

$$= 2.0(v - 0.5) + [1.0] \quad (\text{B.4})$$

$$= 2.0v \quad (\text{B.5})$$

The simplified envelope function with its constant values for the threshold and the slope overestimates the accelerations if the eigen-frequency of a fork-lift truck is low. In most relevant cases (fork-lift trucks with a capacity of up to 2500 kg) it is a reasonable fit for the relevant velocities.

For the configuration “outdoors” the constant summand is 3.25 m/s² instead of 0.25 m/s².

In the case of the mean accelerations the slope is $m_{av}(f_n) \approx 0.6m_{95}(f_n)$ and the constant summand remains unchanged indoors and changes to 1.25 m/s² outdoors.

B.5.2 Correlation of velocity and accelerations

For Nissan16 loaded, indoors see Section 2.7.3.3.

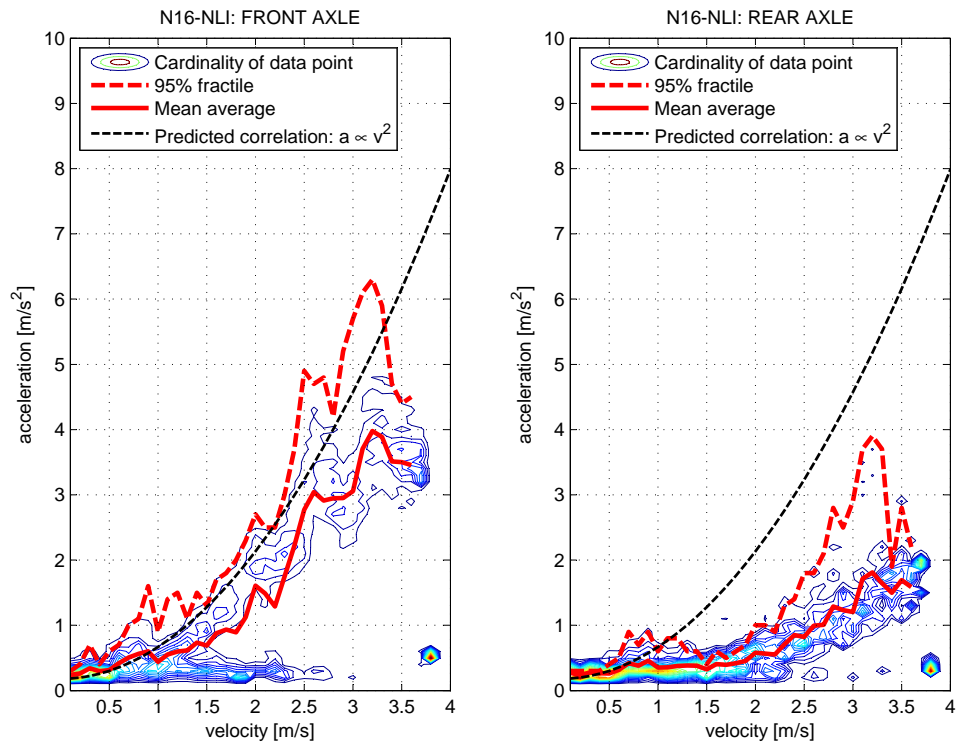


Figure B.46: Nissan16 no payload, indoors, velocity/amplitude

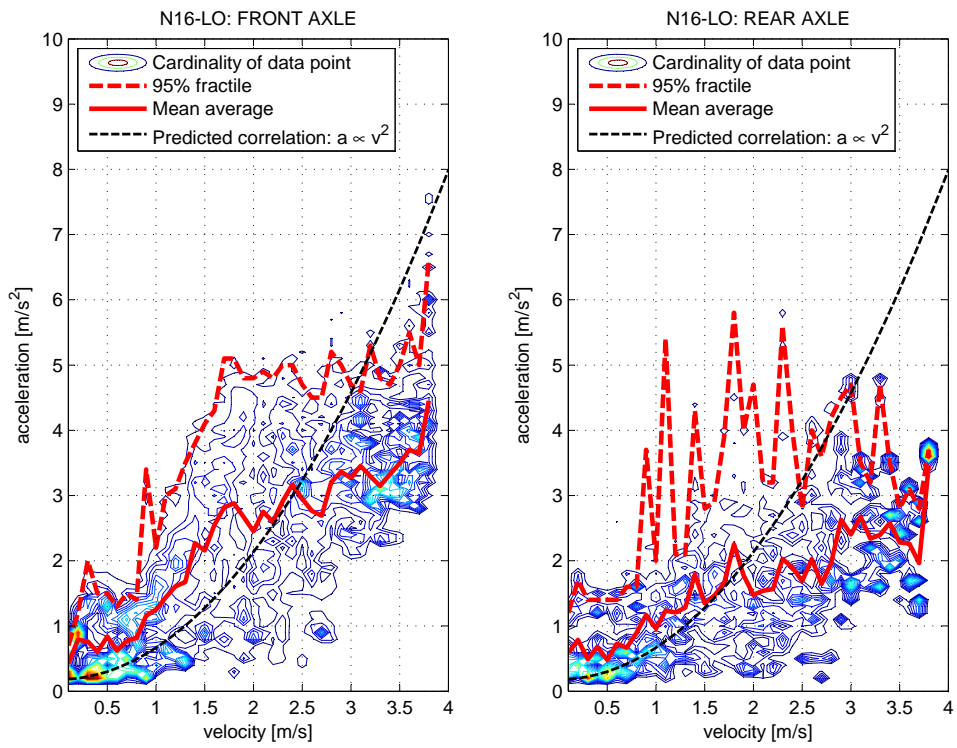


Figure B.47: Nissan16 loaded, outdoors, velocity/amplitude

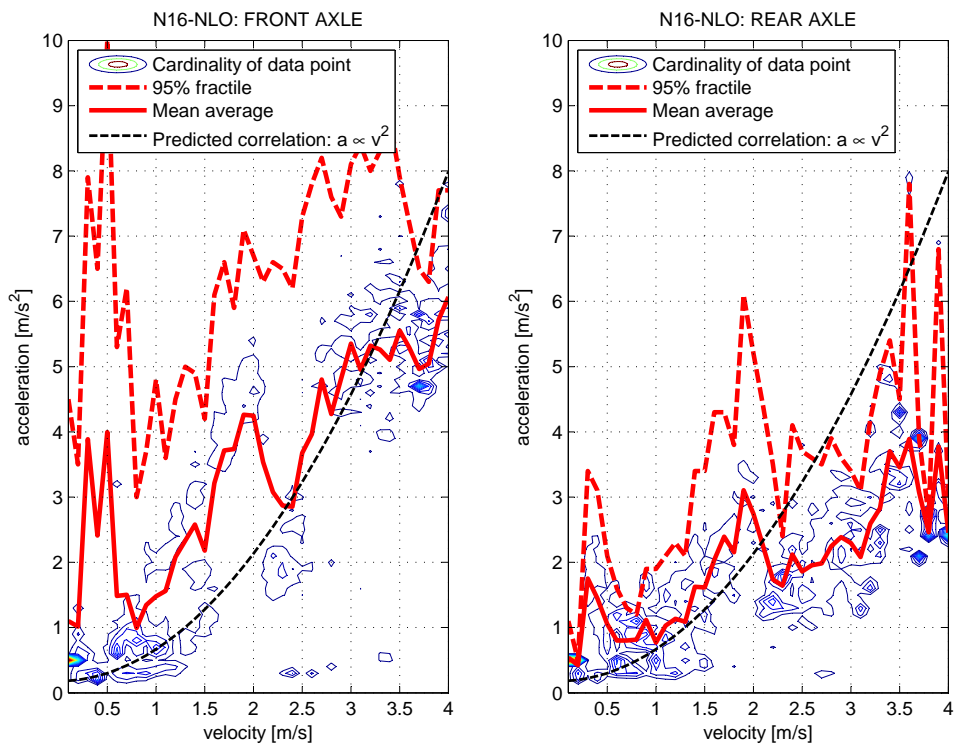


Figure B.48: Nissan16 no payload, outdoors, velocity/amplitude

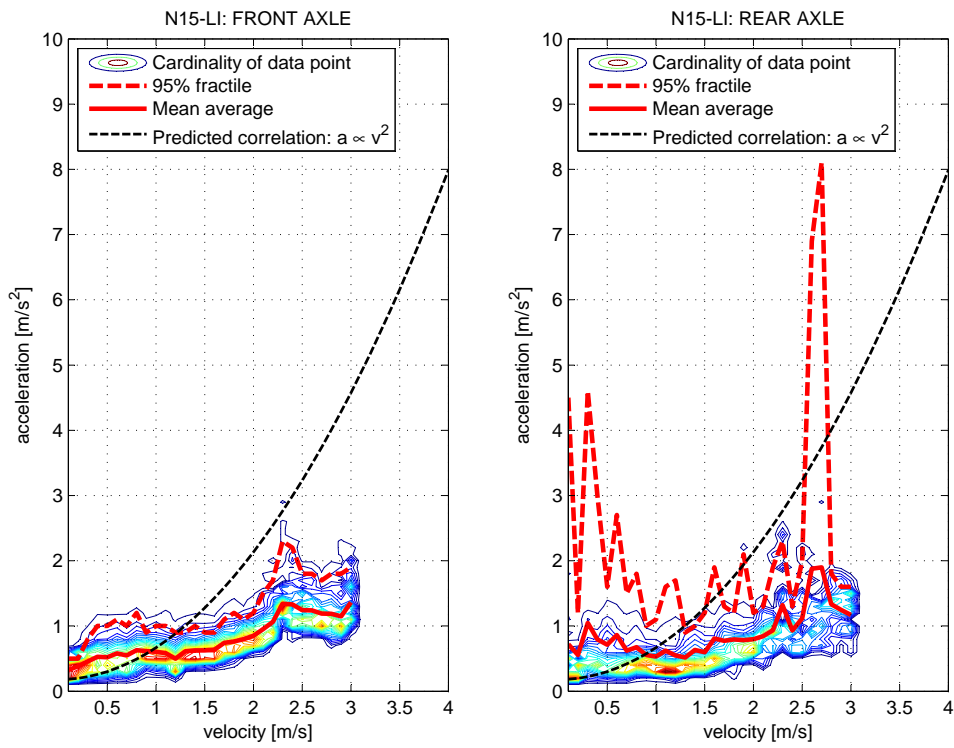


Figure B.49: Nissan15 loaded, indoors, velocity/amplitude

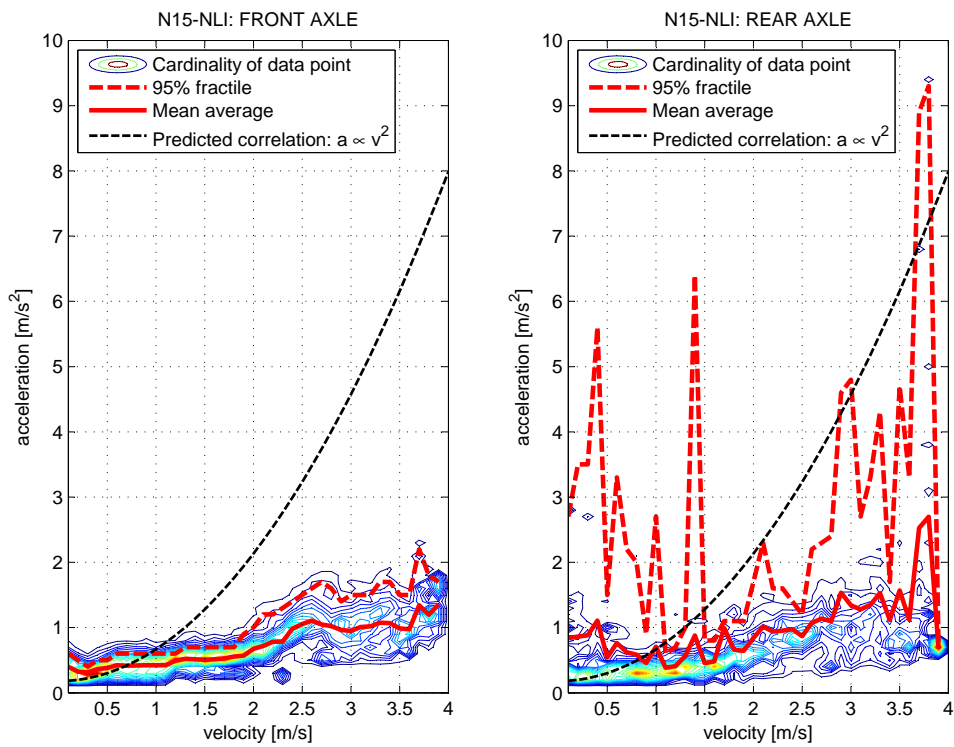


Figure B.50: Nissan15 no payload, indoors, velocity/amplitude

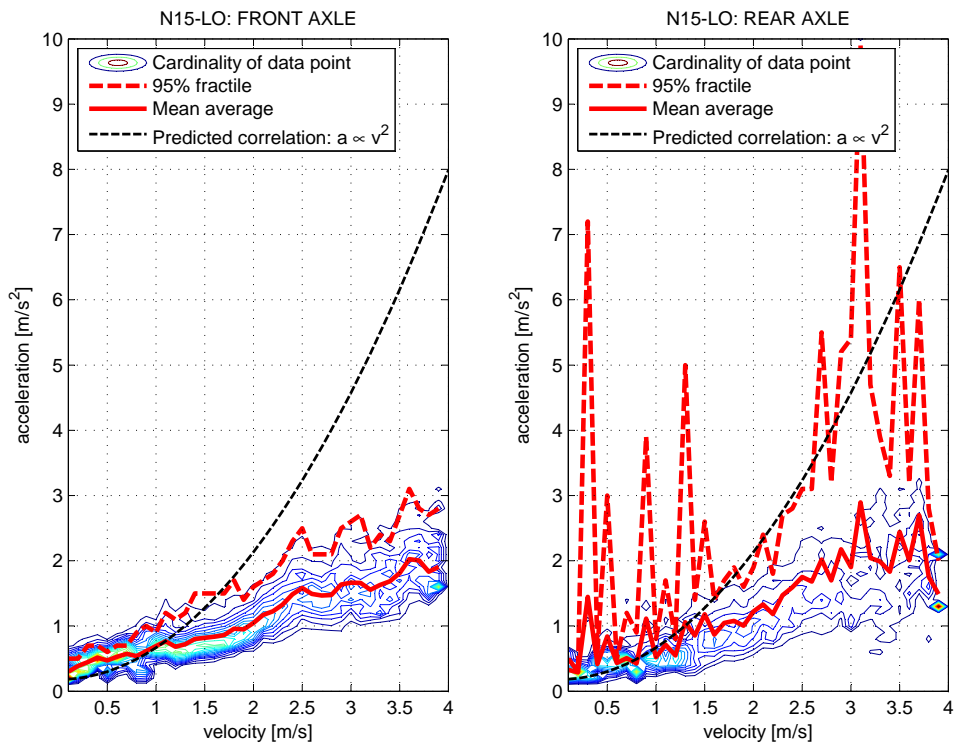


Figure B.51: Nissan15 loaded, outdoors, velocity/amplitude

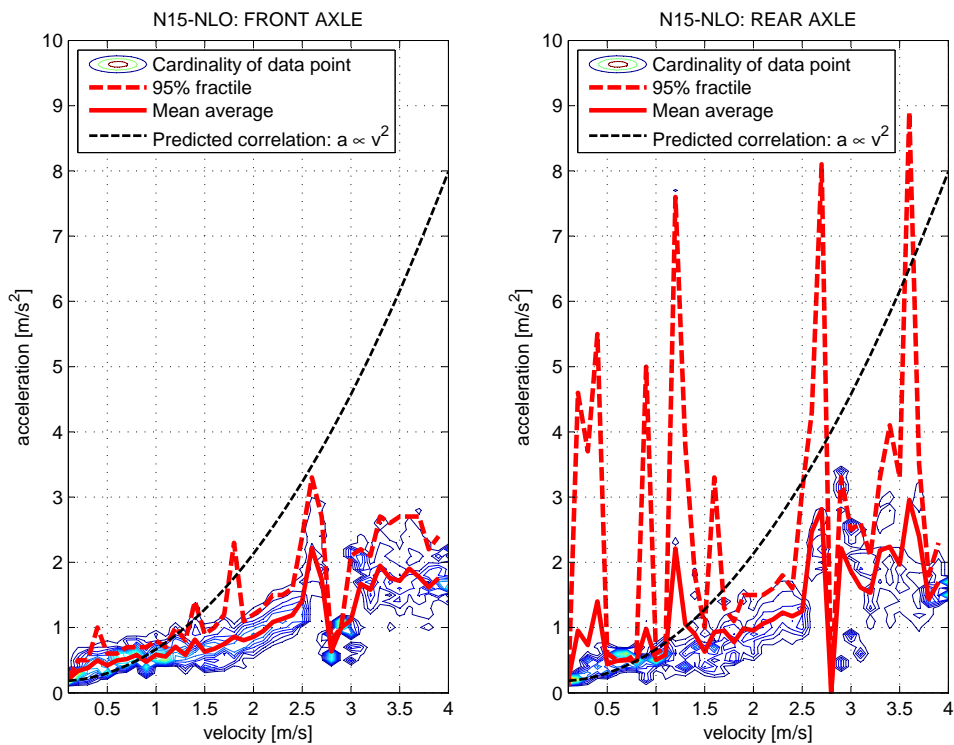


Figure B.52: Nissan15 no payload, outdoors, velocity/amplitude

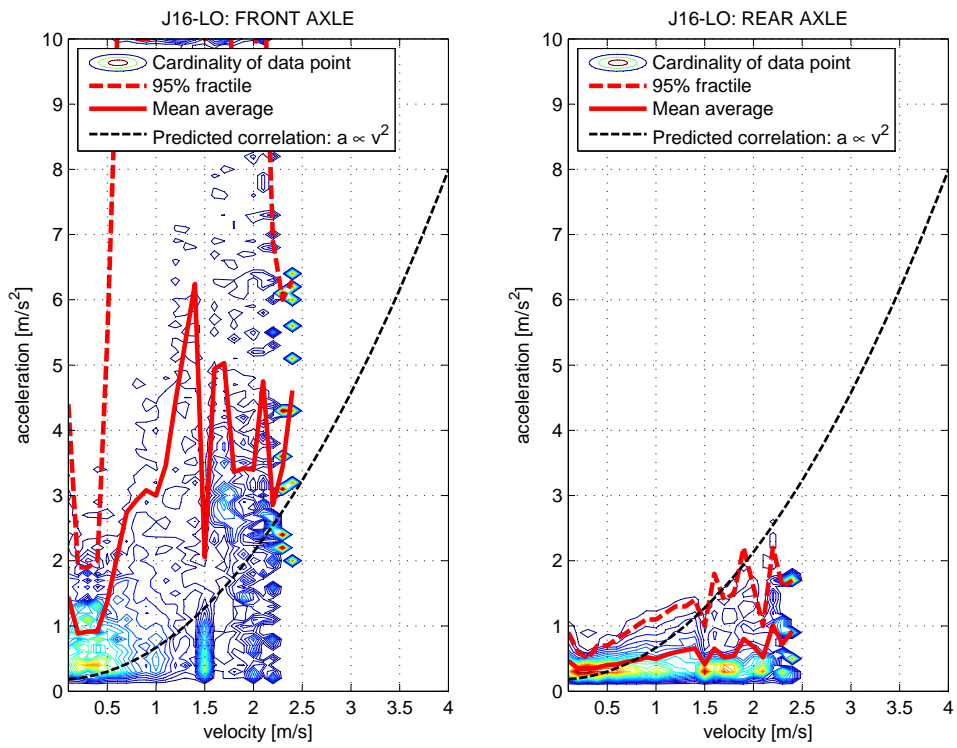


Figure B.53: Jungheinrich16 loaded, outdoors, velocity/amplitude

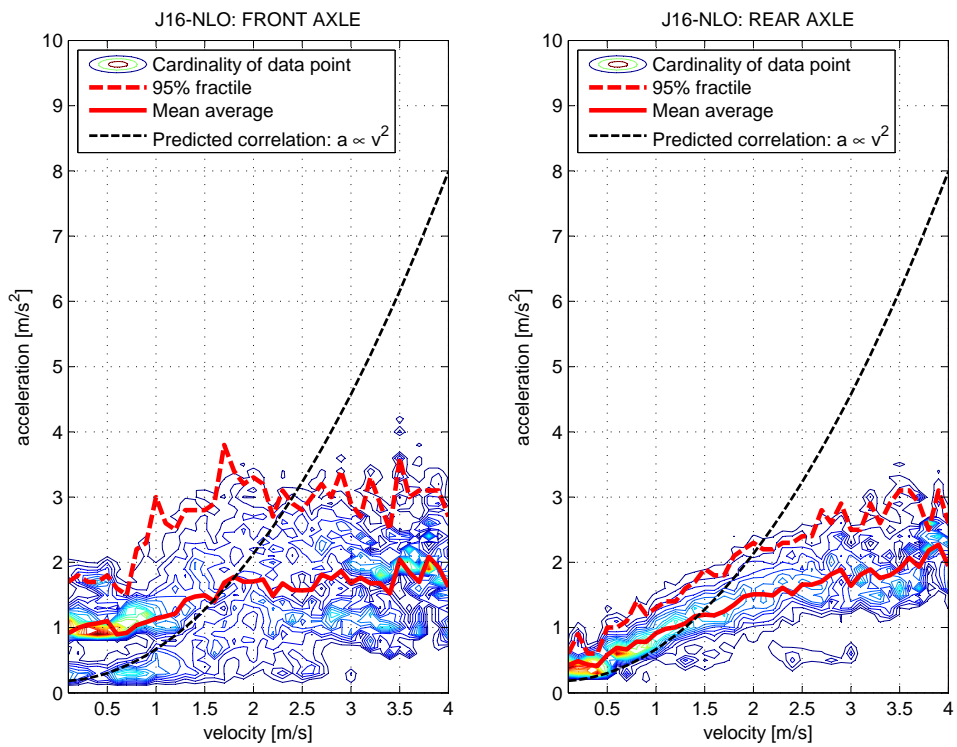


Figure B.54: Jungheinrich16 no payload, outdoors, velocity/amplitude

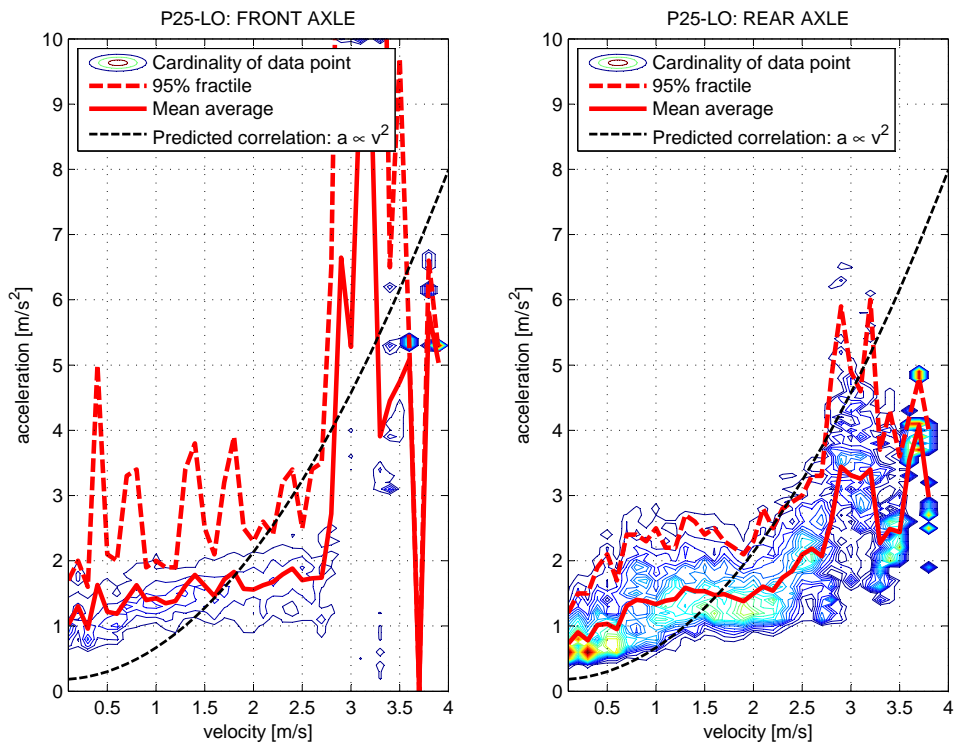


Figure B.55: Pimespo25 loaded, outdoors, velocity/amplitude

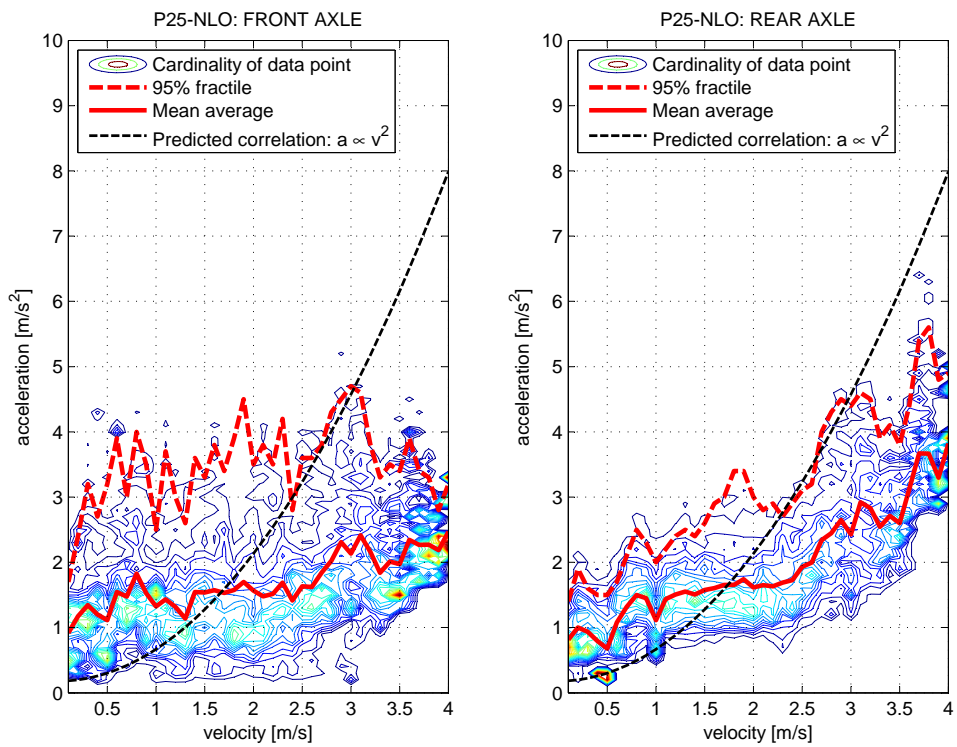


Figure B.56: Pimespo25 no payload, outdoors, velocity/amplitude

In Table B.17 are listed the configurations summarised in the Figures [B.57] to [B.60].

Figure	Configuration displayed	Models analysed
[B.57]	Indoors, front axle	N16, N15
[B.58]	Indoors, rear axle	N16, N15
[B.59]	Outdoors, front axle	N16, N15, J16, P25
[B.60]	Outdoors, rear axle	N16, N15, J16, P25

Table B.17: Allocation legend: Summary of 95% fractiles

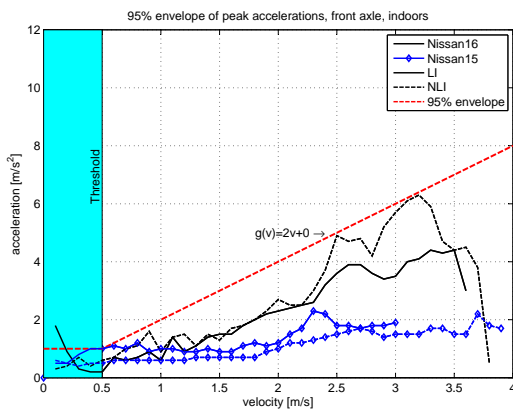


Figure B.57: Summary: accelerations indoors, front axle

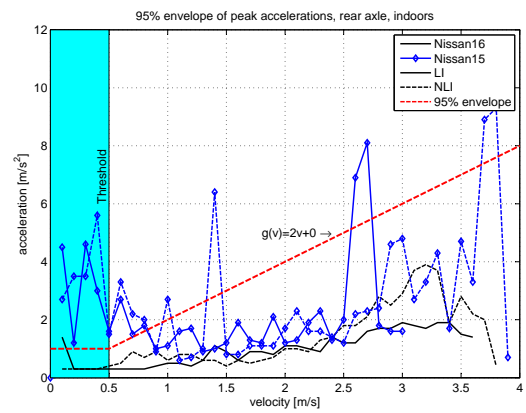


Figure B.58: Summary: accelerations indoors, rear axle

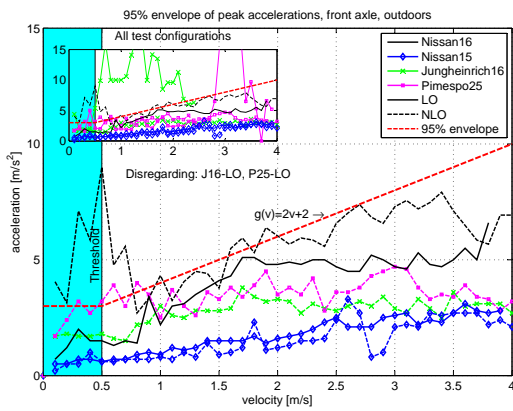


Figure B.59: Summary: accelerations outdoors, front axle

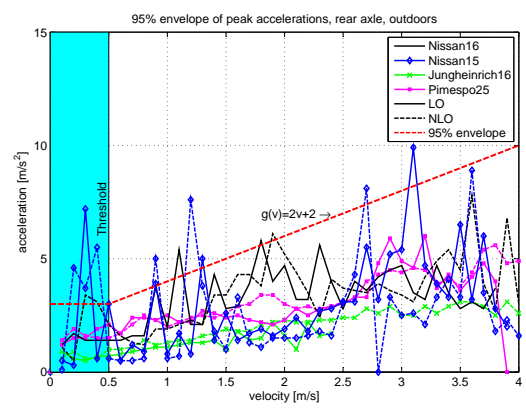


Figure B.60: Summary: accelerations outdoors, rear axle

For the proposed load model an easy function to express the correlation of velocity and the amplitudes is sought. The bi-linear envelope function is suitable for this purpose and fits the data reasonably well¹:

$$A_{95\%}(v) = \begin{cases} T_{95\%} & \text{if } v \leq 0.5 \text{ m/s} \\ C_{95\%}v + D_{95\%} & \text{if } v > 0.5 \text{ m/s} \end{cases} \quad (\text{B.6})$$

with $C_{95\%} = 2.0$ indoors and outdoors

and $D_{95\%} = \begin{cases} 0.0 & \text{indoors} \\ 2.0 & \text{outdoors} \end{cases}$

and $T_{95\%} = \begin{cases} 1.0 & \text{indoors} \\ 3.0 & \text{outdoors} \end{cases}$

B.6 Ratio of amplitudes

For Nissan16 see Section 2.7.4

Nissan 15 Configuration	Axle	Mode 1 [Hz] [-]	Mode 2 [Hz] [-]	μ_f [-]	μ_r [-]	
experimental:						
LI	front	<u>3.3</u>	0.15	5.0	0.35	0.43
	rear	2.9	1.0	5.4	0.9	1.10
NLI	front	4.8	0.25	5.6	0.6	0.42
	rear	4.4	0.9	5.9	1.0	0.90
LO	front	<u>3.3</u>	0.3	5.0	1.0	0.3
	rear	3.1	0.4	5.0	1.0	0.4
NLO	front	<u>4.3</u>	0.1	5.7	1.0	0.1
	rear	4.4	0.7	5.7	1.0	0.7

$x.x$: experimental power spectrum does not show a peak, frequency taken from modal analysis

Table B.18: Nissan 15, ratio of peak sizes in normalised power spectral density

¹A more detailed envelope function is shown in this Appendix, Section B.5.1.

Jungheinrich 16 Configuration	Axle	Mode 1		Mode 2		μ_f	μ_r
		[Hz]	[-]	[Hz]	[-]	[-]	[-]
experimental:							
LO	front	<u>3.6</u>	0.02	<u>5.8</u>	0.15	0.13	
	rear	2.9	0.18	6.1	1.0		0.18
NLO	front	4.5	1.0	<u>6.1</u>	0.8	1.25	
	rear	4.5	1.0	6.2	0.65		1.54
<u>x.x</u> :	experimental power spectrum does not show a peak, frequency taken from modal analysis						

Table B.19: Jungheinrich 16, peak sizes in normalised power spectral density

Pimespo 25 Configuration	Axle	Mode 1		Mode 2		μ_f	μ_r
		[Hz]	[-]	[Hz]	[-]	[-]	[-]
experimental:							
LO	front	<u>3.4</u>	0.45	5.1	1.0	0.45	
	rear	2.9	0.28	5.2	1.0		0.28
NLO	front	<u>4.0</u>	0.3	<u>5.1</u>	0.62	0.48	
	rear	3.5	0.38	5.2	1.0		0.38
<u>x.x</u> :	experimental power spectrum does not show a peak, frequency taken from modal analysis						

Table B.20: Pimespo 25, peak sizes in normalised power spectral density

Appendix C

Calculation procedure in SOFiSTiK and source code of the load model

C.1 Calculation procedure

The input language of SOFiSTiK is “CADINP”, which was developed for a standardised input in CAD programmes in 1976 (Ahn et al., 1976).

The programme is split into several sub-programmes (“modules”) that carry out special tasks and of which some have to be arranged in a given order: firstly, the module “AQUA” defines the materials and the cross sections, then the module “GENF” generates the static system. After that beam loads are defined in the module “STAR2” and the cross-section is designed in the module “AQB”. The further analysis of the dynamic properties is carried out with the stiffnesses calculated in the modules “AQB” and “ASE”.

The modular programme structure is explained briefly:

Module	Description
AQUA	Definition of materials and cross sections
GENF	Definition of statical system
AQB	Definition of prestressing strands (geometry)
STAR2	Load Cases CS0
STAR2	Load Cases CS1
AQB	Creep of precast element
AQB	Creep of assembly
AQB	Design of precast element: double-tee element
AQB	Design of precast element: main beam
STAR2	Deflections in precast plant
STAR2	Deflections in precast plant including creep / shrinkage
STAR2	Deflections during cast of topping
STAR2	Deflections of composite structure in service
STAR2	Deflections of composite structure in service and time dependent effects
ASE	Eigenvalues of composite structure: max stiffness
ASE	Eigenvalues of composite structure: with time dependent effects
ASE	Fork-lift truck placed at midspan (1 load case)
ASE	Fork-lift truck accelerates to max velocity (several load cases)
ASE	Fork-lift truck drives with max velocity (several load cases)
ASE	Fork-lift truck decelerate to halt (several load cases)

Table C.1: SOFiSTiK modules

C.2 The input file for the fork-lift truck model

Parameters are defined which are constant throughout the analysis, simplifying changes of the model:

```

$ FORK-LIFT TRUCK capacity: 1000 kg
$ Constants for dynamic load model acc. to Exp. 6.23,
$ Thesis: Chapter 3, Section 3.7.2
dt=0.01 $ seconds, step width of analysis
$ Loading:
AxLf=29.0 $ kN front axle load
AxLr=6.0 $ kN rear axle load
$ Geometry:
WB=1.000 $m
m=3500 $kg
Lf=0.170 $m
Lr=0.830 $m
J=2500 $kgm^2
$ Eigen-frequencies from modal analysis:
f1=5.3 $Hz
f2=2.0 $Hz
vflt=3.0 $m/s
a=1.00 $ m/s^2 acceleration of flt (horizontal)
$
K1=($m)*$(Lr)^2+$(J)
K2=($m)*$(Lf)*$(Lr)-$(J)

```

C.2 The input file for the fork-lift truck model

```
K3=$(m)*$(Lf)^2-$(J)
A1=(360*$(f1))
A2=(360*$(f2))
$ Definition of start position relative to node
$ node 1126:
locax=0 $ initial position for parallel
$
$ Define driving path for sub-moduls of ASE...
$ parallel:
$ primary load case: LC 1000
dtx1=3 $ seconds
st1=$(dtx1)/$(dt) $ no of steps
ste1=$(st1)+1000
px1=0.5*$(a)*$(dtx1)^2 $ position at end of dtx1...
dtx2=2 $ seconds
st2=$(dtx2)/$(dt) $no of steps
ste2=$((st2))+$(ste1))
px2=$(px1)+$(vflt)*$(dtx2)
dtx3=3 $ seconds
st3=$(dtx3)/$(dt) $ no of steps
ste3=$((st3))+$(ste2))
px3=$(px2)+0.5*$(a)*$(dtx3)^2
dtx4=3 $ seconds
st4=$(dtx4)/$(dt) $ no of steps
ste4=$((st4))+$(ste3))
px4=$(px3)+0.5*(-1)*$(a)*$(dtx4)^2
dtx5=9 $ seconds
st5=$(dtx5)/$(dt) $no of steps
ste5=$((st5))+$(ste4))
px5=$(px4)-$(vflt)*$(dtx5)
dtx6=3 $ seconds
st6=$(dtx6)/$(dt) $ no of steps
ste6=$((st6))+$(ste5))
px6=$(px5)-0.5*$(a)*$(dtx6)^2
dtx7=3 $ seconds
st7=$(dtx7)/$(dt) $ no of steps
ste7=$((st7))+$(ste6))
px7=$(px6)+0.5*$(a)*$(dtx7)^2
dtx8=8 $ seconds
st8=$(dtx8)/$(dt) $no of steps
ste8=$((st8))+$(ste7))
px8=$(px7)+$(vflt)*$(dtx8)
dtx9=3 $ seconds
st9=$(dtx9)/$(dt) $ no of steps
ste9=$((st9))+$(ste8))
px9=$(px8)+0.5*$(a)*$(dtx9)^2
```

The “ASE” modules define the movement and the dynamic action on the floor and the time-history analysis is carried out:

```
-PROG ASE urs:196
HEAD MOVING TRUCK: parallel (1)
LET#dt $(dt) $ time step [s]
LET#factor 0.0
LET#vflt 0.0
LET#locax $(locax)
```

C.2 The input file for the fork-lift truck model

```
$
LET#plc 1000
MASS 0
$
let#step 0
LOOP#1 $(st1)
  LET#step #step+1
  LET#timea #dt*#1
  LET#timee #timea+#dt
  LET#time (#timea+#timee)/2 $ middle of time step
  $
  let#vflt $(a)*#time ; let#factor 1.0
  LET#C ((1.2*#vflt+0.4)/(1.5*$(WB)^2))
  $      adjtmt N->kN
  LET#Forcef $(AxLf)+(0.001*#C*($K1)*(sin$(A1)*#time)+0.5*sin$(A2)*#time))+...
  ...+$K2*(sin$(A1)*#time)+0.5*sin$(A2)*#time)))
  LET#Forcer $(AxLr)+(0.001*#C*($K2)*(sin$(A1)*#time)+0.5*sin$(A2)*#time))+...
  ...+$K3*(sin$(A1)*#time)+0.5*sin$(A2)*#time+180)))
  LET#locax (#locax+#factor*#vflt*#dt)
  $TXB Testprint to .erg file:      $ #(timea,8.3) prints #time with 3 digits
  TXB Parallel: Step #step from time #(timea,4.3)sec., Forcef=#(Forcef,4.2)kN, x=#(locax,3.2)m
  $
  STEP 1 DT #dt ALF 0.25 0.50 1.0
  SYST PROB LINE PLC #plc ;
  GRP ALL FACS 1 FACL 1 FACP 1 RADA $(RDM0) RADB $(RDS1)
  LET#plc #plc+1
  LC #plc DLZ 1.0
  POLO 1126 X #locax      Y 0.50 Z 0.0 TYPE PZP P #Forcer NOG 800
  POLO 1126 X #locax+$(WB) Y 0.50 Z 0.0 TYPE PZP P #Forcef NOG 800
  END
ENDLOOP
END
```

Appendix D

Results of the field test in Helmstadt

Here the results of the configurations

- parallel with payload (Figures [D.1] and [D.2])
- transverse without payload (Figures [D.3] and [D.4])
- transverse with payload (Figures [D.5] and [D.6])

are summarised. For each configuration the time history and the frequency response are plotted.

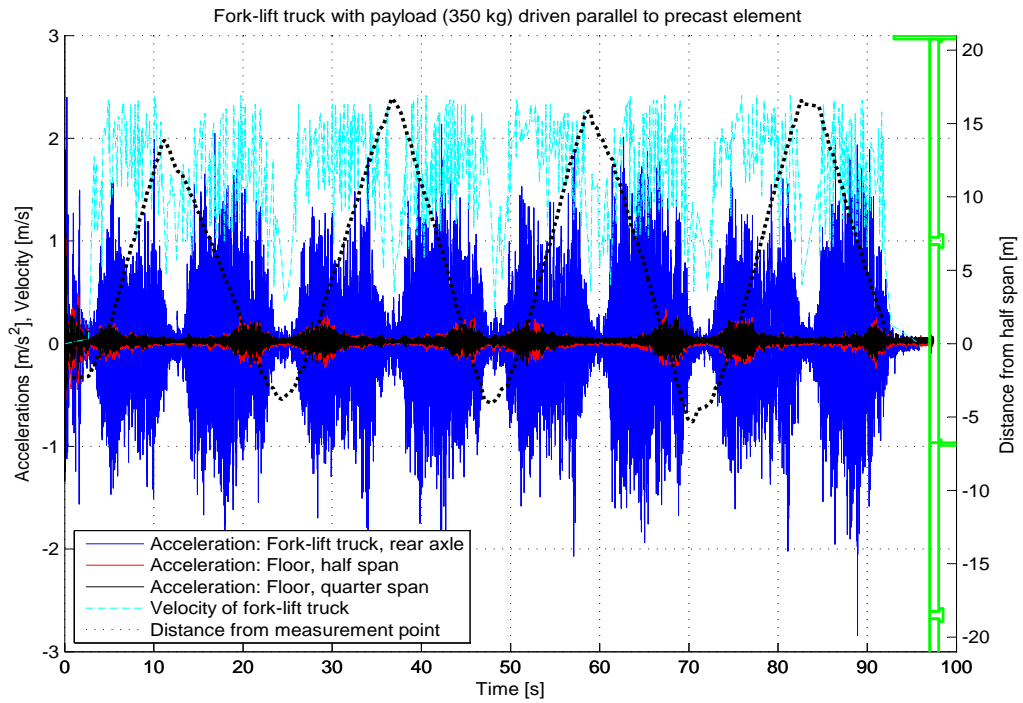


Figure D.1: Fork-lift truck with payload parallel to precast elements

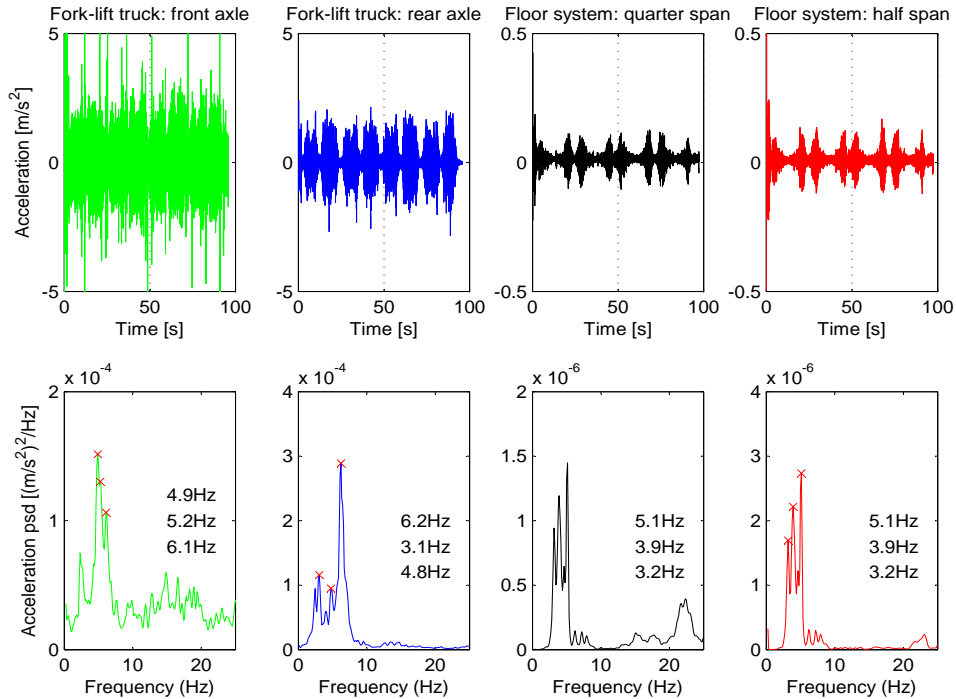


Figure D.2: Frequency content of the above record (Figure [D.1])

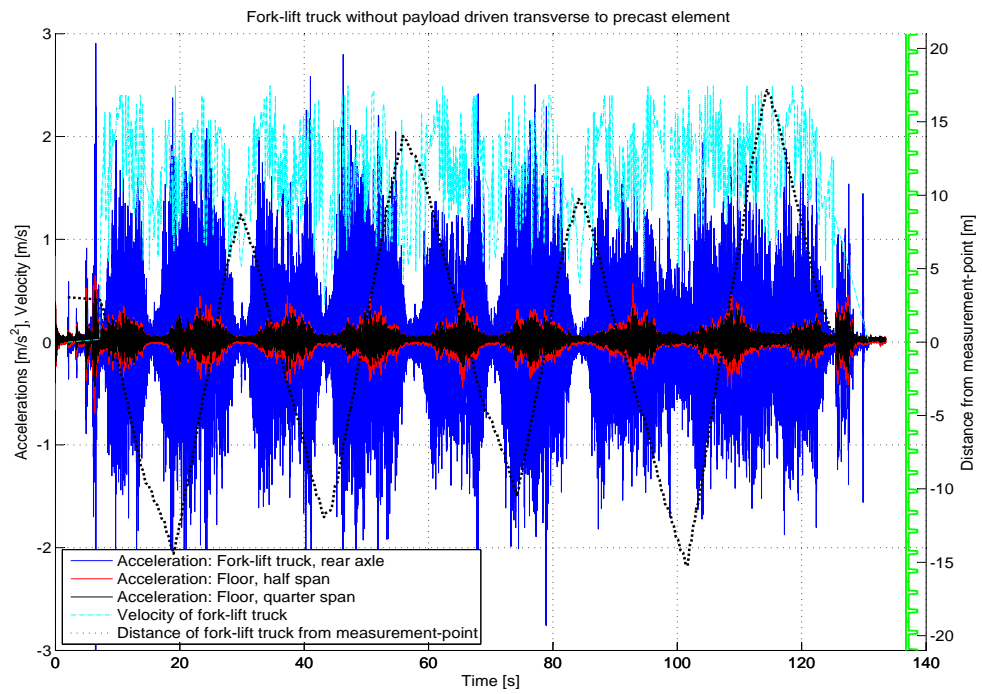


Figure D.3: Fork-lift truck without payload transverse to precast elements

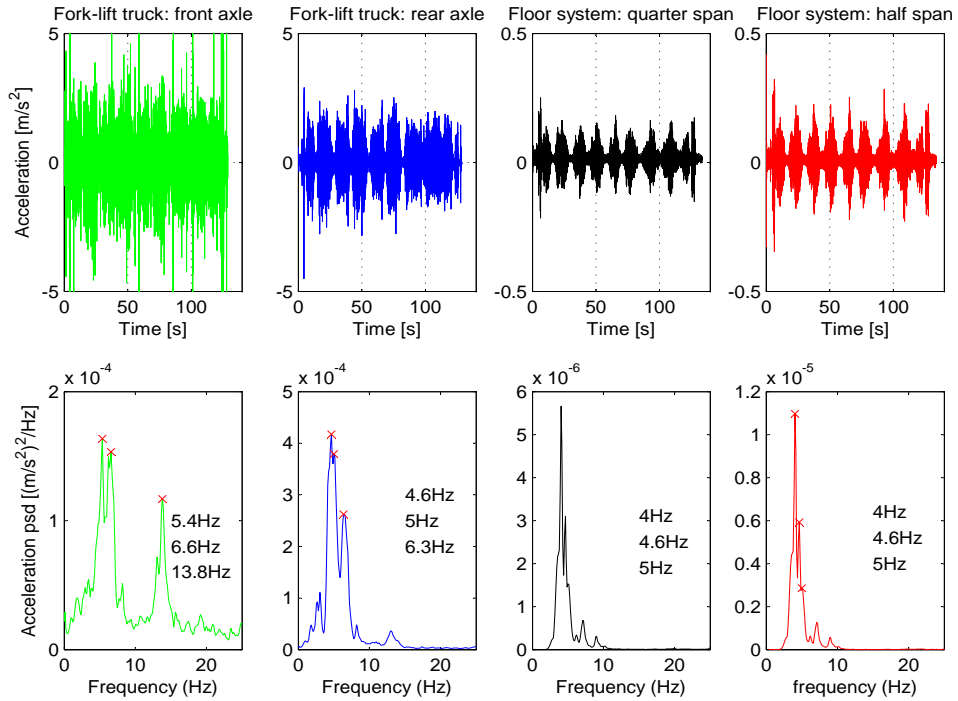


Figure D.4: Frequency content of the above record (Figure [D.3])

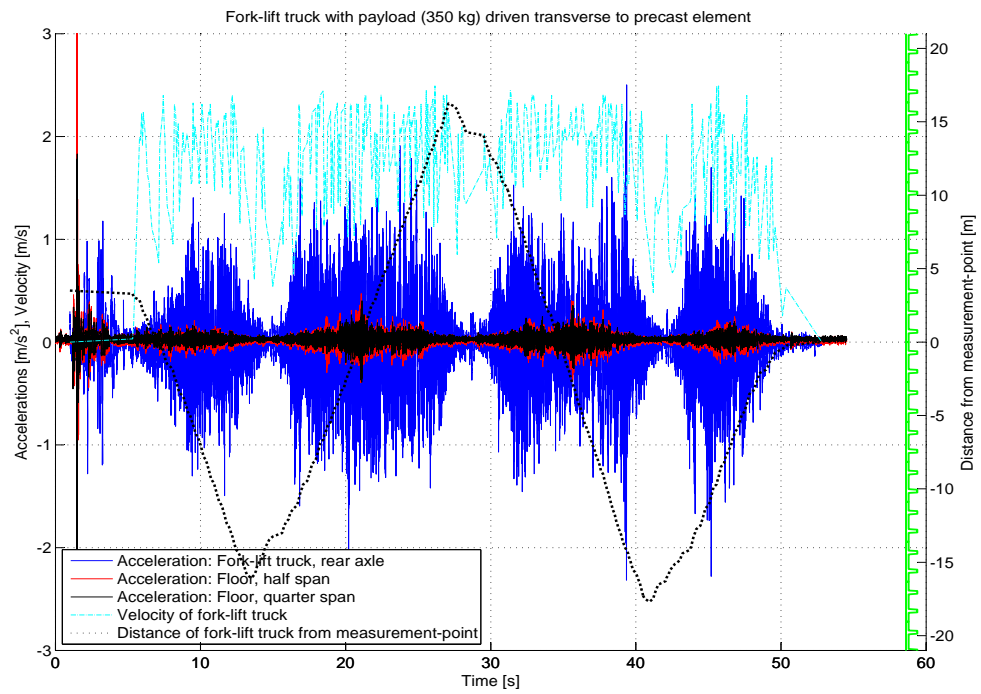


Figure D.5: Fork-lift truck with payload transverse to precast elements

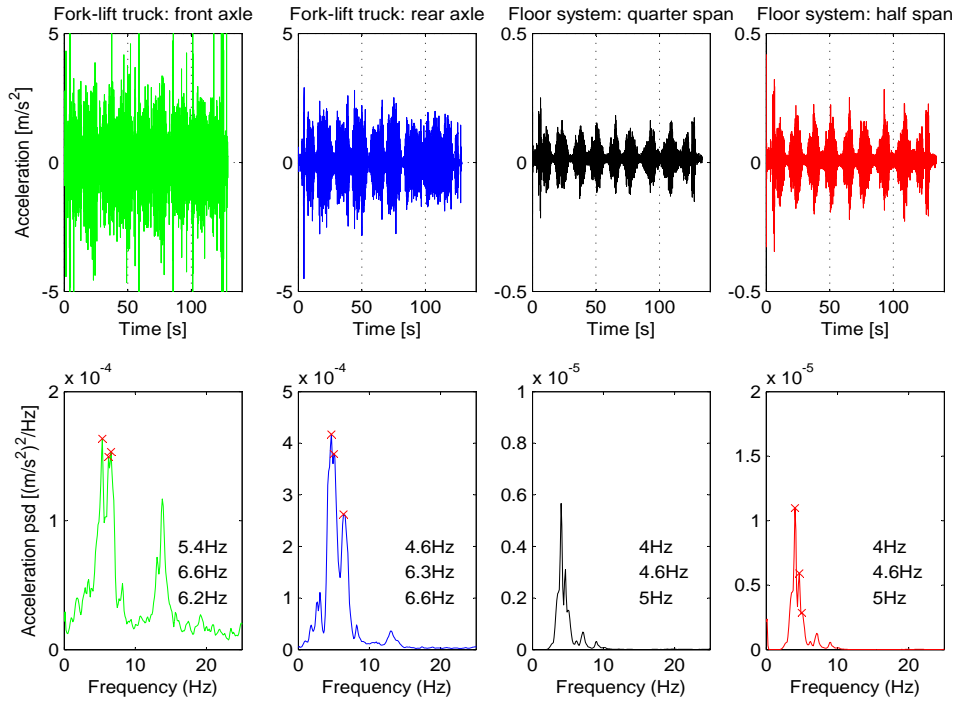


Figure D.6: Frequency content of the above record (Figure [D.5])

Appendix E

Results of the finite-element simulations of the floor in Helmstadt

Here the results of the configurations

- parallel with payload (Figures [E.1] and [E.2])
- transverse with payload (Figures [E.3] and [E.4])
- transverse without payload (Figures [E.5] and [E.6])

are summarised. For each configuration the time history and the frequency response are plotted.

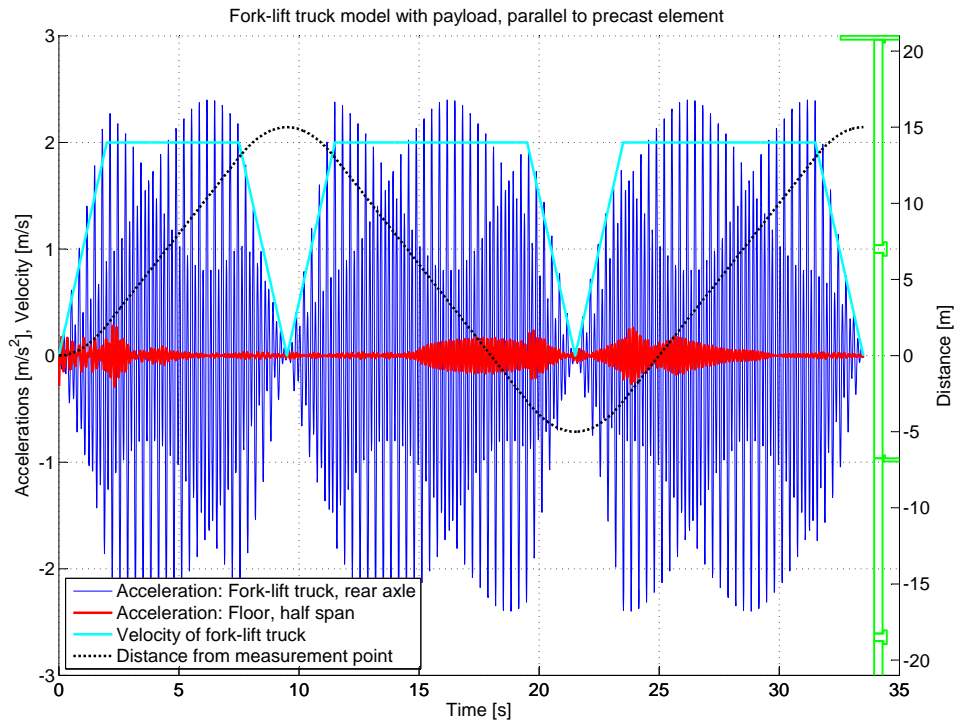


Figure E.1: Time history of calculated accelerations: “parallel with payload”

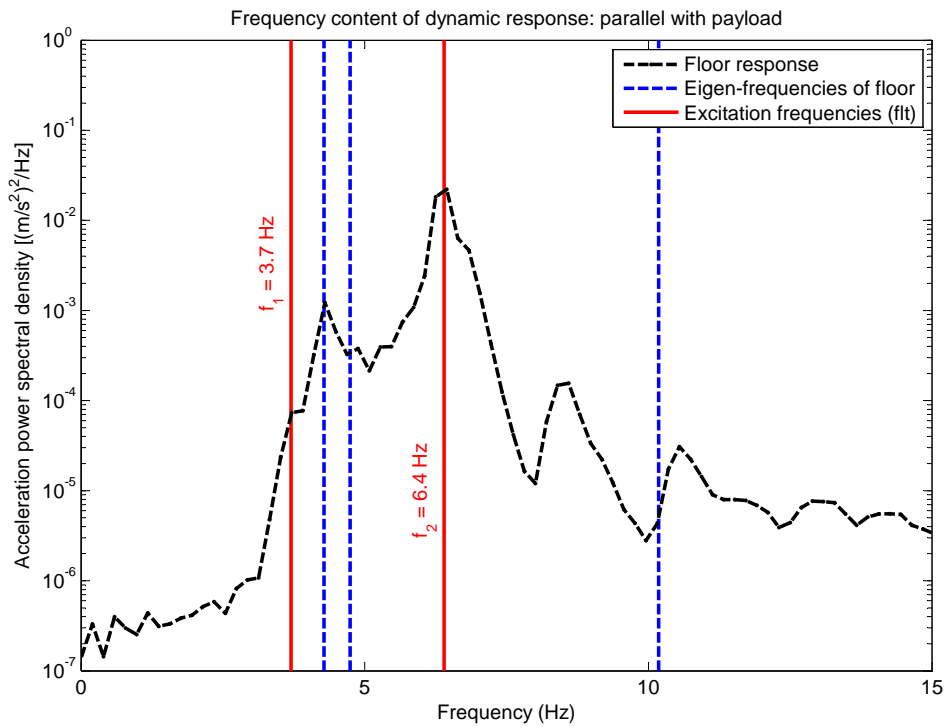


Figure E.2: Frequency content of the above calculated floor accelerations

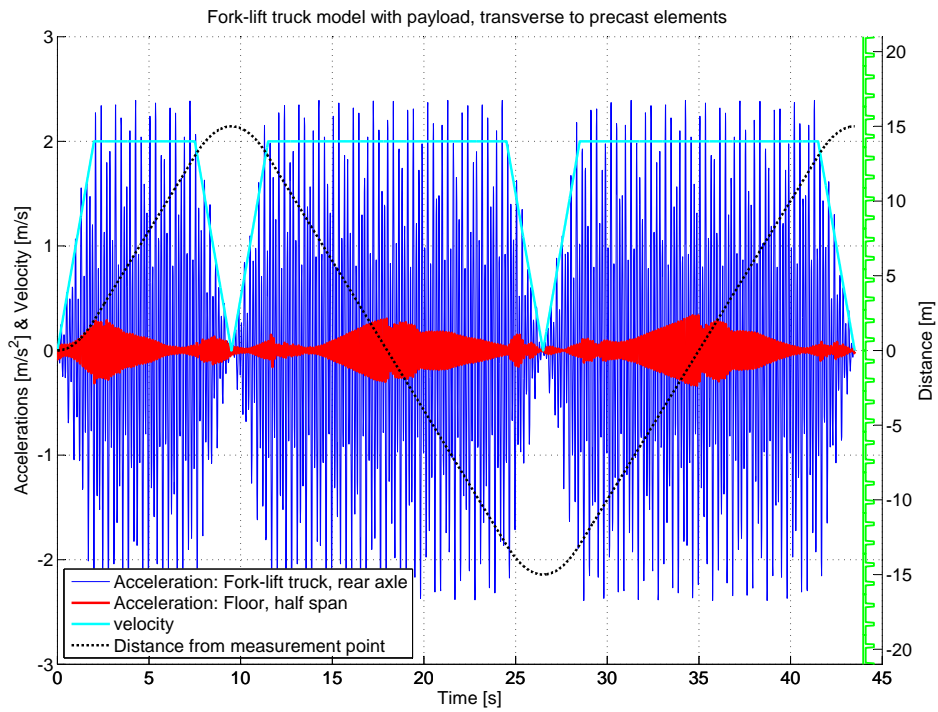


Figure E.3: Time history of calculated accelerations: “transverse with payload”

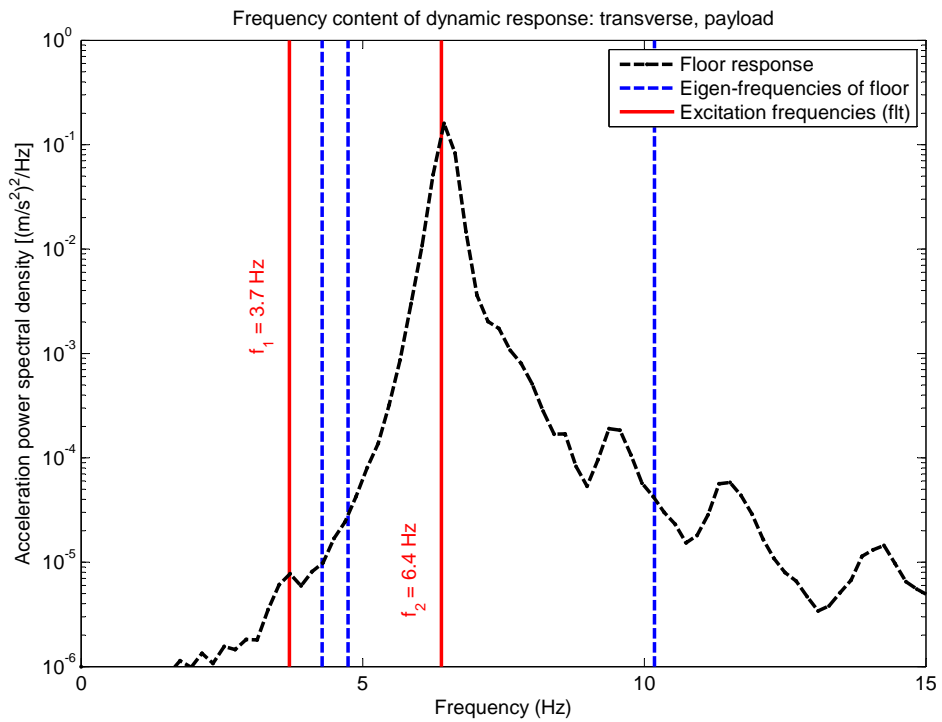


Figure E.4: Frequency content of calculated floor accelerations: “transverse with payload”

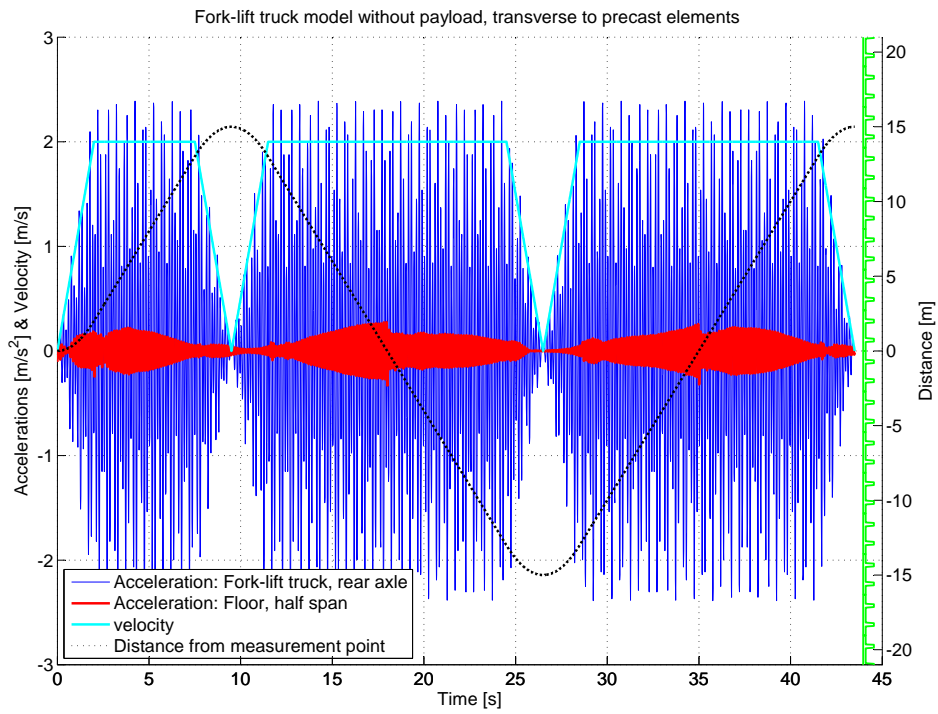


Figure E.5: Time history of calculated accelerations: “transverse without payload”

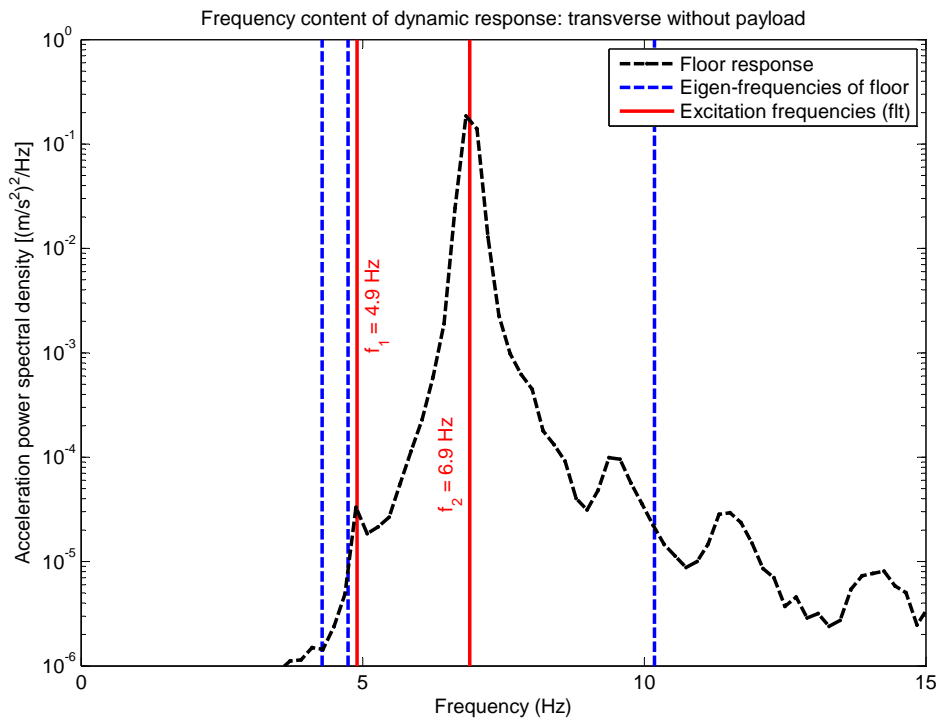


Figure E.6: Frequency content of calculated floor accelerations: “transverse without payload”

References

- O.N.J. Abraham and J.A. Brandon. The modelling of the opening and closure of a crack. *Journal of Vibration and Acoustics Transactions of the ASME*, 117:370–377, 1995.
- M. Ahn, K.H. Böckeler, and W. Haas. Eingabekonventionen für CAD-Programme, CAD-Bericht Kfk-CAD 39. Technical report, Kernforschungszentrum Karlsruhe, 1976.
- AISC D811. *Floor vibrations due to human activity. AISC publication D811*. American Institute of Steel Construction, Chicago, 1997.
- D.E. Allen and J.H. Rainer. Vibration criteria for long-span floors. *Canadian Journal of Civil Engineering*, 3:165–173, 1976.
- ASCE. Structural serviceability: a critical appraisal and research needs. *ASCE Journal of Structural Engineering*, 112:2646–2664, 1986.
- H. Bachmann, editor. *Vibration problems in structures - practical guidelines*. Birkhaeuser Verlag, Basel, 1995.
- H. Bachmann and R. Dieterle. Experiments and models for the damping behaviour of vibrating reinforced concrete beams in the uncracked and cracked condition. *International Association for Bridge and Structural Engineering*, 34:69–82, 1981. IABSE Colloquium, Delft, 1981.
- C.F. Beards. *Structural Vibration - Analysis and Damping*. Arnold, London, 1996.
- E.F. Beha. *Dynamische Beanspruchung und Bewegungsverhalten von Gabelstaplern*. PhD thesis, Universität Stuttgart, 1989.
- D. Bertram and N. Bunke, editors. *Erläuterungen zu DIN 1045, Beton und Stahlbeton 07.88 (DAfStb Heft400)*. Beuth Verlag GmbH, Berlin, 1994.
- K. Billig. *Precast Concrete*. Macmillan & Co. Ltd, London, 1955.

-
- P.H. Bischoff. Effects of shrinkage on tension stiffening and cracking in reinforced concrete. *Canadian Journal of Civil Engineering*, 28(3):363–374, 2001.
- M. Bovenzi, I. Pinto, and N. Stacchini. Low back pain in port machinery operators. *Journal of Sound and Vibration*, 253:3–20, 2002.
- M. Bovenzi, F. Rui, C. Negro, F. D’Agostin, G. Angotzi, S. Bianchi, L. Brmamanti, G. Festa, S. Gatti, I. Pinto, L. Rondina, and N. Stacchini. An epidemiological study of low back pain in professional drivers. *Journal of Sound and Vibration*, 298:514–539, 2006.
- J.M.W. Brownjohn. Energy dissipation from vibrating floor slabs due to human-structure interaction. *Journal of Shock and Vibration*, 8:315–323, 2001.
- J.M.W. Brownjohn, A.A. Dumanoglu, R.T. Severn, and A.B. Blakeborough. Ambient vibration survey of the Bosphorus suspension bridge. *Earthquake Engineering and Structural Dynamics*, 18:263–283, 1989.
- J.M.W. Brownjohn, T.C. Pan, and X.Y. Deng. Correlating dynamic characteristics from field measurements and numerical analysis of a high-rise building. *Earthquake Engineering and Structural Dynamics*, 29:523–543, 2000.
- BS 6399-1. *British Standard BS 6399-1:1996, Loading for buildings - Part 1: Code of practice for dead and imposed loads*. British Standards Institution, London, 1996.
- BS 6472. *BS 6472, Guide to evaluation of human exposure to vibration in buildings (1 Hz to 80 Hz)*. British Standards Institution, London, 1992.
- BS 6841. *BS 6841, Guide to measurement and evaluation of human exposure to whole-body mechanical vibration and repeated shock*. British Standards Institution, London, 1987.
- D. Busjaeger and U. Quast. *Programmgesteuerte Berechnung beliebiger Massivbauquerschnitte unter zweiachsiger Biegung mit Längskraft (DAfStb Heft 415)*. Beuth Verlag GmbH, Berlin, 1990.
- Calenberg Ingenieure. Technical guide, 2003.
- J.O. Caneiro, F.J.Q. deMelo, S. Jalali, V. Teixeira, and M. Tomás. The use of pseudo-dynamic method in the evaluation of damping characteristics in reinforced concrete beams having variable bending stiffness. *Mechanics Research Communications*, 33: 601–613, 2006.
- R.G. Caverson, P. Waldron, and M.S. Williams. Review of vibration guidelines for suspended concrete slabs. *Canadian Journal of Civil Engineering*, 21:931–938, 1994.

-
- CEB. *Bulletin d'Information no. 187: Concrete Structures under Impact and Impulsive Loading*. European Committee for Standardization, 1988.
- CEB. *RC elements under cyclic loading: state of the art report, Comité euro-international du Béton*. European Committee for Standardization, 1996.
- CEB-FIP. *CEB-FIP MODEL CODE 1990, Comité euro-international du Béton*. European Committee for Standardization, 1990.
- Y. Chen. Finite element analysis for walking vibration problems for composite precast building floors using ADINA: modelling, simulation and comparison. *Computer & Structures*, 72:109–126, 1999.
- S.M. Cheng, X.J. Wu, and W. Wallace. Vibrational response of a beam with a breathing crack. *Journal of Sound and Vibration*, 225:201–208, 1999.
- S.H. Chowdhury, Y.C. Loo, and S. Fragomeni. Damping formulae for reinforced and partially prestressed concrete beams. *Advances in Structural Engineering*, 3(4):327–334, 2000.
- R.W. Clough and J. Penzien. *Dynamic of structures*. McGraw-Hill, New York, 1975.
- Concrete Society TR43. *Post-tensioned concrete floors, Design handbook, 2nd edition*. The Concrete Society, 2005.
- S. Constantine. *Finite Element Modelling in Engineering Practice*. Algor Inc. Publishing Division, Pittsburgh, 1994.
- R.R.(Jr.) Craig. *Structural Dynamics: An introduction to Computer methods*. John Wiley & Sons, New York, 1981.
- DIN 1055. *Lastannahmen für Bauten (07.78)*. Beuth Verlag, Berlin, 1978.
- DIN 1055 Teil 3. *Lastannahmen für Bauten (03.2006)*. Beuth Verlag, Berlin, 2006.
- DIN 18202. *Toleranzen im Hochbau (10.2005)*. Beuth Verlag, Berlin, 2005.
- DIN 4150 Teil 2. *Erschütterungen im Bauwesen - Einwirkungen auf Menschen in Gebäuden (06.99)*. Beuth Verlag, Berlin, 1999.
- EC 1. *EUROCODE 1991-1-1:2002, Action on structures. General actions. Densities, self-weight, imposed loads for buildings*. CEN Comité Européen de Normalisation, 2002.

- EC 2. *EUROCODE 1992-1-1:1991, Design of concrete structures; Part 1: General rules and rules for buildings (German Version)*. CEN Comité Européen de Normalisation, 1991.
- EC 2. *EUROCODE 1992-1-1:2004, Design of concrete structures; Part 1: General rules and rules for buildings (British Standard)*. CEN Comité Européen de Normalisation, 2004.
- EC 4. *EUROCODE 1994-1-1:2004, Design of composite steel and concrete structures*. CEN Comité Européen de Normalisation, 2004.
- K.S. Elliott. *Multi-storey Precast Concrete Framed Structures*. Blackwell Science Ltd., Oxford, 1996.
- K.S. Elliott. *Precast Concrete Structures*. Butterworth-Heinemann, Oxford, 2002.
- B.R. Ellis and T. Ji. Human-structure interaction in vertical vibration. *Proceedings of the ICE Structures and Buildings*, 122:1–9, 1997.
- B.R. Ellis and J.D. Littler. Dynamic response of nine similar tower blocks. *Journal of Wind Engineering and Industrial Aerodynamics*, 28:339–349, 1988.
- P.E. Eriksson. *Vibration of Low-Frequency Floors - Dynamic Forces and Response Prediction*. PhD thesis, Chalmers University of Technology, 1994.
- D.J. Ewins. *Modal Testing: Theory, Practice and Application*. Research Studies Press Ltd, Baldock, 2000.
- S. Falati. *The contribution of non-structural members on the overall dynamic behaviour of concrete floor slabs*. PhD thesis, University of Oxford, 1999.
- L. Fryba. *Vibration of solids and structures under moving loads*. Thomas Telford, London, 1999.
- N.J. Gardner. Comparison of prediction provisions for drying shrinkage and creep of normal strength concretes. *Canadian Journal of Civil Engineering*, 31(5):767–775, 2004.
- C.W. Glover. *Structural Precast Concrete*. C.R. Books Limited, London, 1964.
- M.F. Green and D. Cebon. Dynamic response of highway bridges to heavy vehicle loads: theory and experimental validation. *Journal of Sound and Vibration*, 170: 51–78, 1994.
- M.F. Green and D. Cebon. Dynamic interaction between heavy vehicle and highway bridges. *Computer and Structures*, 62:253–264, 1997.

-
- E. Hamed and Y. Frostig. Free vibrations of cracked prestressed beams. *Engineering Structures*, 26:1611–1621, 2004.
- M.S.A. Hardy and D. Cebon. Response of continuous pavements to moving dynamic loads. *Journal of Engineering Mechanics*, 119:1762–1780, 1993.
- J. He and Z-F. Fu. *Modal Analysis*. Butterworth-Heinemann, Oxford, 2001.
- ISO 10137. *ISO 10137, Bases for design of structures - Serviceability of buildings against vibration*. International Organization for Standardization, 2007.
- ISO 2631-1. *ISO 2631-1, Mechanical vibration and shock evaluation of human exposure to whole-body vibration. Part 1: general requirements*. International Organization for Standardization, 1997.
- ISO 2631-2. *ISO 2631-2, Mechanical vibration and shock evaluation of human exposure to whole-body vibration. Part 2: vibration in buildings (1 Hz to 80 Hz)*. International Organization for Standardization, 2003.
- A.P. Jeary. Damping in tall buildings - a mechanism and a predictor. *Earthquake Engineering and Structural Dynamics*, 14:733–750, 1986.
- A.P. Jeary. The description and measurement of nonlinear damping in structures. *Journal of Wind Engineering and Industrial Aerodynamics*, 59:103–114, 1996.
- E. Júlio, F. Branco, and V. Silva. Concrete-to-concrete bond strength. Influence of roughness of substrate surface. *Construction and Building Materials*, 18:675–681, 2004.
- R.E. King and D. Rea. An analysis of damped free vibrations of slender prestressed beams. *International Journal of Mechanical Sciences*, 7:211–219, 1965.
- K. Kordina, editor. *Bemessungshilfsmittel zu Eurocode 2 (DAfStb Heft 425)*. Beuth Verlag GmbH, Berlin, 1992.
- J.W. Kwark, E.S. Choi, Y.J. Kim, B.S. Kim, and S.I. Kim. Dynamic behaviour of two-span continuous concrete bridges under moving high-speed train. *Computer & Structures*, 82:463–474, 2004.
- S.S. Law and X.Q. Zhu. Dynamic behaviour of damaged concrete bridge structures under moving vehicular loads. *Engineering Structures*, 26:1279–1293, 2004.
- P. Lemerle, P. Boulanger, and R. Poirot. A simplified method to design suspended cabs for counterbalance trucks. *Journal of Sound and Vibration*, 253:283–293, 2002.

- C.H. Lewis and M.J. Griffin. A comparison of evaluations and assessments obtained using alternative standards for predicting the hazards of whole-body vibration and repeated shocks. *Journal of Sound and Vibration*, 215:915–926, 1998.
- J. Li and Y. Yao. A study on creep and drying shrinkage of high performance concrete. *Cement and Concrete Research*, 31:1203–1206, 2001.
- Q.S. Li, D.K. Liu, J.Q. Fang, A. P. Jeary, and C.K. Wong. Damping in buildings: its neural network model and ar model. *Engineering Structures*, 22:1216–1223, 2000.
- Q.S. Li, K. Yang, C. K. Wong, and A. P. Jeary. The effect of amplitude-dependent damping on wind-induced vibrations of a super tall building. *Journal of Wind Engineering and Industrial Aerodynamics*, 91:1175–1198, 2003.
- J.R. Libby. *Modern prestressed concrete*. Van Nostrand Reinhold Co., New York, 1984.
- J.H. Lin. Response of a bridge to a moving vehicle load. *Canadian Journal of Civil Engineering*, 33:49–57, 2006.
- C. Liu, D. Huang, and T-L. Wang. Analytical dynamic impact study based on correlated road roughness. *Computers & Structures*, 80:1639–1650, 2002.
- M. Los and U. Quast. *ABaS W32 Documentation (Online)*, 2000.
- F.D. Lydon and R.V. Balendran. Some observations on elastic properties of plain concrete. *Cement and Concrete Research*, 16(3):314–324, 1986.
- A. Major. *Dynamics in Civil Engineering*. Akadémiai Kiadó, 1980.
- J. Malchaire, A. Piette, and I. Mullier. Vibration exposure on fork-lift trucks. *The Annals of Occupational Hygiene*, 40:79–91, 1996.
- T.M. Murray. Design to prevent floor vibrations. *AISC Engineering Journal*, 12:62–70, 1975.
- NBC. *Serviceability criteria for deflections and vibrations*. National Research Council Canada, 1995.
- S.A. Neild, P.D. McFadden, and M. S. Williams. A discrete model of a vibrating beam using a time-stepping approach. *Journal of Sound and Vibration*, 239:99–121, 2001.
- S.A. Neild, M.S. Williams, and P.D. McFadden. Non-linear behaviour of reinforced concrete beams under low amplitude cyclic and vibrations loads. *Engineering Structures*, 24:707–718, 2002.
- A.M. Neville. *Properties of concrete*. Longman Group Ltd., Harlow, 1995.

-
- J. Palamas, O. Coussy, and Y. Bamberger. Effects of the surface irregularities upon the dynamic response of bridges under suspended moving loads. *Journal of Sound and Vibration*, 99:235–245, 1985.
- T-C. Pan, A. Mita, and J. Li. Vehicle-induced floor vibrations in a multistory factory building. *Journal of performance of constructed facilities*, 15:54–61, 2001.
- A. Pavic, R. Crouch, and P. Waldron. Experimental validation of FE models for modal analysis of a full-scale prestressed concrete floor structure. *5th international conference on reliability of finite element methods for engineering*, pages 319–330, 1995.
- A. Pavic and P. Reynolds. Vibration serviceability of long-span concrete building floors. part 1: Review of background information. *The Shock and Vibration Digest*, 34(3), 2002a.
- A. Pavic and P. Reynolds. Vibration serviceability of long-span concrete building floors. part 2: Review of mathematical modelling approaches. *The Shock and Vibration Digest*, 34(4), 2002b.
- A. Pavic and P. Reynolds. Modal testing and dynamic FE model correlation and updating of a prototype high-strength concrete floor. *Cement & Concrete Composites*, 25:787–799, 2003.
- B. Persson. Poisson’s ratio of high-performance concrete. *Cement and Concrete Research*, 29:1647–1653, 1999.
- U. Pfeiffer. *INCA 2.62 Documentation (Online)*, 2004.
- W.H. Press, B.P. Flannery, S.A. Teukolsky, and W.T. Vetterling. *Numerical Recipes - The Art of Scientific Computing*. Cambridge University Press, 1988.
- J.H. Rainer, G. Pernica, and D.E. Allen. Dynamic loading and response of footbridges. *Canadian Journal of Civil Engineering*, 15:66–71, 1988.
- P. Reynolds and A. Pavic. Vibration performance of a large cantilever grandstand during an international football match. *Journal of performance of constructed facilities*, 20:202–212, 2006.
- J.G. Richardson. *Quality in Precast Concrete*. Longman Group UK Ltd, Harlow, 1991.
- R. Sachse, A. Pavic, and P. Reynolds. Human-structure dynamic interaction in civil engineering dynamics: a literature review. *The Shock and Vibration Digest*, 35:3–18, 2003.

-
- R. Sachse, A. Pavic, and P. Reynolds. Parametric study of modal properties of a damped two-degree-of-freedom crowd-structure dynamic system. *Journal of Sound and Vibration*, 274:461–480, 2004.
- E.J. Sapountzakis and J.T. Katsikadelis. Creep and shrinkage effect on the dynamic analysis of reinforced concrete slab-and-beam structures. *Journal of Sound and Vibration*, 260:403–416, 2003.
- SCI 076. *Design guide on the vibration of floors. SCI publication 076*. The Steel Construction Institute, Ascot, 1989.
- R.H. Scott. Technical note 372 - the short-term moment-curvature relationship for reinforced concrete beams. *Proceedings of the Institution of Civil Engineers, Part 2*, 75:725–734, 1983.
- J. Senthilvasan, D.P. Thambiratnam, and G.H. Bramfeld. Dynamic response of a curved bridge under moving truck load. *Engineering Structures*, 24:1283–1293, 2002.
- The MathWorks. *MATLAB R2006a*, 2006.
- W.T. Thomson. *Theory of Vibration with Applications*. Unwin Hyman, London, 1988.
- L.I. Torres, F. López-Alamansa, and L.M. Bozzo. Tension-stiffening model for cracked flexural concrete members. *Journal of Structural Engineering*, 130(8):1242–1251, 2004.
- H. Trost and J. Wolff. Zur wirklichkeitsnahen Ermittlung der Beanspruchung in abschnittsweise hergestellten Spannbetonstragwerken. *Der Bauingenieur*, 45:155–169, 1970.
- S. Zivanovic, A. Pavic, and P. Reynolds. Vibration serviceability of footbridges under human-induced excitation: A literature review. *Journal of Sound and Vibration*, 279:1–74, 2005.
- Z-H. Zong, B. Jaishi, J-P. Ge, and W-X. Ren. Dynamic analysis of a half-through concrete-filled steel tubular arch bridge. *Engineering Structures*, 27:3–15, 2005.